METHODS FOR EVALUATING THE PREDICTIVE ACCURACY OF STRUCTURAL DYNAMIC MODELS

FINAL REPORT

p.306

Technical Report No. TR-91-1152

By

T.K. Hasselman
and
Jon D. Chrostowski

Prepared for

National Aeronautics and Space Administration
Washington, D.C. 20546-0001

NASA Resident Office - JPL
4800 Oak Grove Drive
Pasadena, CA 91109

By

Engineering Mechanics Associates, Inc.
3820 Del Amo Boulevard, Suite 318
Torrance, CA 90503

December, 1991

Report Documentation Page

NASA National Aeronautics and Space Administration

1. Report No.	2. Government Accession No.	3. Recipient's Catalog No.

4. Title and Subtitle

Methodology for Evaluating the Predictive Accuracy of Structural Dynamic Models - Final Report

5. Report Date

December, 1991

6. Performing Organization Code

7. Author(s)

Timothy K. Hasselman and Jon D. Chrostowski

8. Performing Organization Report No.

TR-91-1152

10. Work Unit No.

9. Performing Organization Name and Address

Engineering Mechanics Associates, Inc.
3820 Del Amo Blvd., Suite 318
Torrance, CA 90503-2155

11. Contract or Grant No.

NAS-7-1064

13. Type of Report and Period Covered

Final Report
July 1989 - Dec. 1991

12. Sponsoring Agency Name and Address

National Aeronautics and Space Administration
Washington, D.C. 20546-0001
Jet Propulsion Laboratory

14. Sponsoring Agency Code

15. Supplementary Notes

16. Abstract

Modeling uncertainty is defined in terms of the difference between predicted and measured eigenvalues and eigenvectors. Data compiled from 22 sets of analysis/test results was used to create statistical databases for large truss-type space structures and both pretest and posttest models of conventional satellite-type space structures. Modeling uncertainty is propagated through the model to produce intervals of uncertainty on frequency response functions, both amplitude and phase. This methodology was used successfully to evaluate the predictive accuracy of several structures, including the NASA CSI Evolutionary Structure tested at Langley Research Center. Test measurements for this structure were within ± one-sigma intervals of predicted accuracy for the most part, demonstrating the validity of the methodology and computer code.

17. Key Words (Suggested by Author(s))

Structural Dynamics
Predictive Accuracy
Interval Prediction
Modeling Uncertainty
Modeling Error

18. Distribution Statement

[redacted]

19. Security Classif. (of this report)	20. Security Classif. (of this page)	21. No. of pages	22. Price
Unclassified	Unclassified	293	

NASA FORM 1626 OCT 86

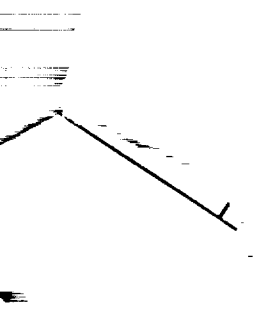

SUMMARY

The purpose of this research was to develop, implement and demonstrate a methodology for evaluating the predictive accuracy of structural dynamic models. Implementation includes a general purpose computer code, and databases residing within the code which quantify modeling accuracy for large truss–type space structures, and both pretest and posttest models of conventional satellite–type space structures.

The research included the collection of modal analysis and test data for twenty–two structure–model combinations. The differences between predicted and measured eigenvalues and eigenvectors were used to generate statistical databases of mass and stiffness uncertainty. Methods were also developed to estimate a full modal damping matrix based on experimentally measured complex eigenvalues and eigenvectors. Multiple estimates based on different tests provide the information necessary to quantify damping uncertainty.

Several methods for propagating the uncertainty through the model were developed, including linear covariance propagation, a fuzzy set method for possibility bounding, and a Monte Carlo method for numerical simulation. These methods are implemented in the PDAC computer code which computes uncertainty intervals on both the amplitude and phase of frequency response functions.

The methodology was demonstrated by applying PDAC to several real structures for which both analysis and test data were available. Intervals of predictive accuracy were computed on the basis of the analytical models and the modeling uncertainty database. These intervals were compared with test results to demonstrate the methodology. Test measurements were found to lie for the most part within ± one–sigma of the nominal (analytically predicted) response, demonstrating that the methodology produces realistic results. This represents the first time that data from previously analyzed and tested structures have been used to evaluate the predictive accuracy of models of other structures.

FOREWORD

This final report documents the work performed under SBIR Phase II Contract NAS7–1064 during the period July, 1989 through December, 1991. The report is complete and self–contained. It documents the methodology for evaluating the predictive accuracy of structural dynamic models, demonstration of the methodology by application to practical problems, and the databases for both conventional and large space structures used in the methodology demonstration. Additional details describing the development of the methodology may be found in eight quarterly reports numbered TR–89–1152–1 through TR–89–1152–8, submitted during the course of the contract. Two interim briefings were presented at the Jet Propulsion Laboratory in May of 1990 and 1991. The authors wish to express their gratitude for the support of Mr. John Garba, the JPL Technical Monitor and Ms. G. Veronica Stickley, the NASA Contracting Officer.

Key data for this project were provided by a number of government agencies and commercial aerospace companies, without whose support the project could not have been completed. Data contributions by the Jet Propulsion Laboratory, NASA Langley Research Center, Air Force Wright Laboratories, Martin Marietta Corporation, TRW Space and Technology Group, Hughes Space and Communications Division, and General Electric Astro Space Division are acknowledged. The authors extend their personal thanks to the numerous individuals within these organizations who were instrumental in providing the data, for their interest and cooperation.

Significant contributions to the project were made by Professor Timothy Ross and his graduate student, Steve Verzie, under a subcontract to the University of New Mexico. Professor Ross was instrumental in developing the fuzzy set approach used for computing possibility bounds on frequency response functions.

Finally, the authors wish to acknowledge the contributions of other EMA personnel, including George Lee who helped with some of the early investigations, John Piersol who helped with coding and check–out, and Wendy Keener who produced the final report and software documentation.

TABLE OF CONTENTS

TABLE OF CONTENTS (Cont'd)

TABLE OF CONTENTS (Cont'd)

LIST OF FIGURES

LIST OF FIGURES (Cont'd)

LIST OF FIGURES (Cont'd)

LIST OF FIGURES (Cont'd)

LIST OF FIGURES (Cont'd)

LIST OF FIGURES (Cont'd)

LIST OF TABLES

LIST OF TABLES (Cont'd)

LIST OF TABLES (Cont'd)

EXECUTIVE SUMMARY

Introduction

The goal of this SBIR project has been to develop a practical tool for evaluating the predictive accuracy of structural dynamic models. Phases I and II have focused on initial application to space structures for two reasons: NASA has identified the need to quantify the accuracy of models used to simulate the performance of flight hardware, and sufficient analysis and testing have been performed on space structures to establish a meaningful database. Phase III will seek uses for the tools developed under this contract in practical aerospace applications, and attempt to extend their application to civil and commercial structures such as high–rise buildings and offshore platforms.

The objectives of Phase II were to develop a methodology, implement it in a suitable computer code complete with the necessary database, and finally to demonstrate the methodology by applying the code to real structures. Specific objectives are outlined as follows:

1. Develop a methodology for:
   - Realistically quantifying mass and stiffness uncertainty,
   - Estimating damping and damping uncertainty, and
   - Propagating these uncertainties through a model to evaluate predictive accuracy.

2. Implement the methodology in:
   - A general purpose computer code, and
   - A database to be accessed by the computer code.

3. Demonstrate the methodology for:
   - Simple examples, and
   - Real structures

Application of the methodology to space structures has provided a contextual framework for the project. Space structures are thoroughly analyzed and tested prior to flight. The need for the quantification of predictive accuracy therefore relates to posttest models which

have been tuned and verified in accordance with test data. Linking the predictive accuracy code to a model verification code was therefore found to benefit both codes. The predictive accuracy code PDAC has been linked to the model verification code SSID. PDAC uses many of the computational modules found in SSID, while SSID benefits from PDAC's ability to compute intervals of uncertainty.

Figure 1 shows typical results from PDAC. Part (a) of the figure shows a drawing of the CSI Evolutionary Structure, identifying locations of sensors and actuators. Part (b) shows the $\pm 1\sigma$ uncertainty intervals computed by PDAC for FRF acceleration amplitude at Coordinate 1 due to force at Coordinate 1. A database of mass and stiffness uncertainty for large space structures was used to compute these intervals. The CSI Evolutionary Structure was not part of the database. Measured FRF amplitude is plotted on the same graph for purposes of comparison. The plot shows that the measured FRF amplitude falls within the predicted $\pm 1\sigma$ uncertainty intervals across the entire frequency spectrum in this case, demonstrating that PDAC produces realistic results. This represents the first time that data from previously analyzed and tested structures have been successfully used to evaluate the predictive accuracy of other structures.

The remainder of the Executive Summary briefly describes how these results were obtained.

Development of Methodology

Mass and Stiffness Uncertainty

Mass and stiffness uncertainty is based on the difference between analytically predicted and experimentally measured eigenvalues and eigenvectors. It is expressed in the form of linear perturbations to the modal mass and stiffness matrices of a model. These perturbations, Δm and Δk, represent a first order correction to the analytical modal mass and stiffness matrices which are both diagonal. When the analytical modes are normalized to unit modal mass, these matrices are the identity matrix, I, and the diagonal matrix of system eigenvalues denoted by ${}^{o}\lambda$. The "corrected" modal mass and stiffness matrices, designated m and k, respectively, are then given by

$$m = I + \Delta m$$
$$k = {}^{o}\lambda + \Delta k$$

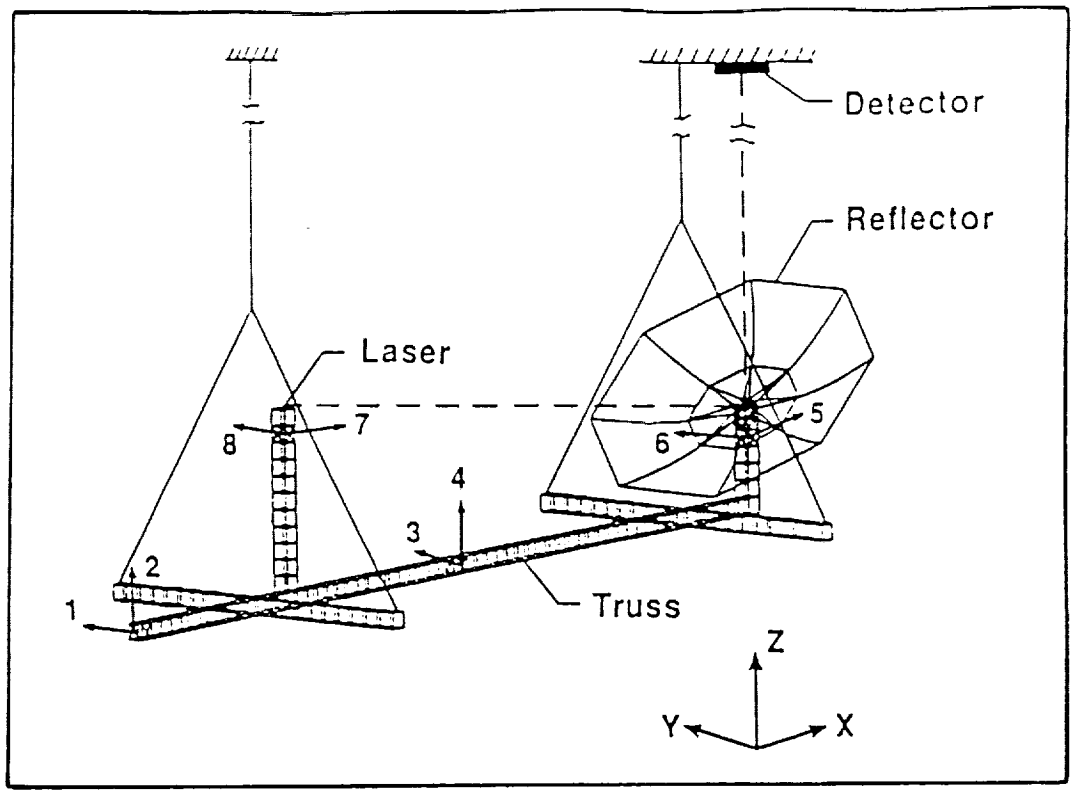

(a) NASA CSI Evolutionary Structure

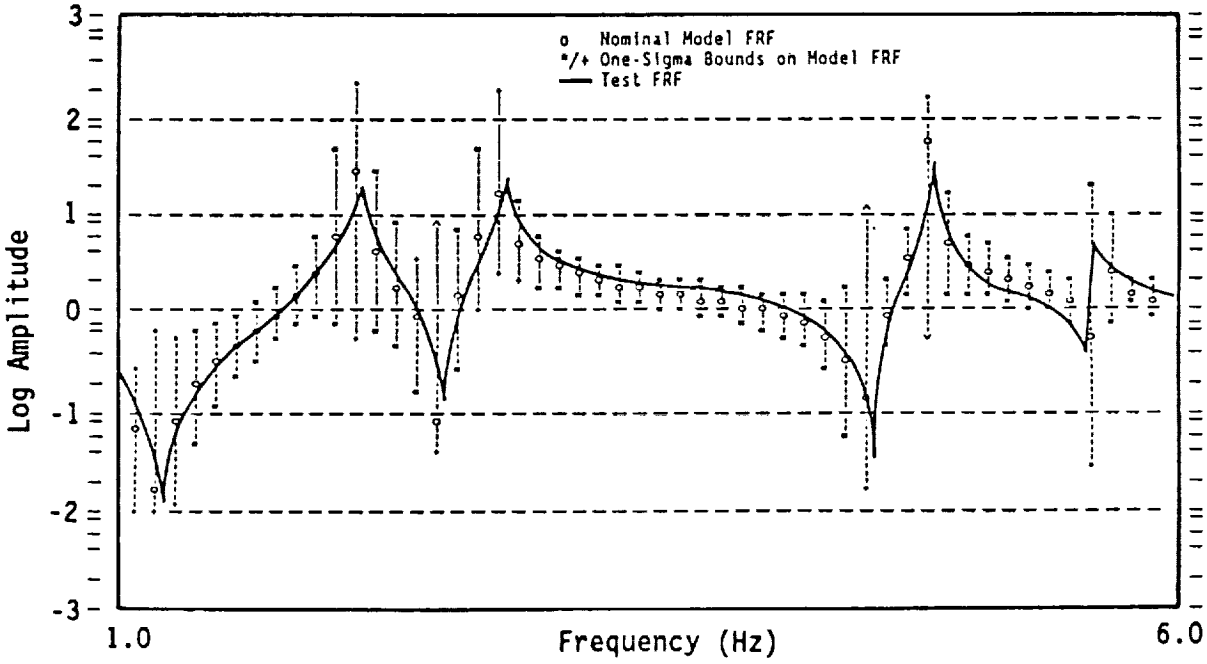

(b) FRF Amplitude Response [Coord 1/Force Coord 1]

Figure 1. Illustration of Typical PDAC Results for NASA CSI Evolutionary Structure.

The correction terms, Δm and Δk, can be expressed in terms of the difference between measured and predicted eigenvalues,

$$\Delta\lambda = \lambda - {}^{o}\lambda$$

and the cross–orthogonality between the measured and predicted eigenvectors,

$${}^{o}\phi^{T}{}^{o}M\phi = \psi$$

where ${}^{o}\phi$ is the matrix of predicted eigenvectors, ϕ is the matrix of measured eigenvectors, ${}^{o}M$ is the analytical mass matrix in physical coordinates, and ψ is the cross–orthogonality matrix. Ideally, the diagonal terms of ψ will be close to unity while the off–diagonal terms are close to zero. The correction terms, Δm and Δk are found by linear perturbation analysis to be

$$\Delta m = (I - \psi) + (I - \psi)^{T}$$

$$\Delta k = \Delta\lambda + {}^{o}\lambda\,(I - \psi) + (I - \psi)^{T}{}^{o}\lambda$$

By putting Δk in the dimensionless form (and thus removing frequency dependence),

$$\Delta\tilde{k} = {}^{o}\lambda^{-1/2}\,\Delta k\,{}^{o}\lambda^{-1/2}$$

these differences in modal mass and stiffness can be averaged over a number of structures to create a statistical database. In particular, a covariance matrix of the Δm's and $\Delta\tilde{k}$'s is derived. This covariance matrix embodies the mass and stiffness uncertainty for the type of structures represented in the database.

Estimation of Damping and Damping Uncertainty

Since damping in general cannot be modeled, it must be determined experimentally. It is current practice to represent damping in terms of equivalent (linear) viscous damping. The damping matrix expressed in the physical coordinate system is denoted by C. The modal damping matrix is defined in terms of C by

$$c = {}^{o}\phi^{T} C {}^{o}\phi$$

Unfortunately, C cannot be measured directly. While it is common practice to assume that the modal damping matrix, c, is diagonal, in reality it is not. The off–diagonal elements of c are generally of the same order as the diagonal terms. As long as the modal frequencies are well separated, the off–diagonal terms may be neglected. When modes are closely spaced in frequency, the off–diagonal terms may be important. If so, the inherent uncertainty in estimates of these terms is also likely to be important.

A previously proposed method for estimating the full modal damping matrix, c, has been refined and demonstrated for two real structures using complex eigenvalues and eigenvectors derived experimentally by the ERA method. This is believed to be the first time a full modal damping matrix has been successfully estimated using digitally recorded and processed data. Early attempts using analog data achieved only limited success, with great effort. The basic method is simple. If the complex modes are normalized such that

$$\phi = \phi_R + i\delta\phi_I$$

where now ϕ represents a matrix of complex modes consisting of a real part, ϕ_R, and a small imaginary part $i\delta\phi_I$, then the modal damping matrix, c, is obtained from

$$c = (\psi^T)^{-1} [2\zeta\omega + \phi_R^T M\delta\phi_I\omega + \omega\delta\phi_I^T M\phi_R] \psi^{-1}$$

where ζ is a diagonal matrix of critical damping ratios, ω is a diagonal matrix of circular modal frequencies, and M is the physical mass matrix of the structure.

Since c is estimated for a particular structure, uncertainties in c must be quantified in terms of multiple estimates. Multiple estimates may be derived from the same measurements by varying the estimation parameters as was done here. A more realistic estimate of the uncertainty would be obtained by varying the experiment (e.g. relocating the shakers). This was not done.

Both SSID and PDAC are structured to handle a full modal damping matrix. However, the option is not active in the present version of PDAC because the technology is not considered to be sufficiently mature. It is felt that estimates of damping uncertainty should be based on multiple experiments, rather than multiple estimates using the same data. Until realistic estimates of damping uncertainty are available, its effect on response predictions cannot be assessed. Until then, it is considered better to withhold the capability. The current version of PDAC therefore accepts only the diagonal elements of c specified in terms of ζ, consistent with current practice.

Uncertainty Propagation

One of the advantages of expressing model uncertainty in terms of modal parameters is that it is readily propagated through a model to determine either (1) eigenvalue/eigenvector uncertainty, (2) response uncertainty, or (3) the uncertainty of physical design parameters. The first two are referred to as forward propagation because the propagation follows the direction of analysis; the latter is called backward propagation or reverse propagation because the propagation is opposite to the direction of analysis.

Three essentially different methods are used for forward uncertainty propagation:

1. Linear covariance propagation;
2. The Vertex Method for evaluating functions of fuzzy variables; and
3. Numerical simulation using the Monte Carlo Method.

All three of the forward propagation methods have been implemented in deliverable software; each has its particular advantages and disadvantages which make it more suitable for some applications than others. The software has been written to select the best combination of methods for general application, i.e. execution defaults to the most suitable combination of methods for general application based on current experience. Default overrides are available. Each of the three methods is discussed in the paragraphs which follow.

Linear covariance propagation is represented by the triple matrix product

$$S_{uu} = T_{ur} S_{rr} T_{ur}^{T}$$

where S_{rr} is the covariance matrix of modal mass, stiffness and damping matrix elements discussed previously, and S_{uu} is the covariance matrix of response variables, e.g. frequency response function (FRF) amplitude and phase at various frequencies. The matrix, T_{ur}, is the sensitivity matrix of the response variables, u, with respect to the modal parameters, r.

$$T_{ur} = \frac{\partial u}{\partial r}$$

Linear covariance propagation is valid at frequencies which are not near resonances or anti–resonances (i.e. poles or zeros). The method breaks down near those frequencies as shown later.

A fuzzy set approach is used to bound the uncertainty intervals near poles and zeros. This approach makes use of the Vertex Method, where response for all possible combinations of the upper and lower limits of each parameter are computed. These combinations correspond to the vertices of a rectangular hyperspace, thus the name Vertex Method. The upper limit of the response interval is taken to be the largest response computed from all of these combinations (vertices) while the lower limit is taken to be the smallest response. This process is illustrated in Figure 2a where a response surface is plotted as a function of only two parameters, modal mass and stiffness. In this case, the parameter interval for m is (m_1, m_2) and for k is (k_1, k_2). The intervals (m_1, m_2) and (k_1, k_2) might correspond to $m_o \pm \sigma_m$ and $k_o \pm \sigma_k$, for example, in which case (u_a, u_c) would represent the possibility interval associated with $\pm 1\sigma$ parameter intervals.

In the case of frequency response functions, the response surface often includes an extremum at some point (or points) other than the vertices of the parameter space, but within the rectangular hyperspace. When this happens, the extremum (or extrema) must be evaluated and included with the responses computed for all of the vertices, when searching for the maximum and minimum response. Such a response surface is illustrated in Figure 2b.

In Figure 2b, the line from the origin through the nominal parameter point in the m, k plane corresponds to the nominal resonant frequency, ${}^o\omega = \sqrt{{}^ok/{}^om}$. The line through

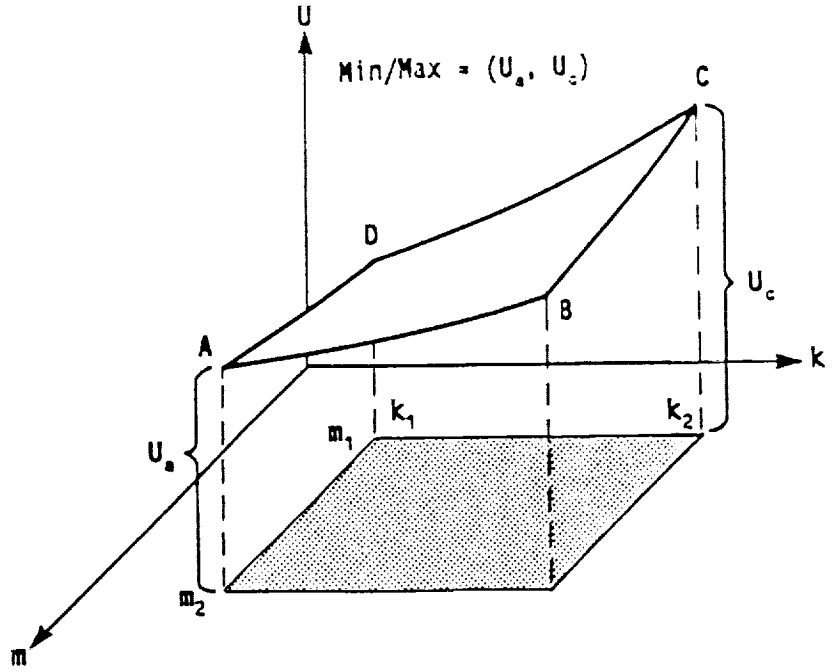

(a) Response Surface Without Included Extrema

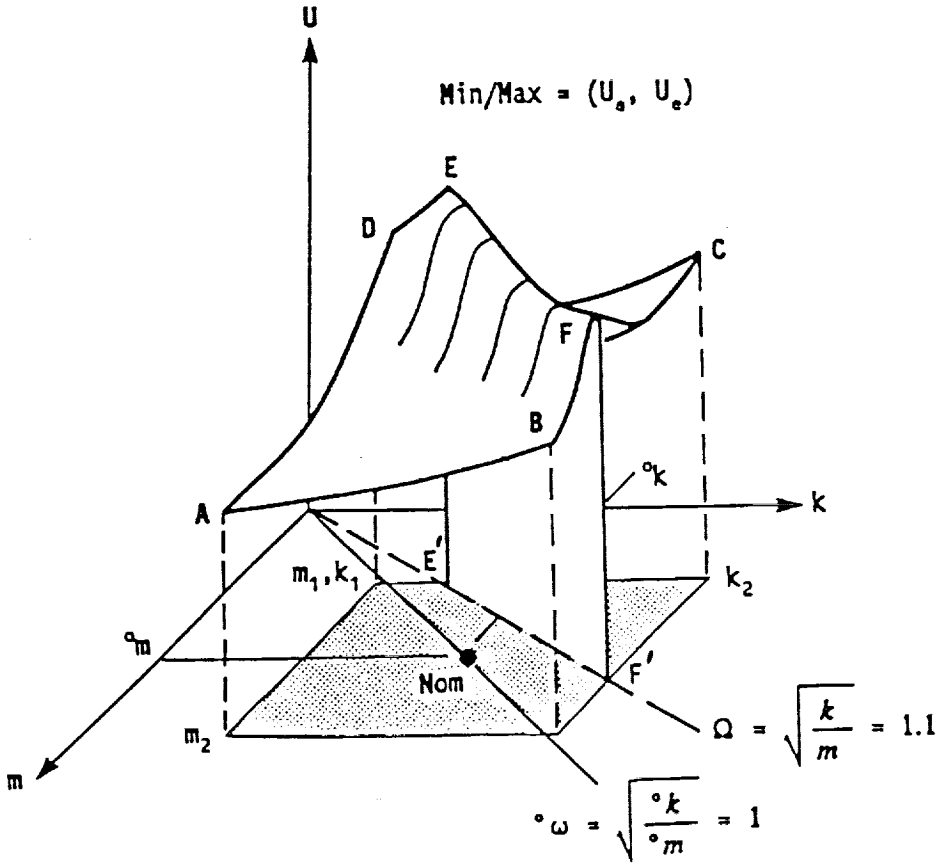

(b) Response Surface With Included Maxima

Figure 2. Illustration of the Vertex Method.

E′F′ corresponds to an excitation frequency, $\Omega = \omega = \sqrt{k/m}$, which is greater than ${}^{0}\omega$, but for which some combination of k and m results in a resonance at that excitation frequency. As a result, the response surface displays a ridge line EF. Thus, while the minimum response is still u_a in this case, the maximum response is now u_e, so that the response possibility interval is (u_a, u_e). PDAC offers several options for evaluating u_e, including random search and constrained optimization techniques.

A third method for evaluating response uncertainty in PDAC is the Monte Carlo method. With this method one can determine the entire distribution of response, not just its upper and lower bounds, or standard deviation. This method is also more useful near poles and zeros where response is dominated by fewer modal parameters.

Implementation of Methodology

SSID/PDAC

A computer code was written to implement the three methods of uncertainty propagation described above. This code is named PDAC (an acronym for PreDictive ACcuracy). Since model uncertainty is expressed in terms of modal parameters, it was convenient to formulate PDAC in terms of modal models. This meant that PDAC would require modeling data in the form of modal mass, damping and stiffness matrices, along with a modal transformation to convert input and output quantities (forces and forced response) to physical coordinates. Also required were an eigensolver, response computation modules, and modules to compute eigenvalue/eigenvector and FRF amplitude and phase derivatives which are used for uncertainty propagation.

These capabilities were available in a previously developed code called SSID (for Structural System IDentification). The modules could have been lifted from SSID to create a separate PDAC code; however, several ways were perceived in which PDAC could enhance the capabilities of SSID as well. The recognition that PDAC and SSID would mutually benefit each other led to combining the codes into the code called SSID/PDAC.

A top level functional diagram of SSID/PDAC is shown in Figure 3. This figure shows three types of information being input to the code: an analytical model, model

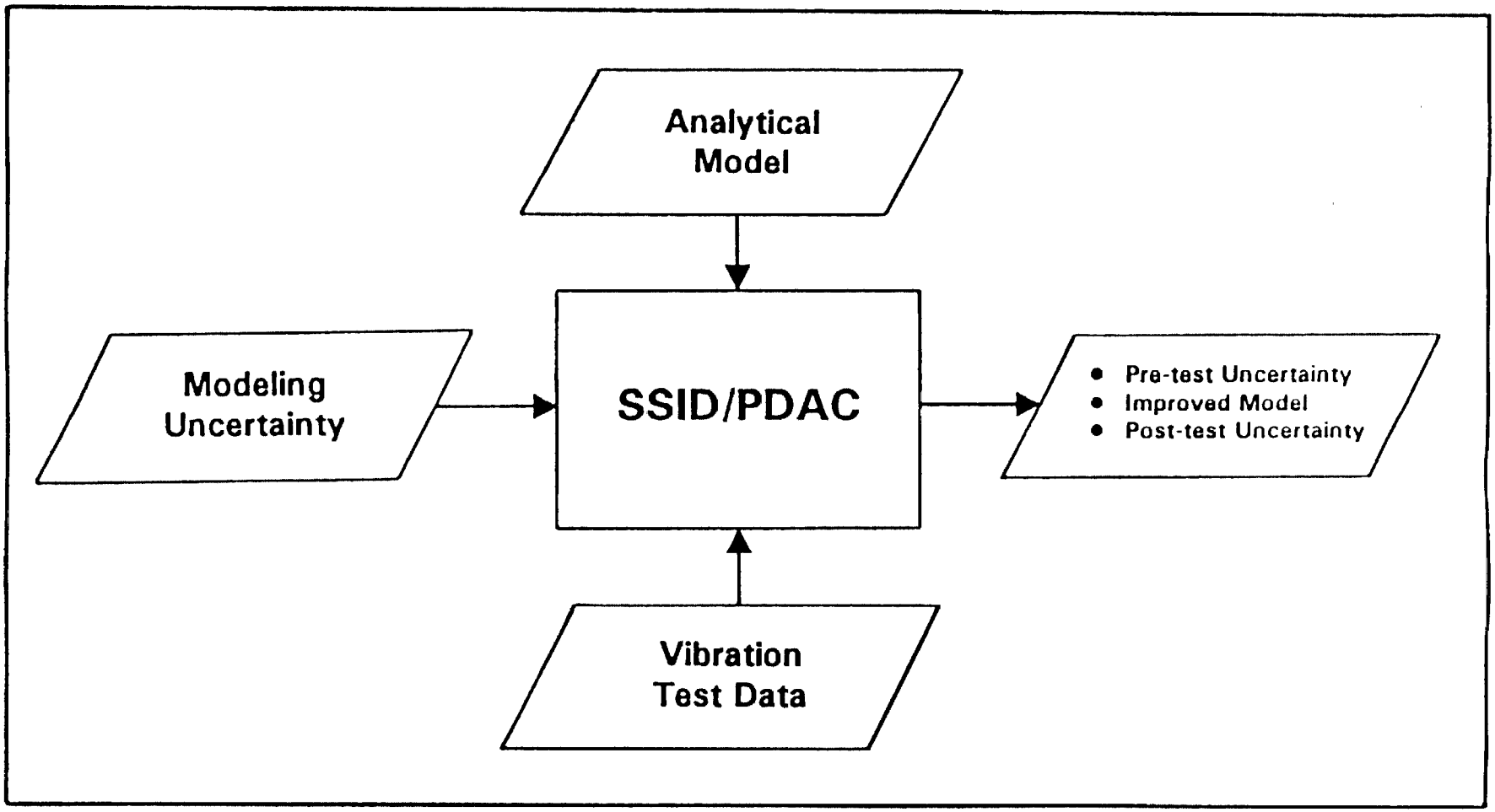

Figure 3. Top Level Functional Diagram of SSID/PDAC.

uncertainty, and vibration test data. The inputs are shown separately because they are read as separate data files. Three types of output are provided. They include pretest response, either with or without pretest uncertainty, a revised model with revised parameter uncertainty, or posttest response, either with or without posttest uncertainty.

Figure 4 shows a top level flow diagram for SSID/PDAC. SSID is designed to operate in conjunction with a finite element modeling code such as NASTRAN. It can function in a stand–alone mode, however, once the necessary modeling data are received from the FEM code. The PDAC option of SSID/PDAC does not require detailed modeling data from a FEM code because it works directly with modal parameters rather than physical parameters. The only modeling data required by PDAC are a list of modal frequencies, corresponding modal displacements (at selected coordinates only), and a list of (diagonal) modal damping constants with corresponding uncertainty estimates. Mass and stiffness uncertainty data are stored internally and are not required as user input. This makes PDAC very simple to run. Frequency response printer–plots are generated by PDAC for either screen viewing or hard copy.

Databases

The method described above for processing eigenvalue and eigenvector differences to obtain covariance matrices of modal mass and stiffness elements was applied to generate three independent databases and one combined database stored as data files within PDAC. The three independent databases are Research Models of Large (truss–type) Space Structures, and both Pretest and Posttest Models of Conventional (Satellite–type) Space Structures in their launch configuration.

The data acquired for these databases is listed in Tables 1 and 2. The identity and sources of the CSS data are not revealed to protect the proprietary interests of contributing organizations. Both tables, however, indicate the number of paired analysis and test modes available for each situation and the frequency range spanned by those modes. Data for a total of 22 structure–model combinations were obtained from seven different organizations, both government and commercial. These data are divided into 7 data sets for LSS Research Models, 7 data sets for CSS Pretest Models and 8 data sets for CSS Posttest Models.

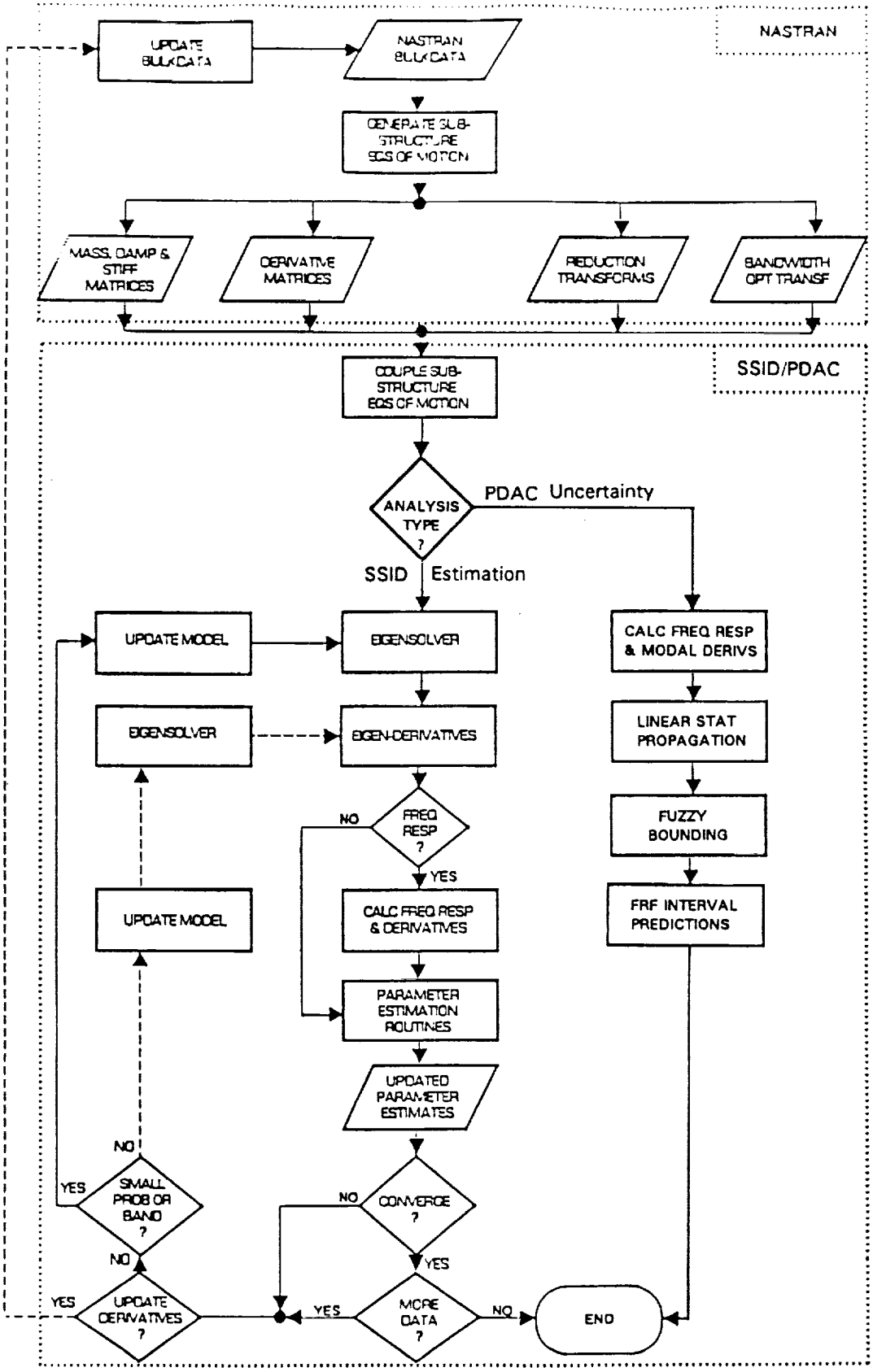

Figure 4. Flow Diagram Illustrating Operations Performed Within NASTRAN and SSID/PDAC.

Table 1. Structures in LSS Database.

Structure Frequency No.	Description	Source	Modes	No. Range (Hz)
LSS 1	LaRC Minimast 3-Longeron Deployable Truss Beam	NASA Langley Research Center	5	0.85 - 6.11
LSS 2	LaRC Ten Bay 4-Longeron Cantilevered Erectable Truss Beam	NASA Langley Research Center	9	18.05 - 200.20
LSS 3	JPL 4-Longeron Cantilevered Precision Truss Structure	Jet Propulsion Laboratory	4	8.31 - 35.53
LSS 4	JPL 3-Longeron Cantilevered Tetrahedral Bay Truss Beam	Jet Propulsion Laboratory	5	10.61 - 71.83
LSS 5	JPL 3-Longeron Free-Free Tetrahedral Bay Truss Beam	Jet Propulsion Laboratory	6	17.94 - 69.17
LSS 6	PACOSS Free-Free Dynamic Test Article (DTA)	Martin Marietta Corporation	22	1.03 - 9.26
LSS 7	PACOSS Cantilevered Solar Array (Substructure of DTA)	Martin Marietta Corporation	9	0.93 - 16.6

Table 2. Structures in CSS Database.

Structure No.	No. Modes Pretest Model	Frequency Range (Hz)	No. Modes Posttest Model	Frequency Range(Hz)
CSS 1	9	13.71 - 23.58	N/A	
CSS 2	5	16.27 - 52.70	5	16.27 - 52.70
CSS 3	6	14.49 - 49.97	6	14.49 - 49.97
CSS 4	6	14.45 - 50.29	N/A	
CSS 5	9	29.38 - 95.99	9	29.38 - 95.99
CSS 6	5	15.11 - 27.35	N/A	
CSS 7	N/A		34	7.04 - 46.50
CSS 8	N/A		4	41.64 - 93.77
CSS 9	N/A		14	5.84 - 24.51
CSS 10	N/A		12	12.50 - 35.67
CSS 11	16	16.15 - 46.60	27	16.15 - 50.76

Demonstration of Methodology

The three types of uncertainty propagation described above were first demonstrated for the simple 2–DOF model shown in Figure 5. In addition to a schematic drawing of the model the figure shows the SSID/PDAC model input data and nominal FRF amplitude and phase plots.

Figure 6 shows ± 1σ interval plots of FRF amplitude and phase generated by PDAC using linear covariance propagation and the CSS Posttest database, for the 2–DOF model. These plots show how the uncertainty intervals tend to "blow up" near resonance. The intervals are truncated for plotting purposes when they exceed two decades on either side of the nominal response. When this truncation occurs, the intervals are delimited by arrows to indicate that the computed intervals are actually greater than those shown.

Figure 7 shows ± 1σ interval plots bounded by the Vertex Method. These plots were generated by computing possibility intervals within ± 10% of the resonant frequency, and then taking the smaller of the one–sigma interval obtained by linear covariance propagation, and the one–sigma possibility bounds obtained by the Vertex Method. At frequencies within the half power point frequency band, the possibility bounds override the linear covariance propagation because partial derivatives of amplitude with respect to modal mass and stiffness go to zero at resonance.

Figure 8 shows amplitude and phase distributions at the selected frequencies shown in Figure 7. These distributions extend beyond the ± 1σ intervals shown in Figure 7 because the parameter ranges are not bounded in this case.

The ultimate objective of this project was to demonstrate the methodology for real structures. Three structures were selected for this purpose: the NASA Mini–mast Structure, the NASA Ten Bay Truss, and the NASA CSI Evolutionary Structure. Results for the latter best exemplify application of the methodology because this structure has the highest modal density and was not included in the LSS database. Figure 1a shows the structural configuration with sensor and actuator locations identified. Figures 9 and 10 show measured FRF acceleration amplitude and phase plots (solid lines) for Coordinates 1 and 6 due to force applied at Coordinate 1. Figures 11 and 12 show the PDAC ± 1σ interval plots for the same locations. Measured FRF amplitude from Figures 9 and 10 are

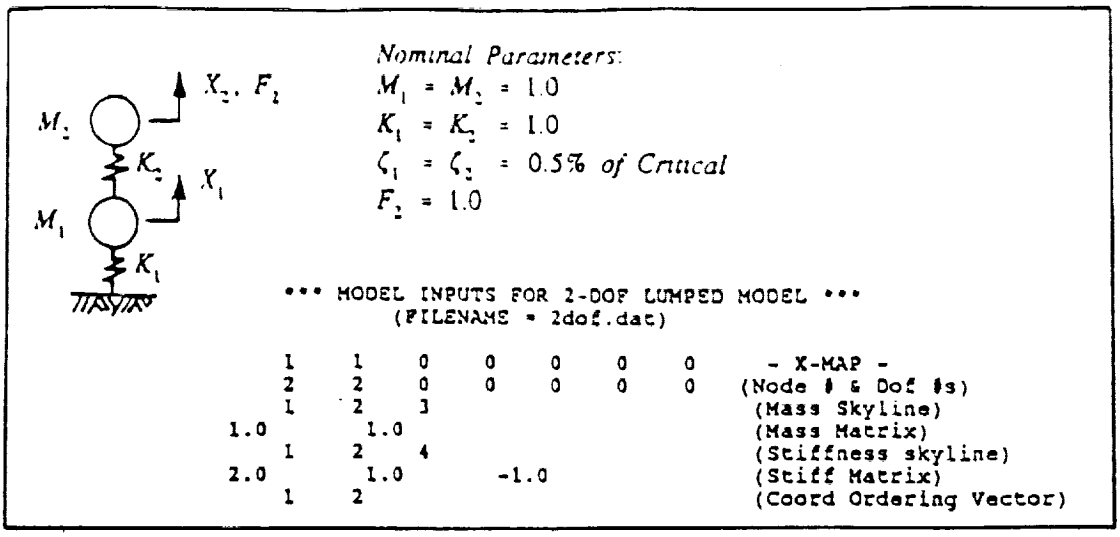

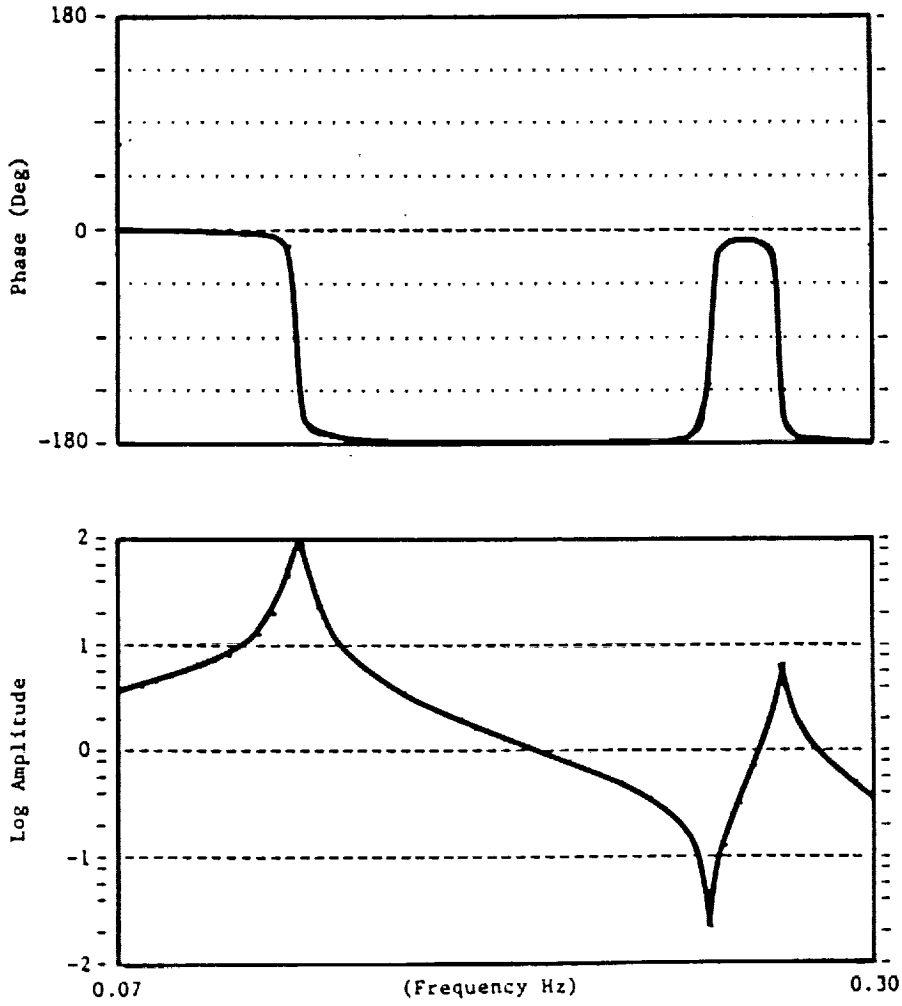

Figure 5. Two-DOF Model.

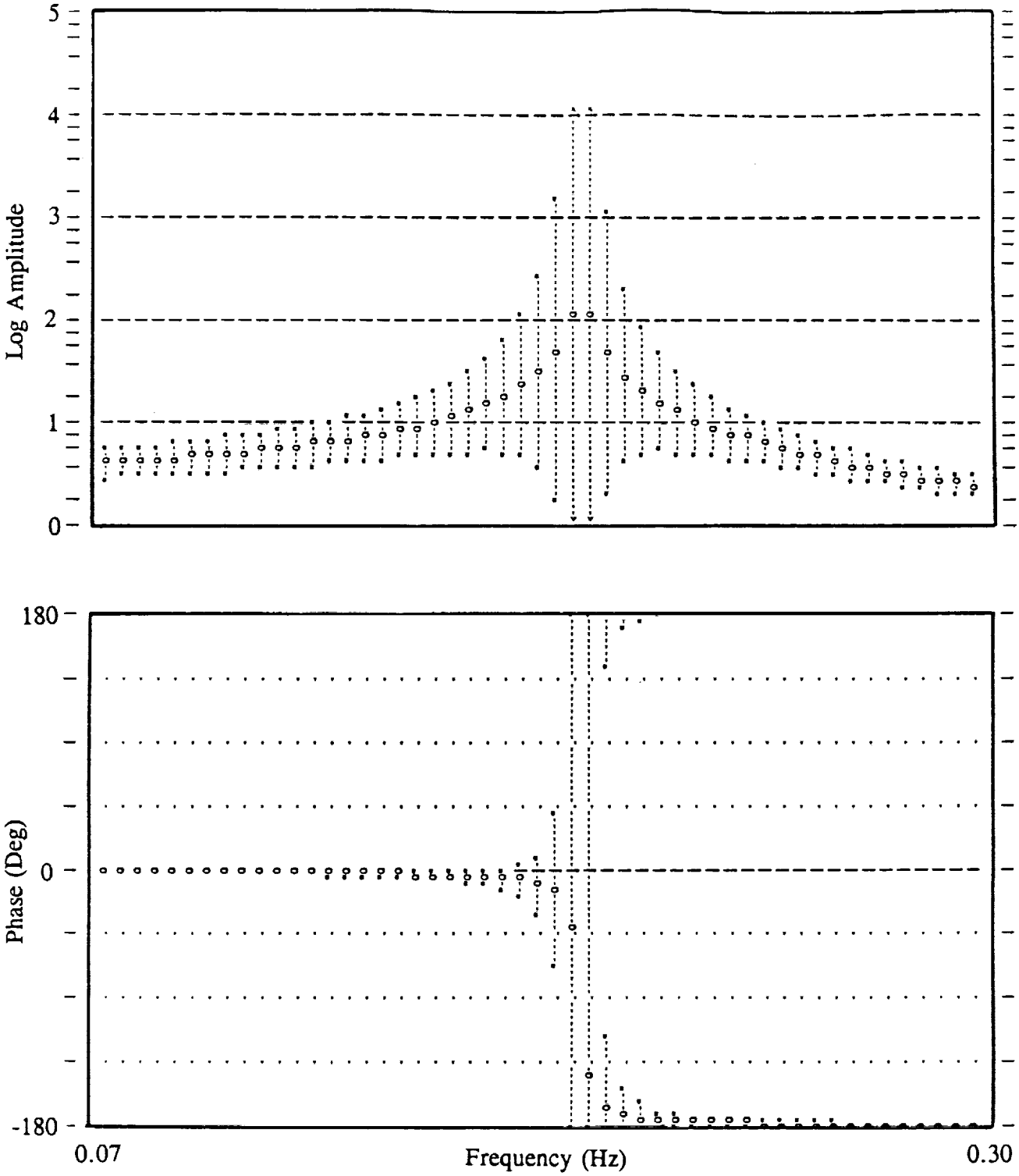

Figure 6. One-sigma Uncertainty Intervals on FRF for 2-DOF Model Using Linear Covariance Propagation.

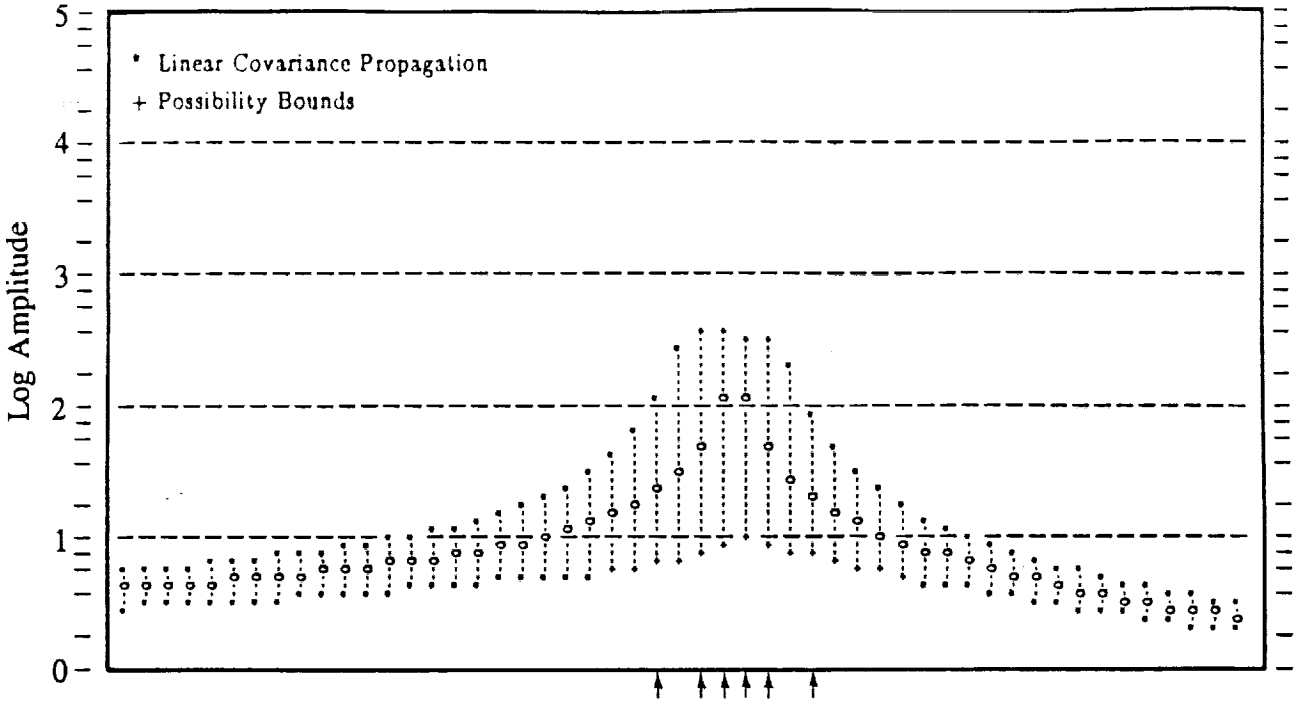

Frequencies for which distributions are shown in Figure 8.

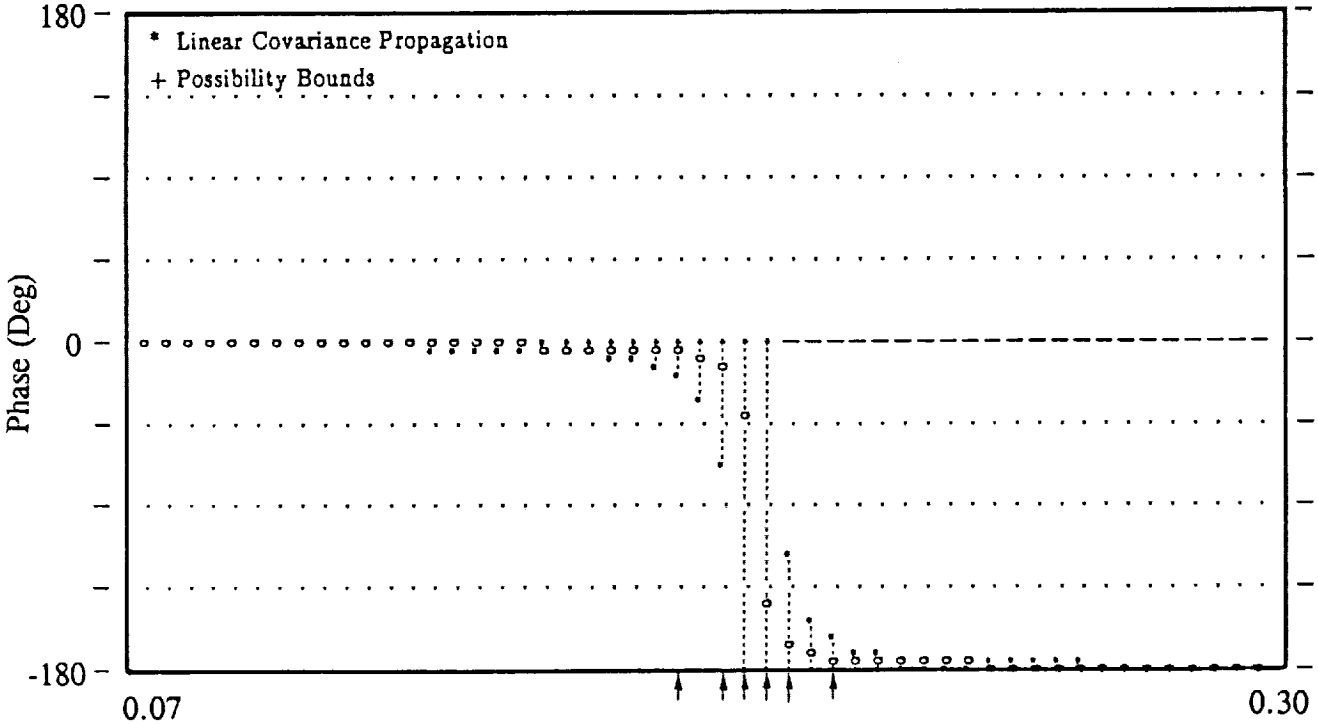

Frequencies for which distributions are shown in Figure 8.

Figure 7. One-sigma Uncertainty Intervals on FRF for 2-DOF Model Using Linear Covariance Propagation Limited by Possibility Bounds.

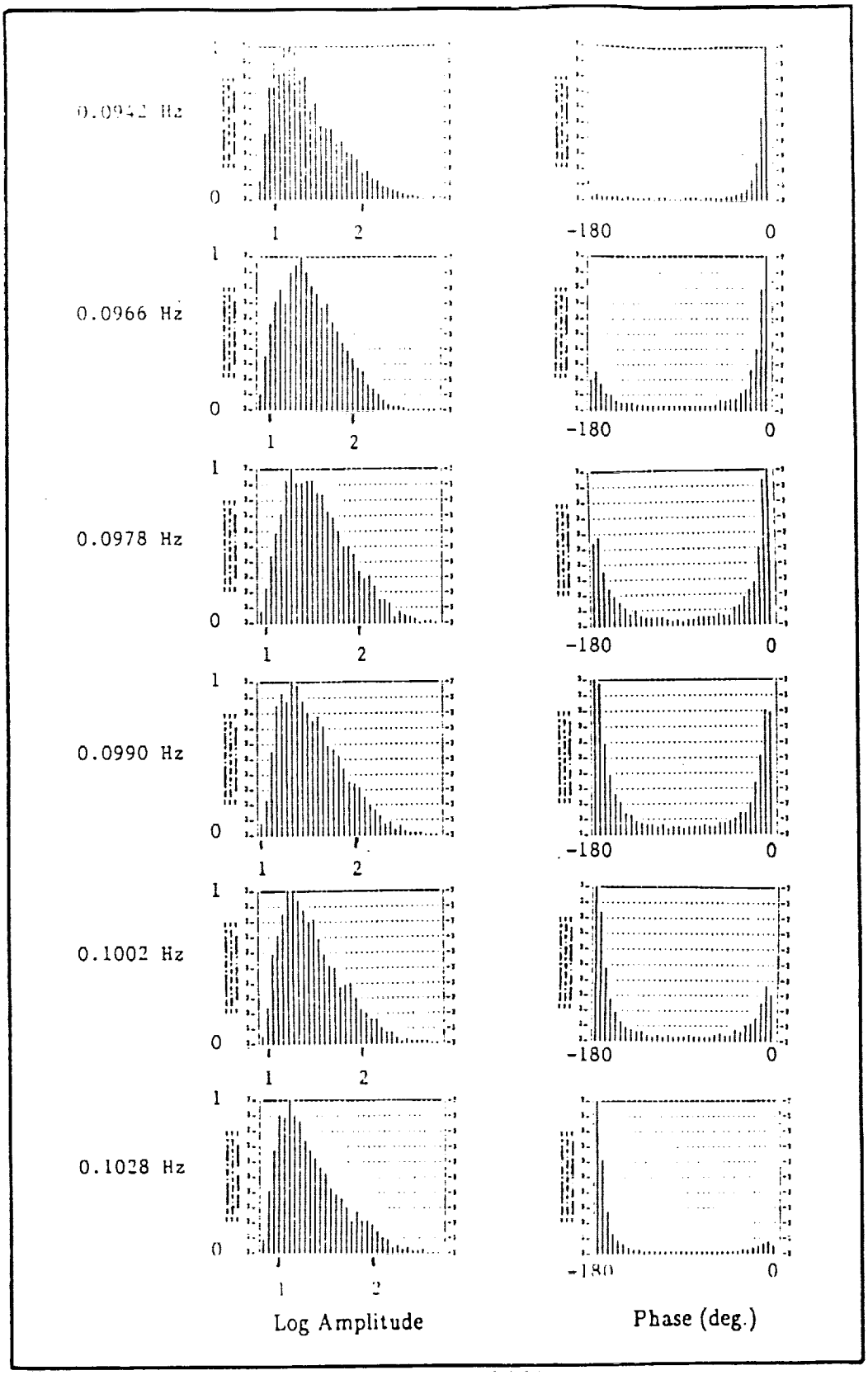

Figure 8. FRF Amplitude and Phase Distributions for 2-DOF Example.

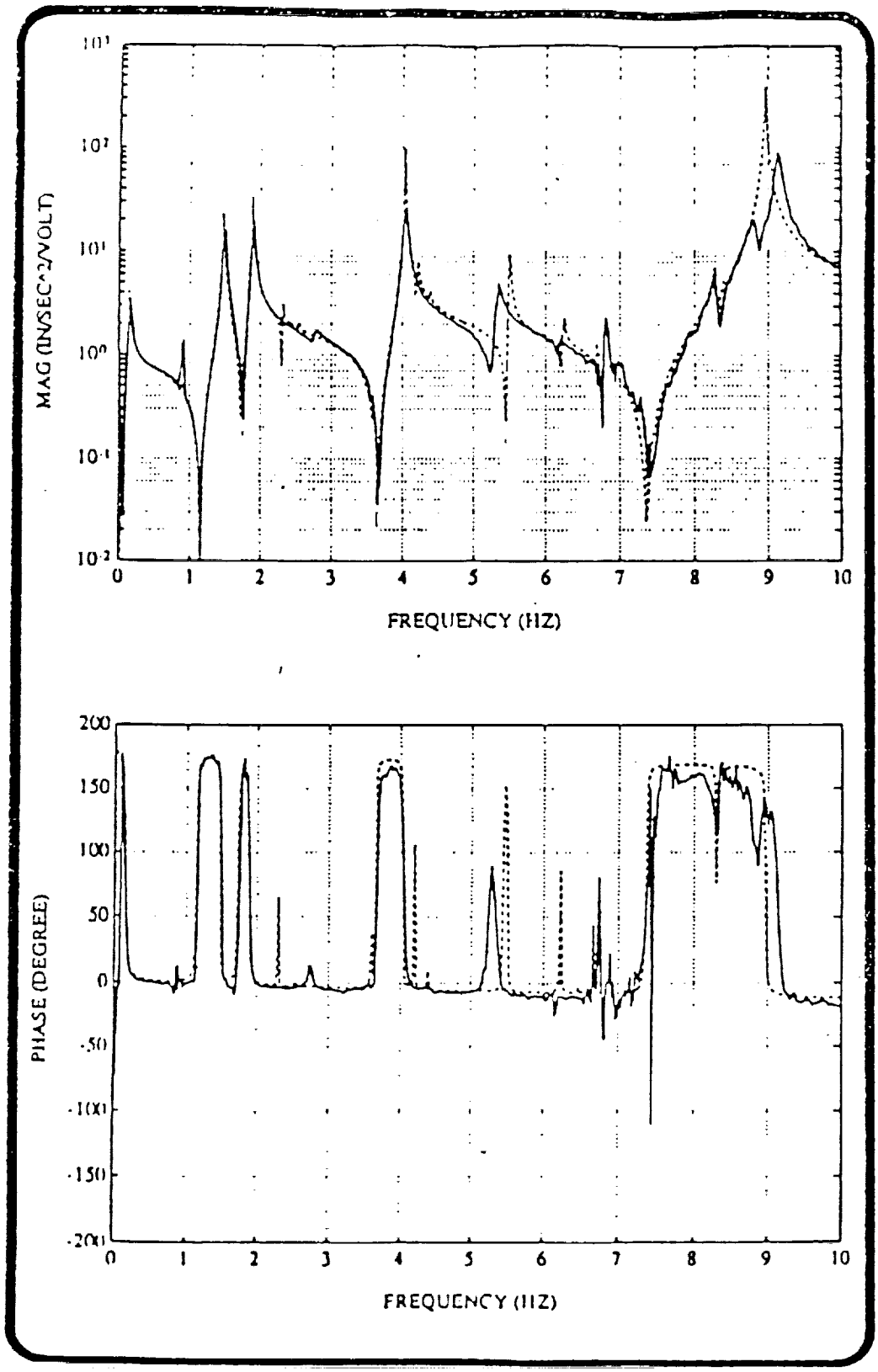

Figure 9. CSI FRF Comparison (Response at Thruster 1/Force at Thruster 1).

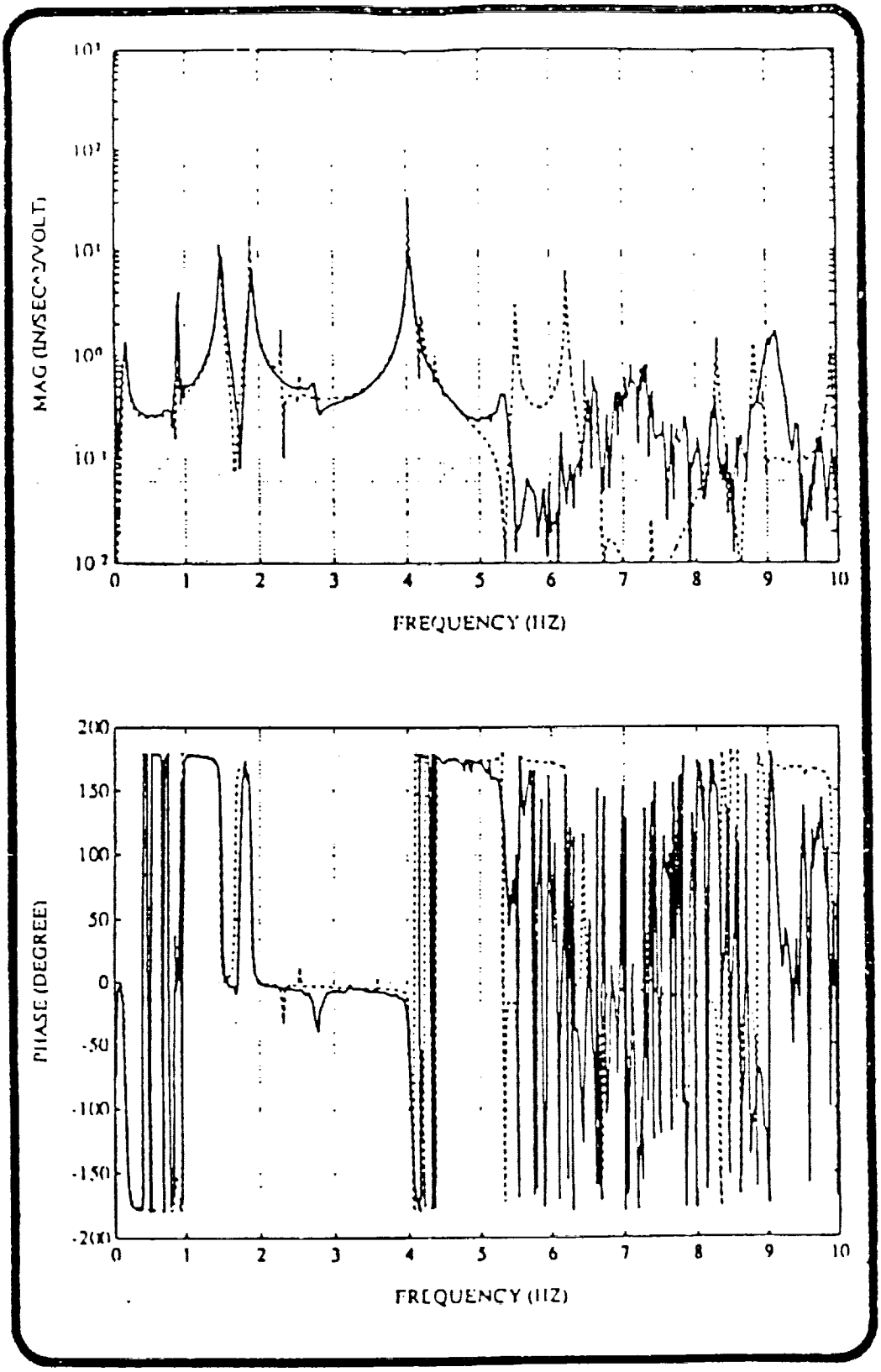

Figure 10. CSI FRF Comparison (Response at Thruster 6/Force at Thruster 1).

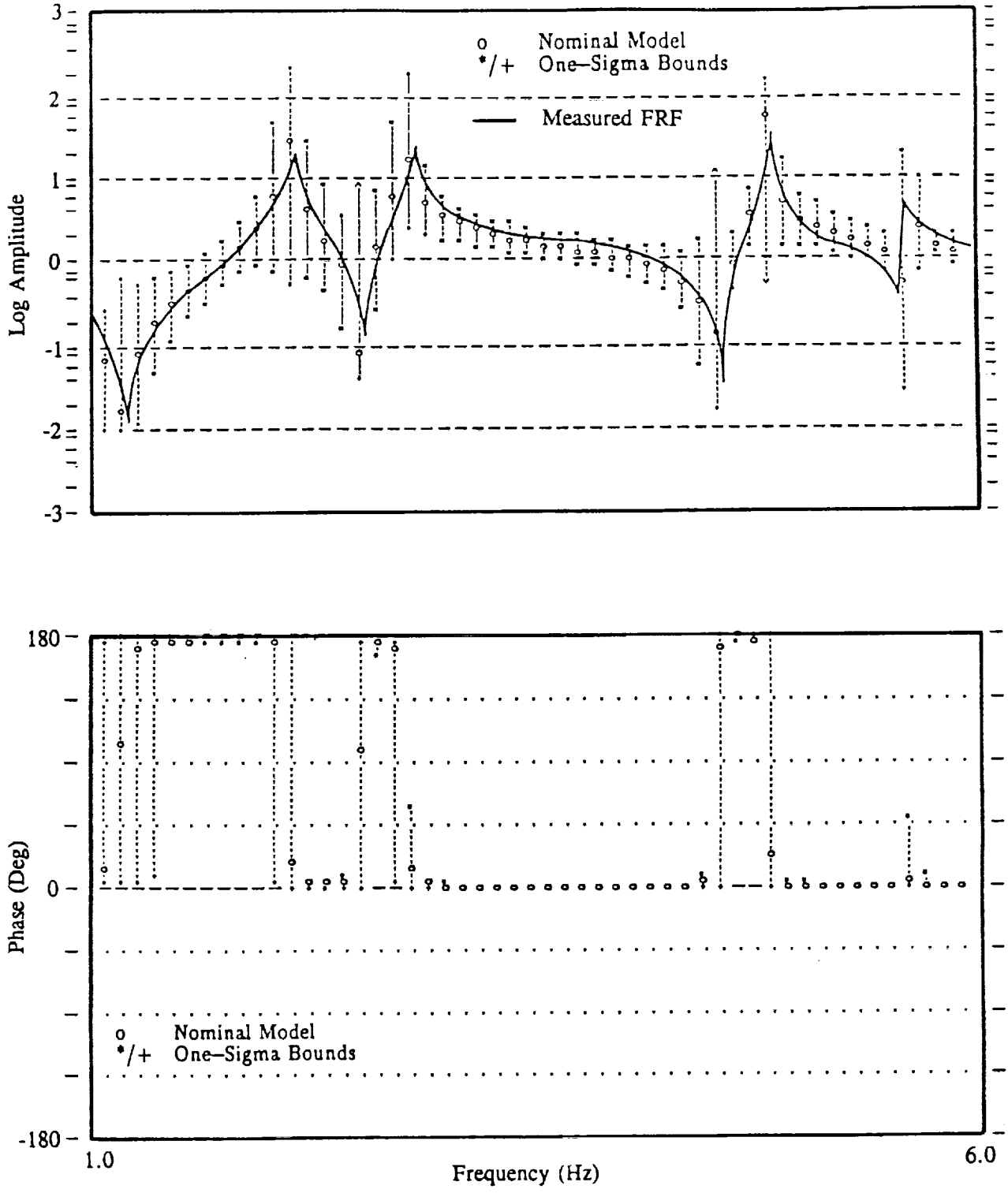

Figure 11. Predictive Accuracy of CSI Evolutionary Structure Model, Coordinate 1 Acceleration/Coordinate 1 Force FRF.

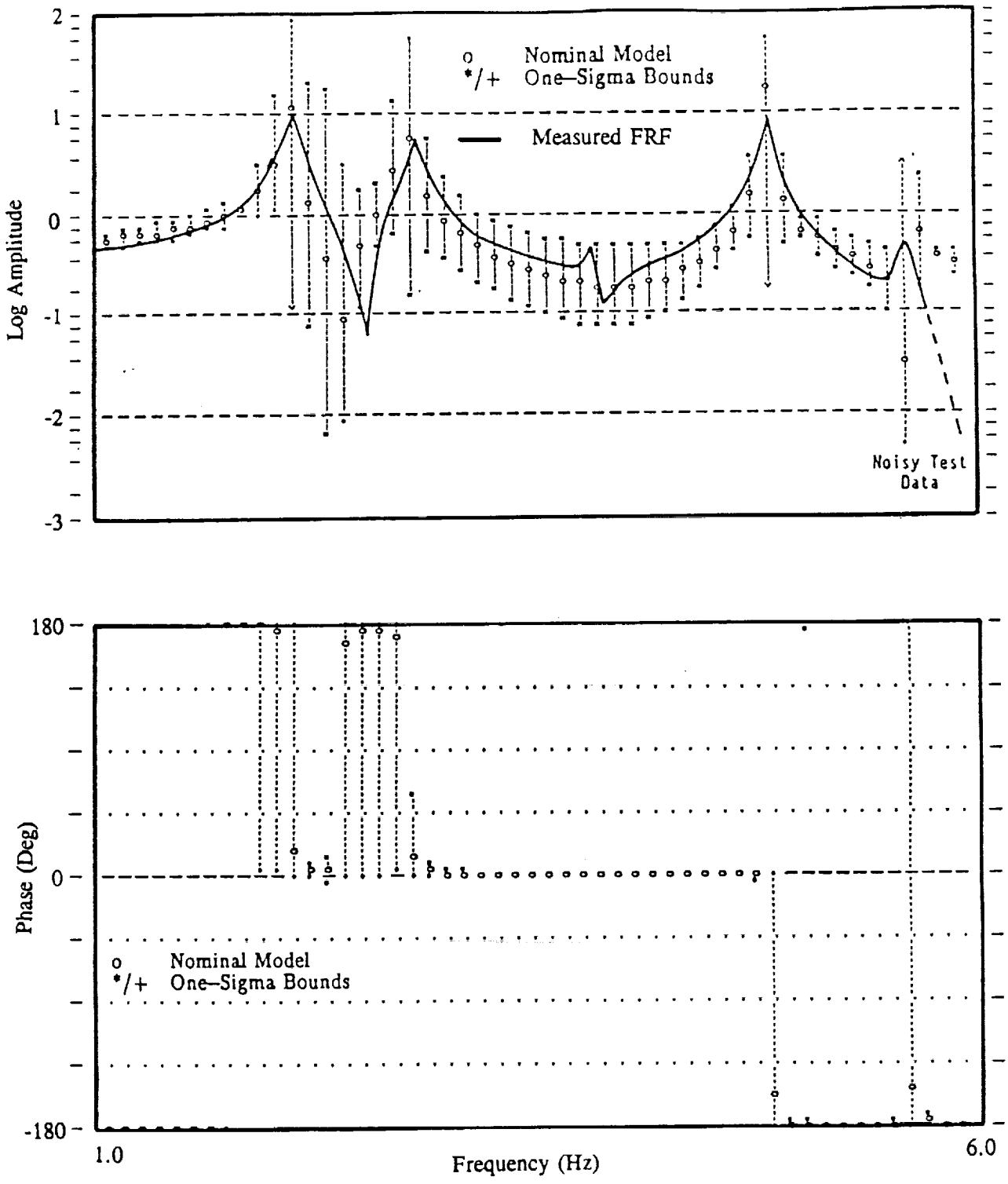

Figure 12. Predictive Accuracy of CSI Evolutionary Structure Model, Coordinate 3 Acceleration/Coordinate 1 Force FRF.

replotted on these figures for direct comparison. Measured phase plots did not contain sufficient resolution to replot and therefore are not shown. These comparisons show that response uncertainty predictions made by PDAC are realistic. Measured FRF amplitude tends to fall within the $\pm 1\sigma$ uncertainty intervals.

Practical Applications – Phase III

Engineering Mechanics Associates is currently working with an SBIR Program Consultant to develop a market for this technology. A secondary market survey of computerized databases is presently being conducted in an attempt to determine whether there are any similar tools on the market, and to identify potential market segments. Following the secondary market survey, a primary market survey will be conducted. The primary market survey will include direct interviews with key persons in the technical community, and may also include workshops where key individuals are brought together to focus on specific applications. Following the market surveys, a business plan will be prepared.

One potential Phase III opportunity has already been identified. EMA has been contacted by a major aerospace company which has received an Air Force contract to build a large number of satellites. The company is contractually obligated to develop a structural dynamic model which matches test frequencies to within ± 3% up to 50 Hz, and matches test mode shapes such that the diagonal terms of the cross–orthogonality matrix are at least 0.95 while the off–diagonal terms are no greater than 0.10. None of the eight models in the CSS Posttest database satisfy these criteria. A preliminary statement of work has already been received which will require the use of both SSID and PDAC. Negotiations are expected to lead to a Phase III contract.

This application is typical of potential applications in the aerospace industry, where structural dynamic models are required to perform launch loads analysis. The accuracy criteria presently being written into contracts are very stringent. The combination of a model verification tool like SSID with a predictive accuracy tool like PDAC may provide the means to satisfy these criteria. So far, to the best of the authors' knowledge, these criteria have not been met.

Other potential applications in the aerospace industry relate to large space structures such as Space Station Freedom. Although requirements for precision control are not as great on this structure as they are on large antennas, for example, there is strong interest in determining the accuracy of the structural dynamic model as evidenced by programs such as NASA LaRC's Dynamic Scale Model Technology (DSMT) Program and plans for conducting on–orbit identification.

Structures which do require precision control must be modeled very accurately to achieve desired levels of control system performance. This realization has been one of the driving factors behind the development of the present technology. What is not yet clear is how best to present modeling uncertainty for purposes of robust control design. This is an area where a workshop might be beneficial.

A different type of problem has been encountered in the commercial sector. It seems that finite element models of large offshore platforms consistently over predict the fundamental frequency. Attempts to use system identification methods to identify the source of this problem have so far been unsuccessful. This is a case where there appears to be an inherent bias–type error, or systematic error in current modeling techniques. Part of the reason for not being able to identify the source of error could be that random error combined with the systematic error may be confusing the estimator. This problem could conceivably be solved by averaging the errors (differences between prediction and measurement) over a number of structures so as to suppress the random type error. Then system identification to identify the source of the remaining bias–type error might be more successful.

In summary, applications for this new technology are being sought in civil and commercial areas as well as the aerospace industry. Application to aerospace structures is likely to occur sooner because the necessary databases already exist. These databases will be enlarged as more data become available.

1. INTRODUCTION

1.1 Background

Structural dynamic models are used in a wide variety of applications including design verification, test support, flight load prediction, and in–flight control. These models offer what may be called "point prediction" in the sense that the models, which are themselves deterministic, yield deterministic response when acted upon by deterministic inputs. Occasionally, stochastic inputs are applied to yield stochastic response. In this case, response may be expressed in terms of response intervals, such as the mean plus or minus one standard deviation. Rarely is the model itself considered to be stochastic, e.g. Reference [1–1]. In practical applications, model uncertainty is accounted for either by perturbing selected model parameters, or by adjusting input levels in an attempt to offset model uncertainty. Heretofore, there have been no general tools for realistically quantifying the effects of model uncertainty on response predictions.

The problem lies in acquiring and processing the data necessary to quantify model uncertainty. Attempts have been made to express model uncertainty in terms of design parameters at the finite element level, such as material properties and local geometry, e.g. Reference [1–2]. However, it is not practically feasible to gather sufficient data at this level because of the diversity of materials, shapes, sizes and methods of fabrication. Other attempts have been made to gather data at the modal level. These data, however, have been limited to modal frequencies and damping. Mode shape data have not been used, possibly because a means for homogenizing the data has not been apparent.

This report documents the methodology and database which have been developed under contract to obtain interval predictions of structural dynamic response resulting from model uncertainty. A database representing mass and stiffness uncertainty was derived from observed differences between analytically predicted and experimentally measured natural frequencies and mode shapes. Estimates of damping uncertainty have been derived from the statistics of damping measurements on truss beams. These data, however, are presently too limited to form a generic database. Alternative means are therefore provided to account for the effects of estimated damping uncertainty, until more data become available.

1.2 Project Objectives

The goal of this SBIR project has been to develop a practical tool for evaluating the predictive accuracy of structural dynamic models. Phases I and II have focused on initial application to space structures for two reasons: NASA has identified the need to quantify the accuracy of models used to simulate the performance of flight hardware, and sufficient analysis and testing have been performed on space structures to establish a meaningful database. Phase III will seek uses for the tools developed under this contract in practical aerospace applications, and attempt to extend their application to civil and commercial structures such as high–rise buildings and offshore platforms.

The objectives of Phase II were to develop a methodology, implement it in a suitable computer code complete with the necessary database, and finally to demonstrate the methodology by applying the code to real structures. Specific objectives are outlined as follows:

1. Develop a methodology for:
   - Realistically quantifying mass and stiffness uncertainty,
   - Estimating damping and damping uncertainty, and
   - Propagating these uncertainties through a model to evaluate predictive accuracy.

2. Implement the methodology in:
   - A general purpose computer code, and
   - A database to be accessed by the computer code.

3. Demonstrate the methodology for:
   - Simple examples, and
   - Real structures

Application of the methodology to space structures has provided a contextual framework for the project. Space structures are thoroughly analyzed and tested prior to flight. The need for the quantification of predictive accuracy therefore relates to posttest models which have been tuned and verified in accordance with test data. Linking the predictive accuracy code to a model verification code was found to benefit both codes. The predictive accuracy

code PDAC (for PreDictive ACcuracy) has been linked to the model verification code SSID (for Structural System IDentification). PDAC uses many of the computational modules found in SSID, while SSID benefits from PDAC's interval prediction capabilities. The following section defines the scope of this SBIR project.

1.3 Scope of Research Effort

The research documented in this report covers the objectives listed above. The methodology for modeling mass and stiffness uncertainty is presented in Chapter 2. Chapter 2 is supplemented by Appendix A which documents three generic mass and stiffness uncertainty databases. The methodology for estimating full modal damping matrices from complex mode data is presented and discussed in Chapter 3. The approach taken here is that damping is estimated on the basis of structure–specific tests, rather than being modeled. Damping uncertainty is therefore derived from repeated estimates involving the same structure, rather than the difference between model predictions and experimental measurements on different structures. The propagation of mass, stiffness and damping uncertainty through a structural model is discussed in Chapter 4, where three different methods for propagating damping uncertainty are presented.

The predictive accuracy computer code, PDAC, and its integration with the model verification code, SSID, are summarized in Chapter 5. Details of code implementation are documented in three separate manuals:

- Theoretical Manual;
- User's Manual; and
- Demonstration Manual.

The Theoretical Manual is a modified version of the SSID Theoretical Manual which documents the mathematical basis of SSID. The mathematical basis of PDAC is included as an appendix of that manual. The User's Manual extends the previous SSID User's Manual by adding the new PDAC input requirements. The Demonstration Manual is presented in two volumes; the first volume presents SSID demonstration problems while the second volume presents PDAC–type demonstration problems.

Primary demonstration of the methodology is contained in Chapter 6, where application to three real structures is presented. The damping estimation methodology presented in Chapter 3 is not utilized in the demonstration problems of Chapter 6, however. Instead, the demonstration problems assume diagonal modal damping with one–sigma multiplicative uncertainty factors. The methodology of Chapter 3 is demonstrated with real data and application to real structures in Chapter 3.

In addition to the demonstration problems of Chapter 6, simple numerical examples selected to illustrate various aspects of the methodology are scattered throughout the text. These examples are included to facilitate a better understanding of the concepts involved.

Some avenues of research pursued as part of this investigation are not documented because they did not produce fruitful results, or because other methods proved to be superior. Lessons learned from these research efforts are briefly summarized in Chapter 7.

2. MASS AND STIFFNESS UNCERTAINTY

2.1 Methodology

Mass and stiffness uncertainty can be expressed in terms of the difference between analytically predicted and experimentally measured eigenvalues and eigenvectors. As in many engineering problems, the mathematical formulation is often the key to obtaining a useful solution. In this case, it will be seen that expressing the mass and stiffness uncertainty of a model in terms of modal mass and stiffness matrices offers a number of advantages including the following:

- The parameters which contain the mass and stiffness uncertainty information can be non–dimensionalized so that statistics from different structures may be combined. This allows statistical databases to be compiled for generically similar structures. The normalized statistics can then be rescaled to match the mass and stiffness properties of other structures belonging to that generic category.

- Having rescaled the normalized modal mass and stiffness uncertainties for a particular structure, they can be propagated forward through the analysis chain to determine eigenvalue, eigenvector and response uncertainties, either in the frequency domain or the time domain.

- The modal mass and stiffness uncertainties can also be propagated backward through the analysis chain subject to certain conditions, to evaluate uncertainties in the basic design variables of the structure.

The development of this methodology is based on perturbation analysis which assumes that variations between analysis and test results are "small." The term "small" is used subjectively in the application of this methodology, even though the perturbation analysis is based on the mathematical definition of small as being of higher order. Here, the coefficients of variation on modal mass and stiffness matrix elements turn out to be in the range of approximately 10% to 30%, with a few higher and a few lower, as will be shown. This is indicative of the accuracy of the present analysis which is based on comparisons of analysis and test results for 22 different data sets contributed by seven different organizations, including both government and industry.

The remainder of this section will establish the mathematical basis for that portion of the methodology concerning mass and stiffness uncertainty.

2.1.1 Linear Perturbation Analysis

Since mass and stiffness uncertainty is considered to be independent of damping and forcing function, only the undamped homogeneous equations of motion need to be considered at this point. They are written as

$$M\ddot{x} + Kx = 0 \tag{2–1}$$

where x is a vector of displacements in the physical coordinate system, and M and K are respectively the "true" (but unknown) mass and stiffness matrices corresponding to x; the mass and stiffness matrices of the analytical model will be denoted by ${}^{o}M$ and ${}^{o}K$, respectively. The undamped eigenproblem may be stated as

$$(K - \lambda_j M)\phi_j = 0 \tag{2–2}$$

where λ_j and ϕ_j are the jth eigenvalue and eigenvector, respectively, of the "true" system.

The parameters and modal characteristics of the analytical model are related to those of the "true" model as follows:

$$K = {}^{o}K + \Delta K \tag{2–3a}$$

$$M = {}^{o}M + \Delta M \tag{2–3b}$$

$$\lambda_j = {}^{o}\lambda_j + \Delta\lambda \tag{2–3c}$$

$$\phi_j = {}^{o}\phi_j + \Delta\phi_j \tag{2–3d}$$

Substitution of these equations into (2–2) gives

$$({}^{o}K - {}^{o}\lambda_j\,{}^{o}M)\Delta\phi_j + (\Delta K - {}^{o}\lambda_j\Delta M - \Delta\lambda_j\,{}^{o}M){}^{o}\phi_j = 0 \tag{2–4}$$

upon neglecting second and third order terms.

Premultiplication of (2–4) by ${}^{o}\phi_j^T$ results in the following for $\Delta\lambda_j$ since ${}^{o}K$ and ${}^{o}M$ are symmetric, assuming that the modes, ${}^{o}\phi_j$, are normalized to unit modal mass.

$$\Delta\lambda_j = {}^{o}\phi_j^T (\Delta K - {}^{o}\lambda_j \Delta M) {}^{o}\phi_j \tag{2–5}$$

Premultiplication of (2–4) by ${}^{o}\phi_i^T$ gives

$${}^{o}\phi_i^T[({}^{o}K - {}^{o}\lambda_j\, {}^{o}M)\Delta\phi_j + (\Delta K - {}^{o}\lambda_j \Delta M - \Delta\lambda_j {}^{o}M) {}^{o}\phi_j] = 0 \tag{2–6}$$

If $\Delta\phi_j$ can be written as a linear combination of the original eigenvectors, then

$$\Delta\phi_j = {}^{o}\phi \Delta\psi_j \tag{2–7}$$

Substitution of (2–7) into (2–6) gives

$$({}^{o}\lambda_j - {}^{o}\lambda_i)\Delta\psi_{ij} = {}^{o}\phi_i^T (\Delta K - {}^{o}\lambda_j \Delta M) {}^{o}\phi_j \tag{2–8}$$

since ${}^{o}\phi_i$ and ${}^{o}\phi_j$ are orthogonal with respect to ${}^{o}M$. It is convenient to define the following terms and notation:

$m = {}^{o}\phi^T M {}^{o}\phi$ = "true" modal mass matrix in ${}^{o}\phi$ coordinates

$k = {}^{o}\phi^T K {}^{o}\phi$ = "true" modal stiffness matrix in ${}^{o}\phi$ coordinates

${}^{o}m = {}^{o}\phi^T {}^{o}M {}^{o}\phi = I$ (identity matrix)

${}^{o}k = {}^{o}\phi^T {}^{o}K {}^{o}\phi = {}^{o}\lambda$ (diagonal matrix of analytical eigenvalues)

$\Delta m = {}^{o}\phi^T \Delta M {}^{o}\phi = m - I$

$\Delta k = {}^{o}\phi^T \Delta K {}^{o}\phi = k - {}^{o}\lambda$

With these substitutions, (2–8) becomes

$$({}^{o}\lambda_j - {}^{o}\lambda_i)\Delta\psi_{ij} = \Delta k_{ij} - {}^{o}\lambda_j \Delta m_{ij} \tag{2–9a}$$

$$({}^{o}\lambda_i - {}^{o}\lambda_j)\Delta\psi_{ji} = \Delta k_{ij} - {}^{o}\lambda_i \Delta m_{ij} \tag{2–9b}$$

since Δm and Δk are symmetric. Taking the difference of these two equations gives

$$\Delta m_{ij} = -(\Delta\psi_{ij} + \Delta\psi_{ji}) \tag{2–10}$$

for $i \neq j$. Adding the equations and using (2–10) for $i \neq j$ gives

$$\Delta k_{ij} = -({}^{o}\lambda_i \Delta\psi_{ij} + {}^{o}\lambda_j \Delta\psi_{ji}) \tag{2–11}$$

It remains only to determine the diagonal terms of Δm and Δk. The term Δm_{jj} is obtained from the normalization condition on ϕ_j which is

$$\phi_j^T M \phi_j = 1 \tag{2–12}$$

Substitution of (2–3b) and (2–3d) into (2–12) while neglecting second and third order terms gives

$$\Delta m_{jj} = -2\Delta\psi_{jj} \tag{2–13}$$

Substitution of (2–13) into (2–5) gives

$$\Delta k_{jj} = \Delta\lambda_j - 2\,{}^{o}\lambda_j \Delta\psi_{jj} = \Delta\lambda_j + {}^{o}\lambda_j \Delta m_{jj} \tag{2–14}$$

Combining Equations (2–10) and (2–13), and Equations (2–11) and (2–14) gives

$$\Delta m = -(\Delta\psi + \Delta\psi^T) \tag{2–15}$$

$$\Delta k = \Delta\lambda - {}^{o}\lambda\Delta\psi - \Delta\psi^{T\,o}\lambda \tag{2–16}$$

The matrix $\Delta\psi$ is obtained from the cross–orthogonality between the analysis modes, ${}^{o}\phi$, and the test modes, ϕ.

$$ {}^{o}\phi^{T}{}^{o}M\phi = {}^{o}\phi^{T}{}^{o}M{}^{o}\phi\psi = \psi \tag{2–17} $$

where, consistent with Equation (2–7), the test modes, ϕ, are expressed as a linear combination of the analysis modes, ${}^{o}\phi$.

$$ \phi = {}^{o}\phi\psi \tag{2–18} $$

Substitution of (2–7) and (2–18) into (2–3d) gives

$$ \psi = (I + \Delta\psi) \tag{2–19} $$

Finally, substitution of (2–19) into (2–15) and (2–16) gives

$$ \Delta m = (I - \psi) + (I - \psi)^{T} \tag{2–20} $$

$$ \Delta k = \Delta\lambda + {}^{o}\lambda\,(I - \psi) + (I - \psi)^{T}{}^{o}\lambda \tag{2–21} $$

2.1.2 Statistical Analysis

Statistical analysis involves averaging the elements of Δm and Δk over a family of "generically similar" structures and models. Generically similar structures, for example, might include conventional space structures, where a conventional space structure is defined as a stiff bus with flexible appendages stowed in the launch configuration. These structures tend to have a large proportion of nonstructural mass. They may be contrasted with the large truss–type space structures currently being used for research purposes. These structures tend to have relatively little nonstructural mass by comparison. The models of generically similar structures may also be segregated into pretest models which have not had the benefit of experimental verification, and posttest models which have been tuned to match test data as closely as possible. These are rather broad generic categories. They are largely dictated by the availability of data, and serve to provide a means of discerning the importance of data segregation. By partitioning the available data into several groups and comparing the results of using different databases in the evaluation of

predictive accuracy, one may judge whether it is advantageous to segregate the data and obtain higher resolution, or combine the data to achieve a larger sample size with more homogeneous characteristics.

In order to perform a statistical analysis of the Δm and Δk data, Δk must first be normalized to remove frequency dependence. This is accomplished by computing $\Delta \tilde{k}$ defined as

$$\Delta \tilde{k} = {}^{o}\lambda^{-1/2}\, \Delta k\, {}^{o}\lambda^{-1/2} \tag{2–22}$$

Having done this, the matrices Δm and $\Delta \tilde{k}$ are then vectorized such that

$$\text{Vec}\,(\Delta m) = \begin{Bmatrix} \Delta m_{11} \\ \Delta m_{12} \\ \vdots \\ \Delta m_{22} \\ \Delta m_{23} \\ \vdots \\ \Delta m_{nn} \end{Bmatrix} \tag{2–23a}$$

$$\text{Vec}\,(\Delta \tilde{k}) = \begin{Bmatrix} \Delta \tilde{k}_{11} \\ \Delta \tilde{k}_{12} \\ \vdots \\ \Delta \tilde{k}_{22} \\ \Delta \tilde{k}_{23} \\ \vdots \\ \Delta \tilde{k}_{nn} \end{Bmatrix} \tag{2–23b}$$

Then the modal parameter vector, $\Delta \tilde{r}$, is formed by combining Vec (Δm) and Vec $(\Delta \tilde{k})$ as follows:

$$\Delta \tilde{r} = \begin{Bmatrix} \text{Vec}\,(\Delta m) \\ \text{Vec}\,(\Delta \tilde{k}) \end{Bmatrix} \tag{2–24}$$

The covariance matrix of the normalized modal mass and stiffness matrix elements, m_{ij} and $\tilde{k}_{ij}$, may be defined as

$$S_{\tilde{r}\tilde{r}} = E\left[\Delta\tilde{r}\ \Delta\tilde{r}^T\right] = \frac{1}{N}\sum_{k=1}^{N}\left[\Delta\tilde{r}\ \Delta\tilde{r}^T\right]_k \qquad (2\text{–}25)$$

where E denotes the expectation operator and $\Delta\tilde{r}$ is understood to represent the difference between analysis (i.e. the nominal model) and test (assumed to represent the "truth" based on experimental observation). In reality, the actual truth may not be known; however, it is reasonable to define predictive accuracy in terms of the difference between predicted and observed behavior, even if the observations are not perfect.

2.2 Databases

The data required to generate covariance matrices of the modal mass and stiffness matrix elements consist of the following:

1. A set of test frequencies and mode shapes normalized to unit modal mass,

2. A corresponding set of analysis frequencies and mode shapes normalized to unit modal mass, and

3. The analytical mass matrix used to normalize the analysis and test modes.

The analytical model must be reduced to the test degrees of freedom (sometimes referred to as a "Test Analysis Model" or "TAM"); alternatively, the test modes may be expanded to match the original analytical model for purposes of computing the cross orthogonality matrix (Equation (2–17)). If the cross–orthogonality matrix is available, then it and the analysis and test frequencies are all that are needed to compute the covariance matrix, $S_{\tilde{r}\tilde{r}}$.

It was originally proposed that two separate databases be developed, one for large truss–type space structures (LSS) and one for conventional space structures (CSS) as described in Section 2.1.2. At the outset, four structures were identified for the LSS database, and six for the CSS database. As the project progressed, however, additional structures were identified and substantially more data were acquired. Furthermore, it was found that both pretest and posttest models of some CSS were available. In other cases, either pretest or posttest models were available, but not both.

To date, complete data sets have been acquired for almost twice as many structures: 7 LSS and 11 CSS. Of the 11 CSS, data for 7 pretest and 8 posttest models were acquired.

The seven LSS models are considered to be neither pretest nor posttest models. They are not pretest models in the strict sense because all of them have been adjusted to some extent to resolve differences between the pretest models and test data. However, the models were not "fine–tuned" as required on models of flight hardware. The models are therefore not considered posttest models in the same sense as those of CSS. The LSS models are therefore referred to as "research models" for purposes of this project.

2.2.1 Research Models of Large Space Structures

Data sets were obtained for the seven large space structures listed in Table 2–1. The number of modes indicated are the number of analysis–test mode pairs in the frequency range indicated, beginning with the fundamental mode. In the case of large space structures, the mode sets are complete within the given frequency range, i.e., none of the analysis modes were omitted because a test mode was not found to correlate with it. This is not strictly true in the case of conventional space structures, as discussed later. For the most part, however, the frequency range for the paired modes was dictated by the range of paired modes having cross–orthogonalities of at least 0.50, where no analysis modes were skipped. Exceptions are noted in Appendix A where the data are presented.

LaRC Mini–Mast

Mini–Mast is a 20–meter long, 18–bay, deployable generic space truss, manufactured by the Astro Aerospace Corporation [2–1]. It was deployed vertically and cantilevered from its base on a rigid foundation for purposes of testing. At the time of its construction in 1986, the design duplicated (except in length) the 60–meter MAST truss under development for the COFS–I flight experiment. The total weight of the structure is approximately 674 lbs. Its geometry is shown in Figure 2–1.

LaRC Ten Bay Truss

The Ten Bay Truss is a 10–meter long erectable–type truss beam cantilevered from its base [2–2]. The total weight of the structure is approximately 43 lbs. Its geometry is shown in Figure 2–2.

Table 2-1. Structures in LSS Database.

Structure No.	Description	Source	No. Modes	Frequency Range (Hz)
LSS 1	LaRC Minimast 3-Longeron Deployable Truss Beam	NASA Langley Research Center	5	0.85 - 6.11
LSS 2	LaRC Ten Bay 4-Longeron Cantilevered Erectable Truss Beam	NASA Langley Research Center	9	18.05 - 200.20
LSS 3	JPL 4-Longeron Cantilevered Precision Truss Structure	Jet Propulsion Laboratory	4	8.31 - 35.53
LSS 4	JPL 3-Longeron Cantilevered Tetrahedral Bay Truss Beam	Jet Propulsion Laboratory	5	10.61 - 71.83
LSS 5	JPL 3-Longeron Free-Free Tetrahedral Bay Truss Beam	Jet Propulsion Laboratory	6	17.94 - 69.17
LSS 6	PACOSS Free-Free Dynamic Test Article (DTA)	Martin Marietta Corporation	22	1.03 - 9.26
LSS 7	PACOSS Cantilevered Solar Array (Substructure of DTA)	Martin Marietta Corporation	9	0.93 - 16.6

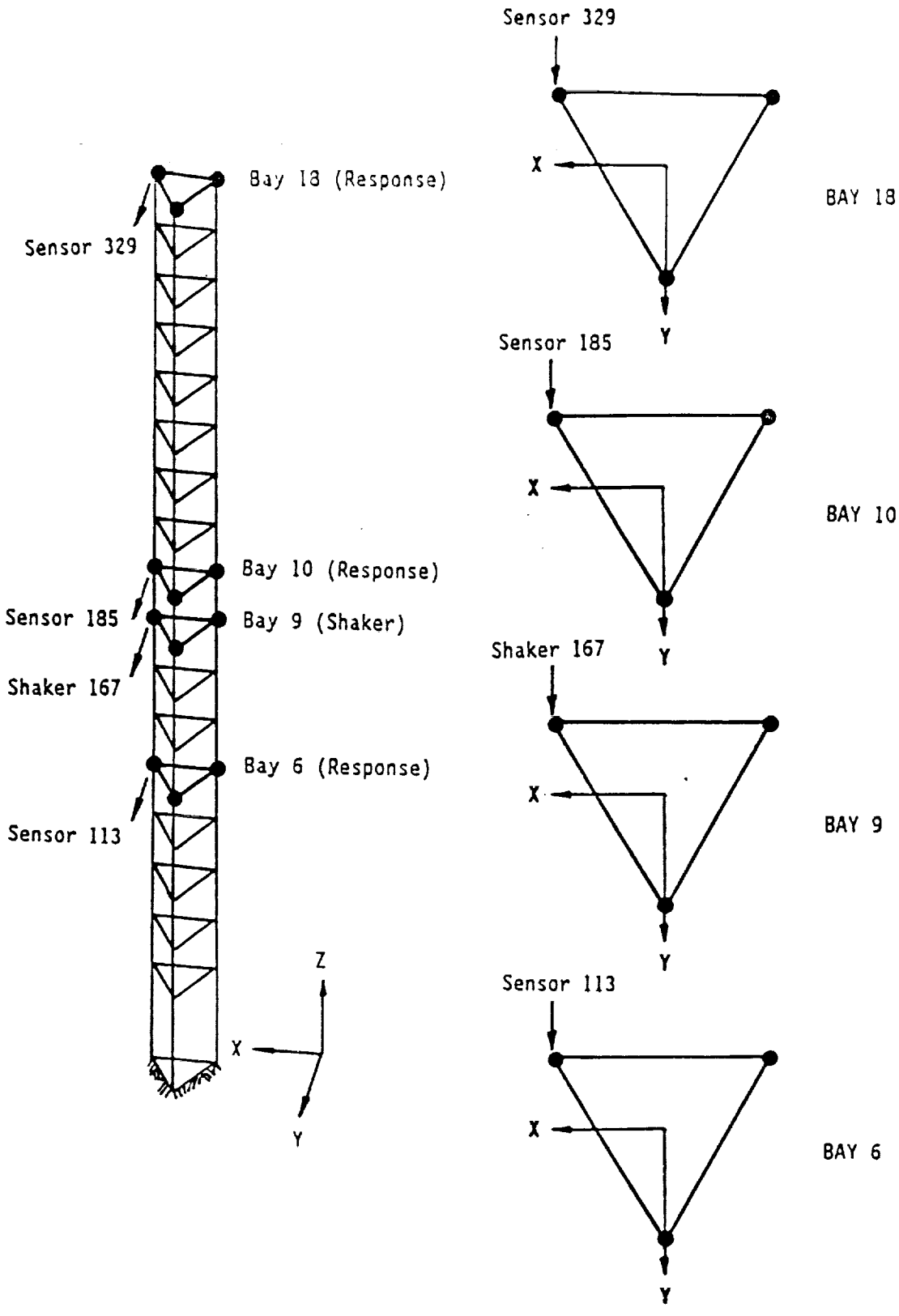

Figure 2–1. LaRC Mini–Mast Structure [2–1].

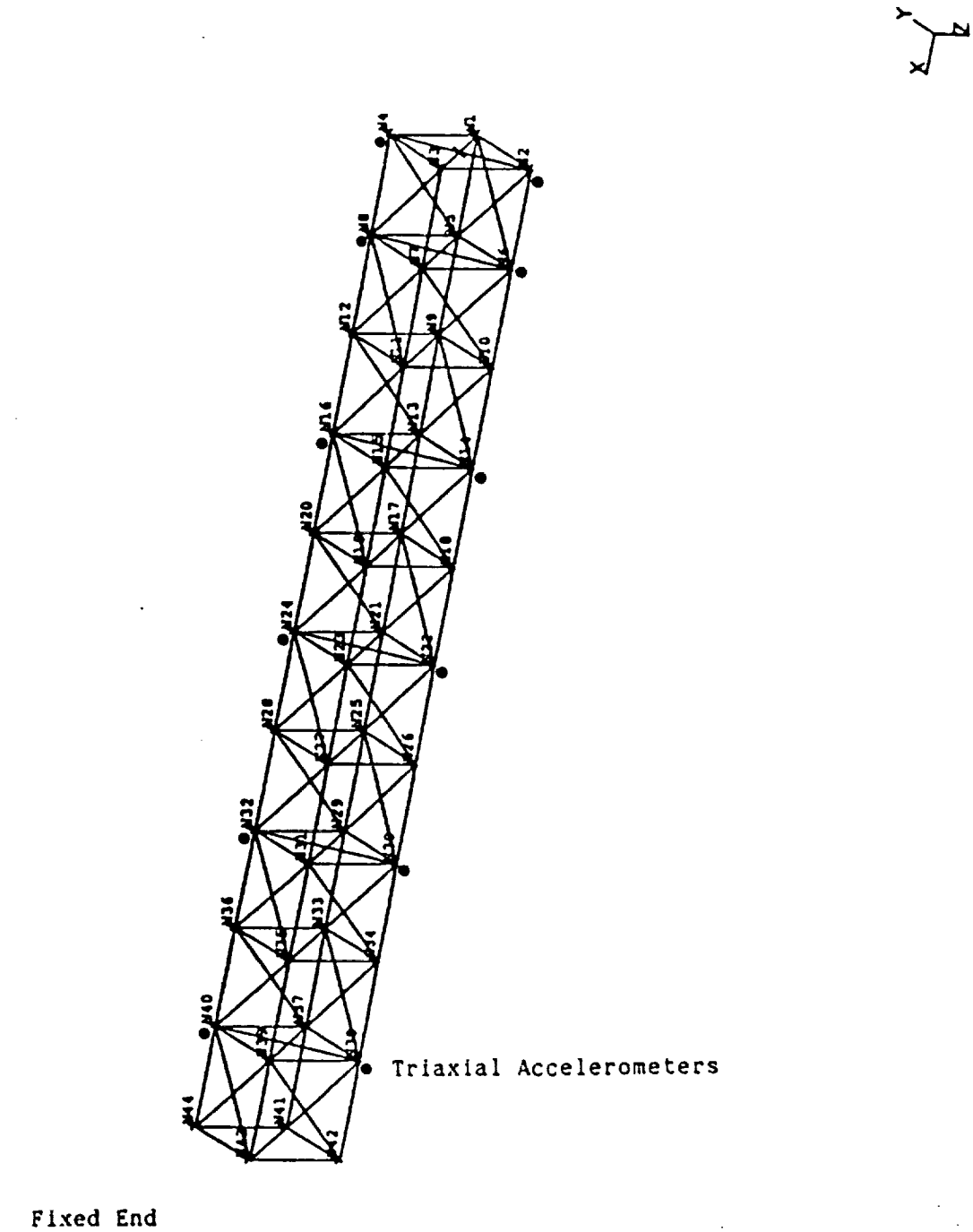

Figure 2–2. LaRC Ten Bay Truss [2–2].

JPL 4–Longeron Precision Truss

The JPL Precision Truss Structure is shown in Figure 2–3 [2–3]. It is essentially a truss beam consisting of six bays approximately 12 x 12 x 8.6 inches in dimension. The structure is cantilevered from its base and stands 72.75 inches tall.

JPL Tetrahedral Bay Truss Beams

Two versions of the JPL Tetrahedral Bay Truss Beam were modeled and tested: (1) a 6–bay cantilevered truss beam and (2) a 13–bay free–free truss beam. See Figure 2–4. As shown in Figure 2–4, each bay is 1 ft. long, making the overall lengths 6 ft. and 13 ft, respectively. The total weight of the 13 ft. truss beam is 13 lbs.

In both cases, excitation was applied by active strut members. In the cantilevered configuration the active member was a longeron in the 4th bay from the tip (Active Member No. 39 in Figure 2–4a). In the free–free configuration, the active member was a longeron in the 10th bay from the left end (Active Member No. 37 in Figure 2–4b). No active damping was applied in either of these particular tests.

PACOSS Dynamic Test Article

The PACOSS Dynamic Test Article (DTA) is shown in Figure 2–5 [2–5]. It consists of seven components as indicated in the figure. All seven components were separately modeled and tested. A component mode model of the complete system was then synthesized and vibration tests were performed on the complete DTA. Figure 2–6 shows the measurement locations on the DTA. Five different shaker configurations, each employing up to four shakers were used to excite the modes of the DTA.

Although each of the seven components was modeled and tested separately, analysis and test frequency and modal cross–orthogonality data were obtained only from one of the solar arrays. The finite element model of this solar array is shown in Figure 2–7.

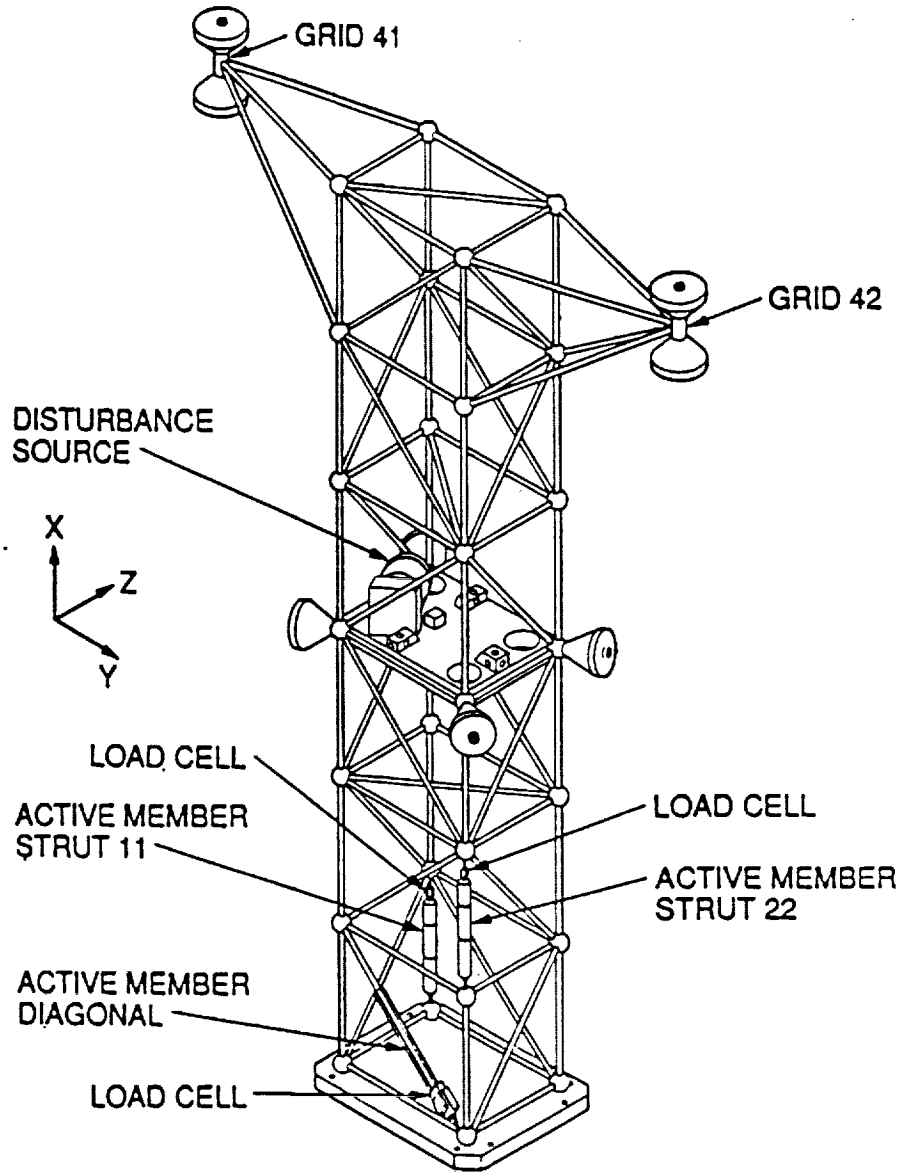

Figure 2–3. JPL Precision Truss [2–3].

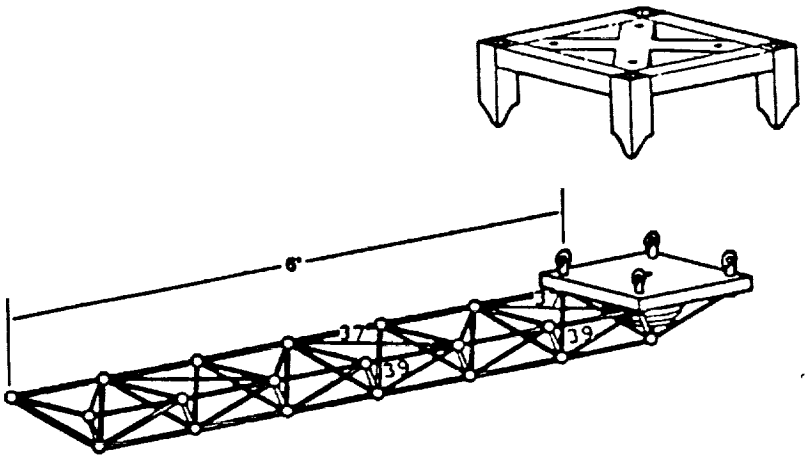

(a) Cantilevered Configuration

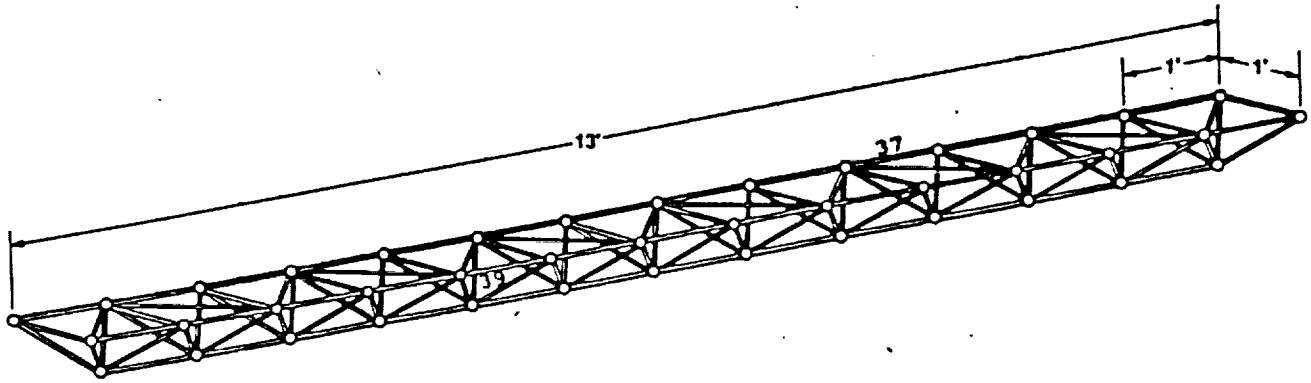

(b) Free-Free Configuration

Figure 2–4. JPL Tetrahedral Bay Truss Beams [2–4].

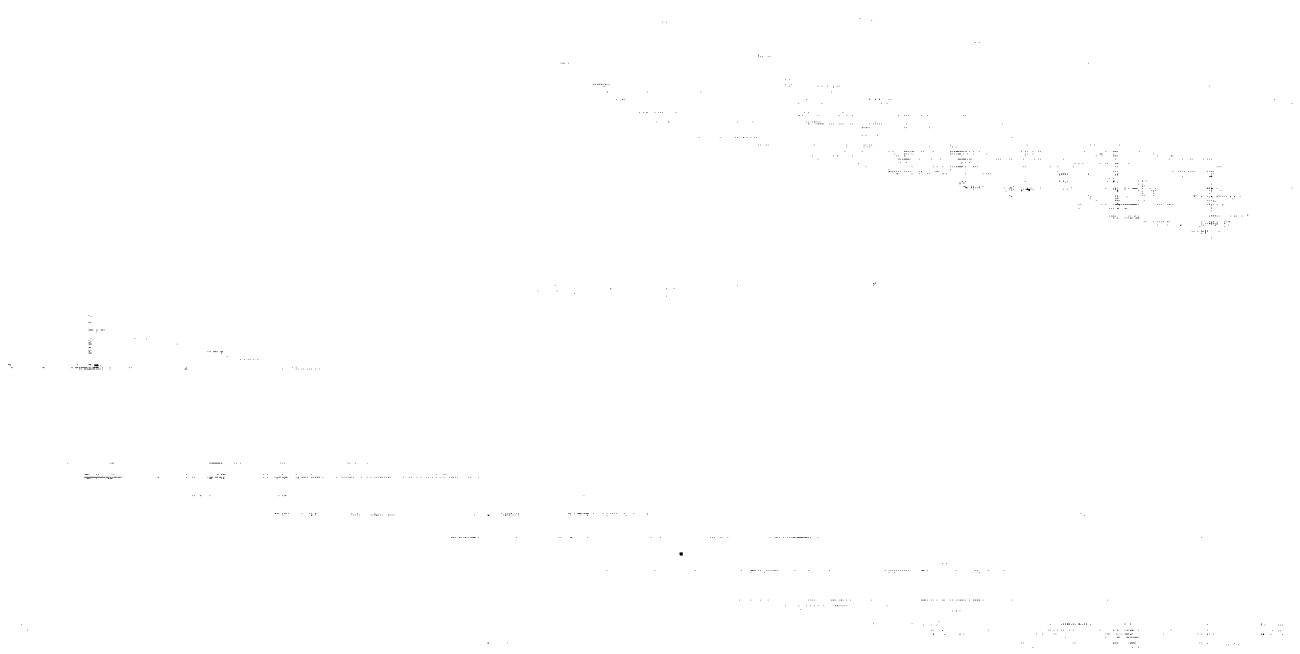

COMPONENT	DIMENSION, m	MASS*, kg
1) Box Truss	2.59 x 2.59 x 0.324	201.5
2) Ring Truss	Diameter: 2.91	116.7**
3) Tripod	Diameter at Base: 2.59 Height: 2.59	29.9
4) Equipment Platform	Length: 1.30	7.94
5) Antenna	Diameter: 0.65	2.24
6,7) Solar Arrays	Length: 2.59	8.93

* Includes Mass of DTA Modal Survey Accelerometers
** Includes: 16.4 kg Mass of Actuators
12.0 kg Active Mass of Zero Spring Rate Mechanisms

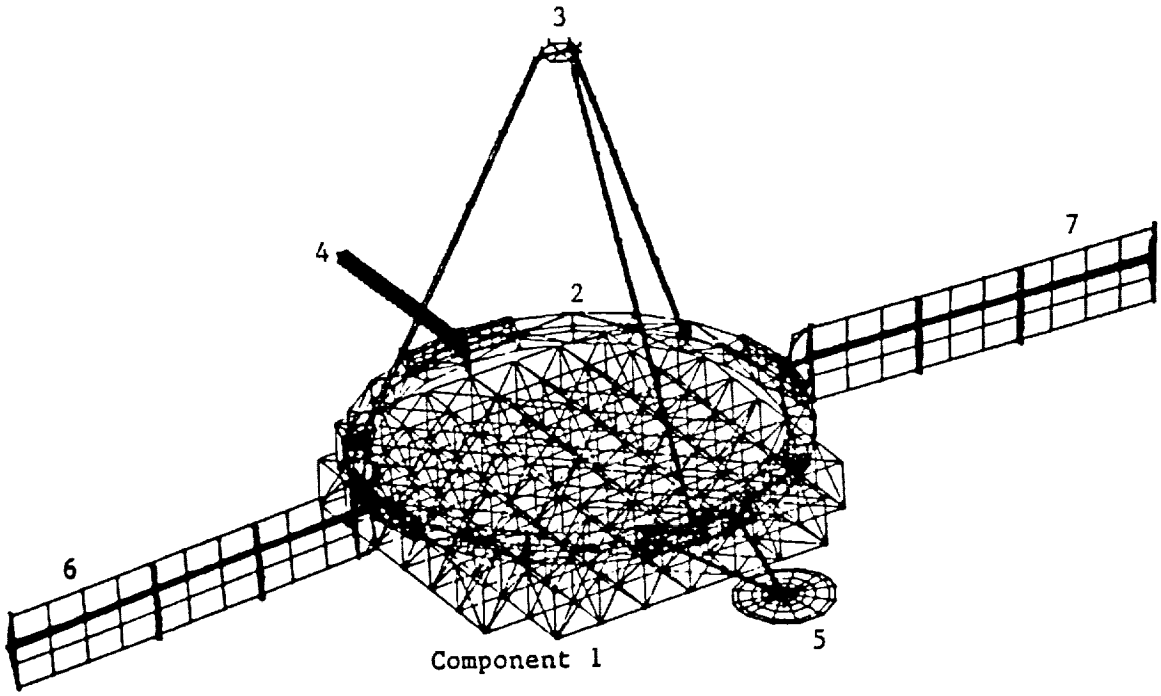

Figure 2–5. Finite Element Model of PACOSS Dynamic Test Article [2–5].

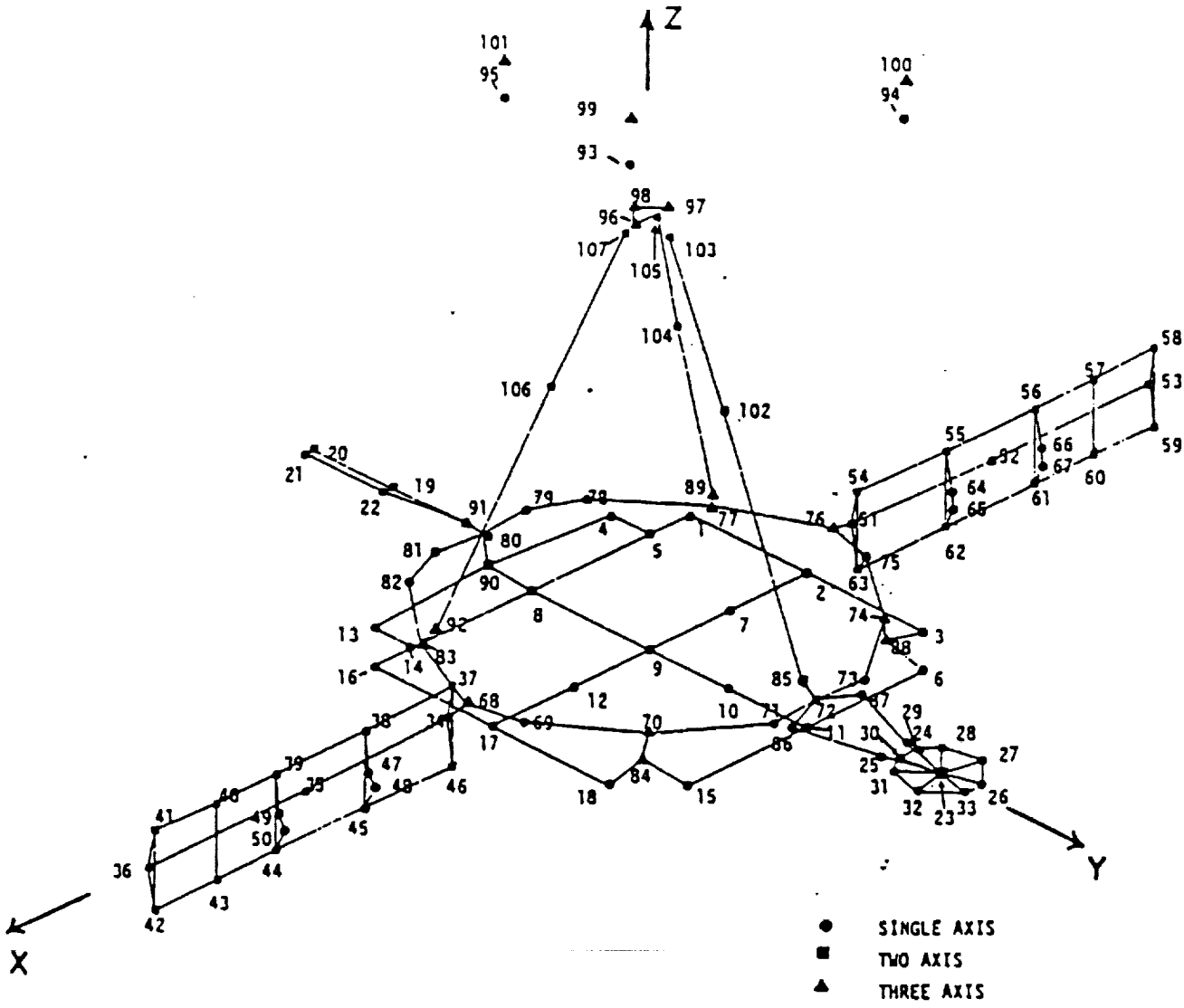

Figure 2–6. PACOSS DTA Measurement Point Diagram [2–5].

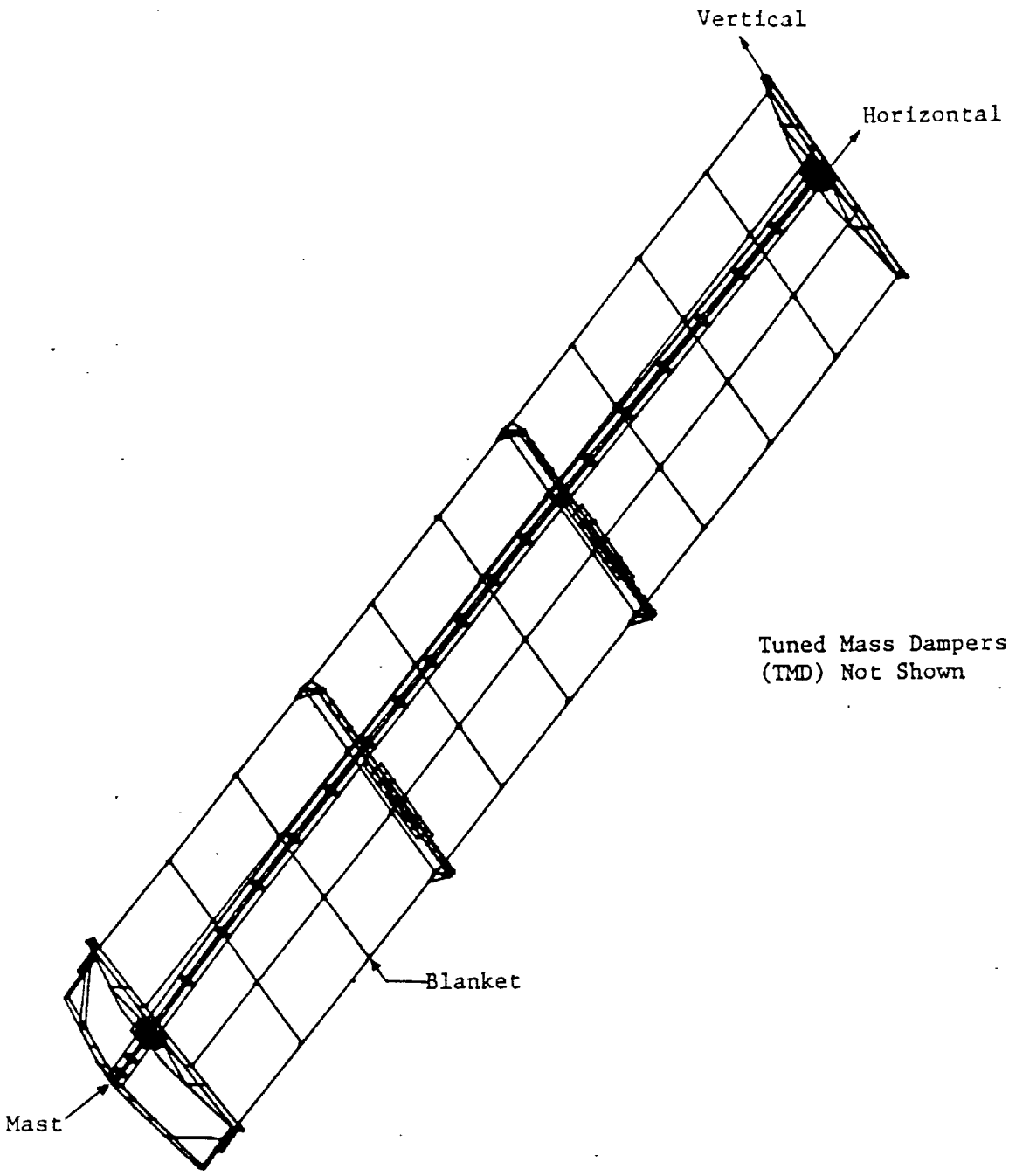

Figure 2–7. Finite Element Model of PACOSS Solar Array [2–5].

Covariance Matrix

The covariance matrix, $S_{\tilde{r}\tilde{r}}$, of modal mass and normalized modal stiffness matrix elements for the first five modes of structures in the LSS Research Model database is presented in Table 2–2. Since only four modes of data were available for LSS 3, it was omitted from this computation, leaving 6 structures in the database. The covariance matrix is presented in terms of its correlation matrix, $\rho_{\tilde{r}\tilde{r}}$, and the square roots of its diagonal elements which correspond to standard deviations $\sigma_{\tilde{r}}$, of the normalized modal matrix elements relative to their nominal values (unity for the diagonals and zero for the off–diagonals). With $\sigma_{\tilde{r}}$ defined as a diagonal (square) matrix,

$$S_{\tilde{r}\tilde{r}} = \sigma_{\tilde{r}} \rho_{\tilde{r}\tilde{r}} \sigma_{\tilde{r}} \tag{2–26}$$

The correlation matrix is presented in partitioned form in Table 2–2 as follows:

$$\rho_{\tilde{r}\tilde{r}} = \begin{bmatrix} \rho_{mm} & \vdots & \rho_{m\tilde{k}} \\ \cdots & \cdots & \cdots \\ \rho_{m\tilde{k}}^T & \vdots & \rho_{\tilde{k}\tilde{k}} \end{bmatrix} \tag{2–27}$$

where ρ_{mm} is the correlation matrix of modal mass matrix elements, $\rho_{\tilde{k}\tilde{k}}$ is the correlation matrix of normalized modal stiffness matrix elements, and $\rho_{m\tilde{k}}$ is the cross–correlation matrix of modal mass and normalized modal stiffness matrix elements. The submatrices ρ_{mm} and $\rho_{\tilde{k}\tilde{k}}$ are presented with the standard deviations of individual matrix elements listed in the first column of the table. The submatrix $\rho_{m\tilde{k}}$ follows ρ_{mm} and $\rho_{\tilde{k}\tilde{k}}$ (without the additional first column).

2.2.2 Pretest and Posttest Models of Conventional Space Structures

Data sets were obtained for the eleven conventional space structures listed in Table 2–3. In this case, neither the structures nor the source of data are identified at the request of contributors who consider the data to be proprietary. As shown in Table 2–3, both pretest and posttest models were available for four of the eleven structures. No

Table 2-2. Covariance Matrix of Modal Mass and Normalized Modal Stiffness Matrix Elements for Research Models of LSS.

ST.D. CORRELATION MATRIX $[\rho_{mm}]$

0.185	1.000	-.327	-.339	-.119	0.483	0.841	-.108	-.181	0.152	0.187	0.127	0.282	0.295	-.095	0.315
0.183	-.327	1.000	-.427	0.162	-.631	0.189	-.438	0.349	-.374	0.328	0.318	-.113	-.113	-.685	-.337
0.248	-.339	-.427	1.000	0.047	0.109	-.647	0.734	0.005	0.262	-.869	-.733	-.264	0.050	0.078	0.164
0.214	-.119	0.162	0.047	1.000	-.789	-.227	0.453	0.963	-.936	-.483	-.660	0.246	-.831	0.201	-.848
0.104	0.483	-.631	0.109	-.789	1.000	0.272	-.045	-.872	0.880	0.167	0.282	0.134	0.768	0.070	0.789
0.140	0.841	0.189	-.647	-.227	0.272	1.000	-.515	-.174	0.103	0.530	0.493	0.134	0.341	-.447	0.268
0.136	-.108	-.438	0.734	0.453	-.045	-.515	1.000	0.289	-.142	-.871	-.923	0.341	-.097	0.189	-.116
0.235	-.181	0.349	0.005	0.963	-.872	-.174	0.289	1.000	-.938	-.428	-.561	0.102	-.854	0.044	-.889
0.269	0.152	-.374	0.262	-.936	0.880	0.103	-.142	-.938	1.000	0.160	0.358	-.203	0.861	-.167	0.894
0.151	0.187	0.328	-.869	-.483	0.167	0.530	-.871	-.428	0.160	1.000	0.959	-.009	0.260	-.079	0.223
0.191	0.127	0.318	-.733	-.660	0.282	0.493	-.923	-.561	0.358	0.959	1.000	-.163	0.377	-.171	0.348
0.100	0.282	-.113	-.264	0.246	0.134	0.134	0.341	0.102	-.203	-.009	-.163	1.000	0.056	0.083	-.262
0.330	0.295	-.113	0.050	-.831	0.768	0.341	-.097	-.854	0.861	0.260	0.377	0.056	1.000	-.470	0.895
0.143	-.095	-.685	0.078	0.201	0.070	-.447	0.189	0.044	-.167	-.079	-.171	0.083	-.470	1.000	-.225
0.290	0.315	-.337	0.164	-.848	0.789	0.268	-.116	-.889	0.894	0.223	0.348	-.262	0.895	-.225	1.000

ST.D. CORRELATION MATRIX $[\rho_{k\bar{k}}]$

0.271	1.000	-.372	-.652	0.381	0.843	0.912	0.390	-.670	0.001	0.049	0.220	0.298	0.407	-.082	0.398
0.175	-.372	1.000	0.060	-.146	-.239	-.262	-.489	0.302	-.057	0.455	0.106	-.186	-.110	-.729	-.450
0.353	-.652	0.060	1.000	-.321	-.575	-.602	0.255	0.740	0.122	-.509	-.739	-.273	-.036	0.064	0.022
0.098	0.381	-.146	-.321	1.000	0.502	0.307	0.596	0.119	-.432	-.518	-.360	0.446	-.611	0.232	-.608
0.230	0.843	-.239	-.575	0.502	1.000	0.812	0.451	-.632	0.024	-.149	0.121	0.283	0.228	-.272	0.174
0.214	0.912	-.262	-.602	0.307	0.812	1.000	0.398	-.554	-.289	0.133	0.191	0.584	0.532	-.292	0.420
0.204	0.390	-.489	0.255	0.596	0.451	0.398	1.000	0.240	-.283	-.827	-.772	0.432	-.036	0.199	0.044
0.159	-.670	0.302	0.740	0.119	-.632	-.554	0.240	1.000	-.426	-.413	-.759	0.131	-.449	0.096	-.507
0.316	0.001	-.057	0.122	-.432	0.024	-.289	-.283	-.426	1.000	0.026	0.237	-.923	0.188	0.026	0.348
0.165	0.049	0.455	-.509	-.518	-.149	0.133	-.827	-.413	0.026	1.000	0.842	-.063	0.399	-.423	0.209
0.194	0.220	0.106	-.739	-.360	0.121	0.191	-.772	-.759	0.237	0.842	1.000	-.153	0.273	-.160	0.234
0.123	0.298	-.186	-.273	0.446	0.283	0.584	0.432	0.131	-.923	-.063	-.153	1.000	0.044	-.043	-.079
0.296	0.407	-.110	-.036	-.611	0.228	0.532	-.036	-.449	0.188	0.399	0.273	0.044	1.000	-.450	0.914
0.142	-.082	-.729	0.064	0.232	-.272	-.292	0.199	0.096	0.026	-.423	-.160	-.043	-.450	1.000	-.080
0.230	0.398	-.450	0.022	-.608	0.174	0.420	0.044	-.507	0.348	0.209	0.234	-.079	0.914	-.080	1.000

CROSS-CORRELATION MATIX $[\rho_{m\bar{k}}]$

0.945	-.393	-.605	0.489	0.959	0.847	0.479	-.677	0.074	-.142	0.137	0.248	0.273	-.093	0.286
-.263	0.956	-.190	-.150	-.196	-.147	-.630	0.127	-.126	0.657	0.349	-.092	-.074	-.691	-.416
-.438	-.166	0.944	-.242	-.315	-.421	0.452	0.550	0.225	-.666	-.768	-.257	0.066	0.103	0.181
-.134	0.256	0.165	0.735	-.111	-.169	0.408	0.691	-.486	-.450	-.621	0.259	-.717	0.163	-.788
0.432	-.685	-.153	-.293	0.453	0.471	0.200	-.647	0.248	-.051	0.244	0.104	0.639	0.072	0.798
0.826	0.061	-.801	0.279	0.858	0.767	-.003	-.784	0.133	0.334	0.514	0.106	0.314	-.436	0.177
-.115	-.242	0.697	0.222	-.125	0.002	0.794	0.693	-.391	-.717	-.929	0.366	-.007	0.151	0.024
-.234	0.452	0.148	0.674	-.124	-.277	0.239	0.657	-.366	-.355	-.521	0.106	-.767	0.016	-.884
0.122	-.383	0.086	-.683	0.153	0.175	-.113	-.541	0.477	0.149	0.311	-.218	0.749	-.133	0.854
0.317	0.056	-.824	-.225	0.131	0.284	-.697	-.718	0.082	0.841	0.970	-.009	0.223	-.070	0.184
0.205	0.080	-.713	-.396	0.110	0.175	-.773	-.767	0.266	0.831	0.998	-.174	0.294	-.148	0.268
0.307	-.206	-.297	0.479	0.331	0.587	0.443	0.097	-.905	-.094	-.143	0.996	0.014	-.038	-.100
0.361	-.159	-.086	-.612	0.300	0.515	-.071	-.541	0.203	0.374	0.349	0.064	0.961	-.457	0.892
-.089	-.732	0.044	0.284	-.258	-.255	0.233	0.132	-.094	-.435	-.180	0.076	-.475	0.991	-.122
0.388	-.359	-.007	-.641	0.228	0.366	-.049	-.600	0.523	0.242	0.312	-.251	0.896	-.165	0.973

Table 2-3. Structures in CSS Database.

Structure No.	No. Modes Pretest Model	Frequency Range (Hz)	No. Modes Posttest Model	Frequency Range(Hz)
CSS 1	9	13.71 - 23.58	N/A	
CSS 2	5	16.27 - 52.70	5	16.27 - 52.70
CSS 3	6	14.49 - 49.97	6	14.49 - 49.97
CSS 4	6	14.45 - 50.29	N/A	
CSS 5	9	29.38 - 95.99	9	29.38 - 95.99
CSS 6	5	15.11 - 27.35	N/A	
CSS 7	N/A		34	7.04 - 46.50
CSS 8	N/A		4	41.64 - 93.77
CSS 9	N/A		14	5.84 - 24.51
CSS 10	N/A		12	12.50 - 35.67
CSS 11	16	16.15 - 46.60	27	16.15 - 50.76

special treatment is accorded data from these structures, however; they are treated as independent data sets belonging to either the pretest or posttest generic categories.

As in the case of Large Space Structures, detailed data for each of the structure–model combinations is given in Appendix A. Data for the pretest models are given in Tables A–8 through A–14 while data for the posttest models are given in Tables A–15 through A–22. Unlike the data presented in Tables A–1 through A–7 for Large Space Structures, the CSS data in Tables A–8 through A–22 reflect the fact that analysis modes are occasionally skipped or omitted from the database whenever a test mode cannot be found to correlate with it. It is assumed that the skipped modes represent either local modes or otherwise unimportant modes which were not excited during test, and therefore do not adversely affect the completeness of the model relative to its intended use (e.g. launch loads analysis). For example, in Table A–11, fourteen of the sixteen skipped modes between 18 and 40 Hz are attributed to local appendage modes, and none of the sixteen modes contribute significantly to the effective mass of the model at its interface with the launch vehicle.

In two isolated cases (Tables A–12 and A–20), mode pairs are listed which have cross–orthogonality coefficients of less than 0.50. Notation is made that the test modes are 94% and 85% represented by linear combinations of the analysis modes listed in their respective tables. This statement requires some explanation. Equations (2–7) and (2–18) imply that the test modes can be represented as linear combinations of the analysis modes. This has been found to be true in an approximate sense. In fact, the test modes, ϕ, are represented by a least squares fit of the modes

$$\hat{\phi} = {}^{o}\phi\psi \tag{2–28}$$

This assertion is easily verified by defining an objective function, J_j, as the weighted sum of the squared differences between the measured mode, ϕ_j, and its approximation, $\hat{\phi}_j$, where the analytical mass matrix, ${}^{o}M$, is used as the weighting matrix.

$$J_j = (\phi_j - \hat{\phi}_j)^T \, {}^{o}M \, (\phi_j - \hat{\phi}_j) \tag{2–29}$$

Substitution of (2–28) into (2–29) gives

$$J_j = (\phi_j - {}^o\phi\psi_j)^T \, {}^oM \, (\phi_j - {}^o\phi\psi_j) \tag{2–30}$$

Setting the gradient of J_j with respect to ψ_j equal to zero gives

$$\nabla_{\psi_j} J_j = - {}^o\phi^T \, {}^oM \, (\phi_j - {}^o\phi\psi_j) = 0 \tag{2–31}$$

from which Equation (2–17) is obtained. From this result it is understood that

$$\phi_j = \hat{\phi}_j + \epsilon_j \tag{2–32}$$

where the vector ϵ_j represents the residual error in the least squares approximation, i.e. the difference between ϕ_j and $\hat{\phi}_j$. A measure of this error is given by the difference, $1 - \psi_j^T \psi_j$. It is recalled that the measured modes, ϕ_j, are normalized such that

$$\phi^T \, {}^oM \, \phi_j = 1 \tag{2–33}$$

Substitution of (2–32) into (2–33) gives

$$({}^o\phi \, \psi_j + \epsilon_j)^T \, {}^oM \, ({}^o\phi \, \psi_j + \epsilon_j) = 1$$

from which it follows that

$$\begin{aligned} 1 - \psi_j^T \psi_j &= \epsilon_j^T \, {}^oM \, (2 \, {}^o\phi \, \psi_j + \epsilon_j) \\ &= \epsilon_j^T \, {}^oM \, (\phi_j + \hat{\phi}_j) \end{aligned} \tag{2–34}$$

In general, then, $\epsilon_j \neq 0$ unless

$$\psi_j^T \psi_j = 1 \tag{2–35}$$

The percent completeness of ψ_j is defined as

$$\text{Percent completeness} = 100\% \sqrt{\psi_j^T \ \psi_j} \qquad (2\text{–}36)$$

Covariance Matrices

The covariance matrices, $S_{\tilde{r}\tilde{r}}$, of modal mass and normalized modal stiffnes matrix elements for the first five modes of structures in the CSS Pretest and Posttest Model databases are presented in Tables 2–4 and 2–5, respectively. One would expect the covariance matrix of modeling error to be smaller for posttest models. It is not immediately apparent that this is the case; the individual standard deviations appear to be roughly equivalent. They are not, however, as shown in the following subsection.

2.2.3 Comparison of Databases

As stated earlier, one of the reasons for segregating the data into three separate databases was to compare them with each other and with the database realized by combining the three. The five–mode covariance matrix for combined LSS and CSS Pretest and Posttest Models is presented in Table 2–6. Again, no significant differences are immediately apparent between the combined database and the three separate databases.

The differences are more apparent when comparing the eigenvalues of these matrices. It will be observed that all four covariance matrices are singular because rank, which is governed by the number of structures in the database, is less than the dimension of the matrices. The dimension is equal to $m^2 + m$, where m is the number of included modes. In this case, $m = 5$ so that the covariance matrices are of dimension 30 x 30. The rank of the matrices in general equals the number of structures in the database, as confirmed by the number of non–zero eigenvalues. Table 2–7 compares the eigenvalues of the four covariance matrices obtained by singular value decomposition [2–6].

The eigenvalues of a covariance matrix provide a measure of its uncertainty. In particular the trace of the covariance matrix which equals the sum of its diagonal elements, or alternatively the sum of its eigenvalues, provides a scalar measure of uncertainty. Now

Table 2-4. Covariance Matrix of Modal Mass and Normalized Modal Stiffness Matrix Elements for Pretest Models of LSS.

ST.D. CORRELATION MATRIX $[\rho_{mm}]$

0.097	1.000	-.707	-.256	0.288	0.046	0.953	0.821	-.644	-.376	0.792	0.724	0.625	0.874	0.120	0.429
0.084	-.707	1.000	0.140	-.533	-.179	-.608	-.834	0.739	0.500	-.386	-.526	-.798	-.751	-.287	-.284
0.137	-.256	0.140	1.000	0.305	0.482	-.249	-.043	0.004	-.368	-.109	-.585	0.013	-.330	0.465	-.514
0.096	0.288	-.533	0.305	1.000	0.699	0.139	0.661	-.624	-.937	0.002	-.131	0.851	0.153	0.766	-.631
0.134	0.046	-.179	0.482	0.699	1.000	0.000	0.254	-.508	-.867	0.138	-.609	0.417	0.044	0.987	-.683
0.117	0.953	-.608	-.249	0.139	0.000	1.000	0.634	-.434	-.264	0.919	0.656	0.416	0.780	0.032	0.530
0.131	0.821	-.834	-.043	0.661	0.254	0.634	1.000	-.878	-.643	0.381	0.566	0.941	0.781	0.383	0.049
0.116	-.644	0.739	0.004	-.624	-.508	-.434	-.878	1.000	0.702	-.274	-.284	-.859	-.766	-.625	0.090
0.062	-.376	0.500	-.368	-.937	-.867	-.264	-.643	0.702	1.000	-.224	0.223	-.782	-.265	-.911	0.597
0.383	0.792	-.386	-.109	0.002	0.138	0.919	0.381	-.274	-.224	1.000	0.378	0.164	0.651	0.115	0.477
0.094	0.724	-.526	-.585	-.131	-.609	0.656	0.566	-.284	0.223	0.378	1.000	0.351	0.686	-.515	0.721
0.109	0.625	-.798	0.013	0.851	0.417	0.416	0.941	-.859	-.782	0.164	0.351	1.000	0.586	0.540	-.221
0.467	0.874	-.751	-.330	0.153	0.044	0.780	0.781	-.766	-.265	0.651	0.686	0.586	1.000	0.136	0.526
0.177	0.120	-.287	0.465	0.766	0.987	0.032	0.383	-.625	-.911	0.115	-.515	0.540	0.136	1.000	-.669
0.278	0.429	-.284	-.514	-.631	-.683	0.530	0.049	0.090	0.597	0.477	0.721	-.221	0.526	-.669	1.000

ST.D. CORRELATION MATRIX $[\rho_{\tilde{k}\tilde{k}}]$

0.193	1.000	-.433	0.025	0.005	0.089	0.675	0.402	-.124	-.259	0.700	0.436	0.261	0.437	0.022	0.562
0.104	-.433	1.000	0.040	-.579	-.555	-.077	-.898	0.390	0.293	-.366	-.591	-.744	-.712	-.294	-.015
0.196	0.025	0.040	1.000	-.033	0.042	-.188	-.160	0.172	-.304	0.024	-.362	0.274	-.223	0.299	-.263
0.072	0.005	-.579	-.033	1.000	0.840	-.077	0.595	0.157	-.600	0.021	-.029	0.761	0.295	0.765	-.404
0.072	0.089	-.555	0.042	0.840	1.000	-.065	0.630	-.276	-.630	-.042	-.119	0.834	0.304	0.919	-.443
0.287	0.675	-.077	-.188	-.077	-.065	1.000	-.098	0.109	0.238	0.889	-.039	-.257	0.488	-.059	0.868
0.133	0.402	-.898	-.160	0.595	0.630	-.098	1.000	-.487	-.413	0.127	0.688	0.817	0.613	0.334	-.156
0.122	-.124	0.390	0.172	0.157	-.276	0.109	-.487	1.000	-.159	0.049	-.386	-.249	-.427	-.025	-.003
0.073	-.259	0.293	-.304	-.600	-.630	0.238	-.413	-.159	1.000	0.264	0.066	-.776	0.288	-.717	0.603
0.634	0.700	-.366	0.024	0.021	-.042	0.889	0.127	0.049	0.264	1.000	0.173	-.062	0.716	-.090	0.850
0.096	0.436	-.591	-.362	-.029	-.119	-.039	0.688	-.386	0.066	0.173	1.000	0.231	0.486	-.440	0.228
0.125	0.261	-.744	0.274	0.761	0.834	-.257	0.817	-.249	-.776	-.062	0.231	1.000	0.267	0.734	-.512
0.407	0.437	-.712	-.223	0.295	0.304	0.488	0.613	-.427	0.288	0.716	0.486	0.267	1.000	0.031	0.535
0.175	0.022	-.294	0.299	0.765	0.919	-.059	0.334	-.025	-.717	-.090	-.440	0.734	0.031	1.000	-.510
0.320	0.562	-.015	-.263	-.404	-.443	0.868	-.156	-.003	0.603	0.850	0.228	-.512	0.535	-.510	1.000

CROSS-CORRELATION MATIX $[\rho_{m\tilde{k}}]$

0.654	-.762	-.409	0.444	0.408	0.411	0.825	-.329	-.122	0.541	0.703	0.473	0.813	0.106	0.368
-.440	0.989	0.016	-.539	-.493	-.118	-.831	0.333	0.271	-.404	-.556	-.691	-.679	-.253	-.057
0.310	0.146	0.847	0.015	0.193	0.171	-.194	0.194	-.434	0.197	-.495	0.255	-.196	0.483	-.080
0.180	-.571	0.298	0.764	0.788	-.334	0.658	-.037	-.919	-.220	0.079	0.951	-.011	0.772	-.647
-.038	-.213	0.287	0.759	0.883	-.018	0.234	0.061	-.658	-.072	-.533	0.649	0.007	0.991	-.478
0.702	-.636	-.469	0.395	0.278	0.616	0.638	-.111	-.045	0.682	0.593	0.286	0.774	0.029	0.546
0.482	-.901	-.019	0.563	0.622	-.038	0.984	-.482	-.418	0.219	0.659	0.836	0.648	0.356	-.103
-.210	0.813	-.005	-.627	-.822	0.086	-.869	0.633	0.326	-.118	-.328	-.819	-.651	-.584	0.226
-.227	0.550	-.229	-.854	-.927	0.103	-.629	0.055	0.850	0.046	0.073	-.920	-.148	-.915	0.504
0.592	-.407	-.409	0.417	0.264	0.768	0.369	0.115	0.043	0.766	0.264	0.116	0.715	0.117	0.623
0.418	-.553	-.473	-.104	-.197	0.126	0.596	-.408	0.294	0.320	0.963	0.059	0.614	-.539	0.427
0.298	-.856	0.094	0.678	0.723	-.273	0.943	-.384	-.625	-.031	0.503	0.951	0.407	0.519	-.406
0.355	-.804	-.313	0.424	0.416	0.281	0.779	-.488	0.156	0.521	0.605	0.419	0.959	0.088	0.330
-.001	-.329	0.307	0.774	0.931	-.074	0.359	-.061	-.682	-.079	-.424	0.747	0.078	0.997	-.509
0.293	-.243	-.440	-.336	-.484	0.531	0.056	-.145	0.741	0.648	0.526	-.450	0.631	-.697	0.833

Table 2-5. Covariance Matrix of Modal Mass and Normalized Modal Stiffness Matrix Elements for Posttest Models of CSS.

ST.D. CORRELATION MATRIX $[\rho_{mm}]$

0.125	1.000	-.167	0.043	0.426	-.631	0.905	0.161	0.118	-.233	0.868	-.902	-.951	0.653	-.700	0.846
0.143	-.167	1.000	-.793	-.101	-.296	-.427	-.968	0.374	-.491	-.514	0.069	0.088	-.086	0.518	-.131
0.042	0.043	-.793	1.000	-.016	0.423	0.317	0.777	-.293	0.492	0.412	0.072	0.116	0.145	-.661	0.175
0.044	0.426	-.101	-.016	1.000	-.813	0.585	0.119	0.713	0.511	0.356	-.243	-.597	0.498	-.327	0.468
0.048	-.631	-.296	0.423	-.813	1.000	-.604	0.301	-.766	-.081	-.386	0.451	0.767	-.659	0.235	-.654
0.132	0.905	-.427	0.317	0.585	-.604	1.000	0.412	0.232	0.190	0.942	-.676	-.860	0.798	-.849	0.911
0.036	0.161	-.968	0.777	0.119	0.301	0.412	1.000	-.450	0.489	0.467	-.112	-.122	0.036	-.550	0.097
0.043	0.118	0.374	-.293	0.713	-.766	0.232	-.450	1.000	0.396	0.035	0.160	-.220	0.563	0.014	0.398
0.030	-.233	-.491	0.492	0.511	-.081	0.190	0.489	0.396	1.000	0.070	0.518	0.157	0.323	-.262	0.114
0.153	0.868	-.514	0.412	0.356	-.386	0.942	0.467	0.035	0.070	1.000	-.666	-.743	0.689	-.821	0.847
0.061	-.902	0.069	0.072	-.243	0.451	-.676	-.112	0.160	0.518	-.666	1.000	0.880	-.282	0.509	-.553
0.105	-.951	0.088	0.116	-.597	0.767	-.860	-.122	-.220	0.157	-.743	0.880	1.000	-.599	0.589	-.764
0.336	0.653	-.086	0.145	0.498	-.659	0.798	0.036	0.563	0.323	0.689	-.282	-.599	1.000	-.692	0.946
0.096	-.700	0.518	-.661	-.327	0.235	-.849	-.550	0.014	-.262	-.821	0.509	0.589	-.692	1.000	-.794
0.297	0.846	-.131	0.175	0.468	-.654	0.911	0.097	0.398	0.114	0.847	-.553	-.764	0.946	-.794	1.000

ST.D. CORRELATION MATRIX $[\rho_{\tilde{k}\tilde{k}}]$

0.163	1.000	-.048	-.088	-.113	-.376	0.849	-.393	-.419	-.090	0.783	-.558	-.622	0.732	-.809	0.764
0.142	-.048	1.000	-.819	-.009	-.111	-.270	-.141	0.548	-.494	-.285	0.087	0.013	-.124	0.289	-.128
0.040	-.088	-.819	1.000	-.345	0.342	0.158	-.035	-.524	0.555	0.268	0.450	0.464	0.130	-.204	-.029
0.049	-.113	-.009	-.345	1.000	-.459	0.115	0.786	0.281	-.757	0.114	-.367	-.639	0.231	0.331	0.345
0.100	-.376	-.111	0.342	-.459	1.000	-.345	-.247	-.133	0.522	-.322	0.360	0.574	-.382	-.204	-.282
0.175	0.849	-.270	0.158	0.115	-.345	1.000	-.139	-.414	-.233	0.971	-.388	-.600	0.920	-.725	0.938
0.023	-.393	-.141	-.035	0.786	-.247	-.139	1.000	-.072	-.538	-.085	-.012	-.223	-.016	0.492	0.029
0.023	-.419	0.548	-.524	0.281	-.133	-.414	-.072	1.000	-.382	-.399	0.157	0.055	-.233	0.595	-.278
0.047	-.090	-.494	0.555	-.757	0.522	-.233	-.538	-.382	1.000	-.282	0.101	0.505	-.471	-.285	-.457
0.233	0.783	-.285	0.268	0.114	-.322	0.971	-.085	-.399	-.282	1.000	-.201	-.482	0.973	-.649	0.912
0.074	-.558	0.087	0.450	-.367	0.360	-.388	-.012	0.157	0.101	-.201	1.000	0.879	-.155	0.452	-.448
0.096	-.622	0.013	0.464	-.639	0.574	-.600	-.223	0.055	0.505	-.482	0.879	1.000	-.508	0.365	-.714
0.383	0.732	-.124	0.130	0.231	-.382	0.920	-.016	-.233	-.471	0.973	-.155	-.508	1.000	-.528	0.917
0.111	-.809	0.289	-.204	0.331	-.204	-.725	0.492	0.595	-.285	-.649	0.452	0.365	-.528	1.000	-.660
0.316	0.764	-.128	-.029	0.345	-.282	0.938	0.029	-.278	-.457	0.912	-.448	-.714	0.917	-.660	1.000

CROSS-CORRELATION MATIX $[\rho_{m\tilde{k}}]$

0.784	-.139	-.306	0.422	-.558	0.743	0.016	-.211	-.308	0.612	-.883	-.955	0.585	-.556	0.767
-.083	0.992	-.786	0.058	-.124	-.253	-.058	0.561	-.574	-.246	0.152	0.024	-.069	0.335	-.095
0.121	-.796	0.764	-.202	0.558	0.326	-.175	-.462	0.530	0.346	0.003	0.091	0.205	-.579	0.269
-.090	-.170	-.177	0.956	-.427	0.196	0.666	0.334	-.661	0.210	-.320	-.604	0.313	0.270	0.390
-.272	-.247	0.539	-.848	0.743	-.384	-.464	-.360	0.879	-.369	0.444	0.780	-.511	-.162	-.549
0.670	-.440	0.041	0.515	-.473	0.832	0.192	-.311	-.301	0.761	-.689	-.855	0.718	-.531	0.847
0.026	-.963	0.727	0.018	0.204	0.194	0.206	-.649	0.530	0.176	-.202	-.056	0.001	-.330	0.088
-.064	0.284	-.259	0.647	-.441	0.192	0.326	0.638	-.820	0.293	0.159	-.269	0.478	0.383	0.348
-.356	-.596	0.668	0.386	0.115	0.093	0.555	-.099	-.142	0.248	0.435	0.179	0.258	0.220	0.131
0.717	-.500	0.142	0.257	-.377	0.863	-.051	-.384	-.049	0.756	-.670	-.736	0.656	-.652	0.793
-.645	0.002	0.495	-.304	0.405	-.440	0.053	0.177	0.131	-.255	0.989	0.883	-.214	0.494	-.485
-.604	0.077	0.417	-.642	0.642	-.580	-.284	0.123	0.472	-.463	0.878	0.988	-.475	0.319	-.665
0.666	-.149	0.063	0.432	-.489	0.888	0.165	-.182	-.583	0.933	-.241	-.621	0.975	-.416	0.920
-.650	0.530	-.272	-.247	-.020	-.802	-.049	0.535	0.061	-.763	0.526	0.619	-.686	0.791	-.842
0.789	-.161	-.060	0.414	-.482	0.942	0.064	-.232	-.485	0.910	-.516	-.791	0.917	-.576	0.972

Table 2-6. Covariance Matrix of Modal Mass and Normalized Modal Stiffness Matrix Elements for all Models of LSS and CSS.

ST.D. CORRELATION MATRIX $[\rho_{mm}]$

0.138	1.000	-.330	-.262	0.019	0.119	0.870	0.204	-.229	0.056	0.497	0.074	-.033	0.543	-.152	0.505
0.140	-.330	1.000	-.309	0.009	-.351	-.190	-.534	0.377	-.250	-.153	0.121	-.185	-.255	-.219	-.238
0.160	-.262	-.309	1.000	0.101	0.261	-.361	0.431	-.003	0.178	-.262	-.655	-.102	-.088	0.168	-.055
0.133	0.019	0.009	0.101	1.000	-.197	-.017	0.477	0.638	-.881	-.111	-.530	0.269	-.246	0.313	-.511
0.102	0.119	-.351	0.261	-.197	1.000	-.012	0.140	-.643	0.308	0.087	-.044	0.366	0.131	0.614	-.173
0.129	0.870	-.190	-.361	-.017	-.012	1.000	0.081	-.173	0.038	0.733	0.285	-.129	0.642	-.338	0.584
0.109	0.204	-.534	0.431	0.477	0.140	0.081	1.000	-.131	-.191	0.079	-.357	0.517	0.369	0.227	-.012
0.148	-.229	0.377	-.003	0.638	-.643	-.173	-.131	1.000	-.701	-.229	-.464	-.220	-.553	-.191	-.361
0.153	0.056	-.250	0.178	-.881	0.308	0.038	-.191	-.701	1.000	0.005	0.333	-.207	0.363	-.261	0.564
0.257	0.497	-.153	-.262	-.111	0.087	0.733	0.079	-.229	0.005	1.000	0.341	-.067	0.575	-.055	0.460
0.124	0.074	0.121	-.655	-.530	-.044	0.285	-.357	-.464	0.333	0.341	1.000	0.176	0.329	-.190	0.249
0.105	-.033	-.185	-.102	0.269	0.366	-.129	0.517	-.220	-.207	-.067	0.176	1.000	0.090	0.407	-.428
0.386	0.543	-.255	-.088	-.246	0.131	0.642	0.369	-.553	0.363	0.575	0.329	0.090	1.000	-.192	0.743
0.142	-.152	-.219	0.168	0.313	0.614	-.338	0.227	-.191	-.261	-.055	-.190	0.407	-.192	1.000	-.541
0.289	0.505	-.238	-.055	-.511	-.173	0.584	-.012	-.361	0.564	0.460	0.249	-.428	0.743	-.541	1.000

ST.D. CORRELATION MATRIX $[\rho_{k\bar{k}}]$

0.211	1.000	-.292	-.389	0.175	0.457	0.770	0.331	-.426	-.039	0.475	0.146	0.072	0.488	-.190	0.538
0.142	-.292	1.000	-.008	-.218	-.238	-.187	-.502	0.303	-.051	-.135	-.036	-.278	-.281	-.278	-.183
0.227	-.389	-.008	1.000	-.221	-.403	-.324	0.129	0.531	0.071	-.075	-.589	-.022	-.080	0.129	-.080
0.075	0.175	-.218	-.221	1.000	0.382	0.100	0.575	0.136	-.427	-.057	-.272	0.345	-.029	0.460	-.251
0.145	0.457	-.238	-.403	0.382	1.000	0.279	0.414	-.475	0.008	-.084	0.121	0.417	0.049	0.029	-.093
0.231	0.770	-.187	-.324	0.100	0.279	1.000	0.117	-.187	-.114	0.760	0.009	-.082	0.608	-.258	0.769
0.137	0.331	-.502	0.129	0.575	0.414	0.117	1.000	-.029	-.285	-.084	-.347	0.496	0.216	0.245	-.041
0.114	-.426	0.303	0.531	0.136	-.475	-.187	-.029	1.000	-.344	-.057	-.583	-.039	-.345	0.061	-.188
0.181	-.039	-.051	0.071	-.427	0.008	-.114	-.285	-.344	1.000	0.049	0.201	-.599	0.080	-.129	0.191
0.410	0.475	-.135	-.075	-.057	-.084	0.760	-.084	-.057	0.049	1.000	0.201	-.125	0.669	-.208	0.715
0.128	0.146	-.036	-.589	-.272	0.121	0.009	-.347	-.583	0.201	0.201	1.000	0.139	0.208	-.140	0.051
0.115	0.072	-.278	-.022	0.345	0.417	-.082	0.496	-.039	-.599	-.125	0.139	1.000	-.031	0.404	-.456
0.368	0.488	-.281	-.080	-.029	0.049	0.608	0.216	-.345	0.080	0.669	0.208	-.031	1.000	-.239	0.756
0.145	-.190	-.278	0.129	0.460	0.029	-.258	0.245	0.061	-.129	-.208	-.140	0.404	-.239	1.000	-.442
0.294	0.538	-.183	-.080	-.251	-.093	0.769	-.041	-.188	0.191	0.715	0.051	-.456	0.756	-.442	1.000

CROSS-CORRELATION MATIX $[\rho_{m\bar{k}}]$

0.829	-.378	-.483	0.453	0.537	0.620	0.484	-.481	0.015	0.293	0.052	-.021	0.502	-.140	0.449
-.239	0.970	-.163	-.173	-.203	-.152	-.539	0.185	-.116	-.077	0.152	-.188	-.206	-.238	-.177
-.168	-.137	0.914	-.156	-.167	-.094	0.252	0.410	0.143	-.015	-.651	-.037	-.021	0.180	0.066
-.049	0.026	0.186	0.728	-.019	-.164	0.468	0.463	-.525	-.161	-.461	0.338	-.244	0.337	-.428
0.119	-.372	0.058	0.129	0.506	0.075	0.183	-.258	0.046	-.092	-.029	0.467	0.073	0.553	-.147
0.733	-.282	-.529	0.361	0.366	0.698	0.206	-.414	0.042	0.533	0.250	-.121	0.620	-.272	0.558
0.132	-.499	0.412	0.338	0.072	-.002	0.843	0.129	-.311	0.046	-.332	0.520	0.297	0.206	-.029
-.201	0.458	0.104	0.300	-.236	-.078	-.056	0.635	-.291	-.101	-.434	-.212	-.441	-.155	-.224
0.035	-.233	0.051	-.575	0.068	0.108	-.169	-.392	0.488	0.051	0.274	-.254	0.313	-.214	0.439
0.469	-.248	-.404	0.193	0.051	0.679	0.003	-.128	0.032	0.765	0.281	-.064	0.585	-.042	0.554
0.138	-.062	-.607	-.303	0.102	0.059	-.376	-.605	0.253	0.262	0.989	0.058	0.252	-.175	0.131
0.048	-.275	-.077	0.272	0.435	-.122	0.505	-.102	-.502	-.121	0.251	0.969	-.006	0.302	-.433
0.415	-.347	-.146	0.053	0.107	0.476	0.302	-.427	0.072	0.543	0.285	0.052	0.957	-.167	0.632
-.154	-.251	0.125	0.399	0.076	-.255	0.253	0.053	-.166	-.208	-.148	0.499	-.246	0.956	-.483
0.462	-.252	-.135	-.266	-.092	0.582	0.000	-.322	0.333	0.554	0.168	-.484	0.796	-.491	0 911

Table 2-7. Eigenvalues of Covariance Matrices.

LSS Research Models		CSS Pretest Models		CSS Posttest Models		Combined LSS and CSS	
Matrix Rank =	6	Matrix Rank =	7	Matrix Rank =	7	Matrix Rank =	20
Singular Value # 1 =	5.69675E-01	Singular Value # 1 =	9.33333E-01	Singular Value # 1 =	5.82411E-01	Singular Value # 1 =	5.99062E-01
Singular Value # 2 =	3.37463E-01	Singular Value # 2 =	2.93328E-01	Singular Value # 2 =	5.90164E-02	Singular Value # 2 =	1.25285E-01
Singular Value # 3 =	2.26366E-01	Singular Value # 3 =	1.70940E-01	Singular Value # 3 =	4.66032E-02	Singular Value # 3 =	1.20427E-01
Singular Value # 4 =	1.25469E-01	Singular Value # 4 =	7.52265E-02	Singular Value # 4 =	2.79430E-02	Singular Value # 4 =	1.10258E-01
Singular Value # 5 =	8.88634E-02	Singular Value # 5 =	4.27559E-02	Singular Value # 5 =	1.36299E-02	Singular Value # 5 =	6.93005E-02
Singular Value # 6 =	3.03972E-02	Singular Value # 6 =	2.19202E-02	Singular Value # 6 =	3.39969E-03	Singular Value # 6 =	5.81738E-02
Singular Value # 7 =	0.00000E+00	Singular Value # 7 =	1.02209E-02	Singular Value # 7 =	1.22147E-03	Singular Value # 7 =	3.24544E-02
Singular Value # 8 =	0.00000E+00	Singular Value # 8 =	0.00000E+00	Singular Value # 8 =	0.00000E+00	Singular Value # 8 =	2.39023E-02
Singular Value # 9 =	0.00000E+00	Singular Value # 9 =	0.00000E+00	Singular Value # 9 =	0.00000E+00	Singular Value # 9 =	2.36756E-02
Singular Value #10 =	0.00000E+00	Singular Value #10 =	0.00000E+00	Singular Value #10 =	0.00000E+00	Singular Value #10 =	1.57983E-02
Singular Value #11 =	0.00000E+00	Singular Value #11 =	0.00000E+00	Singular Value #11 =	0.00000E+00	Singular Value #11 =	1.03530E-02
Singular Value #12 =	0.00000E+00	Singular Value #12 =	0.00000E+00	Singular Value #12 =	0.00000E+00	Singular Value #12 =	6.22819E-03
Singular Value #13 =	0.00000E+00	Singular Value #13 =	0.00000E+00	Singular Value #13 =	0.00000E+00	Singular Value #13 =	5.35949E-03
Singular Value #14 =	0.00000E+00	Singular Value #14 =	0.00000E+00	Singular Value #14 =	0.00000E+00	Singular Value #14 =	4.14099E-03
Singular Value #15 =	0.00000E+00	Singular Value #15 =	0.00000E+00	Singular Value #15 =	0.00000E+00	Singular Value #15 =	3.65832E-03
Singular Value #16 =	0.00000E+00	Singular Value #16 =	0.00000E+00	Singular Value #16 =	0.00000E+00	Singular Value #16 =	2.39505E-03
Singular Value #17 =	0.00000E+00	Singular Value #17 =	0.00000E+00	Singular Value #17 =	0.00000E+00	Singular Value #17 =	9.17409E-04
Singular Value #18 =	0.00000E+00	Singular Value #18 =	0.00000E+00	Singular Value #18 =	0.00000E+00	Singular Value #18 =	3.70913E-04
Singular Value #19 =	0.00000E+00	Singular Value #19 =	0.00000E+00	Singular Value #19 =	0.00000E+00	Singular Value #19 =	2.61047E-04
Singular Value #20 =	0.00000E+00	Singular Value #20 =	0.00000E+00	Singular Value #20 =	0.00000E+00	Singular Value #20 =	1.30769E-04
Singular Value #21 =	0.00000E+00	Singular Value #21 =	0.00000E+00	Singular Value #21 =	0.00000E+00	Singular Value #21 =	0.00000E+00
Singular Value #22 =	0.00000E+00	Singular Value #22 =	0.00000E+00	Singular Value #22 =	0.00000E+00	Singular Value #22 =	0.00000E+00
Singular Value #23 =	0.00000E+00	Singular Value #23 =	0.00000E+00	Singular Value #23 =	0.00000E+00	Singular Value #23 =	0.00000E+00
Singular Value #24 =	0.00000E+00	Singular Value #24 =	0.00000E+00	Singular Value #24 =	0.00000E+00	Singular Value #24 =	0.00000E+00
Singular Value #25 =	0.00000E+00	Singular Value #25 =	0.00000E+00	Singular Value #25 =	0.00000E+00	Singular Value #25 =	0.00000E+00
Singular Value #26 =	0.00000E+00	Singular Value #26 =	0.00000E+00	Singular Value #26 =	0.00000E+00	Singular Value #26 =	0.00000E+00
Singular Value #27 =	0.00000E+00	Singular Value #27 =	0.00000E+00	Singular Value #27 =	0.00000E+00	Singular Value #27 =	0.00000E+00
Singular Value #28 =	0.00000E+00	Singular Value #28 =	0.00000E+00	Singular Value #28 =	0.00000E+00	Singular Value #28 =	0.00000E+00
Singular Value #29 =	0.00000E+00	Singular Value #29 =	0.00000E+00	Singular Value #29 =	0.00000E+00	Singular Value #29 =	0.00000E+00
Singular Value #30 =	0.00000E+00	Singular Value #30 =	0.00000E+00	Singular Value #30 =	0.00000E+00	Singular Value #30 =	0.00000E+00
Trace =	1.377	Trace =	1.547	Trace =	0.734	Trace =	1.210

the relative degrees of uncertainty represented in the four databases may be compared. The pretest models reflect the largest uncertainty as expected, while posttest models reflect the smallest uncertainty. The LSS database involving "research" models lies between the two extremes while the combined database reflects an average of the three. The uncertainty of pretest CSS models is seen to be approximately twice that of the posttest models, while that of the combined database is slightly less than that of the CSS models.

3. DAMPING ESTIMATION AND UNCERTAINTY

Although recent advances have improved the ability to model damping for certain types of structures, there are no general tools available for modeling damping as there are for modeling mass and stiffness; damping is estimated from experimental data. The rationale for quantifying damping uncertainty is therefore different. Instead of defining damping uncertainty in terms of the variability between analytical predictions and experimental measurements for a class of structures, damping uncertainty is defined in terms of the variability among experimental estimates for a particular structure.

The variability in damping estimates arises from many sources, all related to the way damping is commonly defined. In structural dynamics, damping is defined in terms of equivalent viscous damping, More specifically it is defined in terms of modal damping, analogous to the way modal mass and stiffness are defined. Unlike the modal mass and stiffness matrices, however, which are diagonal by virtue of the modal transformation, the modal damping matrix is not diagonal. In general, the off–diagonal elements are the same order of magnitude as the diagonal elements. Nevertheless, the off–diagonal elements are typically neglected, while the diagonal elements are expressed in terms of a critical damping ratio consistent with the assumption that the equations of motion are uncoupled in modal coordinates. The term "modal damping" is thereby taken to mean the critical damping ratio of an equivalent linear single degree of freedom system with viscous damping.

With such an oversimplified damping model, it is not surprising that estimates of its parameters exhibit a high degree of variability. Modal damping represents the energy dissipation per cycle in a particular mode, assuming that the mode vibrates independently of the other structural modes. The modal damping ratio, ζ_j, is proportional to the ratio of modal dissipative energy, D_j, to modal kinetic energy, K_j, which is constant in the case of linear viscous damping.

$$\zeta_j = \frac{1}{4\pi}\left[\frac{D_j}{K_j}\right]$$

In general, the ratio of dissipative to kinetic energy is not constant, but depends on other factors including amplitude, frequency and temperature. Nevertheless, in the absence of more accurate models, the equivalent viscous damping model is commonly accepted with the understanding that the parameters of that model must be determined experimentally, often with a large degree of uncertainty.

3.1 Estimation of a Modal Damping Matrix

A full modal damping matrix has several uses: (1) off–diagonal terms may couple modes when their frequencies are closely spaced [3–1] in which case those terms should be included in response computations; (2) the full modal damping matrix is required to synthesize structural damping from substructure tests [3–2]; and (3) the full modal damping matrix enables the parameters of a physical damping model to be estimated, thereby revealing the type and distribution of damping present in the structure. The first two uses are discussed in the literature; the third is discussed in Section 3.2.

3.1.1 Perturbation Analysis

A method for estimating the full modal damping matrix of a structure based on experimentally measured complex modes was first published in Reference [3–3]. Implicit in the derivation of the method is the assumption that the mass matrix used in the computation of the modal damping matrix is the "true" mass matrix, i.e. that the analytical mass matrix accurately represents the actual mass distribution of the structure in the sense that the real parts of the complex modes diagonalize the matrix, and the real and imaginary parts of each complex mode are orthogonal with respect to it. In reality these assumptions are only true in an approximate sense. The orthogonality of the test modes with respect to themselves through the analytical mass matrix (self–orthogonality) and the orthogonality of the test modes with respect to the analytical modes (cross–orthogonality) are only approximately diagonal. This derivation extends the original derivation of Reference [3–3] to account for these facts.

Equations of motion are first written in the physical (nodal) x–coordinate system:

$$M\ddot{x} + C\dot{x} + Kx = 0 \qquad (3–1)$$

$$\begin{bmatrix} C & M \\ M & 0 \end{bmatrix} \begin{Bmatrix} \dot{x} \\ \ddot{x} \end{Bmatrix} + \begin{bmatrix} K & 0 \\ 0 & -M \end{bmatrix} \begin{Bmatrix} x \\ \dot{x} \end{Bmatrix} = 0 \tag{3–2}$$

or

$$A\dot{y} + By = 0 \tag{3–3}$$

where

$$y = \begin{Bmatrix} x \\ \dot{x} \end{Bmatrix} \tag{3–4}$$

The first order eigenproblem is then written as

$$(B + \Lambda_j A)\Phi_j = 0 \tag{3–5}$$

where

$$y = \Phi z \tag{3–6}$$

and

$$\Phi = \begin{bmatrix} \phi & \phi^* \\ \phi\lambda & \phi^*\lambda^* \end{bmatrix} \tag{3–7}$$

In this chapter, ϕ and ω are used to represent the damped modal displacements and frequencies, respectively, while ϕ_R denotes the real part of the complex modal displacements, ϕ. The asterisks denote complex conjugates. The matrix of complex modes, Φ, diagonalizes both A and B. In particular

$$\Phi^T A \Phi = \begin{bmatrix} \phi^T & \lambda\phi^T \\ \phi^{*T} & \lambda^*\phi^{*T} \end{bmatrix} \begin{bmatrix} C & M \\ M & 0 \end{bmatrix} \begin{bmatrix} \phi & \phi^* \\ \phi\lambda & \phi^*\lambda^* \end{bmatrix} = \text{Diagonal} \tag{3–8}$$

where

$$\lambda_j = \sigma_j + i\omega_j \tag{3–9}$$

$$\phi_j = \phi_{R_j} + \delta\phi_{R_j} + i\delta\phi_{I_j} \approx \phi_{R_j} + i\delta\phi_{I_j} \tag{3–10}$$

and where $i = \sqrt{-1}$. Here it is assumed that ϕ_R are the undamped real modes such that

$$\phi_R^T M \phi_R = I \qquad \text{[modal mass matrix (identity)]} \tag{3–11a}$$

$$\phi_R^T C \phi_R = \xi \qquad \text{[modal damping matrix (full)]} \tag{3–11b}$$

$$\phi_R^T K \phi_R = \lambda_o = \omega_o^2 \qquad \text{[modal stiffness matrix (diagonal)]} \tag{3–11c}$$

The subscript "o" denotes undamped eigenvalues and modal frequencies. Perturbation analysis leads to the following two equations

$$\xi_{jk} = \phi_{R_j}^T C\phi_{R_k} = -(\sigma_j + \sigma_k)\,\phi_{R_j}^T M\phi_{R_k} + \omega_k\,\phi_{R_j}^T M\delta\phi_{I_k} + \omega_j\,\delta\phi_{I_j}^T M\phi_{R_k} \tag{3–12}$$

$$\omega_j\,\phi_{R_j}^T M\delta\phi_{I_k} + \omega_k\,\delta\phi_{I_j}^T M\phi_{R_k} = 0 \tag{3–13}$$

In matrix from these equations may be written as

$$\xi = 2\zeta\omega + \beta\omega + \omega\beta^T \tag{3–14}$$

$$\omega\beta + \beta^T\omega = 0 \tag{3–15}$$

where $2\zeta\omega$ is the diagonal portion of the modal damping matrix, ξ, and

$$\beta_{jk} = \phi_{R_j}^T M\delta\phi_{I_k} \tag{3–16}$$

The requirement that $\xi_{jj} = 2\zeta_{jj}\omega_j$ implies

$$\beta_{jj} = \phi_{R_j}^T \, M\delta_{I_j} = 0 \tag{3–17}$$

which establishes the second normalization condition on the complex mode

$$\phi_j = \phi_{R_j} + i\delta\phi_{I_j} \tag{3–10}$$

the first being Equation (3–11a). This is a condition which heretofore has not been recognized when "converting" experimentally derived complex modes to real modes for comparison with undamped modal analysis. Implementation of this condition is addressed in Section 3.1.2.

Equations (3–14) and (3–15) may be derived from the two equations presented in Reference [3–3]. At this point it is desirable to distinguish between the analytical mass matrix, ^oM, and M such that (see Section 2.1.1)

$$M = {}^oM + \Delta M \tag{2–3b}$$

In addition, ϕ_R and $\delta\phi_I$ are expanded into linear combinations of the analytical (real) modes which are designated $^o\phi_R$. Then

$$\phi_{R_j} = {}^o\phi_R \psi_j \tag{3–18}$$

$$\delta\phi_{I_k} = {}^o\phi_R \gamma_k \tag{3–19}$$

Then (3–16) becomes

$$\beta_{jk} = \psi_j^T \, {}^o\phi_R^T \, ({}^oM + \Delta M) \, {}^o\phi_R \gamma_k$$

$$= \psi_j^T \, (I + \Delta m) \, \gamma_k \tag{3–20}$$

where

$$ {}^{o}\phi_R^{T\,o}M\phi_R = \left[{}^{o}\phi_R^{T\,o}M^{o}\phi_R \right] \psi = \psi \tag{3–21} $$

$$ {}^{o}\phi_R^{T\,o}M\delta\phi_I = \left[{}^{o}\phi_R^{T\,o}M^{o}\phi_R \right] \gamma = \gamma \tag{3–22} $$

Finally, from Equation (2–20) of Chapter 2

$$ \Delta m = (I - \psi) + (I - \psi)^T \tag{2–20} $$

From (3–12) the off–diagonal terms of the modal damping matrix, ξ, are found to be

$$ \xi_{jk} = \omega_k \beta_{jk} + \omega_j \beta_{kj} \tag{3–23} $$

An alternate expression found by combining Equations (3–12) and (3–13) is

$$ \xi_{jk} = (\omega_k - \omega_j)(\beta_{jk} - \beta_{kj}) \tag{3–24} $$

Ideally, Equations (3–23) and (3–24) should give the same result. In reality, however, measurement error affects the complex modes ϕ so that in place of (3–13) one has

$$ \epsilon_{jk} = \omega_j \beta_{jk} + \omega_k \beta_{kj} \tag{3–25} $$

where ϵ_{jk} is considered to be a residual bias error. It is desirable that

$$ \epsilon_{jk} << \xi_{jk} \tag{3–26} $$

To the extent that Equation (3–26) is true, one can expect Equation (3–24) to be true also.

Unfortunately, (3–26) has not been found to hold true with experimentally derived complex eigenvalues and eigenvectors. With the proper normalization of ϕ_R, it does hold true with analytically simulated "data" (complex eigenvalues and eigenvectors

derived from Equation (3–5)). When ϵ_{jk} is not zero, it can be used to obtain a correction term for ξ_{jk} in Equation (3–24).

The correction term is derived by first rewriting Equations (3–24) and (3–25) as

$$\hat{\xi}_{jk} = \omega_k \hat{\beta}_{jk} + \omega_j \hat{\beta}_{kj} \tag{3–27a}$$

$$\hat{\epsilon}_{jk} = \omega_j \hat{\beta}_{jk} + \omega_k \hat{\beta}_{kj} \tag{3–27b}$$

where

$$\hat{\beta}_{jk} = \beta_{jk} + \Delta\beta_{jk} \tag{3–28a}$$

$$\hat{\beta}_{kj} = \beta_{kj} + \Delta\beta_{kj} \tag{3–28b}$$

and then solving for $\Delta\beta_{jk}$ and $\Delta\beta_{kj}$. Substitution of (3–28) into (3–27) gives

$$\hat{\xi}_{jk} = \xi_{jk} + \omega_k \Delta\beta_{jk} + \omega_j \Delta\beta_{kj} \tag{3–29a}$$

$$\hat{\epsilon}_{jk} = \omega_j \Delta\beta_{jk} + \omega_k \Delta\beta_{kj} \tag{3–29b}$$

These equations cannot be solved directly for $\Delta\beta_{jk}$ and $\Delta\beta_{kj}$ because ξ_{jk} is a third unknown and there are only two equations. This problem can be circumvented by imposing an additional condition on $\Delta\beta_{jk}$ and $\Delta\beta_{kj}$, namely that the sum of their squares be minimized, i.e. that $\Delta\beta_{jk}$ and $\Delta\beta_{kj}$ are chosen such that the cost function

$$J = \Delta\beta_{jk}^2 + \Delta\beta_{kj}^2 \tag{3–30}$$

is minimized. Substitution of (3–29b) into (3–30) gives

$$J = \Delta\beta_{jk}^2 + \left[\frac{\hat{\epsilon}_{jk}}{\omega_k} - \frac{\omega_j}{\omega_k} \Delta\beta_{jk} \right]^2 \tag{3–31}$$

Minimization of J with respect to $\Delta\beta_{jk}$ leads to

$$\frac{\partial J}{\partial(\Delta\beta_{jk})} = 2 \left[1 + \frac{\omega_j^2}{\omega_k} \right] \Delta\beta_{jk} - \frac{2\omega_j \hat{\epsilon}_{jk}}{\omega_k^2} = 0 \tag{3–32}$$

which gives

$$\Delta\beta_{jk} = \left[\frac{\omega_j}{\omega_j^2 + \omega_k^2} \right] \hat{\epsilon}_{jk} \tag{3–33a}$$

Substitution of (3–33a) into (3–29b) leads to the companion equation

$$\Delta\beta_{kj} = \left[\frac{\omega_k}{\omega_j^2 + \omega_k^2} \right] \hat{\epsilon}_{jk} \tag{3–33b}$$

Substitution of (3–33) into (3–29a) then gives

$$\xi_{jk} = \hat{\xi}_{jk} - 2 \left[\frac{\omega_j \ \omega_k}{\omega_j^2 + \omega_k^2} \right] \hat{\epsilon}_{jk} \tag{3–34}$$

3.1.2 Data Conditioning

Before Equations (3–27) and (3–34) are applied, several steps are taken to condition the data consisting of experimentally derived complex eigenvectors and the analytical mass matrix. They are as follows:

1. Normalize the complex modes so as to satisfy Equation (3–17);
2. Orthogonalize the real parts of the complex modes; and
3. Adjust the analytical mass matrix to better represent the "true" mass matrix.

These steps are outlined in the subsections which follow.

3.1.2.1 Normalization of Complex Modes

Since complex modes have both a real and an imaginary part, they require two normalization conditions compared with only one condition for real (undamped) modes. The two conditions are chosen as

$$\phi_{R_j}^T \, M \, \phi_{R_j} = 1$$

$$\phi_{R_j}^T \, M \, \delta\phi_{I_j} = 0$$

from Equations (3–11a) and (3–17). For the time being, it will be assumed that M is known.

To begin the normalization process, a complex eigenvector is first normalized such that the element with the greatest magnitude has the value (1,0) (i.e. the real part is unity and the imaginary part is zero). The jth complex eigenvector normalized in this way is designated

$$\hat{\phi}_j = \hat{\phi}_{R_j} + i\delta\hat{\phi}_{I_j} \qquad (3–35)$$

A new eigenvector

$$\phi_j = \phi_{R_j} + i\delta\phi_{I_j} \qquad (3–36)$$

is sought which satisfies the orthogonality condition

$$\phi_{R_j}^T \, M \, \delta\phi_{I_j} = 0 \tag{3–17}$$

The real and imaginary parts of (3–35) can be written in terms of amplitude and phase, where the amplitude and phase of the kth element of the jth eigenvector are

$$\hat{A}_{kj} = (\hat{\phi}_{R_{kj}}^2 + \delta\hat{\phi}_{I_{kj}}^2)^{1/2} \tag{3–37a}$$

$$\hat{\varphi}_{kj} = \tan^{-1}(\delta\hat{\phi}_{I_{kj}} / \hat{\phi}_{R_{kj}}) \tag{3–37b}$$

Then

$$\hat{\phi}_{R_{kj}} = \hat{A}_{kj} \cos \hat{\varphi}_{kj} \tag{3–38a}$$

$$\delta\hat{\phi}_{I_{kj}} = \hat{A}_{kj} \sin \hat{\varphi}_{kj} \tag{3–38b}$$

The problem is to find the rotation angle, φ_{oj}, such that

$$\phi_{R_{kj}} = \hat{A}_{kj} \cos(\hat{\varphi}_{kj} - \varphi_{oj}) \tag{3–39a}$$

$$\delta\phi_{I_{kj}} = \hat{A}_{kj} \sin(\hat{\varphi}_{kj} - \varphi_{oj}) \tag{3–39b}$$

satisfy Equation (3–17). This is accomplished by substitution of (3–39) into (3–17) which gives

$$\sum_k \sum_l \hat{A}_{kj} \, \hat{A}_{lj} \, M_{kl} \cos(\hat{\varphi}_{kj} - \hat{\varphi}_{oj}) \sin(\hat{\varphi}_{lj} - \varphi_{oj}) = 0 \tag{3–40}$$

The rotation angle, φ_{oj}, for the jth mode is found after some algebraic and trigonometric manipulation to be

$$\varphi_{oj} = \frac{1}{2}\tan^{-1}\left[\frac{2\sum_k\sum_l M_{kl}\,\hat{\phi}_{R_{kj}}\,\delta\hat{\phi}_{I_{lj}}}{\sum_k\sum_l M_{kl}\,(\hat{\phi}_{R_{kj}}\,\hat{\phi}_{R_{lj}} - \delta\hat{\phi}_{I_{kj}}\,\delta\hat{\phi}_{I_{lj}})}\right]$$

$$= \frac{1}{2}\tan^{-1}\left[\frac{2\,\hat{\phi}_{R_j}^T M\,\delta\hat{\phi}_{I_j}}{\hat{\phi}_{R_j}^T M\hat{\phi}_{R_j} - \delta\hat{\phi}_{I_j}^T M\delta\hat{\phi}_{I_j}}\right] \qquad (3\text{–}41)$$

This result is similar to the normalization used by Smith at JPL [3–4], where the complex vector

$$X_{kj} = X_{R_{kj}} + iX_{I_{kj}} = \mu_{kj}\,e^{i\varphi_{oj}} + \varepsilon_{kj} \qquad (3\text{–}42)$$

is normalized so as to minimize

$$E_j = \sum_k |\varepsilon_{kj}|^2 \qquad (3\text{–}43)$$

resulting in

$$\varphi_{oj} = \frac{1}{2}\arg\sum_k X_{kj}^2$$

$$= \frac{1}{2}\tan^{-1}\left[\frac{2\sum_k X_{R_{kj}}\,X_{I_{kj}}}{\sum_k (X_{R_{kj}}^2 - X_{I_{kj}}^2)}\right]$$

$$= \frac{1}{2}\tan^{-1}\left[\frac{2\,X_{R_j}^T\,X_{I_j}}{X_{R_j}^T\,X_{R_j} - X_{I_j}^T\,X_{I_j}}\right] \qquad (3\text{–}44)$$

In view of (3–17), Smith's normalization may be interpreted as satisfying the condition

$$X_{R_j}^T X_{I_j} = 0 \tag{3–45}$$

or in the present notation

$$\phi_{R_j}^T \delta\phi_{I_j} = 0 \tag{3–46}$$

as opposed to

$$\phi_{R_j}^T M \delta\phi_{I_j} = 0 \tag{3–17}$$

In other words, the mass matrix is used as a weighting matrix on the eigenvector elements in the present normalization procedure, whereas all eigenvector elements are weighted equally in Smith's procedure. Aside from the perturbation analysis whereby (3–17) was derived, the present method is attractive because of the weighting property. Eigenvector elements (mode shape measurements) corresponding to light appendages, for example, are deemphasized by this procedure. In addition, the present procedure requires that the eigenvectors be complete in the sense that they correspond to a complete mass matrix.

3.1.2.2 Orthogonalization of Real Modes

In some cases, the self–orthogonality of real test modes can be improved by deriving a new set of modes which is a linear combination of the original set. The method proposed by Targoff [3–5] is employed here. It is briefly outlined as follows:

Let $\hat{\phi}_R$ represent the original set of real modes (i.e. real parts of complex modes). A new set of orthogonal modes, ϕ_R, is sought such that

$$\phi_R^T M \phi_R = I \tag{3–47}$$

The original modal matrix, $\hat{\phi}_R$, is expressed as a linear combination of the modes in ϕ_R, i.e.

$$\hat{\phi}_R = \phi_R \hat{C} \tag{3–48}$$

where

$$\hat{C} = I + \alpha \tag{3–49}$$

is symmetric (not to be confused with the damping matrix, C, used elsewhere in this report).

The self–orthogonality matrix of the original modes, [OR] is given by

$$[OR] = \hat{\phi}_R^T M \hat{\phi}_R \tag{3–50}$$

where $\hat{\phi}_{R_j}$ has been normalized to unit modal mass such that

$$\hat{\phi}_{R_j}^T M \hat{\phi}_{R_j} = 1 \tag{3–51}$$

Let

$$\hat{S} = [OR] - I \tag{3–52}$$

Then α has the series representation

$$\alpha = \frac{1}{2}\hat{S} + \frac{1}{8}\hat{S}^2 + \frac{1}{32}\hat{S}^3 + \ldots + \frac{1}{2^{(2n-1)}}\hat{S}^n + \ldots \tag{3–53}$$

The matrix ϕ_R is then obtained by inverting Equation (3–48)

$$\phi_R = \hat{\phi}_R \hat{C}^{-1} \tag{3–54a}$$

It is further assumed that this real transformation can be applied to the complex modes as well such that

$$\phi_I = \hat{\phi}_I \hat{C}^{-1} \tag{3–54b}$$

3.1.2.3 Adjustment of Analytical Mass Matrix

Throughout this chapter, and in particular Equations (3–16) and (3–17), M has represented the "true" mass distribution of the structure. Equation (2–20) suggests a way of updating the original analytical mass matrix, ^oM, to obtain an estimate of M, where

$$M = {}^oM + \Delta M \tag{2–3b}$$

Given that

$$m = {}^o\phi^T M {}^o\phi = {}^o\phi^T ({}^oM + \Delta M) {}^o\phi = I + \Delta m \tag{3–55}$$

it follows that an estimate of ΔM is obtained by recognizing that

$${}^o\phi^T \Delta M {}^o\phi = ({}^o\phi^T {}^oM {}^o\phi) \Delta m ({}^o\phi^T {}^oM {}^o\phi)$$

from which

$$\Delta M = {}^oM {}^o\phi \Delta m {}^o\phi^T {}^oM \tag{3–56}$$

where

$$\Delta m = (I - \psi) + (I - \psi)^T \tag{2–20}$$

and

$$\psi = {}^o\phi^T {}^oM \phi_R \tag{3–57}$$

This estimate is nonunique and ΔM is singular to the extent that $^o\phi$ represents a truncated set of modes. Nevertheless, it may improve ^oM in some (if not all) cases.

3.1.2.4 Iterative Procedure

The foregoing discussion suggests an iterative procedure for evaluating the full modal damping matrix, ξ, based on experimentally derived complex modes. An iterative procedure is indicated because normalization and orthogonalization of the complex eigenvectors utilizes the "true" mass matrix, but adjustment of the analytical mass matrix to obtain an estimate of the "true" mass matrix depends on the eigenvectors. The iterative procedure involves using the analytical mass matrix as a first approximation to the "true" mass matrix, to obtain a properly normalized and orthogonal mode set, which is used to adjust the analytical mass matrix. The adjusted mass matrix is then used to renormalize and orthogonalize the eigenvectors. This process is continued to convergence, after which ξ is finally computed. The entire procedure is summarized below.

Step 1: Normalize the complex mode, $\hat{\phi}_j = \hat{\phi}_{R_j} + i\delta\hat{\phi}_{I_j}$ so that for each mode the element with the largest magnitude is (1,0).

Step 2: Set $M = {}^{o}M$ for the first iteration.

Step 3: Compute the rotation angle, φ_{oj}, for each mode, where

$$\varphi_{oj} = \frac{1}{2}\tan^{-1}\left[\frac{2\,\hat{\phi}_{R_j}^T M \delta\hat{\phi}_{I_j}}{\hat{\phi}_{R_j}^T M \hat{\phi}_{R_j} - \delta\hat{\phi}_{I_j}^T M \delta\hat{\phi}_{I_j}}\right] \tag{3–41}$$

Step 4: Compute ϕ_{R_j} and $\delta\phi_{I_j}$ for each mode where

$$\phi_{R_{kj}} = \hat{A}_{kj}\cos(\hat{\varphi}_{kj} - \varphi_{oj}) \tag{3–39a}$$

$$\delta\phi_{I_{kj}} = \hat{A}_{kj}\sin(\hat{\varphi}_{kj} - \varphi_{oj}) \tag{3–39b}$$

Step 5: Normalize $\phi_j = \phi_{R_j} + i\delta\phi_{I_j}$ for each mode such that

$$\phi_{R_j}^T M \phi_{R_j} = 1$$

Step 6: Set $\hat{\phi}_{R_j}$ and $\delta\hat{\phi}_{I_j}$ equal to ϕ_{R_j} and $\delta\phi_{I_j}$, respectively, for each mode obtained in Step 5.

Step 7: Orthogonalize $\hat{\phi}_R$ to obtain a new set of modes, ϕ_R, where

$$\phi_R = \hat{\phi}_R \hat{C}^{-1} \tag{3–54a}$$

$$\delta\phi_I = \delta\hat{\phi}_I \hat{C}^{-1} \tag{3–54b}$$

Step 8: Update the mass matrix

$$M = {}^oM + \Delta M \tag{2–36}$$

$$\Delta M = {}^oM {}^o\phi \Delta m {}^o\phi^T {}^oM \tag{3–56}$$

$$\Delta m = (I - \psi) + (I - \psi)^T \tag{3–20}$$

$$\psi = {}^o\phi^T {}^oM \phi_R \tag{3–57}$$

Step 9: Repeat Steps 3 – 8 to convergence and use Equation (3–34) to evaluate the full modal damping matrix, ξ.

3.1.3 Analytical Example

A 10–DOF analytical model was studied during the course of the investigation, as a means of better understanding applications involving actual test data. Of primary interest was the question of whether the complex mode data obtained by the ERA method contain useful information relative to damping, or whether the imaginary parts of the

complex modes are dominated by noise. It was hoped that analytical examples might provide some insight into what the imaginary parts of complex modes should look like for known distributions of damping.

An illustration of the 10–DOF analytical example is shown in Figure 3–1. Each of the ten masses and ten springs is assigned the value of unity. The dashpots are assigned values ranging linearly from 0.01 to 0.10 along the length of the spring mass chain. The ten modal frequencies and corresponding modal damping ratios are presented in Table 3–1. Table 3–2 compares the modal damping matrices obtained from

$$\xi = \phi_R^T C \phi_R \tag{3–11b}$$

with those obtained from Equation (3–14) subject to Equations (3–15) and (3–17). It is of interest to note that the comparison between the modal damping matrices computed by (3–27) and (3–14) is better for the lower modes than it is for the higher modes. Scatter plots of the modes in the complex plane (Figure 3–2) reveal that the imaginary parts of the modes are much larger in the higher modes, even though the modal damping remains less than 6%. All modes represented in these figures have been normalized such that the eigenvector element with the largest magnitude is set equal to (1,0) i.e. a real part of 1.0 and an imaginary part of 0.0. The rotation angle shown in each of the plots is the angle through which the mode must be rotated so that the real and imaginary parts of the modes are orthogonal with respect to the original analytical mass matrix. Equation (3–14) was derived by a perturbation method which assumes that $\delta\phi_I$ is much smaller than ϕ_R. Thus, when $\delta\phi_I$ is not small compared to ϕ_R, the perturbation results are no longer valid.

Another case of the same 10–DOF model was run in which the damping values were reduced by an order of magnitude. In this case, all of the imaginary parts of the modes were indeed small and Equations (3–27) and (3–14) were found to be in good agreement for all modes.

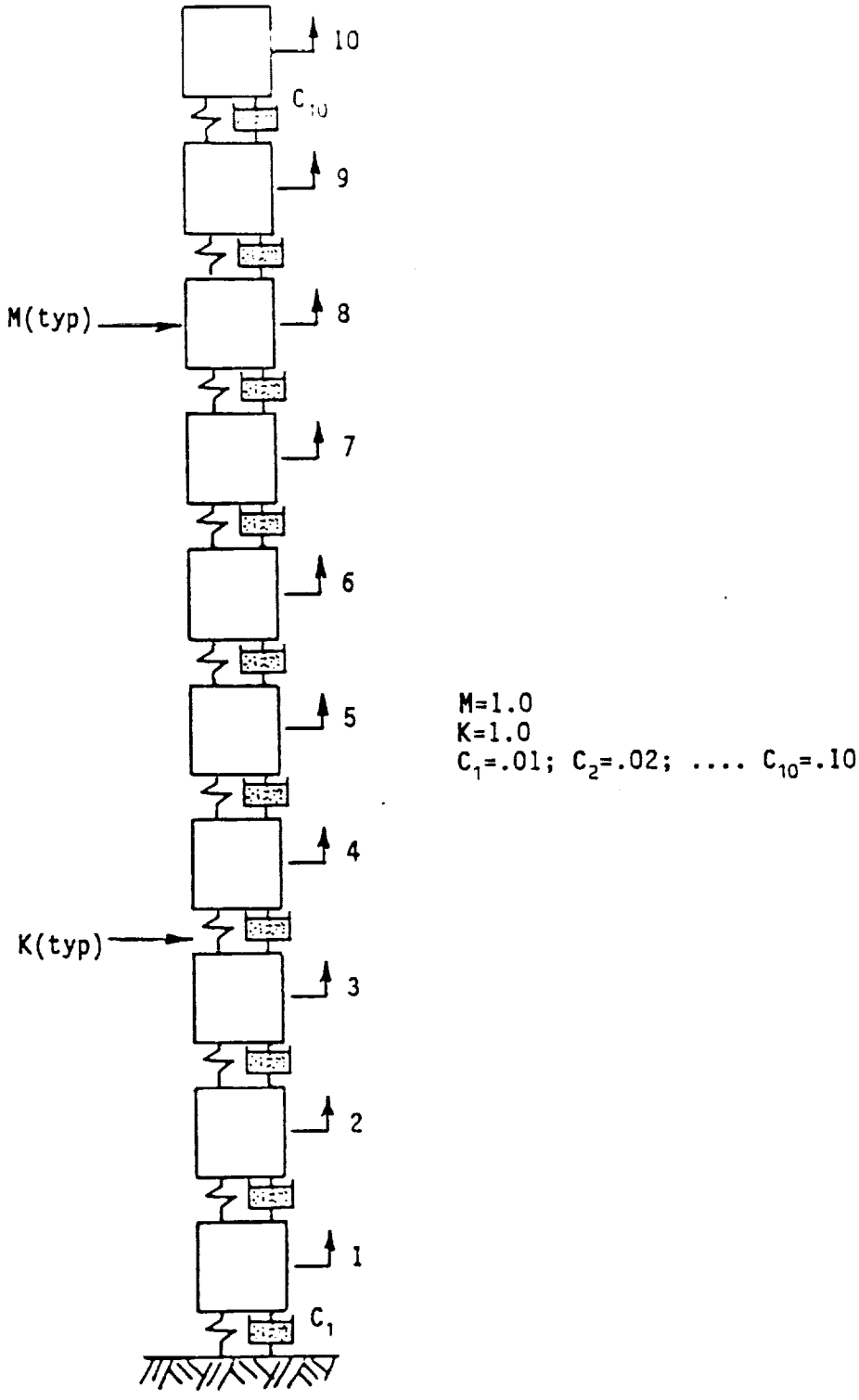

Figure 3–1. 10–DOF Analytical Example.

Table 3–1. Modal Frequencies and Damping for the 10–DOF Analytical Example.

****
**** ****
**** 10-DOF SYSTEM MODAL CHARACTERISTICS ****
**** ****
****

Mode No.	Frequency (Hz)	Damping (%)
1	0.02379	0.271
2	0.07083	1.229
3	0.11629	2.072
4	0.15915	2.856
5	0.19846	3.571
6	0.23336	4.203
7	0.26310	4.739
8	0.28709	5.165
9	0.30582	5.368
10	0.31015	5.847

Table 3–2. Comparison of Modal Damping Matrices for the 10–DOF Analytical Example.

$$\xi = \phi_R^T C \phi_R$$

MODE	1	2	3	4	5	6	7	8	9	10
1	0.0008	-0.0014	-0.0002	0.0003	-0.0001	-0.0002	-0.0001	0.0001	0.0000	0.0000
2	-0.0014	0.0109	-0.0069	0.0003	-0.0012	-0.0002	-0.0005	0.0001	-0.0002	0.0000
3	-0.0002	-0.0069	0.0303	0.0154	-0.0004	-0.0023	-0.0002	0.0008	-0.0001	0.0001
4	0.0003	0.0003	0.0154	0.0571	0.0263	0.0006	0.0033	-0.0002	0.0010	0.0001
5	-0.0001	-0.0012	-0.0004	0.0263	0.0890	-0.0382	-0.0014	0.0038	-0.0002	0.0000
6	-0.0002	-0.0002	-0.0023	0.0006	-0.0382	0.1231	-0.0499	0.0037	-0.0031	-0.0002
7	-0.0001	-0.0005	-0.0002	0.0033	-0.0014	-0.0499	0.1564	0.0593	-0.0085	-0.0084
8	0.0001	0.0001	0.0008	-0.0002	0.0038	0.0037	0.0593	0.1858	0.0688	-0.0339
9	0.0000	-0.0002	-0.0001	0.0010	-0.0002	-0.0031	-0.0085	0.0688	0.1955	0.0591
10	0.0000	0.0000	0.0001	0.0001	0.0000	-0.0002	-0.0084	-0.0339	0.0591	0.2429

$$\xi = 2\zeta\omega + (\phi_R^T M \delta\phi_I)\,\omega + \omega(\delta\phi_I^T M \phi_R)$$

MODE	1	2	3	4	5	6	7	8	9	10
1	0.0008	-0.0014	-0.0003	0.0003	-0.0001	-0.0002	-0.0001	0.0001	0.0000	0.0000
2	-0.0014	0.0109	-0.0069	0.0003	-0.0012	-0.0002	-0.0005	0.0001	-0.0002	0.0000
3	-0.0003	-0.0069	0.0303	0.0155	-0.0003	-0.0023	-0.0002	0.0008	-0.0001	0.0000
4	0.0003	0.0003	0.0155	0.0571	0.0263	0.0002	0.0031	-0.0001	0.0009	0.0002
5	-0.0001	-0.0012	-0.0003	0.0263	0.0891	-0.0385	0.0000	0.0032	0.0000	-0.0003
6	-0.0002	-0.0002	-0.0023	0.0002	-0.0385	0.1233	-0.0508	-0.0002	-0.0014	-0.0003
7	-0.0001	-0.0005	-0.0002	0.0031	0.0000	-0.0508	0.1567	0.0620	0.0022	-0.0158
8	0.0001	0.0001	0.0008	-0.0001	0.0032	-0.0002	0.0620	0.1863	0.0744	0.0133
9	0.0000	-0.0002	-0.0001	0.0009	0.0000	-0.0014	0.0022	0.0744	0.2063	0.0376
10	0.0000	0.0000	0.0000	0.0002	-0.0003	-0.0003	-0.0158	0.0133	0.0376	0.2279

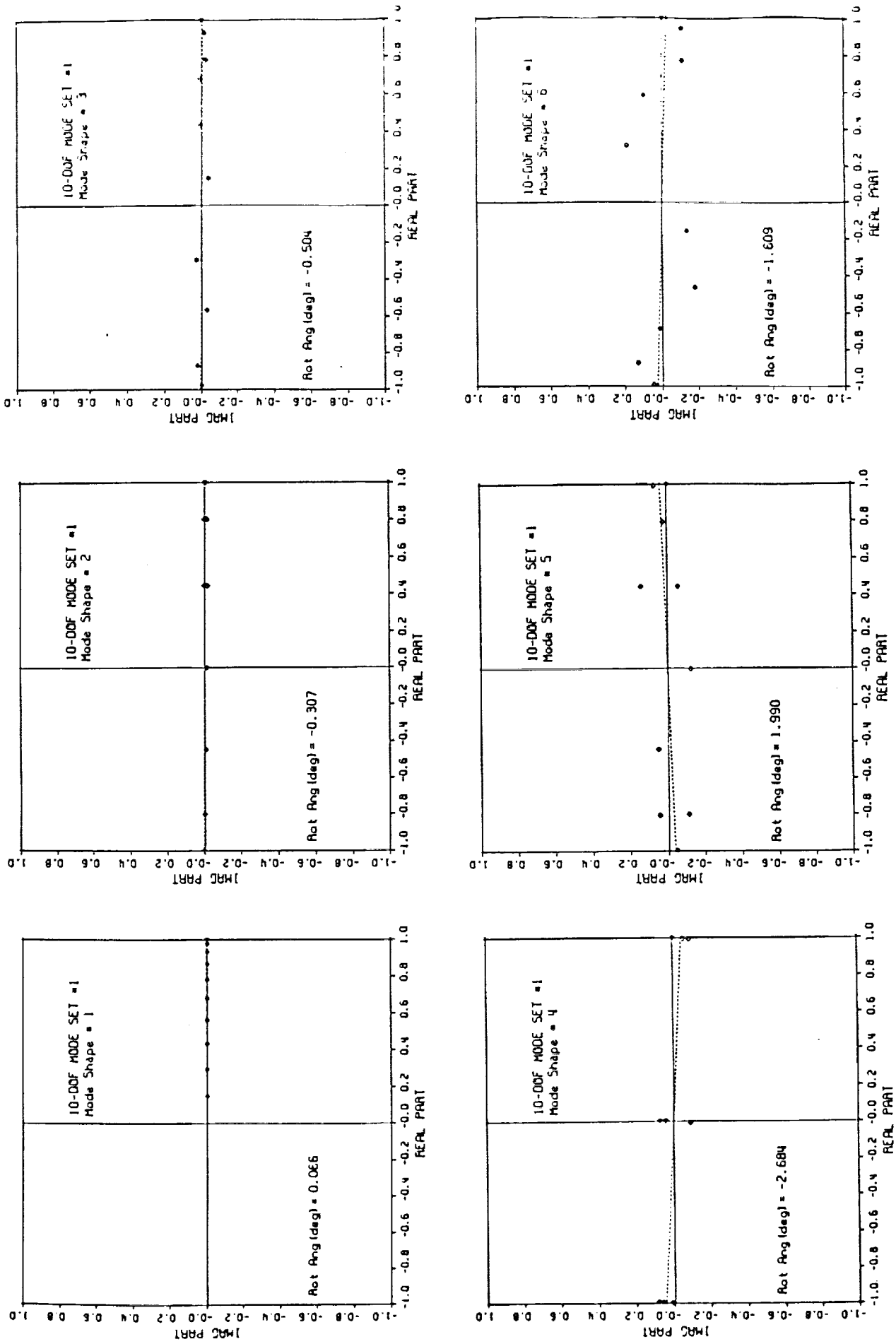

Figure 3–2. Scatter Plots for Complex Modes of the 10–DOF Analytical Example.

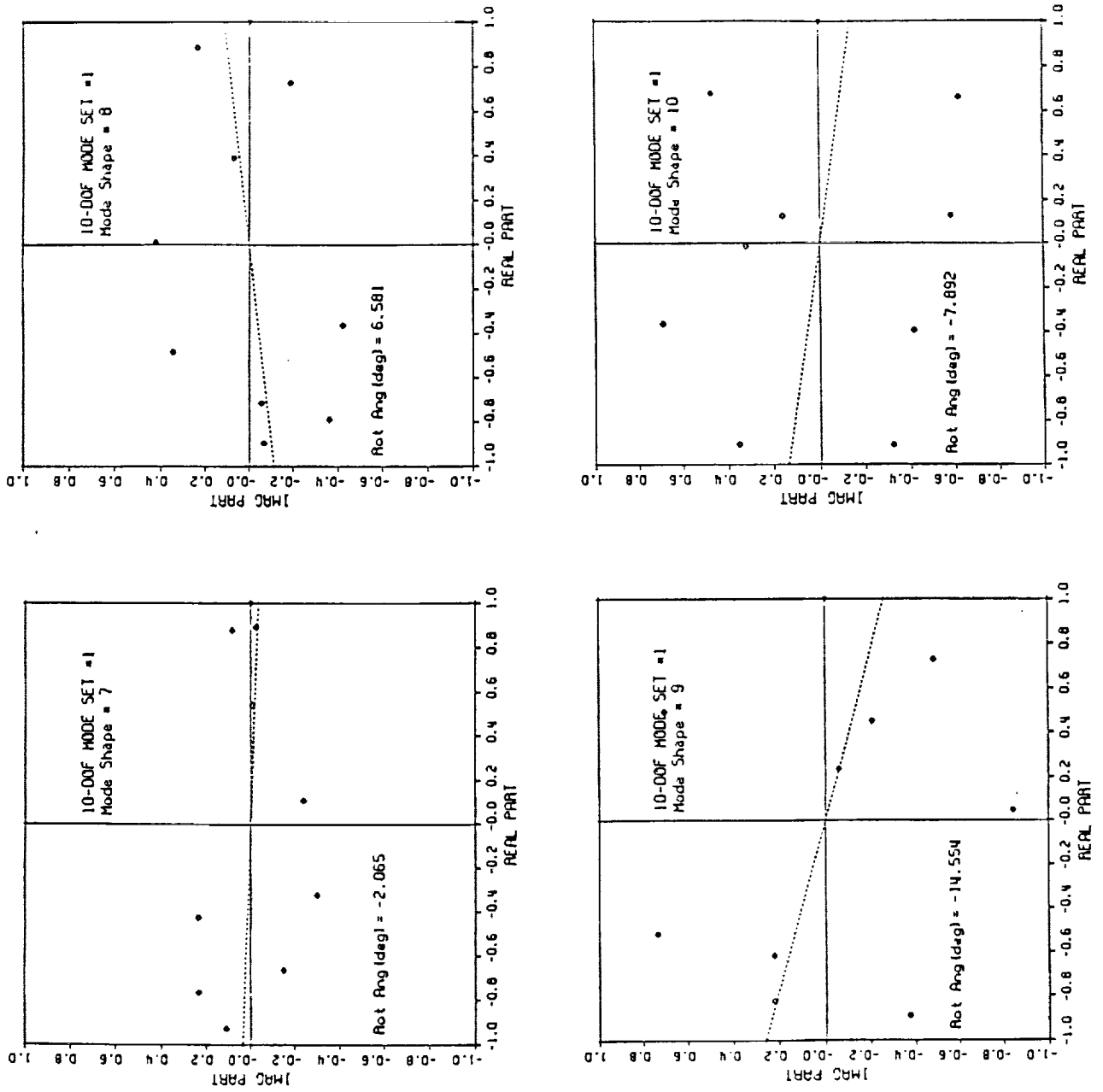

Figure 3–2. Scatter Plots of the Complex Modes of the 10–DOF Analytical Example (Cont'd).

3.1.4 Application to Real Structures

This section documents application of the methods described in Sections 3.1.1 and 3.1.2 to real structures. Data were provided by NASA Langley Research Center. Data provided for two structures, the LaRC Mini–mast Structure and Ten Bay Truss, included multiple ERA realizations of complex modes, and the TAM–type analytical models of the two structures. The ERA modes were generated by Richard Pappa with experimental data provided by Kenny Elliott.

Many realizations of the complex modes were provided. The characteristics of the mode sets varied considerably with respect to (a) the damping reflected in complex eigenvalues, (b) the orthogonality of the real parts of the modes with respect to the analytical mass matrix, and (c) the cross–orthogonality of the real parts of the ERA modes and analytical modes with respect to the analytical mass matrix.

Vibration test data for both structures were generated with multi–point random inputs. Three shakers at fixed locations were used to excite each of the structures. The shakers acted in pairs so that each structure was tested with three different shaker combinations: (1,2), (2,3) and (3,1). The ERA modes used to compute a modal damping matrix were all extracted from the same time–histories so that any variability among them must be attributed to variation among the ERA parameters selected to perform the modal extraction. In other words, none of the variability can be attributed to different time–history records, either from different time sequences or from different shaker configurations.

3.1.4.1 LaRC Mini–mast Structure

Damping estimates for two selected sets of modes were obtained for the Mini–mast Structure. Each set consists of three different realizations of the first five modes. The first set, called "Consistent Test Set" utilized data from Shaker Configuration (2,3) and was selected on the basis that all five modes were obtained from a single realization of the complex modes. See Figure 2–1. The second set, called "Constructed Test Set" was selected to maximize the cross–orthogonality between a given test mode and its analytical counterpart, without regard to maintaining consistent mode sets. In other words, the cross–orthogonality of each test mode was evaluated with respect to each of the

analytical modes. The test mode was then associated with the analysis mode with which it had the highest cross–orthogonality, and rank–ordered with all of the other test modes associated with that analysis mode, according to its cross–orthogonality. The first constructed mode set was then selected as Mode Numbers 1 through 5 with the highest cross–orthogonalities. The second constructed mode set was chosen as Mode Numbers 1 through 5 with the second highest cross–orthogonalities, etc.

Figures 3–3 through 3–7 present scatter plots in the complex plane of both sets of modes for Modes 1 through 5, respectively. As before, the complex modes in each case have been normalized such that the eigenvector element with the largest magnitude is set to (1, 0). It is of particular interest to note the relative magnitudes of the real and imaginary parts of the modes from mode to mode and set to set.

The complex test modes were first conditioned before being used to compute the modal damping matrix. In addition, it was found that with real test data, Equation (3–15) is not satisfied. Thus, the matrix $\hat{\xi}$ was corrected by adjusting each element of $\hat{\xi}$ according to Equation (3–34). Normalization of ξ_{jk} to remove it's frequency dependence produces a full matrix, ζ, whose elements are

$$\zeta_{jk} = \xi_{jk}/2\sqrt{\omega_j \omega_k} \tag{3–58}$$

The diagonal elements, ζ_{jj}, of this matrix are the familiar modal damping ratios.

Table 3–3 presents three sets of modal orthogonality matrices for the consistent test set, evaluated before and after eigenvector conditioning. These matrices correspond to the following:

$^{o}\phi_R^T {}^{o}M\phi_R$ (Cross–orthogonality of real analysis and test modes with respect to analytical mass matrix)

$\phi_R^T M \phi_R$ (Self–orthogonality of real test modes with respect to the "true" mass matrix)

$\phi_R^T M \delta\phi_I$ (Cross–orthogonality of real and imaginary parts of test modes with respect to "true" mass matrix)

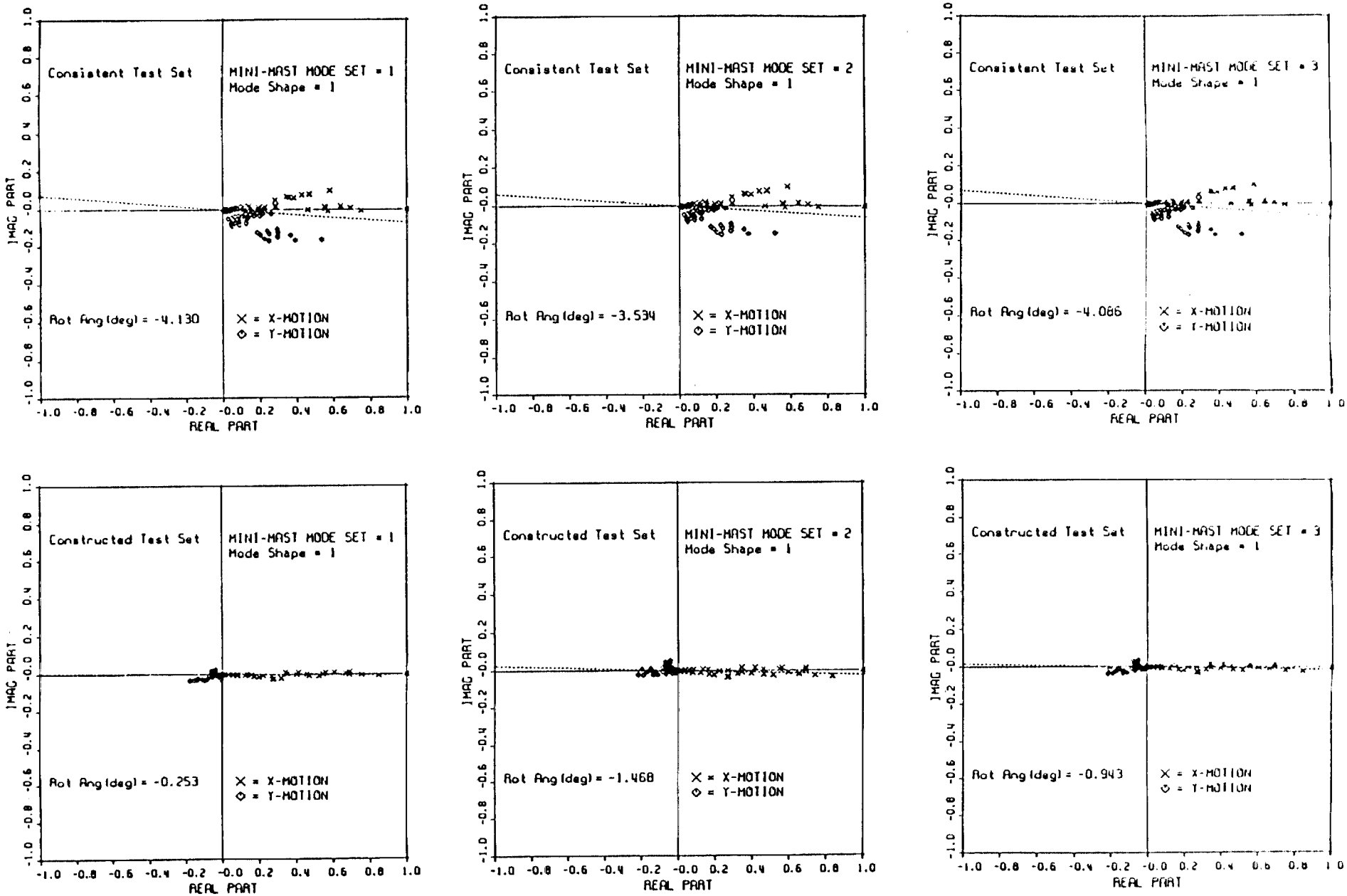

Figure 3–3. Scatter Plots for Mini–mast Consistent and Constructed Test Mode Sets, Mode Shape 1.

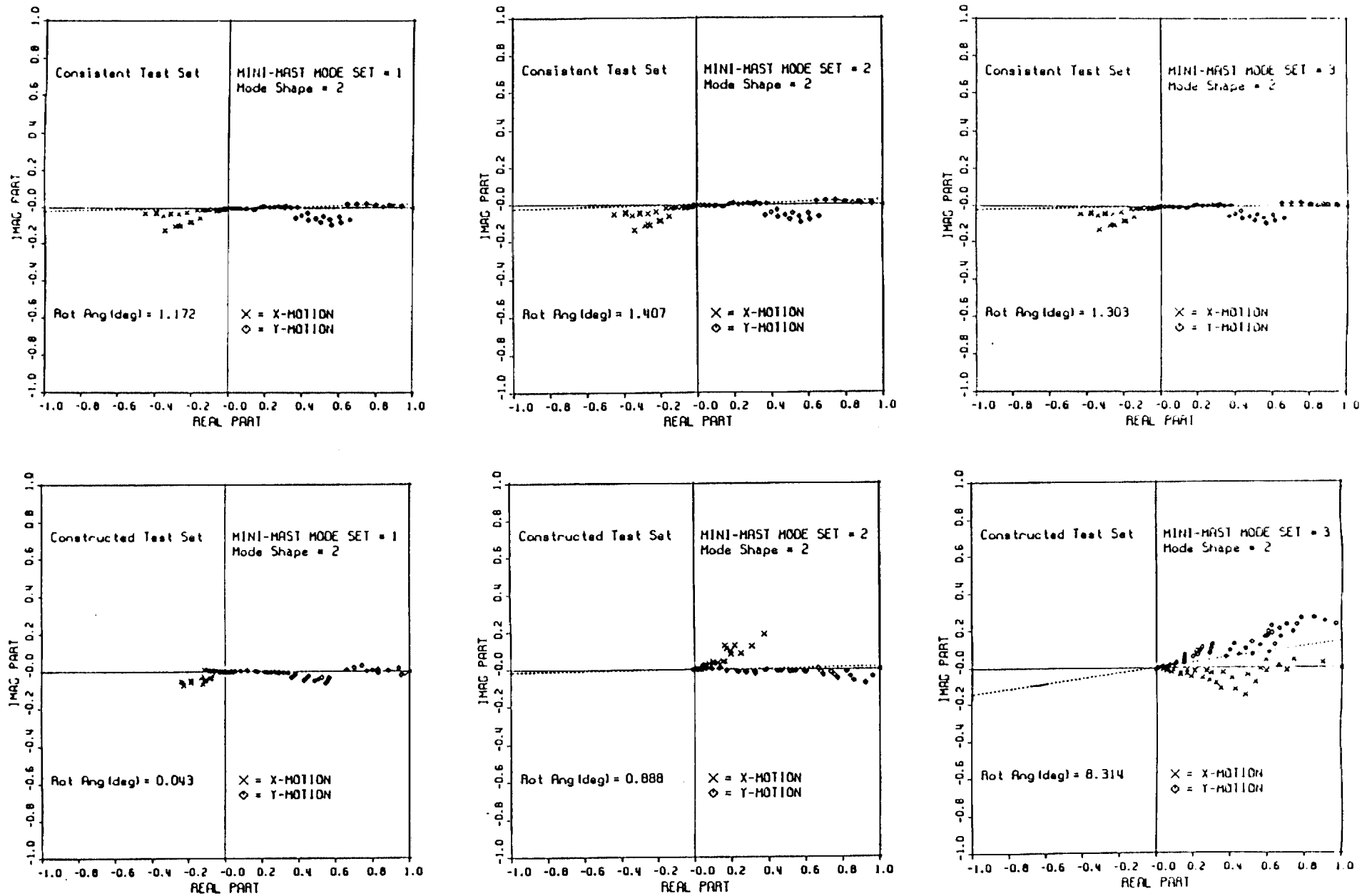

Figure 3–4. Scatter Plots for Mini–mast Consistent and Constructed Test Mode Sets, Mode Shape 2.

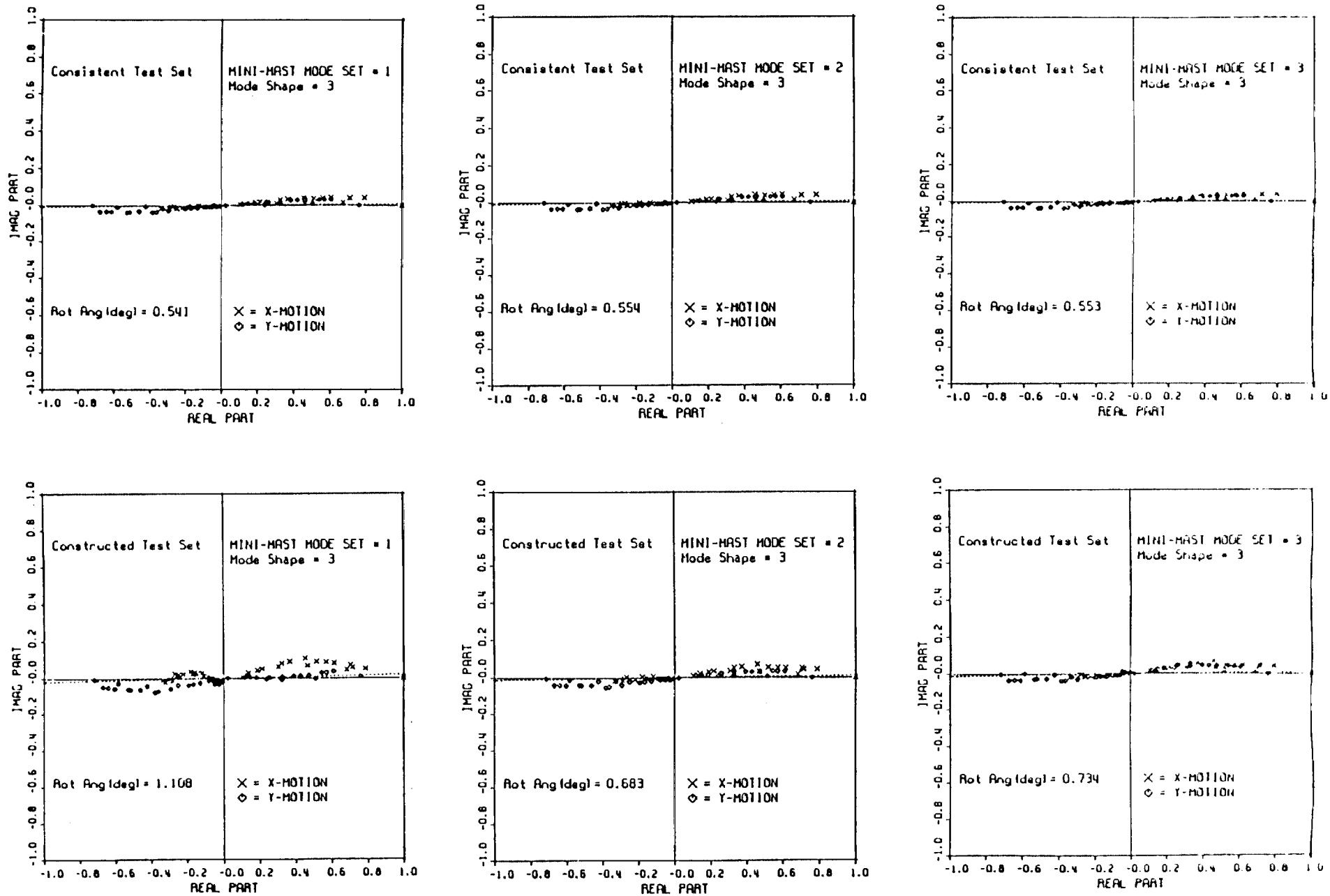

Figure 3–5. Scatter Plots for Mini–mast Consistent and Constructed Test Mode Sets, Mode Shape 3.

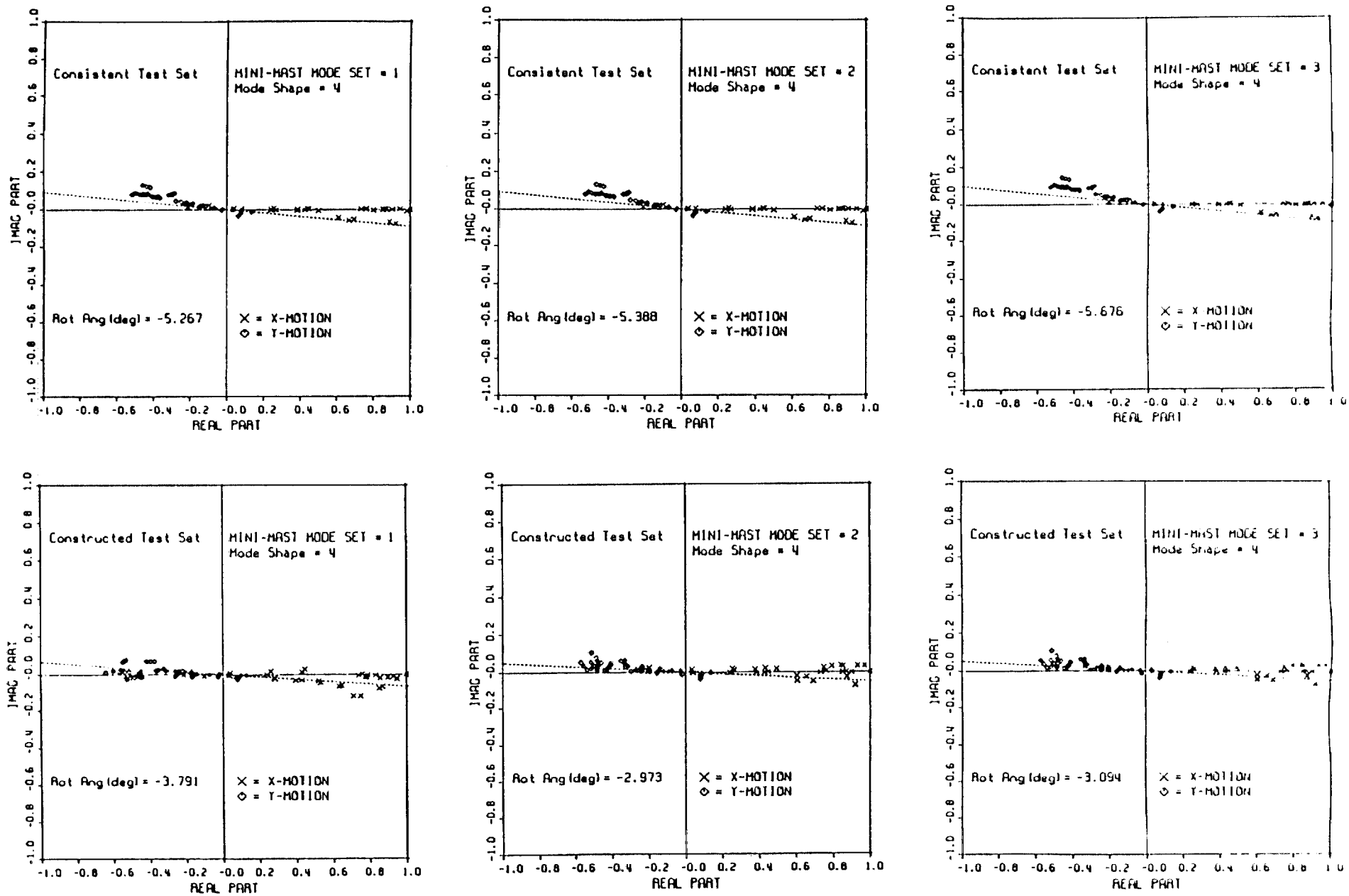

Figure 3–6. Scatter Plots for Mini–mast Consistent and Constructed Test Mode Sets, Mode Shape 4.

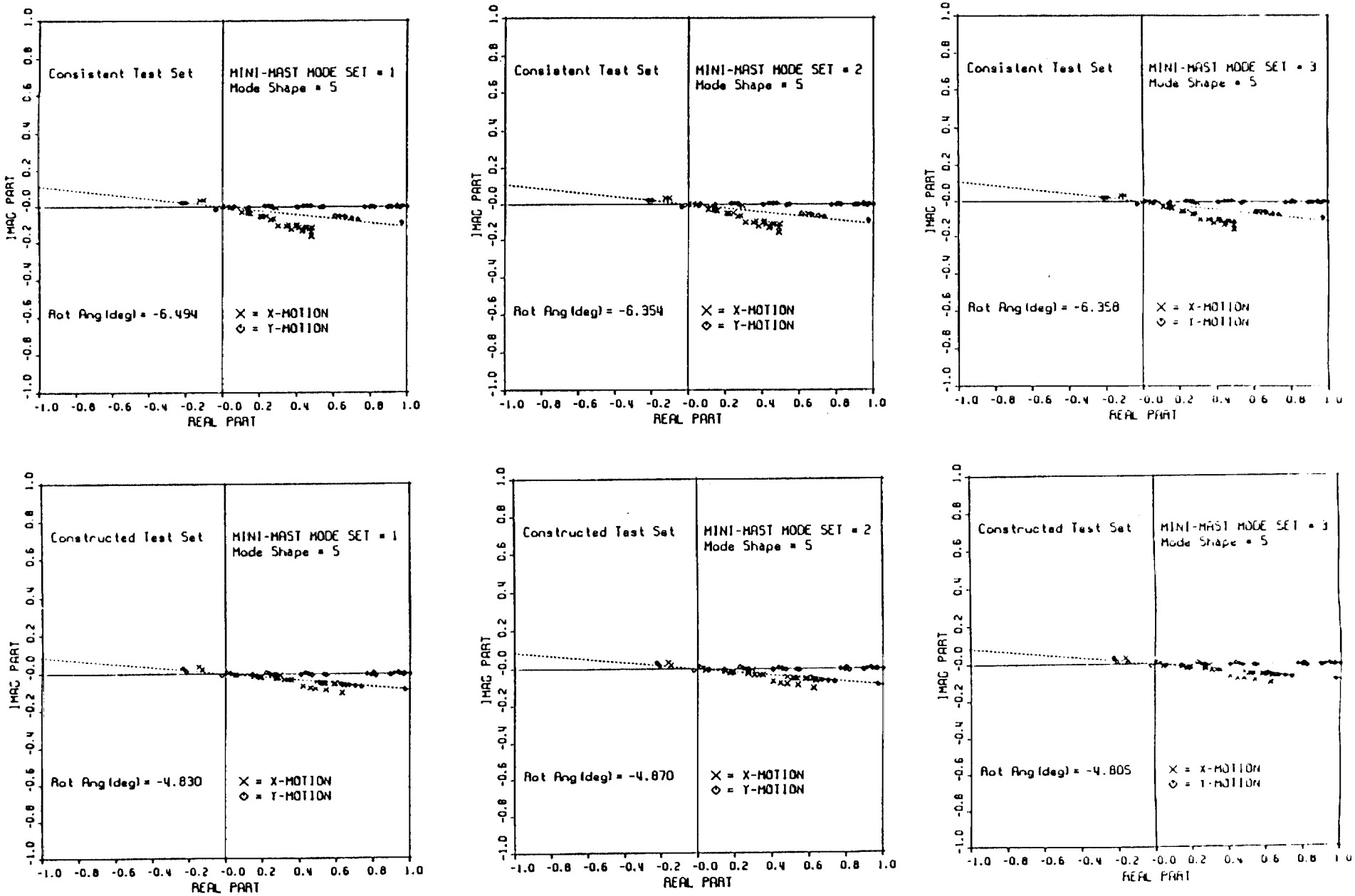

Figure 3–7. Scatter Plots for Mini–mast Consistent and Constructed Test Mode Sets, Mode Shape 5.

Table 3–3a. Comparison of Mini–mast Modal Orthogonality Before and After Eigenvector Conditioning, Consistent Test Set, Mode Set #1.

Before Conditioning

*** ORIG ANAL/TEST REAL CROSS-ORTHOGONALITY ***

MODE	1	2	3	4	5
1	0.8658	-0.4095	0.1120	-0.0051	-0.0134
2	0.4568	0.9063	0.0900	-0.0314	0.0033
3	0.1343	-0.0499	0.9851	0.0081	-0.0302
4	-0.0164	0.0195	-0.0003	0.9604	-0.2421
5	-0.0757	-0.0101	-0.0372	0.2544	0.9667

*** ORIG REAL TEST ORTHOGONALITY ***

MODE	1	2	3	4	5
1	1.0000	0.0424	0.2783	-0.0489	-0.0865
2	0.0424	1.0000	-0.0137	-0.0155	-0.0019
3	0.2783	-0.0137	1.0000	-0.0109	-0.0644
4	-0.0489	-0.0155	-0.0109	1.0000	0.0067
5	-0.0865	-0.0019	-0.0644	0.0067	1.0000

*** ORIG REAL/IMAG TEST ORTHOGONALITY ***

MODE	1	2	3	4	5
1	-0.0702	-0.0355	-0.0030	0.0100	0.0229
2	-0.1650	0.0204	0.0041	-0.0110	0.0104
3	-0.0126	0.0016	0.0094	-0.0117	0.0118
4	0.0205	-0.0037	0.0038	-0.0915	-0.1036
5	0.0090	-0.0082	0.0024	0.0772	-0.1125

After Conditioning

*** FINAL ANAL/TEST REAL CROSS-ORTHOGONALITY ***

MODE	1	2	3	4	5
1	0.8841	-0.4292	-0.0184	0.0151	0.0204
2	0.4469	0.8969	0.0294	-0.0056	0.0280
3	-0.0127	-0.0461	0.9959	0.0191	0.0001
4	0.0034	0.0306	0.0030	0.9634	-0.2342
5	-0.0274	0.0008	-0.0002	0.2441	0.9688

*** REAL TEST ORTHO AFTER ROT & MASS NORMAL ***

MODE	1	2	3	4	5
1	1.0000	0.0001	-0.0001	0.0000	-0.0002
2	0.0001	1.0000	0.0001	-0.0001	0.0000
3	-0.0001	0.0001	1.0000	0.0002	-0.0001
4	0.0000	-0.0001	0.0002	1.0000	0.0000
5	-0.0002	0.0000	-0.0001	0.0000	1.0000

** REAL/IMAG TEST ORTHO AFTER ROT & MASS NORMAL **

MODE	1	2	3	4	5
1	0.0000	-0.0380	-0.0065	0.0111	0.0112
2	-0.1680	0.0000	0.0316	-0.0193	0.0037
3	0.0039	0.0059	0.0000	-0.0116	0.0039
4	0.0120	-0.0046	-0.0013	0.0000	-0.1011
5	0.0061	-0.0080	0.0029	0.0775	0.0000

Table 3–3b. Comparison of Mini–mast Modal Orthogonality Before and After Eigenvector Conditioning, Consistent Test Set, Mode Set #2.

Before Conditioning

*** ORIG ANAL/TEST REAL CROSS-ORTHOGONALITY ***

MODE	1	2	3	4	5
1	0.8742	-0.4102	0.1121	-0.0047	-0.0134
2	0.4395	0.9060	0.0898	-0.0318	0.0029
3	0.1356	-0.0501	0.9851	0.0079	-0.0304
4	-0.0167	0.0197	-0.0010	0.9617	-0.2348
5	-0.0754	-0.0099	-0.0372	0.2491	0.9686

*** ORIG REAL TEST ORTHOGONALITY ***

MODE	1	2	3	4	5
1	1.0000	0.0221	0.2788	-0.0479	-0.0868
2	0.0221	1.0000	-0.0143	-0.0157	-0.0020
3	0.2788	-0.0143	1.0000	-0.0115	-0.0645
4	-0.0479	-0.0157	-0.0115	1.0000	0.0087
5	-0.0868	-0.0020	-0.0645	0.0087	1.0000

*** ORIG REAL/IMAG TEST ORTHOGONALITY ***

MODE	1	2	3	4	5
1	-0.0603	-0.0528	-0.0032	0.0096	0.0220
2	-0.1502	0.0245	0.0045	-0.0117	0.0100
3	-0.0114	-0.0031	0.0097	-0.0130	0.0111
4	0.0201	-0.0030	0.0038	-0.0935	-0.0974
5	0.0089	-0.0069	0.0025	0.0789	-0.1102

After Conditioning

*** FINAL ANAL/TEST REAL CROSS-ORTHOGONALITY ***

MODE	1	2	3	4	5
1	0.8885	-0.4202	-0.0193	0.0149	0.0209
2	0.4378	0.9013	0.0313	-0.0066	0.0272
3	-0.0116	-0.0457	0.9958	0.0193	0.0001
4	0.0029	0.0307	0.0027	0.9648	-0.2282
5	-0.0272	0.0005	0.0000	0.2381	0.9703

*** REAL TEST ORTHO AFTER ROT & MASS NORMAL ***

MODE	1	2	3	4	5
1	1.0000	0.0001	-0.0001	0.0000	-0.0002
2	0.0001	1.0000	0.0001	-0.0001	0.0000
3	-0.0001	0.0001	1.0000	0.0002	-0.0001
4	0.0000	-0.0001	0.0002	1.0000	0.0000
5	-0.0002	0.0000	-0.0001	0.0000	1.0000

** REAL/IMAG TEST ORTHO AFTER ROT & MASS NORMAL **

MODE	1	2	3	4	5
1	0.0000	-0.0547	-0.0065	0.0105	0.0106
2	-0.1544	0.0000	0.0297	-0.0193	0.0039
3	0.0031	0.0038	0.0000	-0.0129	0.0033
4	0.0122	-0.0039	-0.0011	0.0000	-0.0949
5	0.0064	-0.0074	0.0029	0.0793	0.0000

Table 3–3c. Comparison of Mini–mast Modal Orthogonality Before and After Eigenvector Conditioning, Consistent Test Set, Mode Set #3.

Before Conditioning

*** ORIG ANAL/TEST REAL CROSS-ORTHOGONALITY ***

MODE	1	2	3	4	5
1	0.8722	-0.3976	0.1120	-0.0040	-0.0137
2	0.4437	0.9120	0.0898	-0.0318	0.0027
3	0.1352	-0.0470	0.9851	0.0069	-0.0298
4	-0.0167	0.0198	-0.0010	0.9614	-0.2333
5	-0.0758	-0.0103	-0.0372	0.2503	0.9690

*** ORIG REAL TEST ORTHOGONALITY ***

MODE	1	2	3	4	5
1	1.0000	0.0413	0.2785	-0.0478	-0.0875
2	0.0413	1.0000	-0.0091	-0.0161	-0.0028
3	0.2785	-0.0091	1.0000	-0.0126	-0.0640
4	-0.0478	-0.0161	-0.0126	1.0000	0.0116
5	-0.0875	-0.0028	-0.0640	0.0116	1.0000

*** ORIG REAL/IMAG TEST ORTHOGONALITY ***

MODE	1	2	3	4	5
1	-0.0693	-0.0451	-0.0031	0.0081	0.0223
2	-0.1715	0.0227	0.0045	-0.0117	0.0103
3	-0.0137	-0.0006	0.0096	-0.0121	0.0109
4	0.0205	-0.0030	0.0037	-0.0984	-0.0978
5	0.0093	-0.0072	0.0025	0.0898	-0.1102

After Conditioning

*** FINAL ANAL/TEST REAL CROSS-ORTHOGONALITY ***

MODE	1	2	3	4	5
1	0.8900	-0.4170	-0.0181	0.0157	0.0207
2	0.4345	0.9028	0.0289	-0.0063	0.0276
3	-0.0115	-0.0455	0.9959	0.0187	0.0005
4	0.0025	0.0310	0.0033	0.9650	-0.2273
5	-0.0273	0.0010	0.0000	0.2372	0.9705

*** REAL TEST ORTHO AFTER ROT & MASS NORMAL ***

MODE	1	2	3	4	5
1	1.0000	0.0002	-0.0001	0.0000	-0.0002
2	0.0002	1.0000	0.0001	-0.0001	0.0000
3	-0.0001	0.0001	1.0000	0.0001	-0.0001
4	0.0000	-0.0001	0.0001	1.0000	0.0000
5	-0.0002	0.0000	-0.0001	0.0000	1.0000

** REAL/IMAG TEST ORTHO AFTER ROT & MASS NORMAL **

MODE	1	2	3	4	5
1	0.0000	-0.0477	-0.0066	0.0091	0.0109
2	-0.1748	0.0000	0.0328	-0.0201	0.0031
3	0.0030	0.0051	0.0000	-0.0117	0.0031
4	0.0123	-0.0040	-0.0012	0.0000	-0.0950
5	0.0066	-0.0073	0.0030	0.0903	0.0000

Table 3–4 presents the three individual modal damping matrices computed from each of the three consistent mode sets, along with an average of the three and the corresponding covariance matrix presented (as in the case of modal mass and stiffness uncertainty) in terms of the vector of standard deviations and the correlation matrix.

A similar analysis to the foregoing was performed for the constructed test sets of the Mini–mast Structure. Table 3–5 presents a comparison of modal orthogonality characteristics before and after eigenvector conditioning. Table 3–6 presents both the individual and averaged modal damping matrices.

It is interesting to compare the results of the two mode sets as summarized in Tables 3–4 and 3–6. In the first place, there are large differences between the modal damping matrices computed from the constructed test sets and those computed from the consistent mode sets. These large differences occur on both the diagonal and off–diagonal elements corresponding to the first two modes. The large variability within the constructed test set is reflected in the large standard deviations, especially for the first two modes. It may also be noted that the diagonal modal damping term in the first mode is about three times larger in the case of the constructed mode sets. These results seem to correlate with the poorer original real test mode orthogonality evident in Tables 3–5a, b, c. Orthogonalizing the modes prior to evaluation of the modal damping matrices did not appear to help in this case.

3.1.4.2 LaRC Ten Bay Truss

A damping analysis was performed for the LaRC Ten Bay Truss similar to that performed for the Mini–mast Structure. In this case, however, there were no completely consistent test sets available. There were consistent sets including Modes 2 through 5, obtained from Shaker Configuration (1, 2), but these sets did not include Mode 1. Mode 1 was taken from mode sets obtained from Shaker Configuration (1, 3) to obtain complete sets of five modes each. These mode sets are also referred to as "constructed mode sets," although the method of "construction" in this case differs from that used to construct the Mini–mast mode sets. Figures 3–8 through 3–12 present scatter plots of the modes in the complex plane. These plots show a high degree of similarity among the different mode sets.

Table 3–4a. Modal Damping Matrices for the LaRC Mini–mast Structure, Consistent Test Sets.

Mode Set #1

*** MODAL DAMPING (%) MATRIX ***

MODE	1	2	3	4	5
1	0.5620	0.0600	-0.7379	1.2045	1.3367
2	0.0600	0.9950	3.0681	-2.3787	0.6211
3	-0.7379	3.0681	1.4040	-0.2334	0.0444
4	1.2045	-2.3787	-0.2334	2.1160	-0.0828
5	1.3367	0.6211	0.0444	-0.0828	1.1320

Mode Set #2

*** MODAL DAMPING (%) MATRIX ***

MODE	1	2	3	4	5
1	0.6070	0.0459	-0.7197	1.1244	1.2492
2	0.0459	0.9990	2.9204	-2.3923	0.6290
3	-0.7197	2.9204	1.4090	-0.2644	0.0303
4	1.1244	-2.3923	-0.2644	2.1270	-0.0779
5	1.2492	0.6290	0.0303	-0.0779	1.1290

Mode Set #3

*** MODAL DAMPING (%) MATRIX ***

MODE	1	2	3	4	5
1	0.5980	0.0586	-0.7370	0.9514	1.2863
2	0.0586	0.9530	3.2109	-2.5025	0.5242
3	-0.7370	3.2109	1.4090	-0.2390	0.0228
4	0.9514	-2.5025	-0.2390	2.1350	-0.0858
5	1.2863	0.5242	0.0228	-0.0858	1.1330

Average of Three Mode Sets

*** AVERAGE MODAL DAMPING (%) ***

MODE	1	2	3	4	5
1	0.5890	0.0548	-0.7315	1.0935	1.2907
2	0.0548	0.9823	3.0665	-2.4245	0.5914
3	-0.7315	3.0665	1.4073	-0.2456	0.0325
4	1.0935	-2.4245	-0.2456	2.1260	-0.0822
5	1.2907	0.5914	0.0325	-0.0822	1.1313

Table 3–4b. Covariance of Modal Damping Matrix Elements for the LaRC Mini–mast Structure, Consistent Test Sets.

CORRELATION MATRIX

ST.D. (%)															
0.024	1.000	-.718	0.687	-.604	-.970	-.252	-.199	-.420	-.263	0.982	-.774	-.858	0.812	0.319	-.454
0.008	-.718	1.000	-.999	-.121	0.866	-.492	0.825	-.329	-.482	-.574	0.996	0.259	-.178	-.889	0.946
0.010	0.687	-.999	1.000	0.164	-.843	0.530	-.848	0.370	0.520	0.538	-.992	-.216	0.135	0.908	-.959
0.129	-.604	-.121	0.164	1.000	0.392	0.924	-.661	0.977	0.928	-.743	-.037	0.928	-.955	0.563	-.436
0.044	-.970	0.866	-.843	0.392	1.000	0.010	0.431	0.187	0.021	-.907	0.905	0.707	-.646	-.540	0.657
0.025	-.252	-.492	0.530	0.924	0.010	1.000	-.898	0.984	1.000	-.430	-.417	0.714	-.769	0.836	-.748
0.145	-.199	0.825	-.848	-.661	0.431	-.898	1.000	-.806	-.893	-.010	0.774	-.333	0.410	-.992	0.963
0.068	-.420	-.329	0.370	0.977	0.187	0.984	-.806	1.000	0.986	-.584	-.249	0.827	-.871	0.726	-.618
0.058	-.263	-.482	0.520	0.928	0.021	1.000	-.893	0.986	1.000	-.440	-.407	0.721	-.776	0.830	-.740
0.003	0.982	-.574	0.538	-.743	-.907	-.430	-.010	-.584	-.440	1.000	-.641	-.940	0.908	0.135	-.277
0.017	-.774	0.996	-.992	-.037	0.905	-.417	0.774	-.249	-.407	-.641	1.000	0.339	-.260	-.847	0.915
0.011	-.858	0.259	-.216	0.928	0.707	0.714	-.333	0.827	0.721	-.940	0.339	1.000	-.997	0.213	-.068
0.010	0.812	-.178	0.135	-.955	-.646	-.769	0.410	-.871	-.776	0.908	-.260	-.997	1.000	-.293	0.151
0.004	0.319	-.889	0.908	0.563	-.540	0.836	-.992	0.726	0.830	0.135	-.847	0.213	-.293	1.000	-.989
0.002	-.454	0.946	-.959	-.436	0.657	-.748	0.963	-.618	-.740	-.277	0.915	-.068	0.151	-.989	1.000

Table 3–5a. Comparison of Mini–mast Modal Orthogonality Before and After Eigenvector Conditioning, Constructed Test Set, Mode Set #1.

Before Conditioning

*** ORIG ANAL/TEST REAL CROSS-ORTHOGONALITY ***

MODE	1	2	3	4	5
1	0.9909	-0.2389	0.1108	-0.0123	-0.0017
2	-0.0610	0.9682	0.0869	-0.0321	-0.0124
3	0.0844	-0.0190	0.9856	0.0088	-0.0321
4	-0.0351	0.0316	0.0004	0.9789	-0.1311
5	-0.0366	-0.0374	-0.0345	0.1695	0.9885

*** ORIG REAL TEST ORTHOGONALITY ***

MODE	1	2	3	4	5
1	1.0000	-0.2996	0.1924	-0.0519	-0.0371
2	-0.2996	1.0000	0.0402	-0.0032	-0.0506
3	0.1924	0.0402	1.0000	-0.0074	-0.0654
4	-0.0519	-0.0032	-0.0074	1.0000	0.0362
5	-0.0371	-0.0506	-0.0654	0.0362	1.0000

*** ORIG REAL/IMAG TEST ORTHOGONALITY ***

MODE	1	2	3	4	5
1	-0.0044	-0.0599	-0.0021	0.0030	0.0190
2	-0.0293	0.0008	0.0001	-0.0081	0.0111
3	0.0012	-0.0169	0.0193	-0.0152	0.0013
4	-0.0119	0.0164	0.0549	-0.0661	-0.0429
5	0.0020	0.0074	0.0066	0.0119	-0.0842

After Conditioning

*** FINAL ANAL/TEST REAL CROSS-ORTHOGONALITY ***

MODE	1	2	3	4	5
1	0.9947	-0.0959	0.0176	0.0153	0.0127
2	0.0787	0.9932	0.0670	-0.0280	0.0167
3	-0.0179	-0.0346	0.9940	0.0167	-0.0024
4	-0.0055	0.0277	0.0047	0.9821	-0.1447
5	-0.0167	-0.0135	-0.0007	0.1510	0.9869

*** REAL TEST ORTHO AFTER ROT & MASS NORMAL ***

MODE	1	2	3	4	5
1	1.0000	0.0000	0.0000	0.0000	0.0000
2	0.0000	1.0000	0.0000	0.0000	0.0000
3	0.0000	0.0000	1.0000	0.0000	0.0000
4	0.0000	0.0000	0.0000	1.0000	0.0000
5	0.0000	0.0000	0.0000	0.0000	1.0000

** REAL/IMAG TEST ORTHO AFTER ROT & MASS NORMAL **

MODE	1	2	3	4	5
1	0.0000	-0.0633	-0.0020	-0.0006	0.0152
2	-0.0353	0.0000	0.0028	-0.0084	0.0090
3	0.0022	-0.0102	0.0000	-0.0146	-0.0061
4	-0.0176	0.0108	0.0562	0.0000	-0.0375
5	0.0019	0.0057	0.0068	0.0137	0.0000

Table 3–5b. Comparison of Mini–mast Modal Orthogonality Before and After Eigenvector Conditioning, Constructed Test Set, Mode Set #2.

Before Conditioning

*** ORIG ANAL/TEST REAL CROSS-ORTHOGONALITY ***

MODE	1	2	3	4	5
1	0.9875	0.2828	0.1124	-0.0054	-0.0205
2	-0.0940	0.9569	0.0862	-0.0264	-0.0035
3	0.0934	0.0320	0.9855	0.0152	-0.0335
4	-0.0355	0.0037	0.0001	0.9710	-0.1304
5	-0.0352	-0.0442	-0.0351	0.2104	0.9883

*** ORIG REAL TEST ORTHOGONALITY ***

MODE	1	2	3	4	5
1	1.0000	0.1946	0.1995	-0.0421	-0.0552
2	0.1946	1.0000	0.1497	-0.0340	-0.0542
3	0.1995	0.1497	1.0000	-0.0011	-0.0687
4	-0.0421	-0.0340	-0.0011	1.0000	0.0756
5	-0.0552	-0.0542	-0.0687	0.0756	1.0000

*** ORIG REAL/IMAG TEST ORTHOGONALITY ***

MODE	1	2	3	4	5
1	-0.0256	0.1472	-0.0015	0.0228	0.0136
2	-0.0069	0.0152	-0.0012	-0.0041	0.0212
3	0.0181	0.0446	0.0119	-0.0218	0.0007
4	-0.0102	-0.0156	0.0146	-0.0517	-0.0462
5	0.0007	-0.0097	0.0054	0.0429	-0.0849

After Conditioning

*** FINAL ANAL/TEST REAL CROSS-ORTHOGONALITY ***

MODE	1	2	3	4	5
1	0.9780	0.1870	0.0012	0.0166	0.0145
2	-0.1967	0.9805	0.0274	-0.0120	0.0212
3	-0.0012	-0.0478	0.9961	0.0211	-0.0020
4	-0.0215	0.0196	0.0006	0.9782	-0.1622
5	0.0006	-0.0101	-0.0002	0.1732	0.9839

*** REAL TEST ORTHO AFTER ROT & MASS NORMAL ***

MODE	1	2	3	4	5
1	1.0000	0.0000	0.0000	0.0000	0.0000
2	0.0000	1.0000	0.0000	0.0000	0.0000
3	0.0000	0.0000	1.0000	0.0000	0.0000
4	0.0000	0.0000	0.0000	1.0000	0.0000
5	0.0000	0.0000	0.0000	0.0000	1.0000

** REAL/IMAG TEST ORTHO AFTER ROT & MASS NORMAL **

MODE	1	2	3	4	5
1	0.0000	0.1480	-0.0135	0.0263	0.0102
2	-0.0015	0.0000	-0.0006	-0.0067	0.0157
3	0.0208	0.0273	0.0000	-0.0210	-0.0042
4	-0.0131	-0.0139	0.0157	0.0000	-0.0397
5	0.0012	-0.0048	0.0062	0.0464	0.0000

Table 3–5c. Comparison of Mini–mast Modal Orthogonality Before and After Eigenvector Conditioning, Constructed Test Set, Mode Set #3.

Before Conditioning

*** ORIG ANAL/TEST REAL CROSS-ORTHOGONALITY ***

MODE	1	2	3	4	5
1	0.9881	0.6798	0.1108	-0.0041	-0.0205
2	-0.0941	0.7287	0.0845	-0.0284	-0.0035
3	0.0875	0.0393	0.9859	0.0146	-0.0332
4	-0.0355	-0.0164	-0.0016	0.9707	-0.1304
5	-0.0351	-0.0467	-0.0343	0.2115	0.9883

*** ORIG REAL TEST ORTHOGONALITY ***

MODE	1	2	3	4	5
1	1.0000	0.6097	0.1924	-0.0408	-0.0549
2	0.6097	1.0000	0.1800	-0.0515	-0.0615
3	0.1924	0.1800	1.0000	-0.0033	-0.0673
4	-0.0408	-0.0515	-0.0033	1.0000	0.0768
5	-0.0549	-0.0615	-0.0673	0.0768	1.0000

*** ORIG REAL/IMAG TEST ORTHOGONALITY ***

MODE	1	2	3	4	5
1	-0.0164	-0.0214	-0.0050	0.0248	0.0131
2	-0.0294	0.1431	0.0016	0.0074	0.0227
3	0.0117	0.0058	0.0128	-0.0226	-0.0019
4	-0.0100	-0.0336	-0.0005	-0.0538	-0.0463
5	0.0016	-0.0158	0.0154	0.0459	-0.0838

After Conditioning

*** FINAL ANAL/TEST REAL CROSS-ORTHOGONALITY ***

MODE	1	2	3	4	5
1	0.9250	0.4295	-0.0110	0.0248	0.0216
2	-0.3708	0.8977	0.0325	-0.0090	0.0175
3	0.0132	-0.0713	0.9959	0.0212	-0.0031
4	-0.0244	0.0115	0.0007	0.9781	-0.1630
5	0.0051	-0.0071	-0.0001	0.1735	0.9837

*** REAL TEST ORTHO AFTER ROT & MASS NORMAL ***

MODE	1	2	3	4	5
1	1.0000	-0.0001	0.0000	-0.0001	0.0001
2	-0.0001	1.0000	0.0000	0.0000	0.0000
3	0.0000	0.0000	1.0000	0.0001	0.0000
4	-0.0001	0.0000	0.0001	1.0000	0.0000
5	0.0001	0.0000	0.0000	0.0000	1.0000

** REAL/IMAG TEST ORTHO AFTER ROT & MASS NORMAL **

MODE	1	2	3	4	5
1	0.0000	-0.1558	0.0010	0.0258	-0.0016
2	-0.0427	0.0000	0.0013	-0.0030	0.0190
3	0.0209	-0.0188	0.0000	-0.0231	-0.0075
4	-0.0053	-0.0263	0.0006	0.0000	-0.0405
5	0.0031	-0.0082	0.0174	0.0495	0.0000

Table 3–6a. Modal Damping Matrices for the LaRC Mini–mast Structure, Constructed Test Sets.

Mode Set #1

*** MODAL DAMPING (%) MATRIX ***

MODE	1	2	3	4	5
1	1.7950	-0.0339	-0.2457	0.2377	1.9368
2	-0.0339	0.9290	0.4987	-1.2645	1.0498
3	-0.2457	0.4987	1.4700	-1.1587	-0.2396
4	0.2377	-1.2645	-1.1587	2.1260	-0.0217
5	1.9368	1.0498	-0.2396	-0.0217	1.1280

Mode Set #2

*** MODAL DAMPING (%) MATRIX ***

MODE	1	2	3	4	5
1	2.0650	0.2104	-1.8081	3.6247	1.2964
2	0.2104	0.6070	-0.6305	-0.5909	2.0858
3	-1.8081	-0.6305	1.4400	-0.6938	-0.1880
4	3.6247	-0.5909	-0.6938	2.1150	-0.0449
5	1.2964	2.0858	-0.1880	-0.0449	1.1220

Mode Set #3

*** MODAL DAMPING (%) MATRIX ***

MODE	1	2	3	4	5
1	1.9850	-0.0668	-0.3276	3.4143	-0.2650
2	-0.0668	1.3370	0.5219	0.0945	2.5940
3	-0.3276	0.5219	1.4270	-0.5136	-0.4330
4	3.4143	0.0945	-0.5136	2.1140	-0.0469
5	-0.2650	2.5940	-0.4330	-0.0469	1.1220

Average of Three Mode Sets

*** AVERAGE MODAL DAMPING (%) ***

MODE	1	2	3	4	5
1	1.9483	0.0366	-0.7938	2.4256	0.9894
2	0.0366	0.9577	0.1300	-0.5870	1.9099
3	-0.7938	0.1300	1.4457	-0.7887	-0.2869
4	2.4256	-0.5870	-0.7887	2.1183	-0.0378
5	0.9894	1.9099	-0.2869	-0.0378	1.1240

Table 3–6b. Covariance of Modal Damping Matrix Elements for the LaRC Mini–mast Structure, Constructed Test Sets.

ST.D. (%)	CORRELATION MATRIX														
0.139	1.000	0.650	-.760	0.972	-.495	-.223	-.716	0.681	0.813	-.830	0.844	-.030	-.933	-.935	-.958
0.151	0.650	1.000	-.988	0.453	0.339	-.886	-.996	-.113	0.086	-.115	0.140	0.740	-.333	-.337	-.403
0.879	-.760	-.988	1.000	-.586	-.189	0.803	0.998	-.042	-.239	0.268	-.292	-.627	0.475	0.479	0.540
1.898	0.972	0.453	-.586	1.000	-.685	0.012	-.532	0.834	0.927	-.938	0.946	-.264	-.991	-.992	-.998
1.133	-.495	0.339	-.189	-.685	1.000	-.737	-.252	-.973	-.908	0.895	-.884	0.883	0.774	0.772	0.724
0.366	-.223	-.886	0.803	0.012	-.737	1.000	0.840	0.562	0.386	-.359	0.335	-.968	-.143	-.139	-.068
0.659	-.716	-.996	0.998	-.532	-.252	0.840	1.000	0.023	-.176	0.205	-.230	-.676	0.418	0.421	0.485
0.680	0.681	-.113	-.042	0.834	-.973	0.562	0.023	1.000	0.980	-.974	0.968	-.752	-.899	-.897	-.864
0.787	0.813	0.086	-.239	0.927	-.908	0.386	-.176	0.980	1.000	-1.00	0.999	-.606	-.968	-.967	-.946
0.022	-.830	-.115	0.268	-.938	0.895	-.359	0.205	-.974	-1.00	1.000	-1.00	0.582	0.975	0.974	0.956
0.333	0.844	0.140	-.292	0.946	-.884	0.335	-.230	0.968	0.999	-1.00	1.000	-.562	-.980	-.979	-.963
0.129	-.030	0.740	-.627	-.264	0.883	-.968	-.676	-.752	-.606	0.582	-.562	1.000	0.387	0.384	0.317
0.007	-.933	-.333	0.475	-.991	0.774	-.143	0.418	-.899	-.968	0.975	-.980	0.387	1.000	1.000	0.997
0.014	-.935	-.337	0.479	-.992	0.772	-.139	0.421	-.897	-.967	0.974	-.979	0.384	1.000	1.000	0.997
0.003	-.958	-.403	0.540	-.998	0.724	-.068	0.485	-.864	-.946	0.956	-.963	0.317	0.997	0.997	1.000

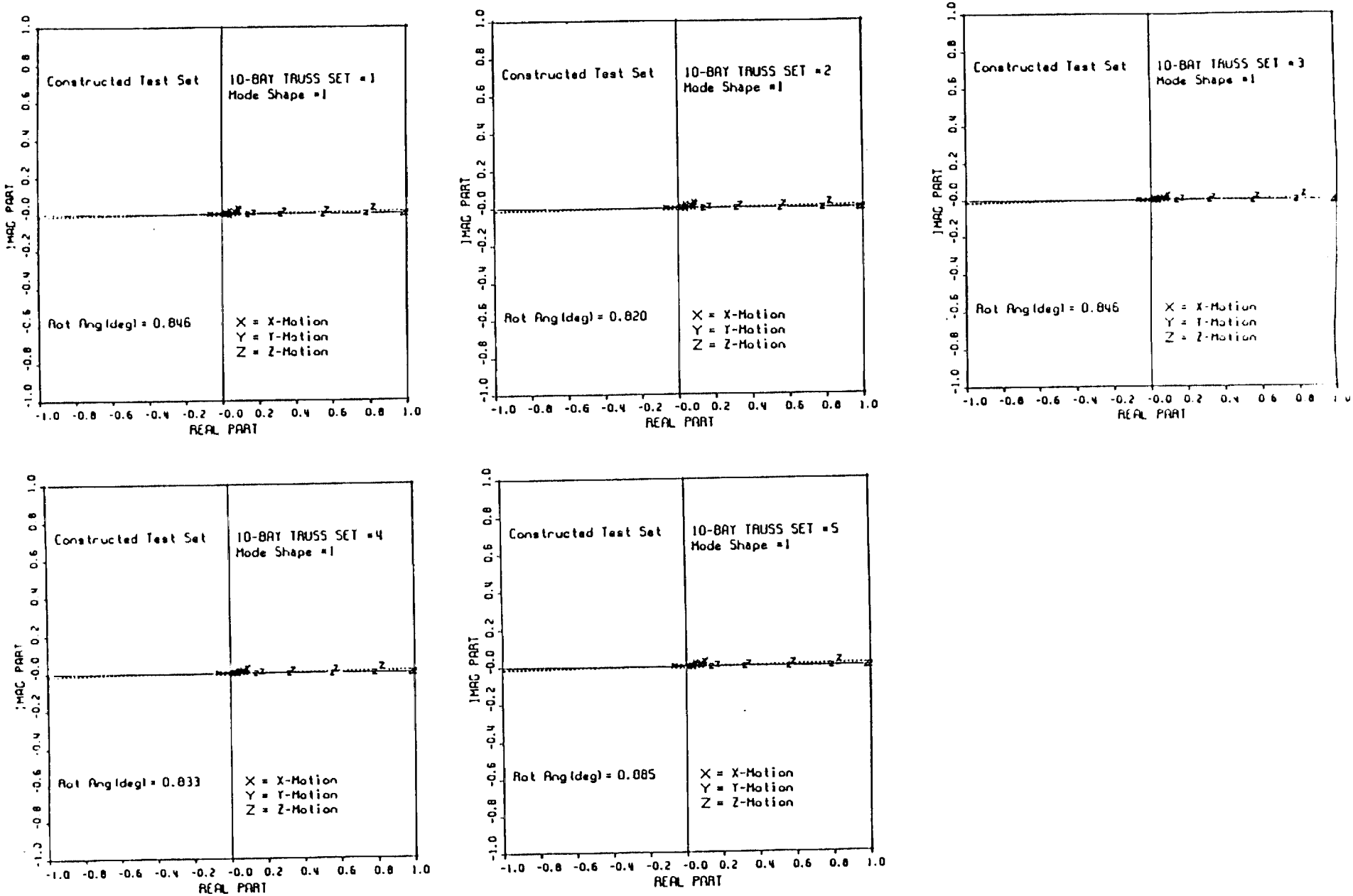

Figure 3–8. Scatter Plots for Ten Bay Truss Constructed Test Sets, Mode Shape 1.

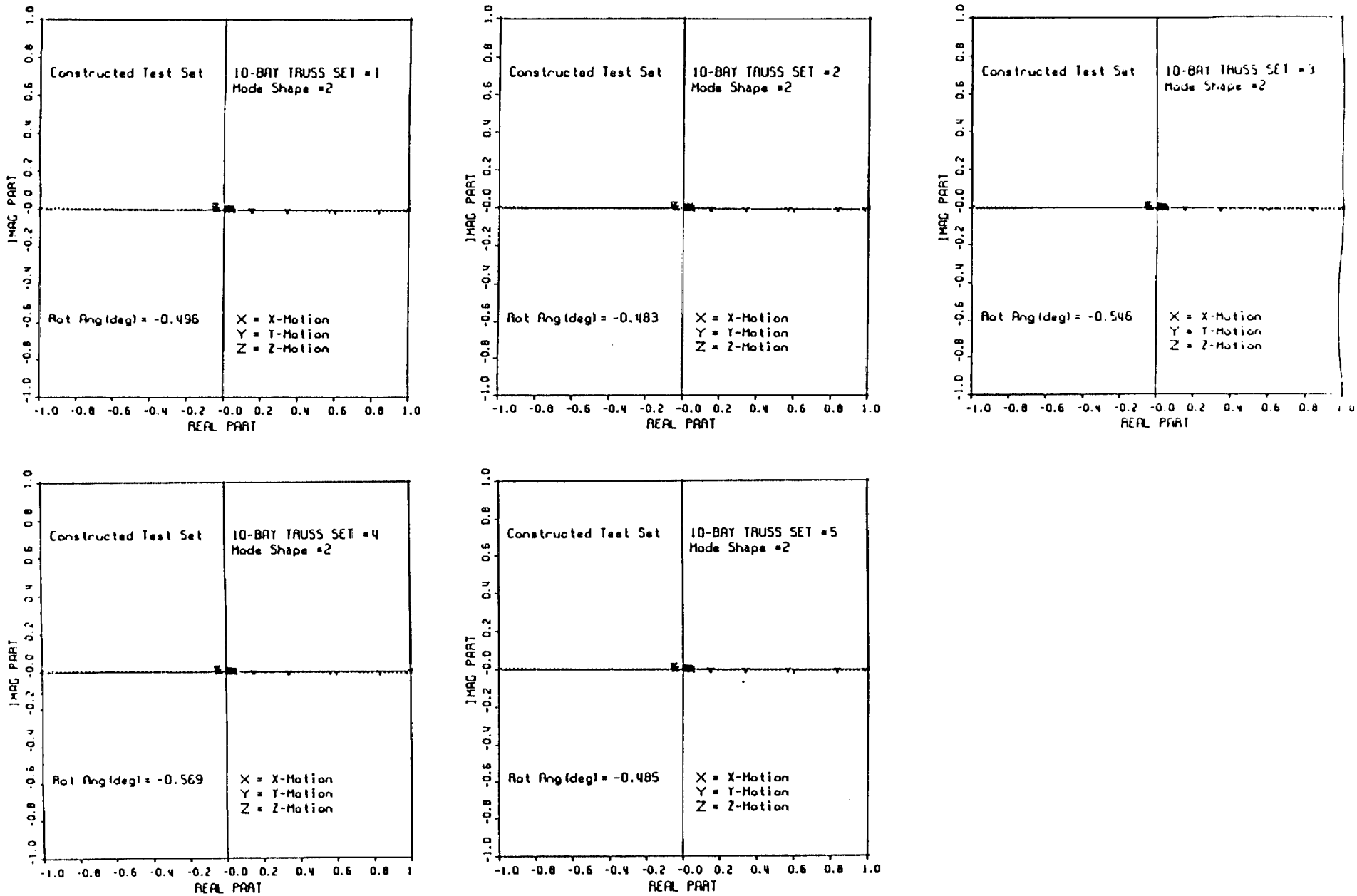

Figure 3–9. Scatter Plots for Ten Bay Truss Constructed Test Sets, Mode Shape 2.

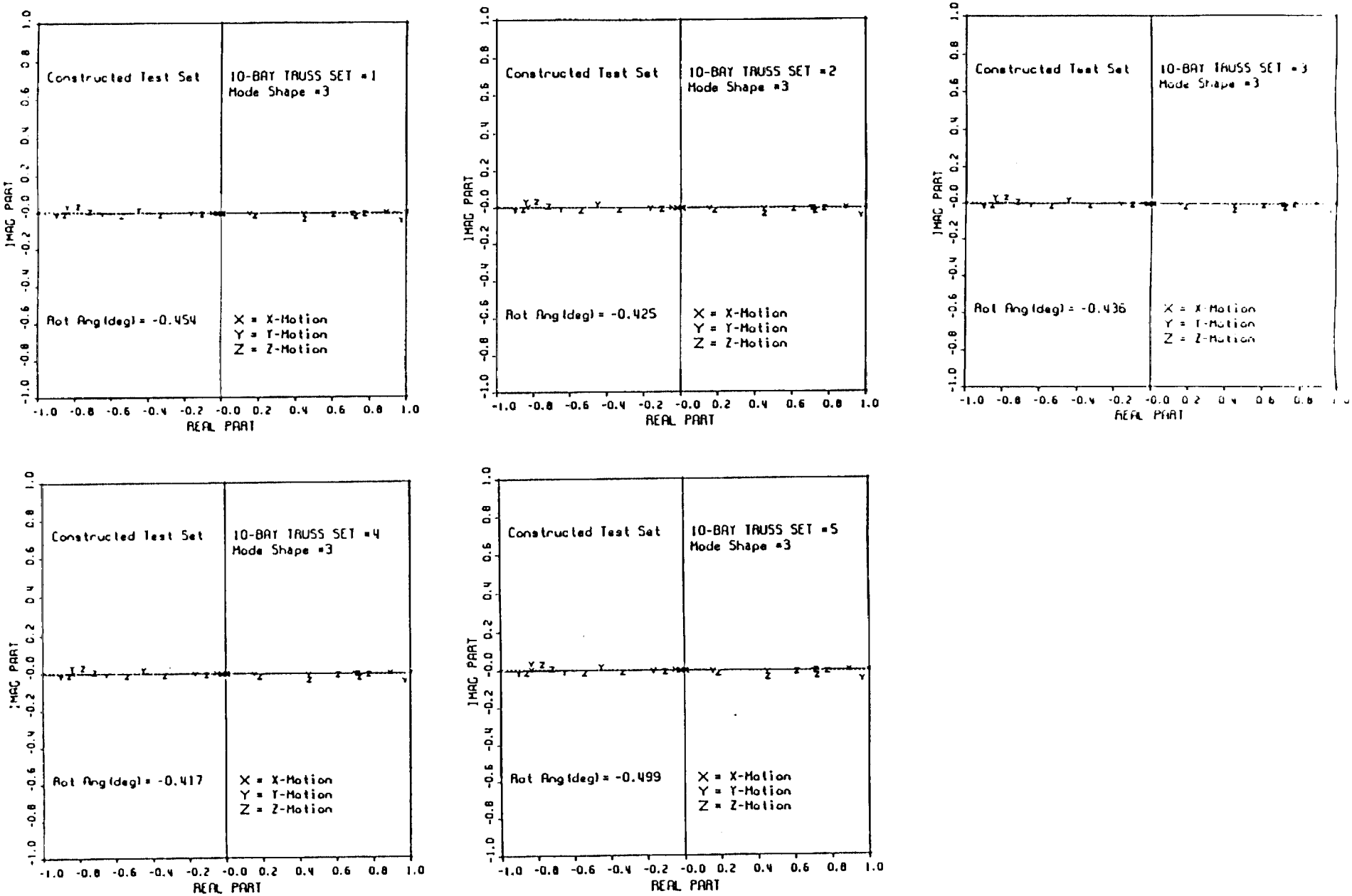

Figure 3–10. Scatter Plots for Ten Bay Truss Constructed Test Sets, Mode Shape 3.

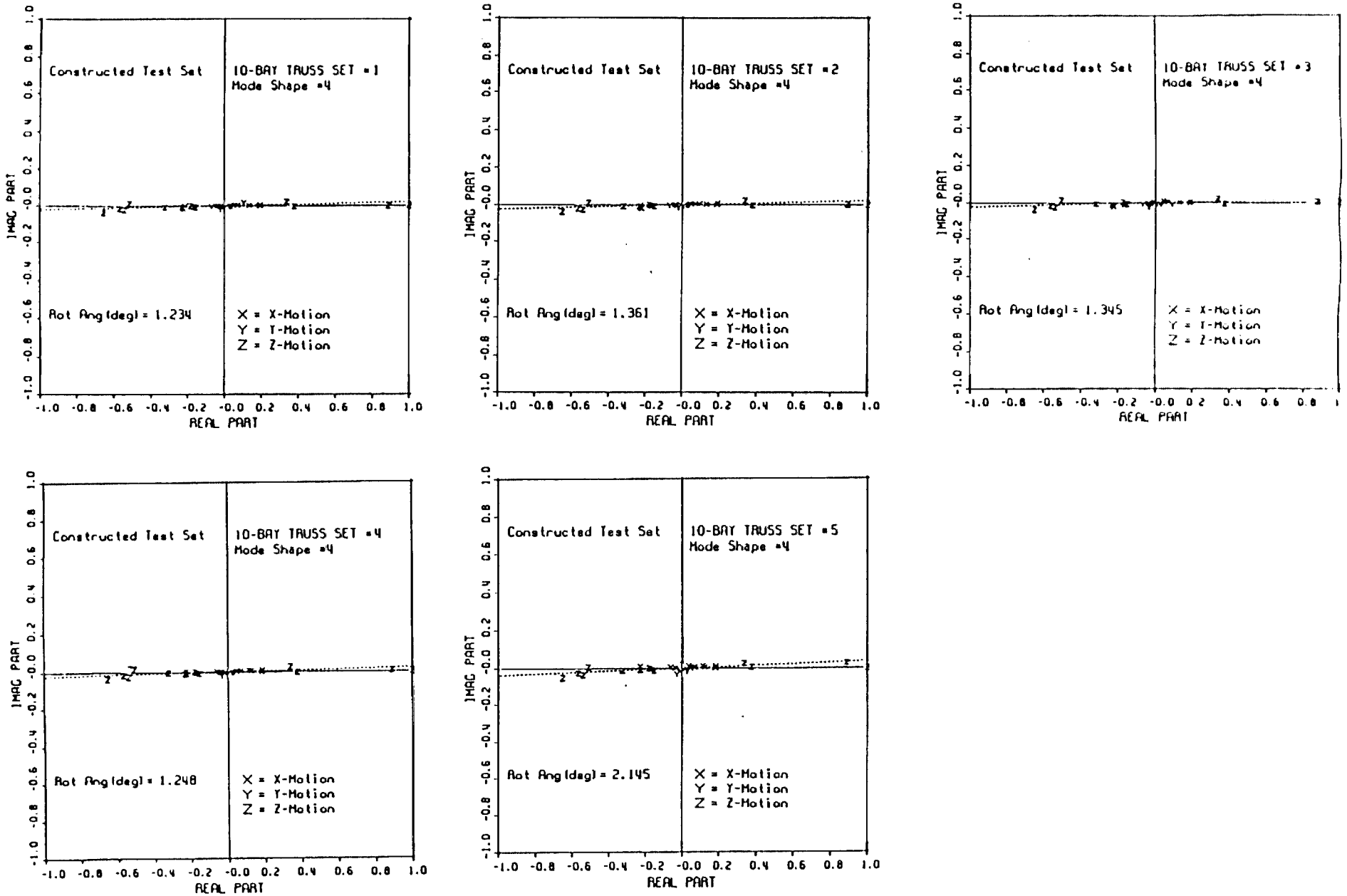

Figure 3–11. Scatter Plots for Ten Bay Truss Constructed Test Sets, Mode Shape 4.

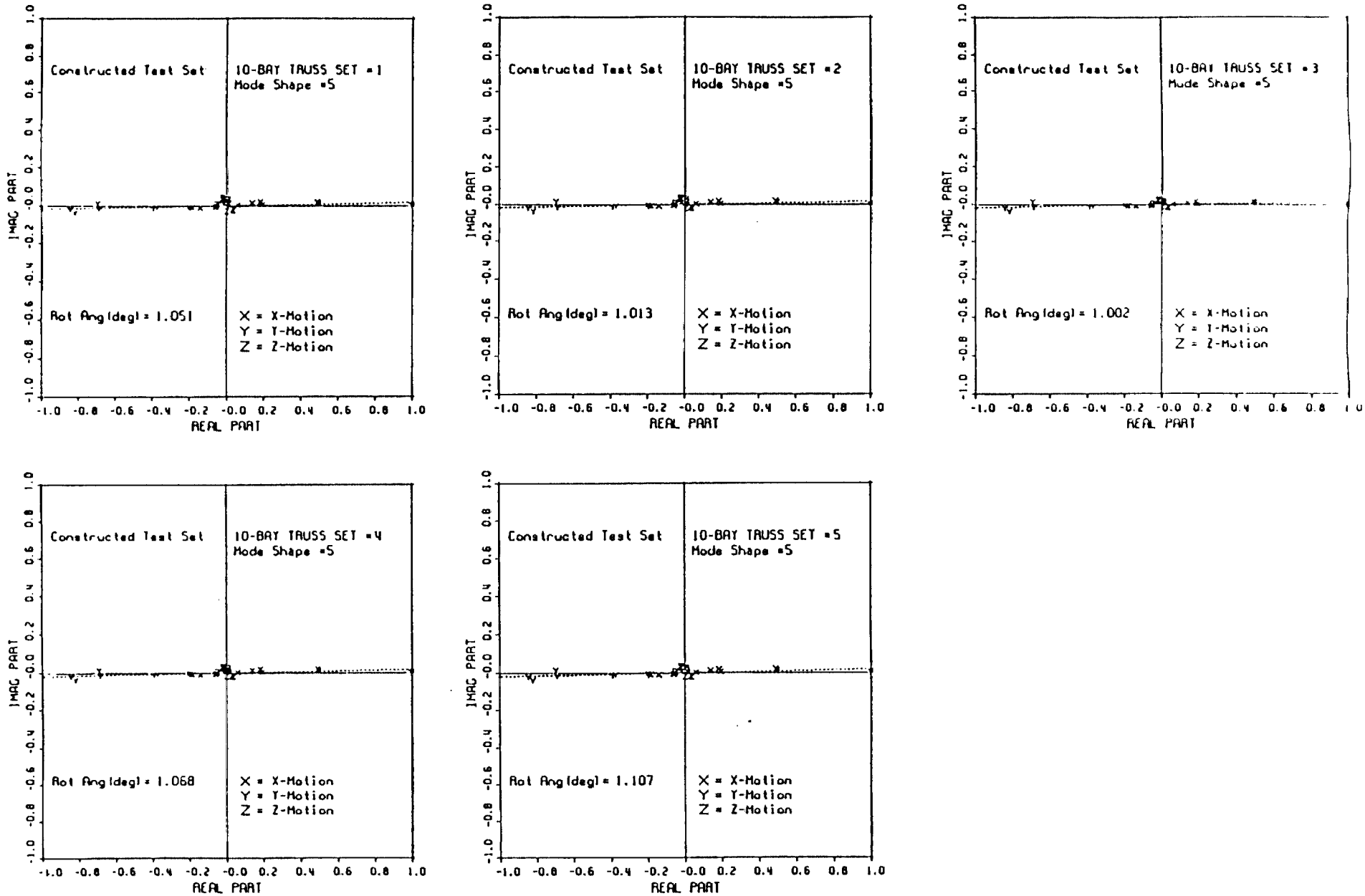

Figure 3–12. Scatter Plots for Ten Bay Truss Constructed Test Sets, Mode Shape 5.

Another notable feature is that the imaginary parts of the complex eigenvector elements are all very small. This is in contrast to some of the Mini–mast plots where imaginary parts as large as 0.2 were observed.

Damping computations were made for all five mode sets. The modal orthog–onality characteristics are presented in Tables 3–7a through 3–7e. Corresponding modal damping matrices and their average statistics are shown in Table 3–8.

It is important to note here that, as in the case of the Mini–mast Structure, the various mode sets were obtained by selecting different processing parameters on the ERA algorithm. The actual vibration test data used in all cases were the same. The different mode sets should therefore not be viewed as completely independent realizations. The variations observed from one mode set to another are a result of differences in the data processing, not the data themselves. Nevertheless, the results presented here are encouraging to the extent that consistent estimates of the modal damping matrices for two different structures have been obtained.

3.2 Estimation of Damping Distribution

Estimating the parameters of a physical damping model requires that a model first be defined. This is not a trivial task, and one should not be mislead by simplistic treatment given here. The emphasis here is not on the damping model itself, but rather on how the modal damping matrix may be used to estimate damping model parameters. To this end one may consider the equivalent viscous damping matrix, C, to reflect contributions from various sources, including damping from nonstructural items such as wiring harnesses, structural material damping, damping due to gravitational preload, and air damping, for example. Such a model might be formulated as follows:

$$C = \sum_i \alpha_i M_i + \sum_j \beta_{E_j} K_{E_j} + \sum_k \beta_{G_k} K_{G_k} + \sum_l \gamma_l A_l \qquad (3–59)$$

where α, β and γ represent model parameters, and the various indices sum over different zones of the structure. (Note that these β's and γ's are unrelated to those used earlier in the chapter.) In this case, M_i represents a portion of the mass matrix, K_{E_j} a portion of the

Table 3–7a. Comparison of Ten Bay Truss Modal Orthogonality Before and After Eigenvector Conditioning, Constructed Test Set, Mode Set #1.

Before Conditioning

*** ORIG ANAL/TEST REAL CROSS-ORTHOGONALITY ***

MODE	1	2	3	4	5
1	-0.9621	0.1661	0.0112	-0.0805	0.0066
2	-0.2687	-0.9852	-0.0337	-0.0360	-0.0183
3	-0.0282	0.0112	-0.9958	-0.0510	-0.0008
4	-0.0113	0.0121	0.0324	-0.9853	-0.0806
5	-0.0056	-0.0049	0.0046	-0.0674	0.9961

*** ORIG REAL TEST ORTHOGONALITY ***

MODE	1	2	3	4	5
1	1.0000	0.1039	0.0265	0.1022	-0.0063
2	0.1039	1.0000	0.0237	0.0084	0.0140
3	0.0265	0.0237	1.0000	0.0171	0.0029
4	0.1022	0.0084	0.0171	1.0000	0.0122
5	-0.0063	0.0140	0.0029	0.0122	1.0000

*** ORIG REAL/IMAG TEST ORTHOGONALITY ***

MODE	1	2	3	4	5
1	0.0148	0.0149	-0.0034	-0.0100	0.0028
2	0.0235	-0.0087	-0.0018	-0.0044	-0.0026
3	0.0044	0.0008	-0.0079	-0.0062	-0.0022
4	-0.0035	0.0026	0.0093	0.0215	-0.0423
5	-0.0008	0.0041	-0.0019	0.0133	0.0183

After Conditioning

*** FINAL ANAL/TEST REAL CROSS-ORTHOGONALITY ***

MODE	1	2	3	4	5
1	0.9746	-0.2167	-0.0251	0.0284	0.0024
2	0.2177	0.9750	0.0163	0.0230	-0.0121
3	0.0101	-0.0259	0.9958	0.0427	-0.0009
4	-0.0405	-0.0109	-0.0391	0.9886	-0.0740
5	-0.0017	0.0119	-0.0054	0.0733	0.9967

*** REAL TEST ORTHO AFTER ROT & MASS NORMAL ***

MODE	1	2	3	4	5
1	1.0000	0.0000	0.0000	0.0000	0.0000
2	0.0000	1.0000	0.0000	0.0000	0.0000
3	0.0000	0.0000	1.0000	0.0000	0.0000
4	0.0000	0.0000	0.0000	1.0000	0.0000
5	0.0000	0.0000	0.0000	0.0000	1.0000

** REAL/IMAG TEST ORTHO AFTER ROT & MASS NORMAL **

MODE	1	2	3	4	5
1	0.0000	0.0159	-0.0037	-0.0121	-0.0052
2	0.0225	0.0000	-0.0018	-0.0053	0.0029
3	0.0041	0.0006	0.0000	-0.0066	0.0019
4	-0.0055	0.0023	0.0098	0.0000	0.0431
5	0.0018	-0.0043	0.0020	-0.0130	0.0000

Table 3–7b. Comparison of Ten Bay Truss Modal Orthogonality Before and After Eigenvector Conditioning, Constructed Test Set, Mode Set #2.

Before Conditioning

*** ORIG ANAL/TEST REAL CROSS-ORTHOGONALITY ***

MODE	1	2	3	4	5
1	-0.9623	0.1665	0.0113	-0.0814	0.0062
2	-0.2681	-0.9851	-0.0335	-0.0365	-0.0185
3	-0.0280	0.0109	-0.9958	-0.0504	-0.0009
4	-0.0114	0.0137	0.0330	-0.9847	-0.0832
5	-0.0056	-0.0052	0.0047	-0.0764	0.9958

*** ORIG REAL TEST ORTHOGONALITY ***

MODE	1	2	3	4	5
1	1.0000	0.1028	0.0263	0.1033	-0.0059
2	0.1028	1.0000	0.0240	0.0072	0.0137
3	0.0263	0.0240	1.0000	0.0158	0.0029
4	0.1033	0.0072	0.0158	1.0000	0.0058
5	-0.0059	0.0137	0.0029	0.0058	1.0000

*** ORIG REAL/IMAG TEST ORTHOGONALITY ***

MODE	1	2	3	4	5
1	0.0143	0.0150	-0.0035	-0.0098	0.0033
2	0.0235	-0.0084	-0.0018	-0.0054	-0.0026
3	0.0047	0.0007	-0.0074	-0.0079	-0.0022
4	-0.0036	0.0029	0.0088	0.0237	-0.0362
5	-0.0007	0.0041	-0.0020	0.0033	0.0177

After Conditioning

*** FINAL ANAL/TEST REAL CROSS-ORTHOGONALITY ***

MODE	1	2	3	4	5
1	0.9746	-0.2165	-0.0249	0.0283	0.0021
2	0.2175	0.9750	0.0161	0.0240	-0.0125
3	0.0101	-0.0257	0.9958	0.0427	-0.0012
4	-0.0410	-0.0120	-0.0390	0.9882	-0.0798
5	-0.0021	0.0120	-0.0056	0.0793	0.9962

*** REAL TEST ORTHO AFTER ROT & MASS NORMAL ***

MODE	1	2	3	4	5
1	1.0000	0.0000	0.0000	0.0000	0.0000
2	0.0000	1.0000	0.0000	0.0000	0.0000
3	0.0000	0.0000	1.0000	0.0000	0.0000
4	0.0000	0.0000	0.0000	1.0000	0.0000
5	0.0000	0.0000	0.0000	0.0000	1.0000

** REAL/IMAG TEST ORTHO AFTER ROT & MASS NORMAL **

MODE	1	2	3	4	5
1	0.0000	0.0160	-0.0039	-0.0121	-0.0054
2	0.0226	0.0000	-0.0018	-0.0062	0.0029
3	0.0045	0.0005	0.0000	-0.0083	0.0019
4	-0.0055	0.0025	0.0093	0.0000	0.0369
5	0.0011	-0.0043	0.0021	-0.0033	0.0000

METHODS FOR EVALUATING THE PREDICTIVE ACCURACY OF STRUCTURAL DYNAMIC MODELS

PART 2

Table 3–7c. Comparison of Ten Bay Truss Modal Orthogonality Before and After Eigenvector Conditioning, Constructed Test Set, Mode Set #3.

Before Conditioning

*** ORIG ANAL/TEST REAL CROSS-ORTHOGONALITY ***

MODE	1	2	3	4	5
1	-0.9618	0.1665	0.0112	-0.0813	0.0063
2	-0.2698	-0.9851	-0.0335	-0.0361	-0.0184
3	-0.0279	0.0109	-0.9958	-0.0512	-0.0009
4	-0.0108	0.0139	0.0333	-0.9841	-0.0803
5	-0.0055	-0.0052	0.0046	-0.0828	0.9961

*** ORIG REAL TEST ORTHOGONALITY ***

MODE	1	2	3	4	5
1	1.0000	0.1047	0.0262	0.1026	-0.0059
2	0.1047	1.0000	0.0240	0.0068	0.0136
3	0.0262	0.0240	1.0000	0.0161	0.0029
4	0.1026	0.0068	0.0161	1.0000	-0.0035
5	-0.0059	0.0136	0.0029	-0.0035	1.0000

*** ORIG REAL/IMAG TEST ORTHOGONALITY ***

MODE	1	2	3	4	5
1	0.0147	0.0147	-0.0036	-0.0091	0.0045
2	0.0238	-0.0095	-0.0018	-0.0060	-0.0026
3	0.0048	0.0006	-0.0076	-0.0078	-0.0021
4	-0.0036	0.0026	0.0083	0.0235	-0.0266
5	-0.0008	0.0043	-0.0019	-0.0131	0.0175

After Conditioning

*** FINAL ANAL/TEST REAL CROSS-ORTHOGONALITY ***

MODE	1	2	3	4	5
1	0.9744	-0.2175	-0.0248	0.0287	0.0018
2	0.2184	0.9748	0.0160	0.0240	-0.0126
3	0.0100	-0.0257	0.9957	0.0435	-0.0015
4	-0.0411	-0.0118	-0.0393	0.9880	-0.0818
5	-0.0024	0.0120	-0.0057	0.0814	0.9961

*** REAL TEST ORTHO AFTER ROT & MASS NORMAL ***

MODE	1	2	3	4	5
1	1.0000	0.0000	0.0000	0.0000	0.0000
2	0.0000	1.0000	0.0000	0.0000	0.0000
3	0.0000	0.0000	1.0000	0.0000	0.0000
4	0.0000	0.0000	0.0000	1.0000	0.0000
5	0.0000	0.0000	0.0000	0.0000	1.0000

** REAL/IMAG TEST ORTHO AFTER ROT & MASS NORMAL **

MODE	1	2	3	4	5
1	0.0000	0.0158	-0.0040	-0.0113	-0.0061
2	0.0228	0.0000	-0.0018	-0.0068	0.0030
3	0.0046	0.0004	0.0000	-0.0082	0.0019
4	-0.0055	0.0022	0.0087	0.0000	0.0270
5	0.0004	-0.0044	0.0019	0.0129	0.0000

Table 3–7d. Comparison of Ten Bay Truss Modal Orthogonality Before and After Eigenvector Conditioning, Constructed Test Set, Mode Set #4.

Before Conditioning

*** ORIG ANAL/TEST REAL CROSS-ORTHOGONALITY ***

MODE	1	2	3	4	5
1	-0.9614	0.1662	0.0110	-0.0784	0.0066
2	-0.2716	-0.9852	-0.0335	-0.0375	-0.0183
3	-0.0276	0.0108	-0.9958	-0.0498	-0.0006
4	-0.0097	0.0138	0.0332	-0.9862	-0.0780
5	-0.0051	-0.0049	0.0048	-0.0555	0.9963

*** ORIG REAL TEST ORTHOGONALITY ***

MODE	1	2	3	4	5
1	1.0000	0.1068	0.0262	0.0988	-0.0059
2	0.1068	1.0000	0.0240	0.0086	0.0139
3	0.0262	0.0240	1.0000	0.0149	0.0030
4	0.0988	0.0086	0.0149	1.0000	0.0215
5	-0.0059	0.0139	0.0030	0.0215	1.0000

*** ORIG REAL/IMAG TEST ORTHOGONALITY ***

MODE	1	2	3	4	5
1	0.0145	0.0143	-0.0036	-0.0068	0.0042
2	0.0233	-0.0099	-0.0018	-0.0059	-0.0027
3	0.0050	0.0004	-0.0073	-0.0081	-0.0020
4	-0.0033	0.0024	0.0083	0.0218	-0.0327
5	-0.0010	0.0039	-0.0021	0.0132	0.0186

After Conditioning

*** FINAL ANAL/TEST REAL CROSS-ORTHOGONALITY ***

MODE	1	2	3	4	5
1	0.9743	-0.2183	-0.0245	0.0278	0.0029
2	0.2191	0.9746	0.0160	0.0247	-0.0120
3	0.0098	-0.0257	0.9958	0.0427	-0.0003
4	-0.0406	-0.0126	-0.0386	0.9891	-0.0669
5	-0.0013	0.0119	-0.0053	0.0660	0.9972

*** REAL TEST ORTHO AFTER ROT & MASS NORMAL ***

MODE	1	2	3	4	5
1	1.0000	0.0000	0.0000	0.0000	0.0000
2	0.0000	1.0000	0.0000	0.0000	0.0000
3	0.0000	0.0000	1.0000	0.0000	0.0000
4	0.0000	0.0000	0.0000	1.0000	0.0000
5	0.0000	0.0000	0.0000	0.0000	1.0000

** REAL/IMAG TEST ORTHO AFTER ROT & MASS NORMAL **

MODE	1	2	3	4	5
1	0.0000	0.0154	-0.0040	-0.0086	-0.0062
2	0.0224	0.0000	-0.0018	-0.0068	0.0030
3	0.0048	0.0002	0.0000	-0.0085	0.0018
4	-0.0051	0.0020	0.0087	0.0000	0.0337
5	0.0019	-0.0041	0.0023	-0.0128	0.0000

Table 3–7e. Comparison of Ten Bay Truss Modal Orthogonality Before and After Eigenvector Conditioning, Constructed Test Set, Mode Set #5.

Before Conditioning

*** ORIG ANAL/TEST REAL CROSS-ORTHOGONALITY ***

MODE	1	2	3	4	5
1	-0.9583	0.1662	0.0111	-0.0799	0.0065
2	-0.2827	-0.9852	-0.0333	-0.0366	-0.0184
3	-0.0278	0.0108	-0.9957	-0.0501	-0.0009
4	-0.0070	0.0136	0.0331	-0.9856	-0.0807
5	-0.0059	-0.0050	0.0046	-0.0588	0.9961

*** ORIG REAL TEST ORTHOGONALITY ***

MODE	1	2	3	4	5
1	1.0000	0.1184	0.0266	0.0973	-0.0064
2	0.1184	1.0000	0.0238	0.0076	0.0138
3	0.0266	0.0238	1.0000	0.0152	0.0030
4	0.0973	0.0076	0.0152	1.0000	0.0209
5	-0.0064	0.0138	0.0030	0.0209	1.0000

*** ORIG REAL/IMAG TEST ORTHOGONALITY ***

MODE	1	2	3	4	5
1	0.0154	0.0143	-0.0044	-0.0081	0.0039
2	0.0236	-0.0085	-0.0018	-0.0049	-0.0026
3	0.0044	0.0007	-0.0087	-0.0047	-0.0020
4	-0.0035	0.0028	0.0071	0.0374	-0.0349
5	-0.0005	0.0039	-0.0016	0.0327	0.0193

After Conditioning

*** FINAL ANAL/TEST REAL CROSS-ORTHOGONALITY ***

MODE	1	2	3	4	5
1	0.9730	-0.2239	-0.0248	0.0299	0.0027
2	0.2247	0.9733	0.0157	0.0243	-0.0122
3	0.0100	-0.0257	0.9957	0.0428	-0.0006
4	-0.0422	-0.0113	-0.0386	0.9885	-0.0693
5	-0.0010	0.0119	-0.0052	0.0684	0.9970

*** REAL TEST ORTHO AFTER ROT & MASS NORMAL ***

MODE	1	2	3	4	5
1	1.0000	0.0000	0.0000	0.0000	0.0000
2	0.0000	1.0000	0.0000	0.0000	0.0000
3	0.0000	0.0000	1.0000	0.0000	0.0000
4	0.0000	0.0000	0.0000	1.0000	0.0000
5	0.0000	0.0000	0.0000	0.0000	1.0000

** REAL/IMAG TEST ORTHO AFTER ROT & MASS NORMAL **

MODE	1	2	3	4	5
1	0.0000	0.0155	-0.0047	-0.0114	-0.0060
2	0.0223	0.0000	-0.0016	-0.0059	0.0030
3	0.0041	0.0005	0.0000	-0.0054	0.0018
4	-0.0055	0.0025	0.0076	0.0000	0.0359
5	0.0023	-0.0041	0.0019	-0.0318	0.0000

Table 3–8a. Modal Damping Matrices for the LaRC Ten Bay Truss, Constructed Test Sets.

Mode Sets #1 through #5

*** MODAL DAMPING (%) MATRIX ***

MODE	1	2	3	4	5
1	0.4340	-0.0025	-0.4089	-1.1533	-0.5818
2	-0.0025	0.8780	-0.1650	-0.5933	0.3898
3	-0.4089	-0.1650	0.5790	-0.2324	0.0066
4	-1.1533	-0.5933	-0.2324	0.2690	0.0384
5	-0.5818	0.3898	0.0066	0.0384	0.3590

*** MODAL DAMPING (%) MATRIX ***

MODE	1	2	3	4	5
1	0.4810	-0.0024	-0.4285	-1.1552	-0.5957
2	-0.0024	0.9260	-0.1623	-0.6940	0.3948
3	-0.4285	-0.1623	0.5790	-0.2540	0.0075
4	-1.1552	-0.6940	-0.2540	0.3880	0.0280
5	-0.5957	0.3948	0.0075	0.0280	0.3590

*** MODAL DAMPING (%) MATRIX ***

MODE	1	2	3	4	5
1	0.4640	-0.0025	-0.4373	-1.0698	-0.6489
2	-0.0025	0.9110	-0.1571	-0.7479	0.4046
3	-0.4373	-0.1571	0.5750	-0.2446	0.0096
4	-1.0698	-0.7479	-0.2446	0.4470	0.0106
5	-0.6489	0.4046	0.0096	0.0106	0.3610

*** MODAL DAMPING (%) MATRIX ***

MODE	1	2	3	4	5
1	0.4320	-0.0024	-0.4493	-0.7983	-0.6891
2	-0.0024	0.8950	-0.1561	-0.7546	0.4015
3	-0.4493	-0.1561	0.5770	-0.2507	0.0016
4	-0.7983	-0.7546	-0.2507	0.3570	0.0327
5	-0.6891	0.4015	0.0016	0.0327	0.3630

*** MODAL DAMPING (%) MATRIX ***

MODE	1	2	3	4	5
1	0.4720	-0.0026	-0.4896	-1.0843	-0.6752
2	-0.0026	0.9090	-0.1504	-0.6675	0.3980
3	-0.4896	-0.1504	0.5650	-0.1849	0.0066
4	-1.0843	-0.6675	-0.1849	0.3970	0.0457
5	-0.6752	0.3980	0.0066	0.0457	0.3620

Average of Five Mode Sets

*** AVERAGE MODAL DAMPING (%) ***

MODE	1	2	3	4	5
1	0.4566	-0.0025	-0.4427	-1.0522	-0.6381
2	-0.0025	0.9038	-0.1582	-0.6915	0.3978
3	-0.4427	-0.1582	0.5750	-0.2333	0.0064
4	-1.0522	-0.6915	-0.2333	0.3716	0.0311
5	-0.6381	0.3978	0.0064	0.0311	0.3608

Table 3–8b. Covariance of Modal Damping Matrix Elements for the LaRC Ten Bay Truss, Constructed Test Sets.

ST.D. (%)	CORRELATION MATRIX														
0.022	1.000	-.396	-.348	-.539	0.086	0.909	0.257	-.132	0.134	-.376	0.223	0.630	0.683	-.176	-.234
0.000	-.396	1.000	0.737	0.304	0.317	-.099	-.682	-.261	-.070	0.939	-.955	-.335	-.275	-.407	-.245
0.030	-.348	0.737	1.000	-.291	0.791	-.323	-.968	0.287	-.449	0.924	-.728	0.177	-.496	-.379	-.726
0.147	-.539	0.304	-.291	1.000	-.772	-.207	0.409	-.656	0.571	0.004	-.225	-.819	0.073	-.015	0.839
0.048	0.086	0.317	0.791	-.772	1.000	-.097	-.890	0.666	-.774	0.598	-.299	0.467	-.486	-.049	-.988
0.018	0.909	-.099	-.323	-.207	-.097	1.000	0.279	-.484	0.374	-.199	-.078	0.395	0.799	-.358	-.040
0.006	0.257	-.682	-.968	0.409	-.890	0.279	1.000	-.443	0.637	-.885	0.632	-.164	0.588	0.193	0.830
0.066	-.132	-.261	0.287	-.656	0.666	-.484	-.443	1.000	-.914	0.011	0.408	0.191	-.739	0.611	-.622
0.006	0.134	-.070	-.449	0.571	-.774	0.374	0.637	-.914	1.000	-.289	-.116	-.018	0.812	-.587	0.718
0.006	-.376	0.939	0.924	0.004	0.598	-.199	-.885	0.011	-.289	1.000	-.906	-.093	-.409	-.408	-.527
0.028	0.223	-.955	-.728	-.225	-.299	-.078	0.632	0.408	-.116	-.906	1.000	0.106	0.026	0.656	0.262
0.003	0.630	-.335	0.177	-.819	0.467	0.395	-.164	0.191	-.018	-.093	0.106	1.000	0.401	-.464	-.572
0.066	0.683	-.275	-.496	0.073	-.486	0.799	0.588	-.739	0.812	-.409	0.026	0.401	1.000	-.574	0.358
0.013	-.176	-.407	-.379	-.015	-.049	-.358	0.193	0.611	-.587	-.408	0.656	-.464	-.574	1.000	0.100
0.002	-.234	-.245	-.726	0.839	-.988	-.040	0.830	-.622	0.718	-.527	0.262	-.572	0.358	0.100	1.000

elastic stiffness matrix, K_{G_k} a portion of the geometric (gravity dependent) stiffness matrix, and A_l a portion of the projected area of the structure related to air damping. Thus, if K_{G_k} and A_l could be defined for a particular ground test configuration, in addition to M_i and K_{E_j}, and all of the parameters α, β and γ successfully estimated, then the contributions of gravity and air damping could be subtracted out as a means of estimating on–orbit damping.

For purposes of illustration, gravity–dependent damping and air damping will be neglected. Equation (3–59) is thus simplified by neglecting the last two terms. Further simplification is achieved by dropping the subscript, E, on β_j and K_j, and zoning the structure the same for M and K. These simplifications lead to

$$C = \sum_k \alpha_k M_k + \sum_k \beta_k K_k \tag{3–60}$$

which is recognized as similar in concept to proportional damping, except that in proportional damping, only one α and one β apply to the entire structure. One might refer to Equation (3–60) as representing piece–wise proportional damping. Again, it is emphasized that this model is not necessarily intended to be realistic, but rather illustrative.

The next step is to transform Equation (3–60) to modal coordinates as in Equation (3–11b).

$$\xi = \phi_R^T C \phi_R = \sum_k \alpha_k \phi_R^T M_k \phi_R + \sum_k \beta_k \phi_R^T K_k \phi_R$$

$$= \sum_k (\alpha_k m_k + \beta_k k_k) \tag{3–61}$$

It follows that the derivatives of ξ with respect to α_k and β_k are

$$\frac{\partial \xi}{\partial \alpha_k} = m_k = \phi_R^T M_k \phi_R \tag{3–62}$$

$$\frac{\partial \xi}{\partial \beta_k} = k_k = \phi_R^T K_k \phi_R \tag{3–63}$$

It is important to note that in this example, ξ is a linear function of the α's and β's, so that the partial derivatives shown in (3–62) and (3–63) are constant. The relationship between ξ and the α's and β's is simplified by arraying the elements of ξ in vector form (following the notational convention of Chapter 2)

$$r = \text{Vec}\,(\xi) \tag{3–64}$$

and forming a single vector of the α's and β's which is designated θ.

$$\theta = \begin{Bmatrix} \alpha_1 \\ \alpha_2 \\ \vdots \\ \alpha_n \\ \beta_1 \\ \beta_2 \\ \vdots \\ \beta_n \end{Bmatrix} \tag{3–65}$$

Then (3–61) may be written simply as

$$r = T\theta \tag{3–66}$$

where

$$T = \frac{\partial \xi}{\partial \theta} = \left[\frac{\partial \xi}{\partial \alpha} \vdots \frac{\partial \xi}{\partial \beta} \right] \tag{3–67}$$

and T is a constant matrix of sensitivity coefficients. Whenever T is a square matrix and nonsingular, Equation (3–66) can be inverted to solve for θ in terms of r.

$$\theta = T^{-1}r \tag{3–68}$$

Usually this will not be the case, however. For example, there may be more r–parameters than θ–parameters, in which case a least squares solution may be sought for θ. A least–squares estimate of θ in this case gives

$$\theta = (T^T T)^{-1} T^T r \tag{3–69}$$

provided that the matrix $(T^T T)$ is not singular. The least squares estimator is obtained by minimizing the quadratic cost function

$$J = (r - T\theta)^T (r - T\theta) \tag{3–70}$$

with respect to θ. This is achieved by setting the gradient of J with respect to θ equal to zero,

$$\nabla_\theta J = -T^T (r - T\theta) = 0 \tag{3–71}$$

from which (3–69) is derived. Equation (3–69) reduces to (3–68) whenever T^{-1} exists.

Finally, it is recognized that the vector, r, in Equation (3–64) is actually a vector of random variables, in which case a statistical estimator for θ is more appropriate than either (3–68) or (3–69). Since r and θ are linearly related, it follows from (3–66) that

$$\bar{r} = T\bar{\theta} \tag{3–72a}$$

$$(r - \bar{r}) = T(\theta - \bar{\theta}) \tag{3–72b}$$

where $\bar{r}$ and $\bar{\theta}$ denote the mean values of r and θ. In addition to $\bar{r}$ which is obtained by averaging the modal damping matrices, the covariance matrix of r, defined by

$$S_{rr} = E\,[(r - \bar{r})(r - \bar{r})^T] \tag{3–73}$$

is also available. One may then define the cost function

$$J = [(r - \bar{r}) - T(\theta - \bar{\theta})]^T\, S_{rr}^{-1}\, [(r - \bar{r}) - T\,(\theta - \bar{\theta})] \tag{3–74}$$

which weights the differences between Δr and $T\Delta\theta$ by S_{rr}^{-1}, regarded as an information matrix on r. Minimizing J with respect to θ now leads to

$$\nabla_\theta J = -T^T S_{rr}^{-1}\, [(r - \bar{r}) - T\,(\theta - \bar{\theta})] = 0 \tag{3–75}$$

which results in the statistical estimator

$$\theta = \bar{\theta} + (T^T S_{rr}^{-1} T)^{-1} T^T S_{rr}^{-1}\,(r - \bar{r}) \tag{3–76}$$

The matrix $(T^T S_{rr}^{-1} T)^{-1}$ has a useful statistical interpretation, realized by substituting (3–76) for $(\theta - \bar{\theta})$ in the covariance matrix of θ:

$$\begin{aligned} S_{\theta\theta} &= E[(\theta - \bar{\theta})(\theta - \bar{\theta})^T] \\ &= E[(T^T S_{rr}^{-1} T)^{-1}\, T^T S_{rr}^{-1}\,(r - \bar{r})\,(r - \bar{r})^T\, S_{rr}^{-1} T\,(T^T S_{rr}^{-1} T)^{-1}] \\ &= (T^T S_{rr}^{-1} T)^{-1}\, T^T S_{rr}^{-1}\, E[(r - \bar{r})\,(r - \bar{r})^T]\, S_{rr}^{-1} T\,(T^T S_{rr}^{-1} T)^{-1} \\ &= (T^T S_{rr}^{-1} T)^{-1} \end{aligned} \tag{3–77}$$

It is important to recognize that (3–77) is only true whenever S_{rr} and $(T^T S_{rr}^{-1} T)$ are nonsingular. In particular, this means that (a) the number of estimates of ξ used in computing $\bar{r} = \text{Vec}\,(\bar{\xi})$ and S_{rr} must be equal to or greater than the number of elements in r, and (b) that the dimension of r be equal to or greater than the dimension of θ.

Attempts were made to estimate a set of α's and β's for the Ten Bay Truss, since this was the simpler of the two structures for which full modal damping matrices had been computed. For purposes of this estimation, the truss beam was divided into five zones of two bays per zone. One α–parameter and one β–parameter were assigned to each zone. The 5 x 5 modal damping matrix produced an S_{rr} matrix of dimension 15 x 15. However, since only five estimates of the modal damping matrix were made, S_{rr} was only of rank 5. A pseudo–inverse based on singular value decomposition was used to obtain S_{rr}^{-1} and $(T^T S_{rr} T)^{-1}$ in Equation (3–76). This attempt yielded a solution for the α's and β's which matched the diagonal elements of the modal damping matrix fairly well, but not the off–diagonal elements. The estimated values of the α's and β's, however, were not meaningful; they were an order of magnitude too large and some were negative. This of course is not surprising since the problem is undetermined.

A second attempt was then made to estimate only four α and β parameters, two α's for the two zones near the free end of the beam and two β's for the two zones near the fixed end. The pseudo–inverse was still used to compute S_{rr}^{-1} and $(T^T S_{rr} T)^{-1}$, but the latter was not singular in this case. This attempt was similarly unsuccessful.

There are several possible reasons for the failure of these attempts:

- The rank deficiency of S_{rr} resulting from insufficient data,
- Bias error in the modal damping matrix, possibly resulting from the fact that all of the data came from only one test, and
- A poor damping model.

It is certainly conceivable that piece–wise proportional damping is incapable of matching the full modal damping matrix. Any future work, however, should begin by running enough tests to obtain a nonsingular S_{rr} matrix with reasonably small coefficients of variation. The different estimates of the modal damping matrix should not all be obtained from the same test.

4. UNCERTAINTY PROPAGATION

Models are used to predict the behavior of physical systems. Structural dynamic models are used to predict how structures respond to dynamic loads. This project has been concerned with the development of methods for evaluating the accuracy of those predictions. Chapters 2 and 3 have addressed the problem of quantifying defacto model uncertainty, based on actual analysis and test experience. This experience is cast in the form of modal mass, stiffness and damping parameters. The present chapter addresses the problem of propagating that uncertainty through a model.

One of the advantages of expressing model uncertainty in terms of modal parameters is that it is readily propagated through a model to determine either (1) eigenvalue/eigenvector uncertainty, (2) response uncertainty, or (3) the uncertainty of physical design parameters. The first two are referred to as forward propagation because the propagation follows the direction of analysis; the latter is called backward propagation or reverse propagation because the propagation is opposite to the direction of analysis.

Three essentially different methods are used for forward uncertainty propagation:

1. Linear covariance propagation;
2. The Vertex Method for evaluating functions of fuzzy variables; and
3. Numerical simulation using the Monte Carlo Method.

All three of the methods have been implemented in deliverable software; each has its particular advantages and disadvantages which make it more suitable for some applications than others. The software has been written to select the best combination of methods for general application, i.e. execution defaults to the most suitable methods for general application based on current experience. Default overrides are available. Each of the three methods is discussed in the subsections which follow.

4.1 Linear Covariance Propagation

Linear covariance propagation is addressed first because it is the simplest, most economical, and most generally applicable method of uncertainty propagation. It may be used for either forward propagation or reverse propagation as long as an explicit functional

relationship exists in at least one of the two directions. The methods used in forward propagation will be addressed first, because this is usually the direction for which an explicit functional relationship exists.

4.1.1 Forward Propagation

Variables "downstream" from the modal parameters (in the flow of analysis) are referred to as response variables and designated by the vector, u, where

$$u = u(r) \tag{4–1}$$

The vector, u, which might represent eigenvalues, eigenvectors or frequency response, may be expanded in a Taylor series about the nominal vector, u_o, such that

$$u = u_o + \frac{\partial u}{\partial r} \Delta r + \text{H.O.T.} \tag{4–2}$$

The matrix, $\partial u / \partial r$, is called the sensitivity matrix and is designated T_{ur},

$$T_{ur} \equiv \frac{\partial u}{\partial r} \tag{4–3}$$

Then $\Delta u = u - u_o$ has the linear approximation

$$\Delta u = T_{ur} \Delta r \tag{4–4}$$

The covariance matrix of u is defined as

$$S_{uu} = E [\Delta u \, \Delta r^T] = T_{ur} E [\Delta r \, \Delta r^T] \, T_{ur}{}^T = T_{ur} S_{rr} T_{ur}{}^T \tag{4–5}$$

In general, S_{rr} represents the covariance of modal mass, stiffness and damping parameters. However, it will be of block–diagonal form, provided that damping uncertainty is estimated independently of mass and stiffness uncertainty, as assumed here. The covariance matrix, S_{rr}, can therefore be expressed in partitioned form as

$$S_{rr} = \left[\begin{array}{cc:c} S_{mm} & S_{mk} & 0 \\ S_{km} & S_{kk} & 0 \\ \hdashline 0 & 0 & S_{\xi\xi} \end{array}\right] \tag{4–6}$$

The matrix S_{rr} is no longer in the dimensionless form of $S_{\tilde{r}\tilde{r}}$, but is obtained from $S_{\tilde{r}\tilde{r}}$ by appropriate frequency scaling. Given $S_{\tilde{r}\tilde{r}}$ in the form

$$S_{\tilde{r}\tilde{r}} = \left[\begin{array}{cc:c} S_{mm} & S_{m\tilde{k}} & 0 \\ S_{\tilde{k}m} & S_{\tilde{k}\tilde{k}} & 0 \\ \hdashline 0 & 0 & S_{\zeta\zeta} \end{array}\right] \tag{4–7}$$

S_{rr} is obtained by multiplying the individual elements of $S_{\tilde{r}\tilde{r}}$ by the appropriate frequencies. Therefore when a particular element of S_{mk} corresponds to m_{gh} and k_{ij}, then

$$S_{m_{gh}k_{ij}} = \omega_i\omega_j \, S_{m_{gh}\tilde{k}_{ij}} \tag{4–8a}$$

Similarly when an element of S_{kk} corresponds to k_{gh} and k_{ij}, then

$$S_{k_{gh}k_{ij}} = \omega_g\omega_h\omega_i\omega_j \, S_{\tilde{k}_{gh}\tilde{k}_{ij}} \tag{4–8b}$$

When an element of $S_{\xi\xi}$ corresponds to ξ_{gh} and ξ_{ij}, then

$$S_{\xi_{gh}\,\xi_{ij}} = 4\sqrt{\omega_g\omega_h\omega_i\omega_j} \; S_{\zeta_{gh}\zeta_{ij}} \tag{4–8c}$$

The derivatives, $\partial u/\partial r$, are particularly simple whenever u represents eigenvalues and/or eigenvectors and r represents modal mass and stiffness parameters. And of course $\partial u/\partial r = 0$ whenever u represents (undamped) eigenvalues and/or eigenvectors and r represents modal damping. When r represents modal mass and stiffness parameters, Reference [4–1] gives

$$\frac{\partial \lambda_j}{\partial r_k} = \begin{cases} 1 & : r_k = k_{jj} \\ -\lambda_j & : r_k = m_{jj} \\ 0 & : \text{otherwise} \end{cases} \tag{4–9}$$

$$\frac{\partial \phi_j}{\partial r_k} = \sum_{h=1}^{m} \phi_{ih} \begin{cases} \left[\frac{1-\delta_{hj}}{\lambda_j - \lambda_h}\right] & : r_k = k_{hj} \\ -\lambda_j \left[\frac{1-\delta_{hj}}{\lambda_j - \lambda_h}\right] - \frac{\delta_{hj}}{2} & : r_k = m_{hj} \\ 0 & : \text{otherwise} \end{cases} \tag{4–10}$$

The eigenvector derivative matrix is written out in Table 4–1 for the case when ϕ, m and k are all 3 x 3 matrices.

The response variables, u, may also represent frequency response function (FRF) amplitude and phase. In this case $\partial u / \partial r$ represents the derivatives of FRF amplitude and phase with respect to the modal parameters, r. These derivatives are obtained in closed form from the forced equations of motion. Consistent with Equations (2–1) and (3–1), the damped non–homogeneous equations of motion are written as

$$M\ddot{x} + C\dot{x} + Kx = f_x(t) \tag{4–11}$$

where C is an equivalent viscous damping matrix and $f_x(t)$ is the time dependent force vector. Whenever $f_x(t)$ can be separated into a constant spatial vector, P_x, and a scalar time function, g(t), Equation (4–11) becomes

$$M\ddot{x} + C\dot{x} + Kx = P_x\, g(t) \tag{4–12}$$

The modal transformation derived from Equation (2–2) gives

$$x = \phi q \tag{4–13}$$

and when applied to (4–10) results in

Table 4–1a. Eigenvector Derivatives with Respect to Modal Mass.

$$\frac{\partial \phi}{\partial m} = \begin{bmatrix}
\frac{\partial \phi_{11}}{\partial m_{11}} & \frac{\partial \phi_{11}}{\partial m_{12}} & \frac{\partial \phi_{11}}{\partial m_{13}} & \frac{\partial \phi_{11}}{\partial m_{22}} & \frac{\partial \phi_{11}}{\partial m_{23}} & \frac{\partial \phi_{11}}{\partial m_{33}} \\
\frac{\partial \phi_{21}}{\partial m_{11}} & \frac{\partial \phi_{21}}{\partial m_{12}} & \frac{\partial \phi_{21}}{\partial m_{13}} & \frac{\partial \phi_{21}}{\partial m_{22}} & \frac{\partial \phi_{21}}{\partial m_{23}} & \frac{\partial \phi_{21}}{\partial m_{33}} \\
\frac{\partial \phi_{31}}{\partial m_{11}} & \frac{\partial \phi_{31}}{\partial m_{12}} & \frac{\partial \phi_{31}}{\partial m_{13}} & \frac{\partial \phi_{31}}{\partial m_{22}} & \frac{\partial \phi_{31}}{\partial m_{23}} & \frac{\partial \phi_{31}}{\partial m_{33}} \\
\frac{\partial \phi_{12}}{\partial m_{11}} & \frac{\partial \phi_{12}}{\partial m_{12}} & \frac{\partial \phi_{12}}{\partial m_{13}} & \frac{\partial \phi_{12}}{\partial m_{22}} & \frac{\partial \phi_{12}}{\partial m_{23}} & \frac{\partial \phi_{12}}{\partial m_{33}} \\
\frac{\partial \phi_{22}}{\partial m_{11}} & \frac{\partial \phi_{22}}{\partial m_{12}} & \frac{\partial \phi_{22}}{\partial m_{13}} & \frac{\partial \phi_{22}}{\partial m_{22}} & \frac{\partial \phi_{22}}{\partial m_{23}} & \frac{\partial \phi_{22}}{\partial m_{33}} \\
\frac{\partial \phi_{32}}{\partial m_{11}} & \frac{\partial \phi_{32}}{\partial m_{12}} & \frac{\partial \phi_{32}}{\partial m_{13}} & \frac{\partial \phi_{32}}{\partial m_{22}} & \frac{\partial \phi_{32}}{\partial m_{23}} & \frac{\partial \phi_{32}}{\partial m_{33}} \\
\frac{\partial \phi_{13}}{\partial m_{11}} & \frac{\partial \phi_{13}}{\partial m_{12}} & \frac{\partial \phi_{13}}{\partial m_{13}} & \frac{\partial \phi_{13}}{\partial m_{22}} & \frac{\partial \phi_{13}}{\partial m_{23}} & \frac{\partial \phi_{13}}{\partial m_{33}} \\
\frac{\partial \phi_{23}}{\partial m_{11}} & \frac{\partial \phi_{23}}{\partial m_{12}} & \frac{\partial \phi_{23}}{\partial m_{13}} & \frac{\partial \phi_{23}}{\partial m_{22}} & \frac{\partial \phi_{23}}{\partial m_{23}} & \frac{\partial \phi_{23}}{\partial m_{33}} \\
\frac{\partial \phi_{33}}{\partial m_{11}} & \frac{\partial \phi_{33}}{\partial m_{12}} & \frac{\partial \phi_{33}}{\partial m_{13}} & \frac{\partial \phi_{33}}{\partial m_{22}} & \frac{\partial \phi_{33}}{\partial m_{23}} & \frac{\partial \phi_{33}}{\partial m_{33}}
\end{bmatrix}$$

$$= \begin{bmatrix}
\frac{-\phi_{11}}{2} & \frac{-\phi_{12}\lambda_1}{\lambda_1-\lambda_2} & \frac{-\phi_{13}\lambda_1}{\lambda_1-\lambda_3} & 0 & 0 & 0 \\
\frac{-\phi_{21}}{2} & \frac{-\phi_{22}\lambda_1}{\lambda_1-\lambda_2} & \frac{-\phi_{23}\lambda_1}{\lambda_1-\lambda_3} & 0 & 0 & 0 \\
\frac{-\phi_{31}}{2} & \frac{-\phi_{32}\lambda_1}{\lambda_1-\lambda_2} & \frac{-\phi_{33}\lambda_1}{\lambda_1-\lambda_3} & 0 & 0 & 0 \\
0 & \frac{-\phi_{11}\lambda_2}{\lambda_2-\lambda_1} & 0 & \frac{-\phi_{12}}{2} & \frac{-\phi_{12}\lambda_2}{\lambda_2-\lambda_3} & 0 \\
0 & \frac{-\phi_{21}\lambda_2}{\lambda_2-\lambda_1} & 0 & \frac{-\phi_{22}}{2} & \frac{-\phi_{22}\lambda_2}{\lambda_2-\lambda_3} & 0 \\
0 & \frac{-\phi_{31}\lambda_2}{\lambda_2-\lambda_1} & 0 & \frac{-\phi_{12}}{2} & \frac{-\phi_{32}\lambda_2}{\lambda_2-\lambda_3} & 0 \\
0 & 0 & \frac{-\phi_{11}\lambda_3}{\lambda_3-\lambda_1} & 0 & \frac{-\phi_{12}\phi_3}{\lambda_3-\lambda_2} & \frac{-\phi_{13}}{2} \\
0 & 0 & \frac{-\phi_{21}\lambda_3}{\lambda_3-\lambda_1} & 0 & \frac{-\phi_{22}\lambda_3}{\lambda_3-\lambda_2} & \frac{-\phi_{23}}{2} \\
0 & 0 & \frac{-\phi_{31}\lambda_3}{\lambda_3-\lambda_1} & 0 & \frac{-\phi_{32}\lambda_3}{\lambda_3-\lambda_2} & \frac{-\phi_{33}}{2}
\end{bmatrix}$$

Table 4–1b. Eigenvector Derivatives with Respect to Modal Stiffness.

$$\frac{\partial \phi}{\partial k} = \begin{bmatrix}
\frac{\partial \phi_{11}}{\partial k_{11}} & \frac{\partial \phi_{11}}{\partial k_{12}} & \frac{\partial \phi_{11}}{\partial k_{13}} & \frac{\partial \phi_{11}}{\partial k_{22}} & \frac{\partial \phi_{11}}{\partial k_{23}} & \frac{\partial \phi_{11}}{\partial k_{33}} \\
\frac{\partial \phi_{21}}{\partial k_{11}} & \frac{\partial \phi_{21}}{\partial k_{12}} & \frac{\partial \phi_{21}}{\partial k_{13}} & \frac{\partial \phi_{21}}{\partial k_{22}} & \frac{\partial \phi_{21}}{\partial k_{23}} & \frac{\partial \phi_{21}}{\partial k_{33}} \\
\frac{\partial \phi_{31}}{\partial k_{11}} & \frac{\partial \phi_{31}}{\partial k_{12}} & \frac{\partial \phi_{31}}{\partial k_{13}} & \frac{\partial \phi_{31}}{\partial k_{22}} & \frac{\partial \phi_{31}}{\partial k_{23}} & \frac{\partial \phi_{31}}{\partial k_{33}} \\
\frac{\partial \phi_{12}}{\partial k_{11}} & \frac{\partial \phi_{12}}{\partial k_{12}} & \frac{\partial \phi_{12}}{\partial k_{13}} & \frac{\partial \phi_{12}}{\partial k_{22}} & \frac{\partial \phi_{12}}{\partial k_{23}} & \frac{\partial \phi_{12}}{\partial k_{33}} \\
\frac{\partial \phi_{22}}{\partial k_{11}} & \frac{\partial \phi_{22}}{\partial k_{12}} & \frac{\partial \phi_{22}}{\partial k_{13}} & \frac{\partial \phi_{22}}{\partial k_{22}} & \frac{\partial \phi_{22}}{\partial k_{23}} & \frac{\partial \phi_{22}}{\partial k_{33}} \\
\frac{\partial \phi_{32}}{\partial k_{11}} & \frac{\partial \phi_{32}}{\partial k_{12}} & \frac{\partial \phi_{32}}{\partial k_{13}} & \frac{\partial \phi_{32}}{\partial k_{22}} & \frac{\partial \phi_{32}}{\partial k_{23}} & \frac{\partial \phi_{32}}{\partial k_{33}} \\
\frac{\partial \phi_{13}}{\partial k_{11}} & \frac{\partial \phi_{13}}{\partial k_{12}} & \frac{\partial \phi_{13}}{\partial k_{13}} & \frac{\partial \phi_{13}}{\partial k_{22}} & \frac{\partial \phi_{13}}{\partial k_{23}} & \frac{\partial \phi_{13}}{\partial k_{33}} \\
\frac{\partial \phi_{23}}{\partial k_{11}} & \frac{\partial \phi_{23}}{\partial k_{12}} & \frac{\partial \phi_{23}}{\partial k_{13}} & \frac{\partial \phi_{23}}{\partial k_{22}} & \frac{\partial \phi_{23}}{\partial k_{23}} & \frac{\partial \phi_{23}}{\partial k_{33}} \\
\frac{\partial \phi_{33}}{\partial k_{11}} & \frac{\partial \phi_{33}}{\partial k_{12}} & \frac{\partial \phi_{33}}{\partial k_{13}} & \frac{\partial \phi_{33}}{\partial k_{22}} & \frac{\partial \phi_{33}}{\partial k_{23}} & \frac{\partial \phi_{33}}{\partial k_{33}}
\end{bmatrix}$$

$$= \begin{bmatrix}
0 & \frac{\phi_{12}}{\lambda_1 - \lambda_2} & \frac{\phi_{13}}{\lambda_1 - \lambda_3} & 0 & 0 & 0 \\
0 & \frac{\phi_{22}}{\lambda_1 - \lambda_2} & \frac{\phi_{23}}{\lambda_1 - \lambda_3} & 0 & 0 & 0 \\
0 & \frac{\phi_{32}}{\lambda_1 - \lambda_2} & \frac{\phi_{33}}{\lambda_1 - \lambda_3} & 0 & 0 & 0 \\
0 & \frac{\phi_{11}}{\lambda_2 - \lambda_1} & 0 & 0 & \frac{\phi_{13}}{\lambda_2 - \lambda_3} & 0 \\
0 & \frac{\phi_{21}}{\lambda_2 - \lambda_1} & 0 & 0 & \frac{\phi_{23}}{\lambda_2 - \lambda_3} & 0 \\
0 & \frac{\phi_{31}}{\lambda_2 - \lambda_1} & 0 & 0 & \frac{\phi_{33}}{\lambda_2 - \lambda_3} & 0 \\
0 & 0 & \frac{\phi_{11}}{\lambda_3 - \lambda_1} & 0 & \frac{\phi_{12}}{\lambda_3 - \lambda_2} & 0 \\
0 & 0 & \frac{\phi_{21}}{\lambda_3 - \lambda_1} & 0 & \frac{\phi_{22}}{\lambda_3 - \lambda_2} & 0 \\
0 & 0 & \frac{\phi_{31}}{\lambda_3 - \lambda_1} & 0 & \frac{\phi_{32}}{\lambda_3 - \lambda_2} & 0
\end{bmatrix}$$

$$I\ddot{q} + \xi\dot{q} + \lambda q = \phi^T P_x\, g(t) = P_q\, g(t) \tag{4–14}$$

where as before (following Equation (2–8))

$$\phi^T M \phi = I \tag{4–15a}$$

$$\phi^T K \phi = \lambda = \omega^2 \tag{4–15b}$$

and in addition

$$\phi^T C \phi = \xi \tag{4–15c}$$

Transformation of (4–14) to the frequency domain gives

$$[(\lambda - \Omega^2 I) + i\Omega\xi]\, H_q\,(i\Omega) = Z_q\,(i\Omega)\, H_q\,(i\Omega) = P_q \tag{4–16}$$

where

$$H_q\,(i\Omega) = \frac{Q(i\Omega)}{G(i\Omega)} \tag{4–17}$$

$$Z_q\,(i\Omega) = [(\lambda - I\Omega^2) + i\Omega\xi\,] \tag{4–18}$$

and $Q(i\Omega)$ and $G(i\Omega)$ are respectively the Fourier transforms of the vector $q(t)$ and the scalar $g(t)$. Then

$$H_q\,(i\Omega) = Z_q^{-1}\,(i\Omega)\, P_q \tag{4–19}$$

Transformation back to the x–coordinates gives

$$H_x\,(i\Omega) = \phi Z_q^{-1}\,(i\Omega)\, \phi^T P_x \tag{4–20}$$

The derivative of the vector $H_x(i\Omega)$ with respect to the (scalar) modal parameter, r_k, (assuming that P_x is not a function of r_k) is

$$\frac{\partial H_x(i\Omega)}{\partial r_k} = \frac{\partial \phi}{\partial r_k} Z_q^{-1}(i\Omega)\, \phi^T P_x + \phi \frac{\partial Z_q^{-1}(i\Omega)}{\partial r_k} \phi^T P_x + \phi Z_q^{-1}(i\Omega) \frac{\partial \phi^T}{\partial r_k} P_x \tag{4–21}$$

where

$$\frac{\partial Z_q^{-1}(i\Omega)}{\partial r_k} = - Z_q^{-1}(i\Omega) \frac{\partial Z_q(i\Omega)}{\partial r_k} Z_q^{-1}(i\Omega) \tag{4–22}$$

and from (4–18)

$$\frac{\partial Z_q(i\Omega)}{\partial r_k} = \frac{\partial \lambda}{\partial r_k} + i\Omega \frac{\partial \xi}{\partial r_k} \tag{4–23}$$

When the structure is base–excited, then P_x (or its equivalent) will be a function of r_k. The equations of motion for a base–excited structure are usually written:

$$M\ddot{x} + C(\dot{x} - \dot{x}_o) + K(x - x_o) = 0 \tag{4–24}$$

The transformation of variables

$$z = x - x_o \tag{4–25}$$

leads to

$$M\ddot{z} + C\dot{z} + Kz = - M\ddot{x}_o = - M\alpha_z \ddot{g}(t) \tag{4–26}$$

where g(t) represents the base input motion and α_z is essentially a distribution vector. Now one may define

$$P_z = -M\alpha_z \tag{4–27}$$

and Equation (4–26) becomes

$$M\ddot{z} + C\dot{z} + Kz = P_z\,\ddot{g}(t) \tag{4–28}$$

which is of the same form as (4–10) except that $\ddot{g}(t)$ replaces g(t) because the forcing function is now a base acceleration instead of an applied force. In order to express M in (4–27) in terms of the modal mass matrix, m, the vector α_z is transformed as follows:

$$\alpha_z = \phi\alpha_q \tag{4–29}$$

$$\alpha_q = (\phi^T\phi)^{-1}\,\phi^T\alpha_z \tag{4–30}$$

Then (4–20) becomes

$$\begin{aligned} H_z(i\Omega) &= -\Omega^2\,\phi Z_q^{-1}(i\Omega)\,\phi^T M\phi\,\alpha_q \\ &= -\Omega^2\,\phi Z_q^{-1}(i\Omega)\,\alpha_q \end{aligned} \tag{4–31}$$

The derivative of $H_z(i\Omega)$ with respect to r_k is

$$\begin{aligned} \frac{\partial H_z(i\Omega)}{\partial r_k} = &-\Omega^2\frac{\partial\phi}{\partial r_k}Z_q^{-1}(i\Omega)\,\alpha_q \\ &-\Omega^2\,\phi\frac{\partial Z_q^{-1}(i\Omega)}{\partial r_k}\alpha_q \\ &-\Omega^2\,\phi\,Z_q^{-1}(i\Omega)\frac{\partial\alpha_q}{\partial r_k} \end{aligned} \tag{4–32}$$

where

$$\frac{\partial \alpha_q}{\partial r_k} = \left[\phi^T \phi \right]^{-1} \left[\frac{\partial \phi^T}{\partial r_k} - \left[\frac{\partial \phi^T}{\partial r_k} \phi + \phi^T \frac{\partial \phi}{\partial r_k} \right] \left[\phi^T \phi \right]^{-1} \phi^T \right] \alpha_z \tag{4–33}$$

It is convenient to express the complex frequency response function, $H_x(i\Omega)$, in terms of amplitude, $A(\Omega)$, and phase, $\varphi(\Omega)$, functions.

$$A(\Omega) = [H_x(\Omega)\, H_x^*(\Omega)]^{1/2}$$

$$= [R_x^2(\Omega) + I_x^2(\Omega)]^{1/2} \tag{4–34a}$$

$$\varphi(\Omega) = \tan^{-1} \left[\frac{I_x(\Omega)}{R_x(\Omega)} \right] \tag{4–34b}$$

The asterisk denotes a complex conjugate and $R_x(\Omega)$ and $I_x(\Omega)$ are the real and imaginary parts of $H_x(i\Omega)$. The derivatives of FRF log–amplitude and phase are

$$\frac{\partial \log A(\Omega)}{\partial r_k} = \frac{\log e}{A^2(\Omega)} \left[R_x(\Omega) \frac{\partial R_x(\Omega)}{\partial r_k} + I_x(\Omega) \frac{\partial I_x(\Omega)}{\partial r_k} \right] \tag{4–35a}$$

$$\frac{\partial \varphi(\Omega)}{\partial r_k} = \frac{1}{A^2(\Omega)} \left[R_x(\Omega) \frac{\partial I_x(\Omega)}{\partial r_k} - I_x(\Omega) \frac{\partial R_x(\Omega)}{\partial r_k} \right] \tag{4–35b}$$

It may be noted that both log–amplitude and phase are dimensionless quantities.

There is a fine point to make here regarding the type of modes represented by λ and ϕ, and the type of mass and stiffness properties represented by M and K. Heretofore, these symbols have represented the (hypothetical) "truth" model, while the same symbols with a left superscript "o" have been used to represent the original analytical model,

assumed to be a close approximation to the "truth." In this chapter, the unsuperscripted symbols may be considered to represent either the pretest or posttest analytical models, or the "truth" model, with one small (but conceptually important) adjustment.

If λ, ϕ, M, K are taken to represent the analytical model, then the full modal damping matrix, ξ, defined in (4–15c) should be replaced by

$$c = (\psi^T)^{-1} \xi \psi^{-1} \tag{4–36}$$

where ξ represents the "measured" modal damping matrix discussed in Chapter 3, and ψ is the transformation matrix relating the true modes, ϕ, to the analytical modes, ${}^o\phi$.

$$\phi = {}^o\phi\psi$$

Equation (4–36) follows from the definition of c as

$$c = {}^o\phi^T C {}^o\phi$$

and ξ as

$$\xi = \phi^T C \phi = \psi^T {}^o\phi^T C {}^o\phi\psi = \psi^T c \psi$$

where C represents the "true" equivalent viscous damping matrix.

4.1.2 Reverse Propagation

Reverse uncertainty propagation refers to the propagation of uncertainty backward through the analysis chain. Suppose the analysis chain is described as moving from design parameters, θ, to modal parameters, r, to response variables, u. This progression may be indicated symbolically as

$$\theta \rightarrow r \rightarrow u$$

In other words, response, u, is computed from the modal parameters, r, which in turn are computed from the design parameters, θ. Forward covariance propagation gives

$$S_{rr} = T_{r\theta}\, S_{\theta\theta}\, T_{r\theta}^{T}, \tag{4–37a}$$

$$S_{uu} = T_{ur}\, S_{rr}\, T_{ur}^{T} \tag{4–37b}$$

$$S_{uu} = T_{u\theta}\, S_{\theta\theta}\, T_{u\theta}^{T} \tag{4–37c}$$

Reverse propagation is employed when computing $S_{\theta\theta}$ from S_{rr}, S_{rr} from S_{uu}, or $S_{\theta\theta}$ from S_{uu}. Equation (3–77) is an example of reverse uncertainty propagation. In the present case, however, the Bayesian form is used because prior knowledge is assumed about the parameters.

In Bayesian parameter estimation [4–2], one has some prior knowledge of the parameters being estimated. This knowledge is contained in the covariance matrix of initial parameter estimates, say $S_{\theta\theta}$. If new knowledge is gained in the form of information about r, contained in the covariance matrix, S_{rr}, then $S_{\theta\theta}$ may be updated by adding the new information

$$S_{\theta\theta}^{*} = [S_{\theta\theta}^{-1} + T_{r\theta}^{T}\, S_{rr}^{-1}\, T_{r\theta}]^{-1} \tag{4–38}$$

Equation (4–38) is seen to be similar to (3–77). The only difference is that prior knowledge is reflected in the covariance matrix $S_{\theta\theta}$. The form of (4–38) is also similar to the equation for the stiffness of two springs in series, where

$$K = \left[\frac{1}{K_1} + \frac{1}{K_2} \right]^{-1}$$

In this analogy, uncertainty (represented by variance or covariance) is analogous to stiffness or rigidity, while information content (represented by the inverse of variance or covariance) is analogous to flexibility.

There are at least two foreseeable uses for reverse uncertainty propagation. The first is to estimate the uncertainty in physical design parameters given the uncertainty in modal parameters. This is potentially useful in Bayesian parameter estimation where a

covariance matrix of the initial parameter estimates is required. Typically, this covariance matrix is assumed to be diagonal, and the diagonal elements are determined by intuitively estimating the coefficient of variation on each parameter estimate. For some parameters, this is not difficult. For example, when lumped masses are used to represent the mass distribution of a structure, the mass values can be estimated fairly accurately because mass properties can be measured. On the other hand, stiffness properties are more difficult to estimate, generally requiring detailed finite element modeling. It is usually not feasible to directly estimate the parameters of these small finite elements based on global test data, so recourse is made to estimating zonal parameters such as linked finite element parameters or submatrix scaling parameters, for example. It is much more difficult to quantify uncertainty in the initial estimates of these zonal parameters. The ability to use uncertainties in modal data to back out uncertainties in zonal parameters could be of significant benefit, since these uncertainties play an important role in revising the initial parameter estimates with Bayesian estimation.

Another possible use for reverse uncertainty propagation is in establishing criteria for modeling accuracy in terms of eigenvalue and eigenvector error. Criteria for modeling accuracy, or analysis–test correlation, are usually specified in terms of the difference between analysis and test frequencies (e.g. less than or equal to ± 3%) and the cross–orthogonality between analysis and test modes (e.g. less than or equal to 0.10). These values are established conservatively on the basis of prior experience, and are rarely if ever fully satisfied. Questions inevitably arise as to what these criteria imply (or guarantee) with regard to predictive accuracy, and whether they can be relaxed. Reverse uncertainty propagation could be used to transform uncertainties in frequency response back to uncertainties in frequency and cross–orthogonality. The uncertainties in frequency response could be specified in terms of tolerances on FRF amplitude, representing, say, two standard deviations. This information would define a diagonal covariance matrix of FRF amplitude, S_{uu}, at selected frequencies, and selected response coordinates. Uncertainties in frequency, f, and cross–orthogonality, ψ, would then be obtained from S_{uu} as follows:

$$S_{ff} = [T_{uf}^T S_{uu}^{-1} T_{uf}]^{-1} \tag{4–39a}$$

$$S_{\psi\psi} = [T_{u\psi} S_{uu}^{-1} T_{u\psi}]^{-1} \tag{4–39b}$$

Since no prior information is known about f and ψ, the form of (3–77) is used rather than that of (4–38). The sensitivity matrices T_{uf} and $T_{u\phi}$ are given by

$$T_{uf} = T_{ur}\, T_{rf} \tag{4–40a}$$

$$T_{u\phi} = T_{ur}\, T_{r\phi} \tag{4–40b}$$

where T_{ur} is given by (4–21) and (4–35a) and T_{rf} and $T_{r\phi}$ are obtained from Equations (2–9), (2–13), (2–14) and (2–19) as

$$T_{rf} = \begin{bmatrix} \frac{\partial m}{\partial f} \\ \cdots \\ \frac{\partial k}{\partial f} \end{bmatrix}; \quad \begin{aligned} \frac{\partial m_{ij}}{\partial f_j} &= 0 \\ \frac{\partial k_{ij}}{\partial f_j} &= 4\pi^2 f_j \delta_{ij} = 2^o \omega_j \delta_{ij} \end{aligned} \tag{4–41a}$$

$$T_{r\phi} = \begin{bmatrix} \frac{\partial m}{\partial \psi} \\ \cdots \\ \frac{\partial k}{\partial \psi} \end{bmatrix}; \quad \begin{aligned} \frac{\partial m_{ij}}{\partial \psi_{gh}} &= -\delta_{ig}\delta_{jh} - \delta_{jg}\delta_{ih} \\ \frac{\partial k_{ij}}{\partial \psi_{gh}} &= -\delta_{ig}\delta_{jh}{}^o\lambda_i - \delta_{jg}\delta_{ih}{}^o\lambda_j \end{aligned} \tag{4–41b}$$

The square roots of the diagonal elements of S_{ff} and $S_{\psi\phi}$ are the standard deviations of the modal frequencies and cross–orthogonality coefficients, respectively.

4.1.3 Example

A simple example is presented to illustrate linear covariance propagation. Figure 4–1 shows a 2–DOF spring–mass system. Damping elements are not shown; however, one–half percent damping is assumed in each of the two modes. Mass and stiffness uncertainty are represented by the covariance matrix of modal mass and stiffness for large space structures (Table 2–2). In this case, the covariance matrix is of dimension 6 x 6, including only those rows and columns of the matrix in Table 2–2 which correspond to the elements m_{11}, m_{12}, m_{22}, $\bar{k}_{11}$, $\bar{k}_{12}$ and $\bar{k}_{22}$, i.e. the intersecting elements of rows and columns 1, 2, 6, 16, 17 and 21. A lognormal distribution on damping was assumed with a median value of 0.5% and a one–sigma multiplicative factor of 2.0.

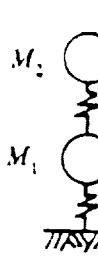

Nominal Parameters:

$M_1 = M_2 = 1.0$

$K_1 = K_2 = 1.0$

$\zeta_1 = \zeta_2 = 0.5\%$ *of Critical*

$F_2 = 1.0$

```
*** MODEL INPUTS FOR 2-DOF LUMPED MODEL ***
        (FILENAME = 2dof.dat)

    1    1    0    0    0    0    0     - X-MAP -
    2    2    0    0    0    0    0   (Node # & Dof #s)
    1    2    3                        (Mass Skyline)
1.0       1.0                         (Mass Matrix)
    1    2    4                       (Stiffness skyline)
2.0       1.0       -1.0              (Stiff Matrix)
    1    2                           (Coord Ordering Vector)
```

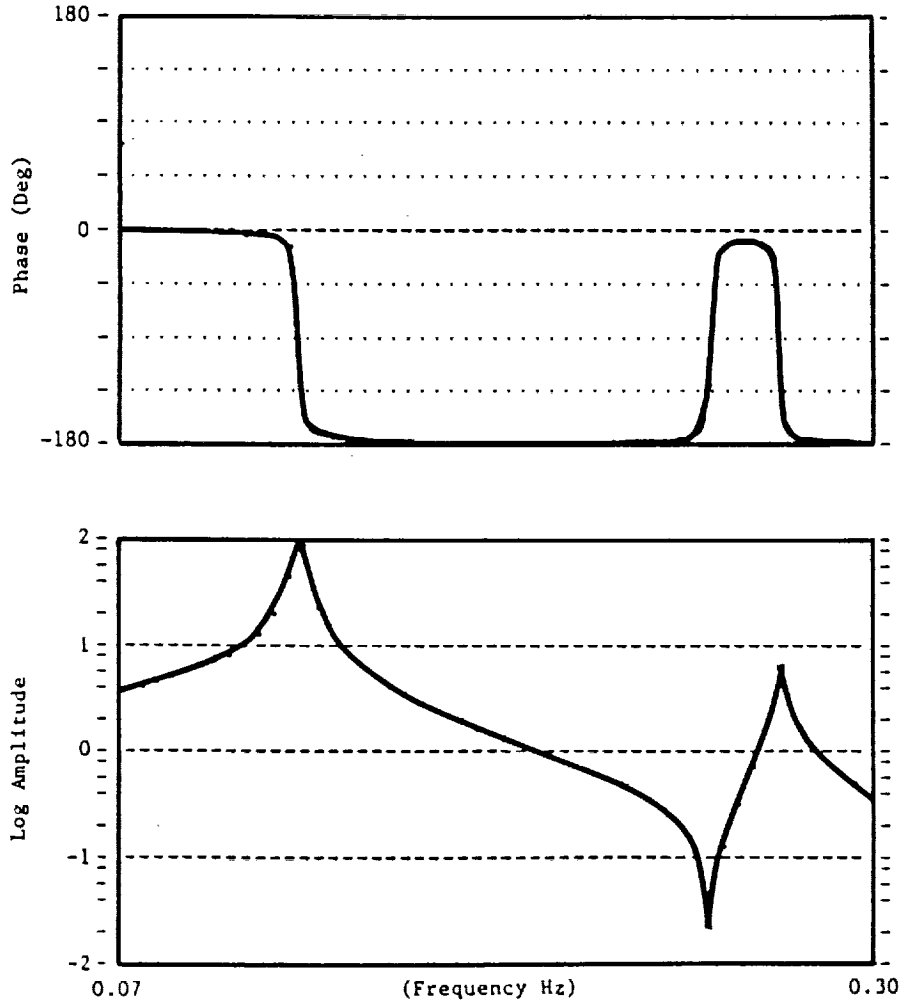

Figure 4–1. Two–DOF Model.

Figure 4–2 shows the nominal and $\pm 1\sigma$ interval response computations for FRF amplitude and phase corresponding to displacement at the end mass due to force applied at that coordinate, and spanning a frequency range which encompasses the first mode. It is noted that the $\pm 1\sigma$ uncertainty intervals tend to become very large near resonance. They are in fact larger than shown. The symbols used to delimit the amplitude intervals are asterisks as long as the one–sided intervals do not exceed two decades. When an interval exceeds that limit, it is truncated at two decades (on either side of the nominal response log–amplitude) for plotting purposes and delimited by arrows indicating that the single–sided interval actually computed exceeded two decades. In the case of phase, when the phase interval exceeds 360°, it simply wraps around.

It is clear from this simple example that linear covariance propagation breaks down near resonances where the derivatives with respect to frequency (and therefore modal mass and stiffness) become large. The same occurs at anti–resonances. Away from these frequencies, however, the uncertainty intervals computed by linear covariance propagation appear to be reasonable. Further evaluation of these results is offered later, when the same 2–DOF example is used to illustrate the fuzzy set approach and numerical simulation.

4.2 Fuzzy Set Approach

The fuzzy set approach was identified in Phase I as providing an alternative to linear covariance propagation for the evaluation of uncertainty intervals in frequency response near poles and zeros. Since uncertainty expressed in terms of fuzzy sets results in possibility intervals, this approach was seen as a means of bounding the uncertainty near poles and zeros where linear covariance propagation yields unreasonably large intervals of uncertainty. The practical feasibility of this approach depends on the assumption that only a few modal parameters contribute to response uncertainty near these frequencies. Otherwise, the computations become prohibitively expensive. Thus, while linear covariance propagation is ineffective at frequencies near poles and zeros but effective elsewhere, the fuzzy set approach is effective near poles and zeros but ineffective elsewhere. The two methods taken together are effective over the entire frequency range.

LINEAR STATISTICAL PROPAGATION

*** DISPL @ TOP MASS DUE TO FORCE @ TOP MASS ***

*** AMPLITUDE ***

FREQ-HZ	NOM DISPL/FORCE
7.00000E-02	3.95191E+00
7.08720E-02	4.05344E+00
7.17549E-02	4.16323E+00
7.26488E-02	4.28227E+00
7.35539E-02	4.41176E+00
7.44702E-02	4.55309E+00
7.53979E-02	4.70791E+00
7.63372E-02	4.87819E+00
7.72882E-02	5.06633E+00
7.82510E-02	5.27520E+00
7.92259E-02	5.50837E+00
8.02129E-02	5.77026E+00
8.12121E-02	6.06642E+00
8.22238E-02	6.40395E+00
8.32482E-02	6.79205E+00
8.42853E-02	7.24283E+00
8.53353E-02	7.77267E+00
8.63983E-02	8.40412E+00
8.74747E-02	9.16926E+00
8.85644E-02	1.01152E+01
8.96677E-02	1.13141E+01
9.07848E-02	1.28825E+01
9.19157E-02	1.50208E+01
9.30608E-02	1.81063E+01
9.42201E-02	2.29401E+01
9.53939E-02	3.15648E+01
9.65823E-02	5.10423E+01
9.77855E-02	1.23417E+02
9.90037E-02	1.14763E+02
1.00237E-01	4.74890E+01
1.01486E-01	2.88793E+01
1.02750E-01	2.05155E+01
1.04030E-01	1.57920E+01
1.05326E-01	1.27629E+01
1.06638E-01	1.06571E+01
1.07967E-01	9.10908E+00
1.09312E-01	7.92368E+00
1.10673E-01	6.98711E+00
1.12052E-01	6.22869E+00
1.13448E-01	5.60215E+00
1.14861E-01	5.07597E+00
1.16292E-01	4.62793E+00
1.17741E-01	4.24189E+00
1.19208E-01	3.90589E+00
1.20693E-01	3.61084E+00
1.22196E-01	3.34974E+00
1.23719E-01	3.11708E+00
1.25260E-01	2.90849E+00
1.26821E-01	2.72044E+00
1.28400E-01	2.55006E+00
1.30000E-01	2.39499E+00

0 *** AMPLITUDE *** 5

*** DISPL @ TOP MASS DUE TO FORCE @ TOP MASS ***

Figure 4–2a. One–Sigma Uncertainty Intervals on FRF Amplitude for 2–DOF Example, Linear Covariance Propagation.

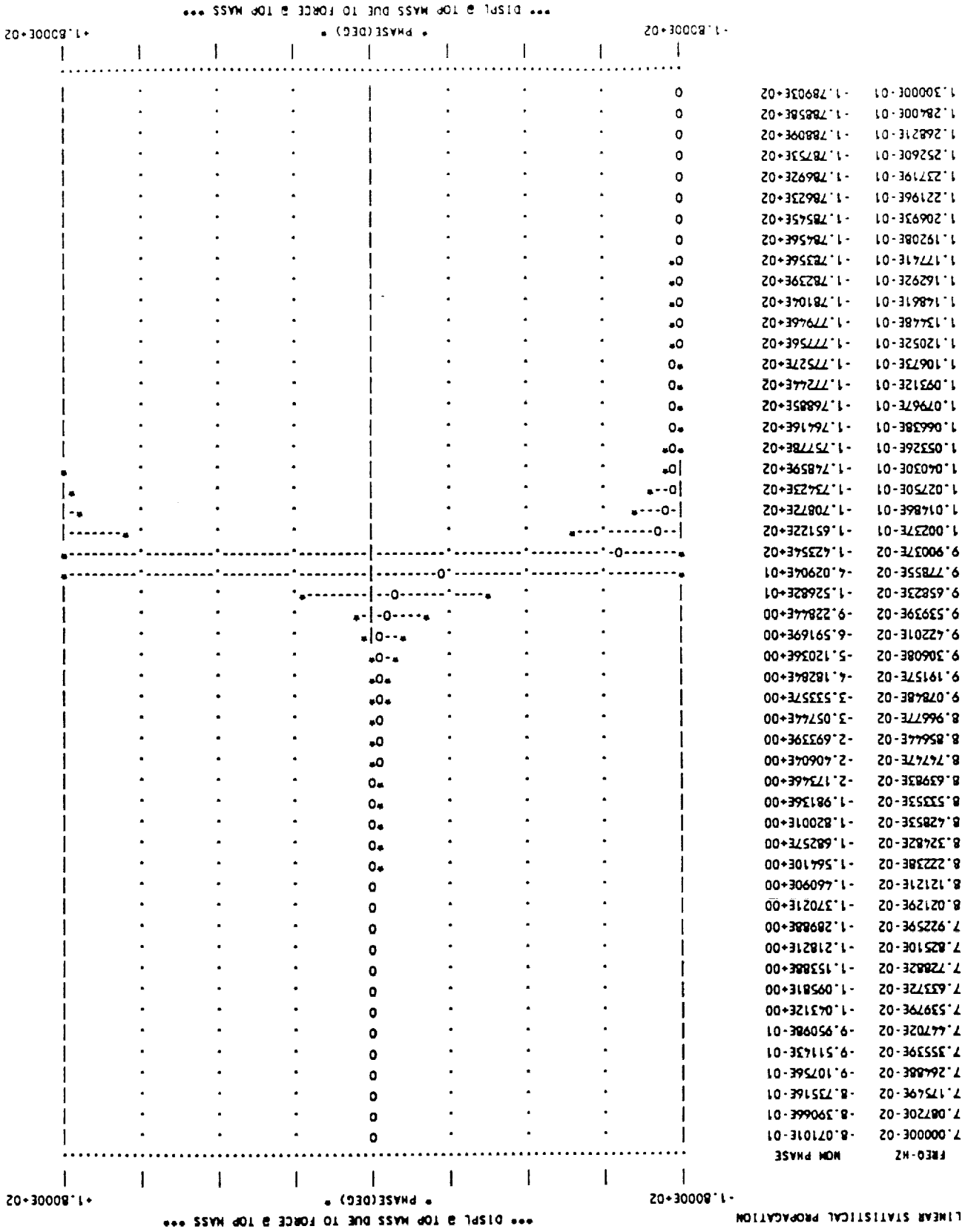

Figure 4–2b. One–Sigma Uncertainty Intervals on FRF Phase for 2–DOF Example, Linear Covariance Propagation.

4.2.1 Fuzzy Sets

Fuzzy sets are axiomatically different from deterministic and probabilistic concepts, but there are interesting comparisons between them. Fuzzy sets are represented by membership functions that can assume values between 0 and 1 and that measure the degree of membership a member of a set S has to a fuzzy subset F of S. Parameters can be thought of as being one of three kinds: deterministic, probabilistic, or fuzzy. The deterministic parameter has complete membership (1) at a distinct value. The probabilistic parameter varies within some domain (usually called the sample space), but its membership within (1), and outside (0) these bounds is certain. The fuzzy parameters may have uncertain membership (between 0 and 1) at a particular level, and may not have complete membership (1) anywhere.

Fuzzy sets offer an alternative to random variables for representing uncertainty [4–3]. The degree of uncertainty in a fuzzy set is defined by its membership function as illustrated in Figures 4–3a. At any particular value of membership (α ; $0 \leq \alpha \leq 1$), the interval defined by the intersection (referred to as the "α–cut" interval) of the membership function with the horizontal line at that level of membership is interpreted as an interval of confidence, or the range of possibility associated with that membership. Any value falling outside of the interval is not possible given that membership. Any value falling outside the range of possibility at the zero membership level is impossible in an absolute sense. Thus, unlike probability density functions which define the relative frequency of occurrence of a random variable as a function of the values which the random variable may assume, the membership function defines the range of possibility of a fuzzy number as a function of membership. In the case of a triangular membership function where the vertex has a membership of unity, the value of the fuzzy number corresponding to the vertex is interpreted as the deterministic value.

It is not necessary to specify the membership function of a fuzzy set in order to define an interval of possibility. For example, one might define the interval of $[-\sigma, +\sigma]$, or $\pm\ 1\sigma$ as an interval of possibility associated with some unspecified membership of an unspecified membership function of a given parameter. In fact, one might define $\pm\ 1\sigma$ intervals for a number of parameters and seek to determine the corresponding possibility interval for structural response. If the $\pm\ 1\sigma$ possibility intervals relate to the same membership level for all of the parameters, then the corresponding possibility interval for

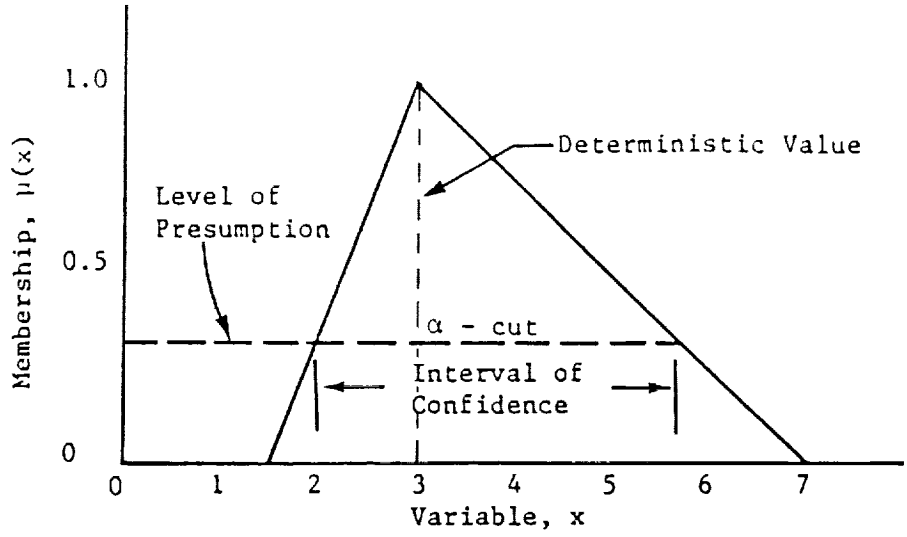

(a) Illustration of Membership Function

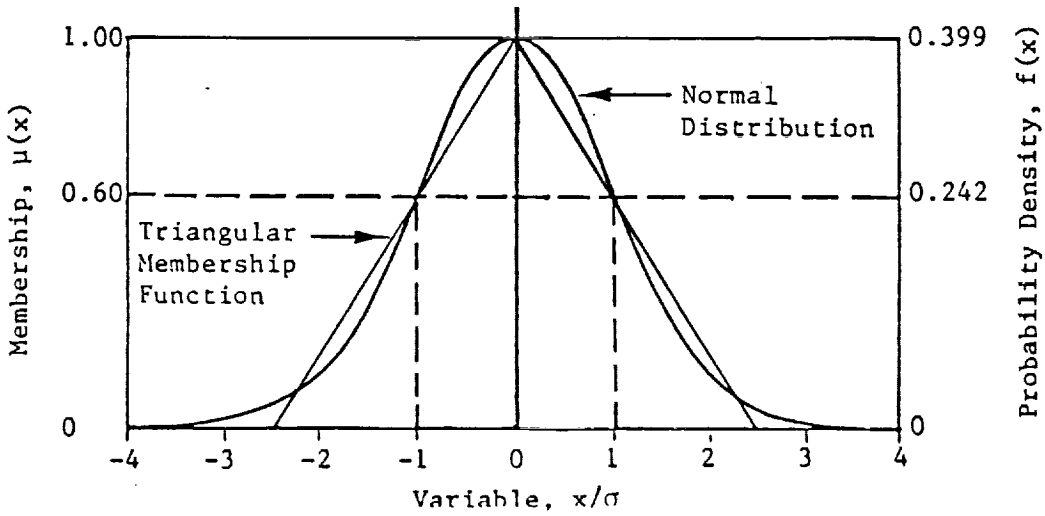

(b) Use of Normal Distribution to Define a Triangular Membership Function

Figure 4–3. Interpretation of Membership Functions.

structural response may be associated with that membership. Otherwise, the possibility interval for structural response cannot be associated with a membership function. Nevertheless, the possibility interval will in itself be meaningful as the interval of response possibility associated with $\pm 1\sigma$ parameter intervals. If one wishes to associate a $\pm n\sigma$ interval with a particular membership function, it is easy to do so. For example, a triangular membership function may be defined to roughly approximate a Gaussian distribution, by letting the vertex of the triangle assume a membership of unity corresponding to the mode of the distribution, and letting the base of the triangle span an interval of $\pm 2.5\sigma$. In this case, the membership associated with an interval of $\pm 1\sigma$ is approximately 0.60 as illustrated in Figure 4–3b.

It is important to keep in mind that the concepts of a density function and a membership function are different. A density function is based on probability theory which in turn is postulated from "crisp set" mathematics. A crisp set merely defines the sample space of a random variable; the variable is either in the set ($\alpha = 1$) or it is not ($\alpha = 0$). A fuzzy set differs from a crisp set by allowing for vagueness in the prescription of the boundaries of the sample space. Graphically, crisp sets have vertical boundaries, whereas fuzzy sets can have sloped or variable boundaries. The degree of the slope is inversely proportional to the fuzziness in the boundary. It is also noted that crisp sets are special subsets of fuzzy sets.

Fuzzy sets have been shown to be useful in the sense that they provide a means of bounding the uncertainty of response predictions, particularly when structural response is a highly nonlinear function of the uncertain model parameters [4–4]. In this situation, first–order methods tend to be unreliable, and random simulation may be too costly.

The propagation of uncertainties using fuzzy sets involves computations with interval variables and functions [4–5]. For example, a variable, x, could have as its value "a", "b" or "3.5", etc., which are real numbers. Similarly, an interval variable denoted by X, will have as its value [a, b] or I. All arithmetic operations on interval numbers can be applied to interval variables. A function of the interval variable X = [a, b] can be defined by

$$Y = f(x) = \{f(x) \mid x \epsilon X\}$$

$$= \{f(x) \mid x \epsilon [a, b]\}$$

whose value usually would be an interval number. When f(x) is continuous and monotonic on X = [a, b], Y can simply be obtained by

$$Y = \{\min[f(a), f(b)], \max[f(a), f(b)]\}$$

4.2.2 The Vertex Method

The Vertex Method can be used to propagate uncertainties whenever Y is a function of many interval variables [4–5]. When $Y = f(X_1, X_2, ..., X_n)$ is continuous in the n–dimensional rectangular region, and no extreme point exists in this region (including the boundaries), then the value of the interval function can be obtained by

$$\begin{aligned} Y &= f(X_1, X_2, ..., X_n) \\ &= \{\min_j [f(c_j)], \max_j [f(c_j)]\};\ j = 1, n \end{aligned} \tag{4–42}$$

where c_j represents the coordinates of the jth vertex.

When $Y = f(X_1, X_2, ..., X_n)$ represents a frequency response function, where X_j are interval variables representing uncertain parameters, there may be extreme points, within the rectangular hyperspace defined by the parameter intervals, corresponding to the zeros and poles of the frequency response function. In this case, a generalized form of Equation (4–42) is appropriate [4–5]:

$$Y = \{\min_{j,k} [f(c_j), f(E_k)], \max_{j,k} [f(c_j), f(E_k)]\};\ \begin{matrix} j = 1, 2, 3, ... n \\ k = 1, 2, 3, ... m \end{matrix} \tag{4–43}$$

where E_k (k = 1, m) define m extreme points within the region. The extreme points may be located by various means including random search and constrained optimization methods.

When using the Vertex Method, the number of required FRF calculations is given by:

$$n = N_a N_f N_r (2^{N_p}) \tag{4–44}$$

where

N_a = number of alpha cuts

N_f = number of frequencies

N_r = number of FRFs

N_p = number of uncertain parameters

The number, n, can become very large as N_p becomes large. Since the basic uncertain parameters in the present analysis are modal parameters, N_p depends on the number of modes represented in the generic uncertainty model. For a system with only 10 modes (considering only mass and stiffness uncertainty), N_p can be shown to be equal to 110 and N_p in Equation (4–45) is on the order to 10^{33}! However, since the fuzzy set method proves most helpful near resonance and anti–resonance, only a few of the uncertain modal parameters should be important in these cases. Therefore, a classification method to identify which of the modal parameters are important near resonance is essential.

4.2.2.1 Clustering

Clustering is the generic term given to the process of grouping parameters into different classes. In this case it is only necessary to group the parameters into two classes: those which contribute significantly to the interval of response uncertainty at a given excitation frequency, and those which do not, i.e. the important and the unimportant parameters. The first step is to define an appropriate measure of importance; the second is to establish a suitable threshold for separating the two classes.

The linearized Taylor series may be used for this purpose, even though the series itself may not approximate the true response. The linearized Taylor series given by Equation (4–4) may be rewritten as

$$\Delta u = T_{u\tilde{r}} \Delta \tilde{r} \tag{4–45}$$

where the dimensionless parameters $\tilde{r}$ replace r. In this case, where only one response variable, u_j, is sought, (4–45) becomes

$$\Delta u_j = \sum_k (T_{u\tilde{r}})_{jk} \Delta \tilde{r}_k \tag{4–46}$$

If $\Delta \tilde{r}_k$ is defined to be one standard deviation of the random variable $\tilde{r}_k$, then the product

$$| \Delta u_{jk} | = | (T_{u\tilde{r}})_{jk} \Delta \tilde{r}_k | \tag{4–47}$$

may be thought of as a measure of the contribution of parameter $\tilde{r}_k$ to the uncertainty of the response variable u_j. The ratio

$$R_{jk} = \left| \frac{\Delta u_{jk}}{u_j} \right| \tag{4–48}$$

is a relative measure of the importance r_k with respect to the uncertainty of u_j. When u_j is log–amplitude, then

$$R_{jk} = 10^{| \Delta u_{jk} |} - 1 \tag{4–49}$$

With R_{jk} defined as the measure of importance, one may proceed to specify a threshold.

Intuitively, one would like to choose R_{jk} to be small, say $R_{jk} << 1$, near the poles where u_j is large. On the other hand, when the excitation frequency is near a zero where u_j is small, then the threshold can be chosen much larger without adversely affecting the computed upper bound on uncertainty. Near the zeros of a FRF, one might choose $R_{jk} < 1$. The error introduced by the truncation of parameters is referred to as the parameter truncation error, ϵ_j. An estimate of this error is given by

$$\epsilon_j = \sum_{k=1}^{N_t} R_{jk} \qquad (4\text{–}50)$$

where R_{jk} is summed over the number of parameters which have been truncated, N_t. One must keep in mind that when the excitation frequency is near a pole this truncation error will be a small fraction of a large number, and when near a zero, it will be a larger fraction of a small number. The estimated parameter truncation error, ϵ_j, can therefore be expressed as "(100 x ϵ_j) percent of (u_j)," where numerical values are given for the quantities in parenthesis.

4.2.2.2 Diagonalization of Covariance Matrix

Before the Vertex Method can be applied, it is necessary to transform the parameter vector, $\tilde{r}$, to a set of uncorrelated parameters $\tilde{s}$. This is accomplished by diagonalizing the covariance matrix $S_{\tilde{r}\tilde{r}}$ which remains after parameter truncation. (The effect of parameter truncation on $S_{\tilde{r}\tilde{r}}$ is to eliminate those rows and columns of $S_{\tilde{r}\tilde{r}}$ corresponding to the parameters being truncated.) Diagonalization may be performed by singular value decomposition [2–6] which identifies all of the non–zero singular values (eigenvalues) and their corresponding eigenvectors. Since $S_{\tilde{r}\tilde{r}}$ is symmetric and non–negative definite, all of the non–zero eigenvalues are positive and there is only one set of eigenvectors. These eigenvectors provide the linear transformation between the original $\tilde{r}$–parameters which are correlated, and the new $\tilde{s}$–parameters which are uncorrelated. In particular,

$$\Delta\tilde{r} = \Theta\Delta\tilde{s} \qquad (4\text{–}51)$$

where Θ is the linear transformation relating $\Delta\tilde{r}$ to $\Delta\tilde{s}$.

Having made the transformation of variables from $\tilde{r}$ to $\tilde{s}$, another clustering operation is performed on the $\tilde{s}$ parameters to reduce N_p in Equation (4–44). This limits the number of response computations required by the Vertex Method. (The first clustering

operation on $\tilde{r}$ limited the size of $S_{\tilde{r}\tilde{r}}$ for singular value decomposition.) The clustering on $\tilde{s}$ is performed in the same manner it was on $\tilde{r}$.

$$\Delta u = T_{u\tilde{r}}\,\Theta\Delta\tilde{s} = T_{u\tilde{s}}\,\Delta\tilde{s} \tag{4–52}$$

$$\Delta u_j = \sum_k (T_{u\tilde{s}})_{jk}\,\Delta\tilde{s}_k \tag{4–53}$$

$$|\,\Delta u_{jk}\,| = |\,(T_{u\tilde{s}})_{jk}\,\Delta\tilde{s}_k\,| \tag{4–54}$$

Then R_{jk} and ϵ_j are given by (4–48), (4–49) and (4–50) as before.

The truncated singular values $\sigma^2_{\tilde{s}_k}$, of $S_{\tilde{r}\tilde{r}}$ are the variances of the truncated vector, $\tilde{s}$. Thus, if one wishes to evaluate the possibility bounds on u_j corresponding to $\pm\, n\sigma$ parameter intervals, one would let

$$\Delta\tilde{s}_k = n\sigma_{\tilde{s}_k} \tag{4–55}$$

Given a particular combination, $\Delta\tilde{s}$, of the scalar parameters $\Delta\tilde{s}_k$, $\Delta\tilde{s}$ is transformed back to $\Delta\tilde{r}$ using (4–51). From $\Delta\tilde{r}$, Δr is obtained by appropriate frequency scaling, thus determining Δm, Δk and $\Delta\xi$, from which one obtains

$$m = I + \Delta m$$

$$k = {}^{o}\lambda + \Delta k$$

$$\xi = {}^{o}\xi + \Delta\xi$$

The undamped eigenvalues, λ, and eigenvectors, ϕ, are computed from

$$(k - \lambda_j m)\,\psi_j = 0;\ \phi = {}^{o}\phi\,\psi$$

Frequency response is then computed from (4–20). Response at the vertices of the rectangular hyperspace corresponding to $\pm$ nσ parameter intervals is determined by computing the response, u_j, for all combinations of $\Delta\tilde{s}_k$ comprising the vector $\Delta\tilde{s}$, with two exceptions:

(1) Any combination, $\Delta\tilde{s}$, resulting in $\Delta m_{jj} < 0$ is discarded because Δm_{jj} as defined by (2–20) is non–negative.

(2) Any combination, $\Delta\tilde{s}$, resulting in negative eigenvalues is discarded because negative eigenvalues imply an unstable system.

Negative eigenvalues and negative Δm_{jj}'s can result from violation of the small perturbation assumption and the symmetric intervals assigned to Δs_k.

4.2.2.3 Included Maxima and Minima

Equation (4–42) is used to compute response uncertainty intervals as long as no extremum exists within the parameter space including its boundaries. A test is made to detect the presence of an extremum. The poles and zeros computed for each combination of truncated parameter values are searched to determine the highest and lowest in each case, thus determining a frequency range for the poles and another for the zeros. If the excitation frequency falls within the range of poles there is an included maximum. If it falls within the range of zeros, there is an included minimum. An included maximum means that there is some combination of parameter values which results in a pole at the excitation frequency. An included minimum means that there is some combination of parameter values which results in a zero at the excitation frequency. Poles are located by solving the undamped eigenproblem. Zeros are located by the Method of Golden Sections [4–6].

Figure 4–4 illustrates the occurrence of an included maximum. These figures shows FRF amplitude of the LaRC Ten Bay Truss (Figure 2–2 and Table A–2) at selected excitation frequencies near the first resonance which is approximately 17.89 Hz. Unlike conventional FRF plots which are functions of excitation frequency given certain parameter

⊙ Maximum and Minimum Vertex Values

▼ Included Maxima

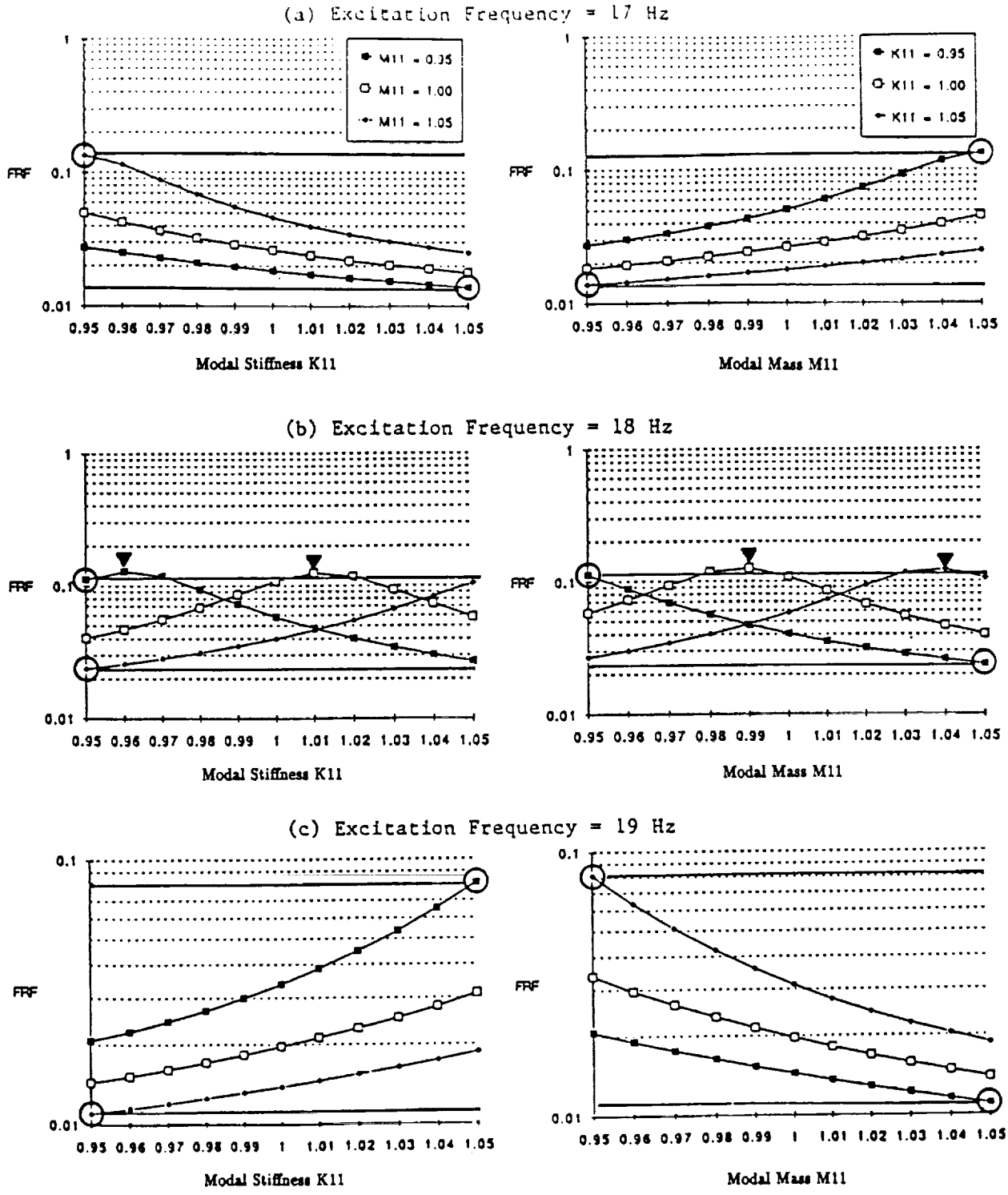

Figure 4–4. Variation of Frequency Response With Modal Mass and Stiffness at Fixed Excitation Frequencies, Ten Bay Truss, Node 2Y Output/Node 2Y Input.

values, these plots are functions of selected modal parameters with excitation frequency fixed. In this case, the modal mass and stiffness of the first mode are varied over the arbitrarily selected intervals of ± 5%. In Figure 4–4, included maxima appear at an excitation frequency of 18 Hz, but not at 17 or 19 Hz. The circled points represent the maximum and minimum FRF amplitudes at the vertices. In each case, the parameter space is a two–dimensional rectangle with four vertices. The four vertices correspond to the following parameter combinations:

1. $\frac{m_{11}}{{}^{o}m_{11}} = 0.95, \quad \frac{k_{11}}{{}^{o}k_{11}} = 0.95$

2. $\frac{m_{11}}{{}^{o}m_{11}} = 0.95, \quad \frac{k_{11}}{{}^{o}k_{11}} = 1.05$

3. $\frac{m_{11}}{{}^{o}m_{11}} = 1.05, \quad \frac{k_{11}}{{}^{o}k_{11}} = 0.95$

4. $\frac{m_{11}}{{}^{o}m_{11}} = 1.05, \quad \frac{k_{11}}{{}^{o}k_{11}} = 1.05$

At the 18 Hz excitation frequency, Combinations 1 and 3 correspond to the maximum and minimum response at the vertices. Included maxima are seen to occur at the combinations:

5. $\frac{m_{11}}{{}^{o}m_{11}} = 0.95, \quad \frac{k_{11}}{{}^{o}k_{11}} = 0.96$

6. $\frac{m_{11}}{{}^{o}m_{11}} = 1.00, \quad \frac{k_{11}}{{}^{o}k_{11}} = 1.01$

7. $\frac{m_{11}}{{}^{o}m_{11}} = 0.99, \quad \frac{k_{11}}{{}^{o}k_{11}} = 1.00$

8. $\frac{m_{11}}{{}^{o}m_{11}} = 1.04, \quad \frac{k_{11}}{{}^{o}k_{11}} = 1.05$

In fact, Combinations 5 through 8 all have the approximate ratio

$$\frac{k_{11}\ {}^{o}k_{11}}{m_{11}\ {}^{o}m_{11}} = 1.01$$

implying that the included maxima lie along a ridge line over the two–parameter space. The ridge line is not quite level, however; the true maximum lies on the $m_{11}/{}^{o}m_{11} = 0.95$ boundary. In this example, the included maxima are only slightly greater than FRF amplitude at the vertices. This is only because the excitation frequency of 18 Hz is so close to the resonance frequency of 17.89 Hz. If the excitation frequency were 17 Hz or 19 Hz, for example, and the parameter intervals were ± 20% instead of ± 5%, the difference between the highest vertex response and the included maximum would be much greater.

Figure 4–5 illustrates the occurrence of included minima. As in Figure 4–4, the maximum and minimum response among the four vertices are circled. Included minima are indicated by the solid triangles. These minima correspond to a zero which occurs between the resonant frequencies of the first two bending modes of the Ten Bay Truss.

When the presence of an included maximum or minimum is detected, the value of that maximum or minimum must be determined so that Equation (4–43) may be evaluated. There are several ways of doing this, but none guarantee that the extremum will be found with a finite computational effort. All of them, however, improve upon the interval obtained by computing response at only the vertices, with accuracy improving as the computational effort increases. The three basic search techniques are:

1. Uniform grid search;
2. Random search; and
3. Constrained optimization.

The uniform grid search simply divides the parameter space into a finer mesh (or grid) and computes response at the nodes of the mesh as well as the vertices of the parameter space. The random search substitutes randomly selected parameter combinations within the parameter space for the regular combinations represented by the refined mesh. In constrained optimization, a search algorithm with multiple starting points is employed to find the extremum within the boundaries of the parameter space.

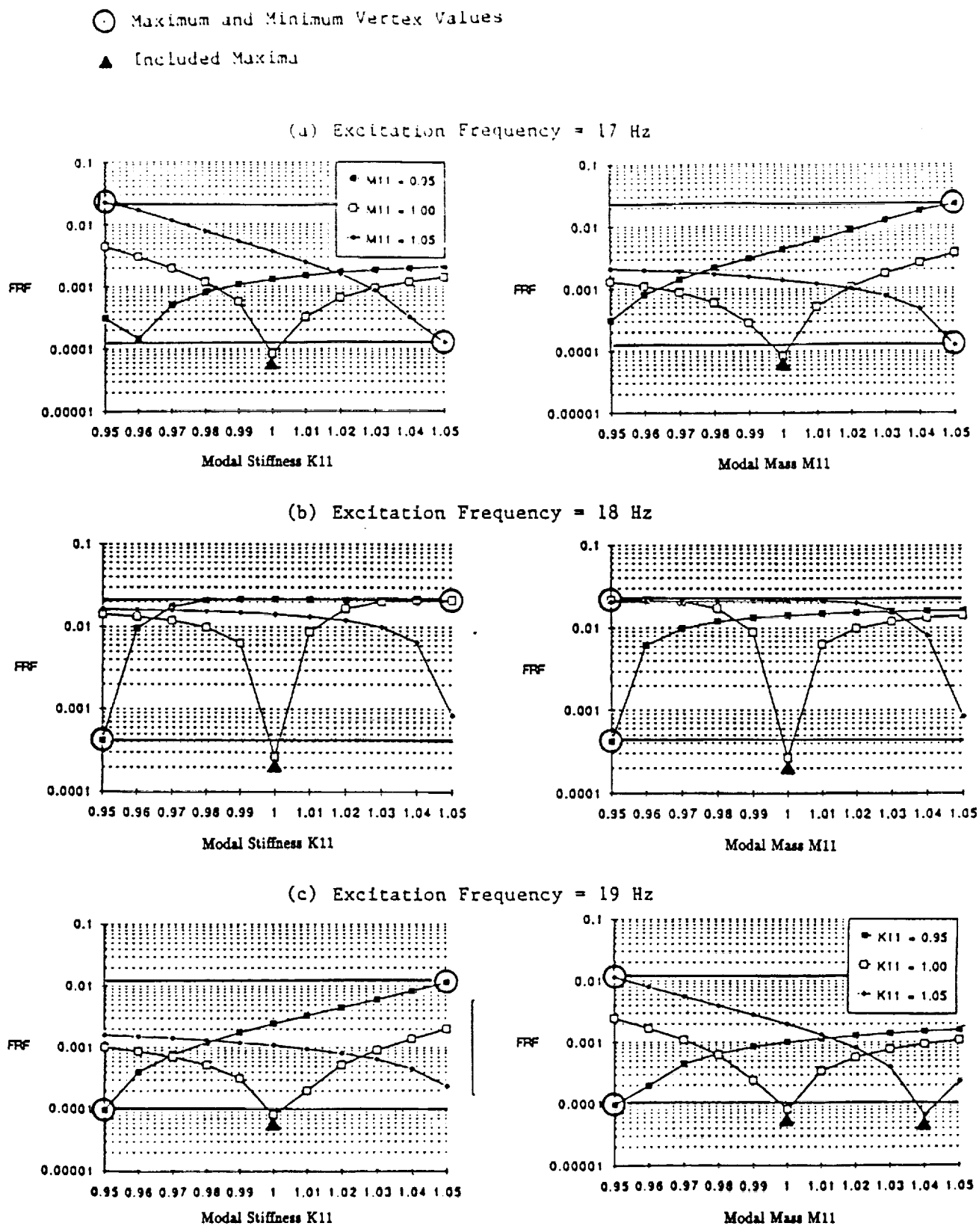

Figure 4–5. Variation of Frequency Response with Modal Mass and Stiffness at Fixed Excitation Frequencies, Ten Bay Truss, Node 2Z Output/Node 2Y Input.

4.2.3 Example

The 2–DOF system shown in Figure 4–1 is used to illustrate the fuzzy set approach. The CSS Posttest modal mass and stiffness covariance matrix is used as before (Section 4.1.3), and 0.5% damping is assumed with a one–sigma uncertainty factor of 2.0. The results are shown in Figure 4–6 and may be compared with the results of linear covariance propagation shown in Figure 4–2. Figure 4–6 shows that both the amplitude and phase intervals have been reduced in the neighborhood of resonance. The plots in Figure 4–6 use different symbols to delimit the intervals computed by the fuzzy set approach. Instead of the asterisks used to delimit intervals computed by linear covariance propagation, plus signs are used to delimit possibility bounds. The composite plot is obtained by computing uncertainty intervals by both linear covariance propagation and the Vertex Method, and plotting the smaller of the two.

4.3 Monte Carlo Simulation

Monte Carlo simulation is performed in basically the same way as the random search for maxima and minima. The only difference is that whereas the random search uses rectangular distributions limited to $\pm\ n\sigma$, Monte Carlo simulation uses normal distributions for mass and stiffness parameters and lognormal for damping. In place of the possibility interval, a frequency–of–occurrence distribution is computed. This distribution could be normalized to unit area to make it a probability density function. However, it is instead normalized to a maximum occurrence rate of unity for plotting purposes. Figure 4–7 shows a sequence of amplitude and phase distributions, for the frequencies shown in Figure 4–6. It is interesting to note the bimodal phase distributions which occur near resonance. These distributions are recognized as being similar to the distribution for $\sin\theta$ where θ is uniformly distributed over the interval $[-\pi/2, \pi/2]$. See Reference [4–2].

The distributions in Figure 4–7 may be compared with the $\pm\ 1\sigma$ uncertainty intervals in Figure 4–6. The two are seen to be generally consistent, except that the nominal response does not necessarily coincide with any particular statistic of the distributions such as the mean, median or mode. It is well to keep in mind, for example, that in the absence of damping uncertainty, the nominal FRF amplitude at resonance will very nearly coincide with the upper limit of the distribution. This was illustrated in [4–2].

FUZZY BOUNDING ANALYSIS

FREQ-HZ	NOM DISPL/FORCE
7.00000E-02	3.95191E+00
7.08720E-02	4.05344E+00
7.17549E-02	4.16323E+00
7.26488E-02	4.28227E+00
7.35539E-02	4.41176E+00
7.44702E-02	4.55309E+00
7.53979E-02	4.70791E+00
7.63372E-02	4.87819E+00
7.72882E-02	5.06633E+00
7.82510E-02	5.27520E+00
7.92259E-02	5.50837E+00
8.02129E-02	5.77026E+00
8.12121E-02	6.06642E+00
8.22238E-02	6.40395E+00
8.32482E-02	6.79205E+00
8.42853E-02	7.24283E+00
8.53353E-02	7.77267E+00
8.63983E-02	8.40412E+00
8.74747E-02	9.16926E+00
8.85644E-02	1.01152E+01
8.96677E-02	1.13141E+01
9.07848E-02	1.28825E+01
9.19157E-02	1.50208E+01
9.30608E-02	1.81063E+01
9.42201E-02	2.29401E+01
9.53939E-02	3.15648E+01
9.65823E-02	5.10423E+01
9.77855E-02	1.23417E+02
9.90037E-02	1.14763E+02
1.00237E-01	4.74890E+01
1.01486E-01	2.88793E+01
1.02750E-01	2.05155E+01
1.04030E-01	1.57920E+01
1.05326E-01	1.27629E+01
1.06638E-01	1.06571E+01
1.07967E-01	9.10908E+00
1.09312E-01	7.92368E+00
1.10673E-01	6.98711E+00
1.12052E-01	6.22869E+00
1.13448E-01	5.60215E+00
1.14861E-01	5.07597E+00
1.16292E-01	4.62793E+00
1.17741E-01	4.24189E+00
1.19208E-01	3.90589E+00
1.20693E-01	3.61084E+00
1.22196E-01	3.34974E+00
1.23719E-01	3.11708E+00
1.25260E-01	2.90849E+00
1.26821E-01	2.72044E+00
1.28400E-01	2.55006E+00
1.30000E-01	2.39499E+00

Figure 4–6a. One–Sigma Uncertainty Intervals on FRF Amplitude for 2–DOF Example, Linear Covariance Propagation Limited by Possibility Bounds.

Frequencies for which distributions are shown in Figure 4–7.

FUZZY BOUNDING ANALYSIS

FREQ-HZ	NOM PHASE
7.00000E-02	-8.07101E-01
7.08720E-02	-8.39066E-01
7.17549E-02	-8.73516E-01
7.26488E-02	-9.10756E-01
7.35539E-02	-9.51143E-01
7.44702E-02	-9.95098E-01
7.53979E-02	-1.04312E+00
7.63372E-02	-1.09581E+00
7.72882E-02	-1.15388E+00
7.82510E-02	-1.21821E+00
7.92259E-02	-1.28988E+00
8.02129E-02	-1.37021E+00
8.12121E-02	-1.46090E+00
8.22238E-02	-1.56410E+00
8.32482E-02	-1.68257E+00
8.42853E-02	-1.82001E+00
8.53353E-02	-1.98136E+00
8.63983E-02	-2.17346E+00
8.74747E-02	-2.40604E+00
8.85644E-02	-2.69339E+00
8.96677E-02	-3.05744E+00
9.07848E-02	-3.53357E+00
9.19157E-02	-4.18284E+00
9.30608E-02	-5.12036E+00
9.42201E-02	-6.59169E+00
9.53939E-02	-9.22844E+00
9.65823E-02	-1.52682E+01
9.77855E-02	-4.02904E+01
9.90037E-02	-1.42354E+02
1.00237E-01	-1.65122E+02
1.01486E-01	-1.70872E+02
1.02750E-01	-1.73423E+02
1.04030E-01	-1.74859E+02
1.05326E-01	-1.75778E+02
1.06638E-01	-1.76416E+02
1.07967E-01	-1.76885E+02
1.09312E-01	-1.77244E+02
1.10673E-01	-1.77527E+02
1.12052E-01	-1.77756E+02
1.13448E-01	-1.77946E+02
1.14861E-01	-1.78104E+02
1.16292E-01	-1.78239E+02
1.17741E-01	-1.78356E+02
1.19208E-01	-1.78456E+02
1.20693E-01	-1.78545E+02
1.22196E-01	-1.78623E+02
1.23719E-01	-1.78692E+02
1.25260E-01	-1.78753E+02
1.26821E-01	-1.78809E+02
1.28400E-01	-1.78858E+02
1.30000E-01	-1.78903E+02

Figure 4–6b. One–Sigma Uncertainty Intervals on FRF Phase for 2–DOF Example, Linear Covariance Propagation Limited by Possibility Bounds.

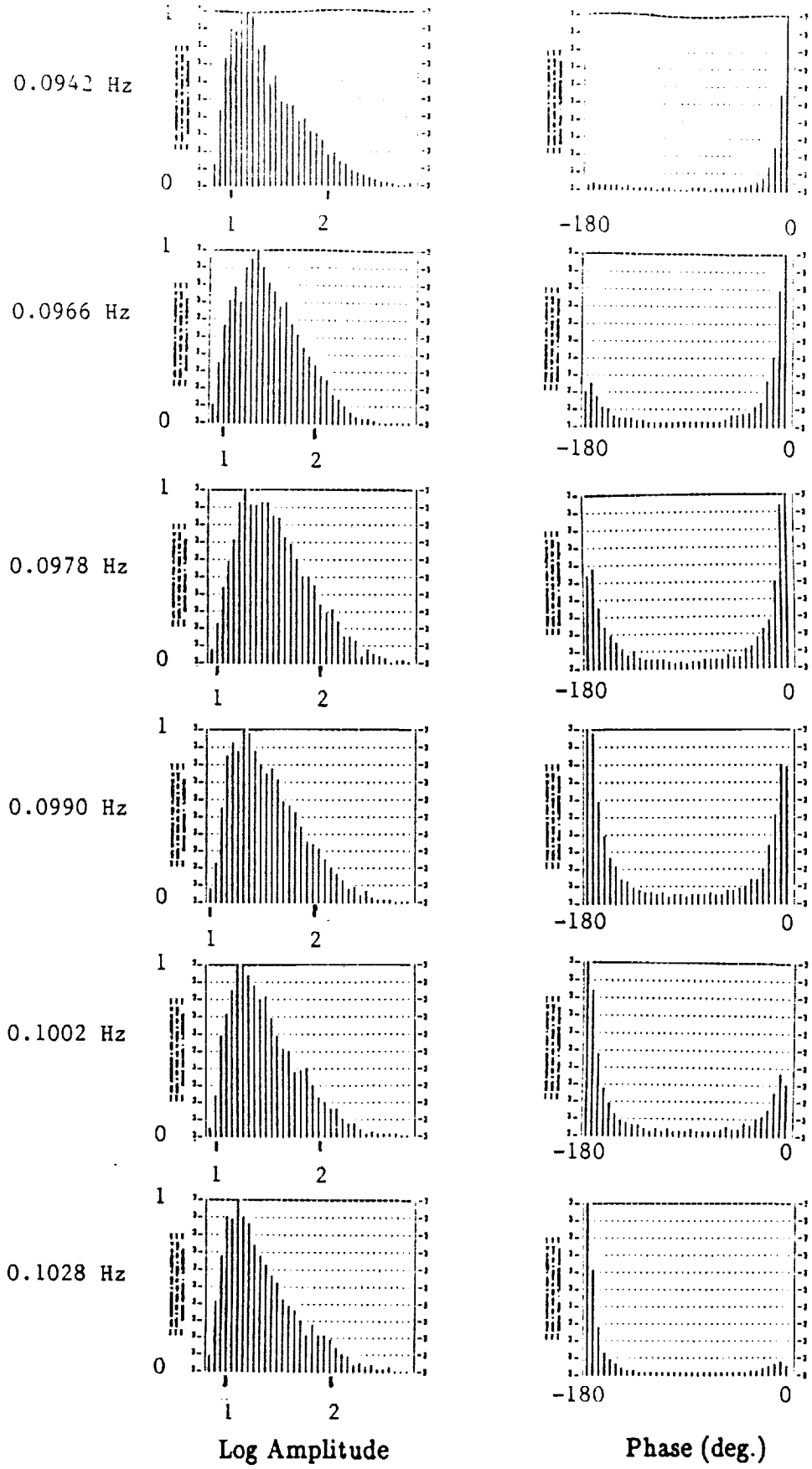

Figure 4–7. FRF Amplitude and Phase Distributions for 2–DOF Example.

As a final comparison between $\pm n\sigma$ uncertainty intervals and corresponding distributions, the $\pm 2\sigma$ uncertainty interval was computed for the 2–DOF example. These results are shown in Figure 4–8. This figure shows that where the uncertainty intervals have been determined by linear covariance propagation, the intervals double as they should. However, the possibility intervals computed near resonance do not double. They tend to increase only in proportion to the increase in damping uncertainty. The increase in mass and stiffness uncertainty tends to broaden the uncertainty bands in the frequency direction, but has little effect in the amplitude direction near resonance.

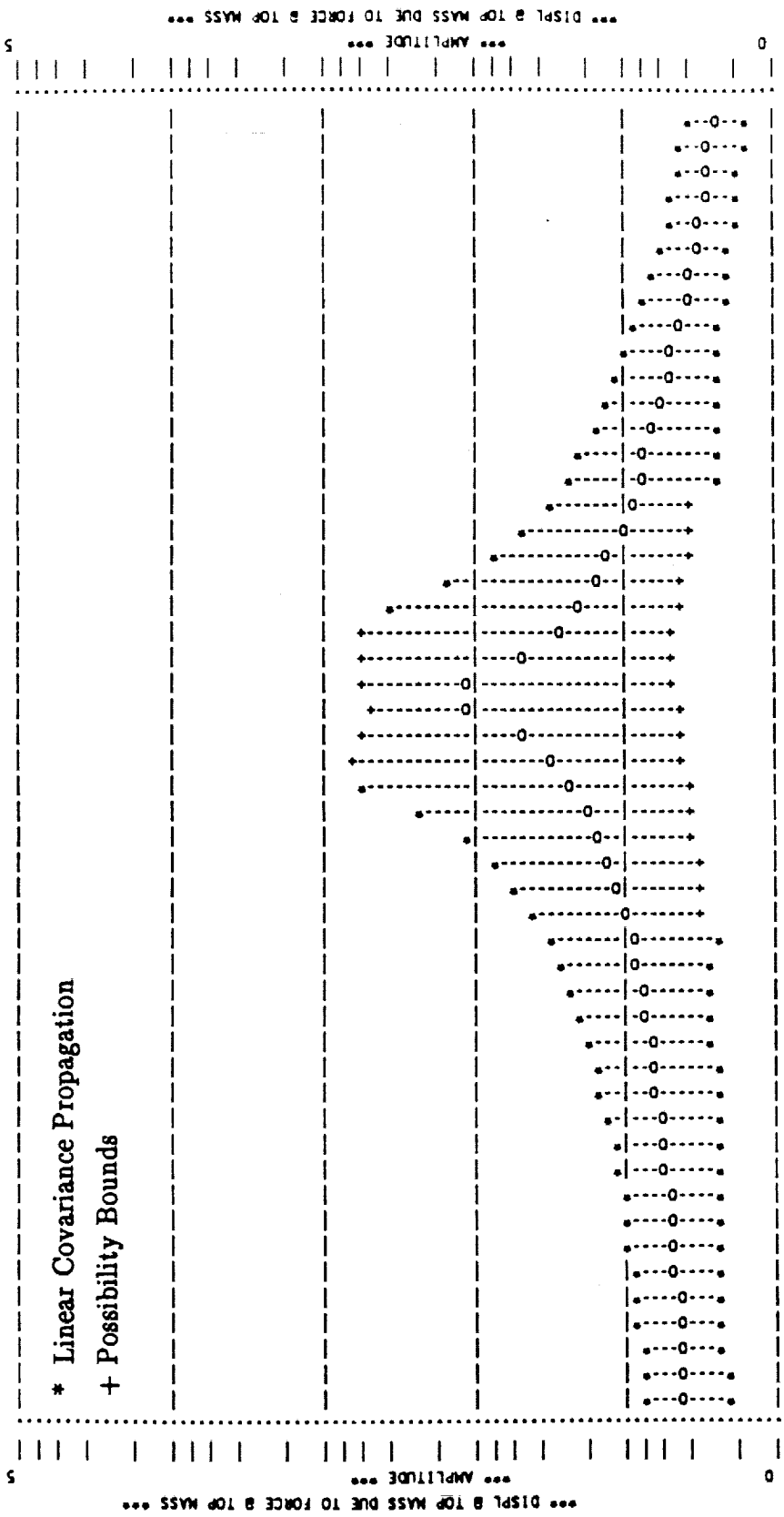

FUZZY BOUNDING ANALYSIS

FREQ-HZ	NOM DISPL/FORCE
7.000000E-02	3.951919E+00
7.087206E-02	4.053446E+00
7.175496E-02	4.163236E+00
7.264886E-02	4.282276E+00
7.355396E-02	4.411746E+00
7.447026E-02	4.553096E+00
7.539796E-02	4.707916E+00
7.633726E-02	4.878196E+00
7.728826E-02	5.066336E+00
7.825106E-02	5.275206E+00
7.922596E-02	5.508376E+00
8.021296E-02	5.770266E+00
8.121216E-02	6.066426E+00
8.222386E-02	6.403956E+00
8.324826E-02	6.792056E+00
8.428536E-02	7.242836E+00
8.533536E-02	7.772676E+00
8.639836E-02	8.404126E+00
8.747476E-02	9.169266E+00
8.856446E-02	1.011526E+01
8.966776E-02	1.131416E+01
9.078486E-02	1.288256E+01
9.191576E-02	1.502086E+01
9.306086E-02	1.810636E+01
9.422016E-02	2.294016E+01
9.539396E-02	3.156486E+01
9.658236E-02	5.104236E+01
9.778556E-02	1.234176E+02
9.900376E-02	1.147636E+02
1.002376E-01	4.748906E+01
1.014866E-01	2.887936E+01
1.027506E-01	2.051556E+01
1.040306E-01	1.579206E+01
1.053266E-01	1.276296E+01
1.066386E-01	1.065716E+01
1.079676E-01	9.109086E+00
1.093126E-01	7.923486E+00
1.106736E-01	6.987116E+00
1.120526E-01	6.228696E+00
1.134486E-01	5.602156E+00
1.148616E-01	5.075976E+00
1.162926E-01	4.627936E+00
1.177416E-01	4.241896E+00
1.192086E-01	3.905896E+00
1.206936E-01	3.610846E+00
1.221966E-01	3.349746E+00
1.237196E-01	3.117086E+00
1.252606E-01	2.908496E+00
1.268216E-01	2.720446E+00
1.284006E-01	2.550066E+00
1.300006E-01	2.394996E+00

Figure 4–8a. Two–Sigma Uncertainty Intervals on FRF Amplitude for 2–DOF Example, CSS Posttest Model Database.

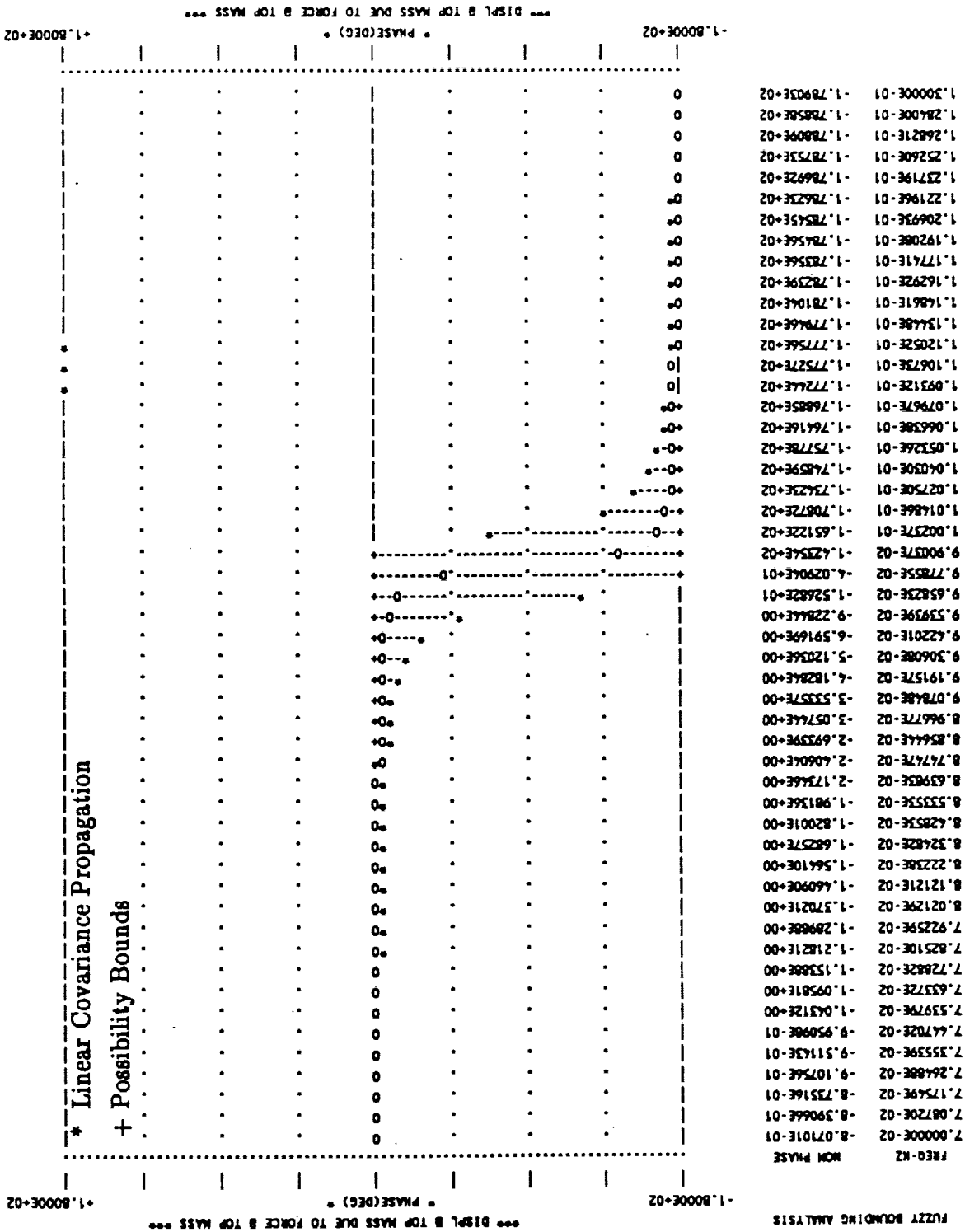

Figure 4–8b. Two–Sigma Uncertainty Intervals on FRF Phase for 2–DOF Example, CSS Postest Model Database.

5. IMPLEMENTATION OF METHODOLOGY

A computer code was written to implement the three methods of uncertainty propagation described in Chapter 4. This code is named PDAC (an acronym for PreDictive ACcuracy). Since model uncertainty is expressed in terms of modal parameters, it was convenient to formulate PDAC in terms of modal models. This meant that PDAC would require modeling data in the form of modal mass, damping and stiffness matrices, along with a modal transformation to convert input and output quantities (forces and forced response) to physical coordinates. Also required were an eigensolver, response computation modules, and modules to compute eigenvalue/eigenvector and FRF amplitude and phase derivatives which are used for uncertainty propagation.

These capabilities were available in a previously developed code called SSID (for Structural System IDentification). The modules could have been lifted from SSID to create a separate PDAC code; however, several ways were perceived in which PDAC could enhance the capabilities of SSID, including the following:

1. Reverse uncertainty propagation could be used to obtain the initial parameter covariance matrices required for Bayesian estimation in SSID. This database approach for defining an initial parameter covariance matrix should provide a better "sense of direction" for the Bayesian estimator, and could conceivably eliminate the need on the part of the analyst to "guestimate" these quantities.

2. The interval prediction capability of PDAC would make it possible to translate the parameter covariance matrices, either input to SSID or computed by SSID, into response intervals. This capability would provide a valuable diagnostic tool for SSID by facilitating the interpretation of parameter covariance matrices.

3. A posttest model uncertainty database combined with PDAC's forward propagation capability would enable SSID to display the accuracy of the models it tuned.

The recognition that PDAC and SSID would mutually benefit each other led to combining the codes into the code called SSID/PDAC. Not all of the SSID enhancements discussed above have been implemented. Since the objective of this project was to

implement the predictive accuracy methodology rather than enhance SSID, only the last of the three SSID benefits has been implemented. Thus while PDAC benefits from many of the code modules resident in SSID, not all of the SSID/PDAC code is needed to compute predictive accuracy. And whereas SSID now benefits from the ability to compute uncertainty intervals on either pretest or posttest models, it does not yet utilize all of the capabilities which PDAC has to offer. The code has been structured so that these capabilities can be added in the future.

A top level functional diagram of SSID/PDAC is shown in Figure 5–1. This figure shows three types of information being input to the code: an analytical model, model uncertainty, and vibration test data. The inputs are shown separately because they are read as separate data files. Three types of output are provided. They include pretest response, either with or without pretest uncertainty, a revised model with revised parameter uncertainty, or posttest response, either with or without posttest uncertainty.

Figure 5–2 shows a top level flow diagram for SSID/PDAC. Mathematical symbols indicate the flow of primary input to SSID/PDAC from the modeling code (NASTRAN), ground vibration testing, model uncertainty databases and user input. The four modal mass and stiffness matrix databases previously discussed reside as data within the code. SSID/PDAC output is also shown symbolically. Here the asterisks denote quantities which have been updated by SSID to better match test data. These symbols are placed on the flow diagram so that the operation of SSID/PDAC can be related to the mathematical derivations of Chapters 2 through 4.

The following two sections summarize the present capabilities of SSID and PDAC.

5.1 Summary of SSID Capabilities

This section summarizes the primary capabilities of the SSID portion of the code. They are grouped according to (1) modeling and analysis capabilities, i.e. the types of models which may be updated, parameters which may be estimated and machines which the code will run on; (2) types of test data which may be used to update the models; and (3) description of parameter estimation algorithms, their limitations, and the format of output presentation.

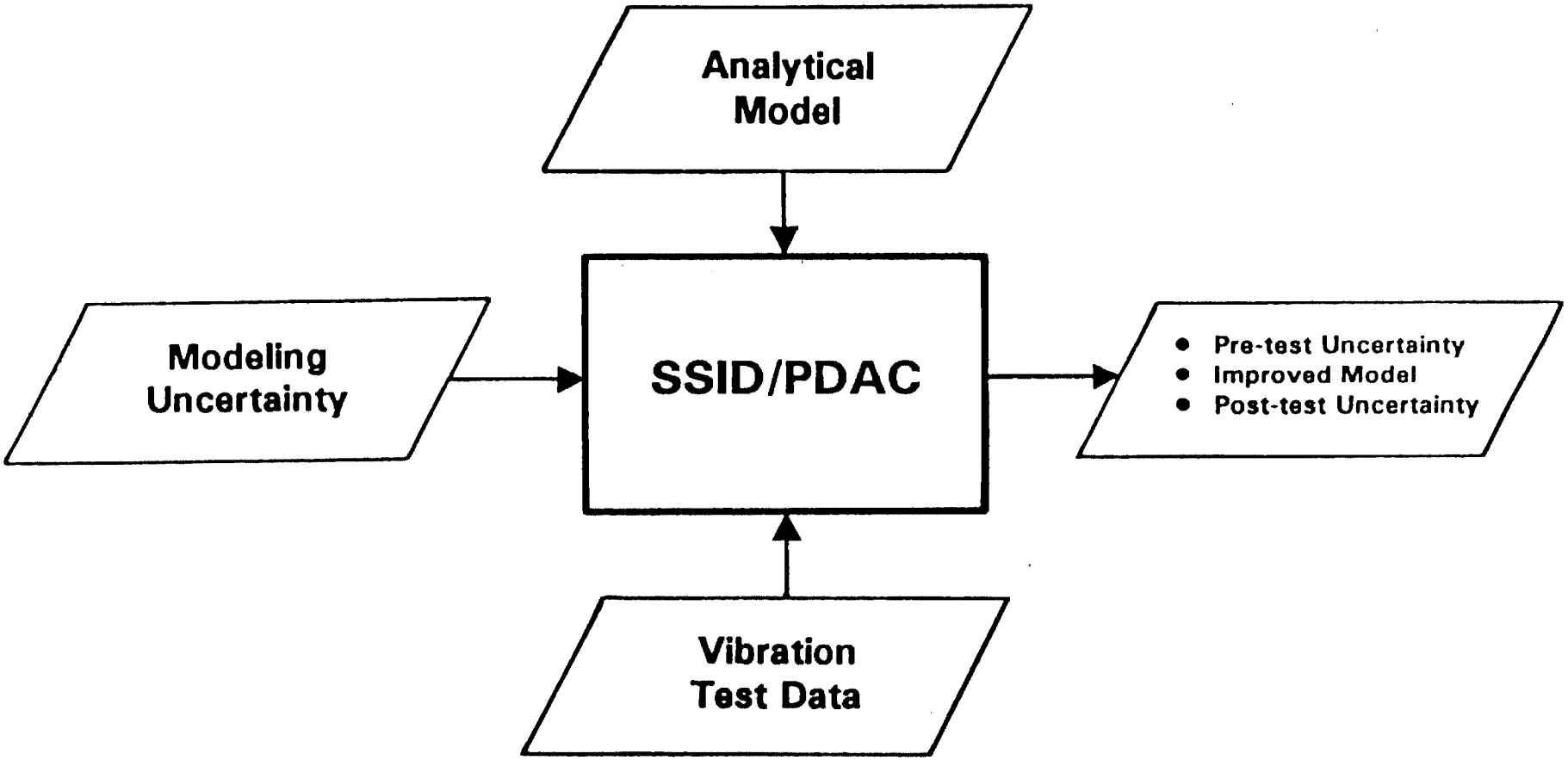

Figure 5–1. Top–Level View of SSID/PDAC Function.

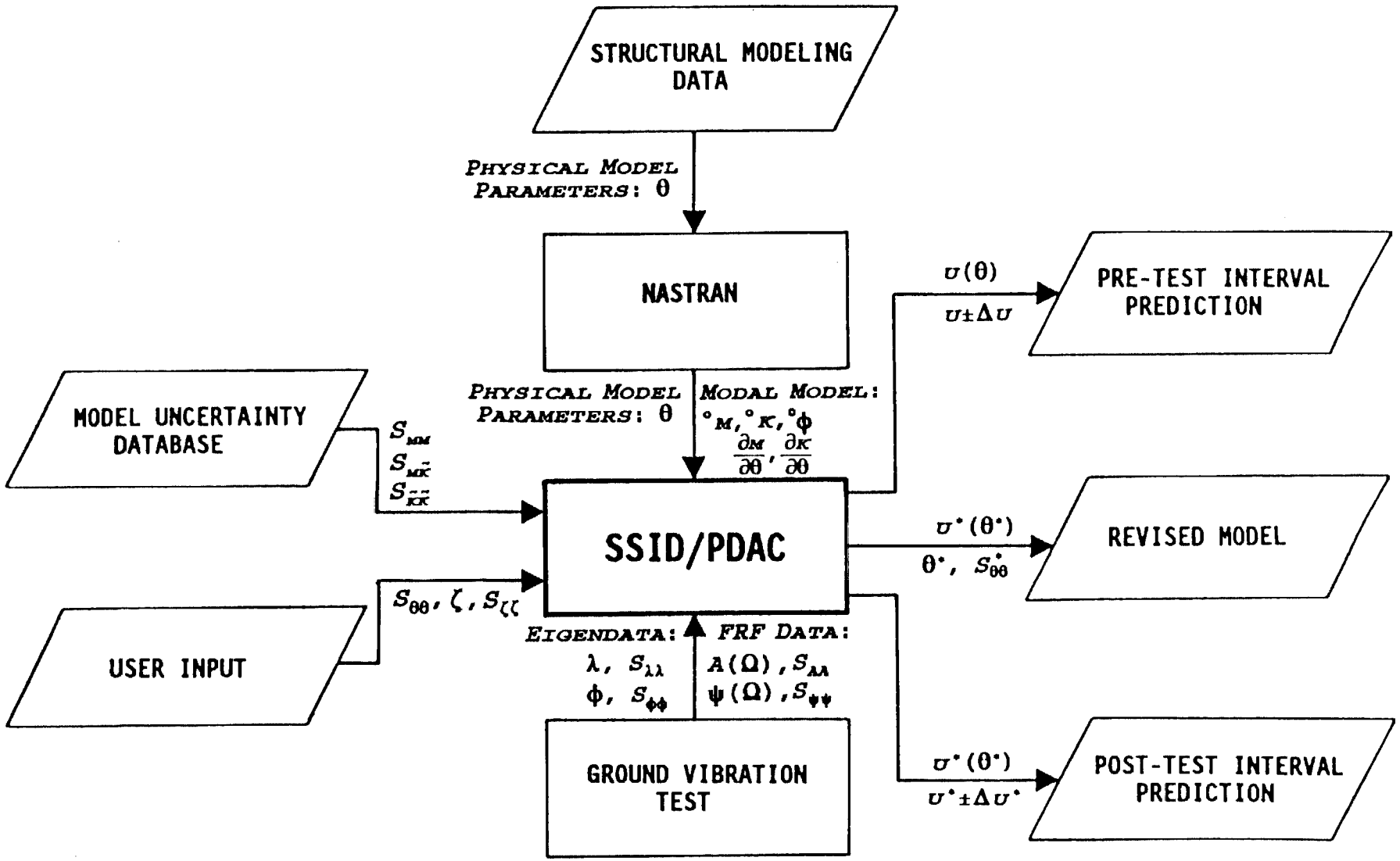

Figure 5–2. Expanded Top–level Flow Diagram for SSID/PDAC.

Modeling and Analyses

- SSID interfaces with NASTRAN via a NASTRAN–to–SSID input data link. NASTRAN's linear modeling capabilities, including substructuring and coordinate reduction can therefore be used to generate finite element models for parameter estimation in SSID. There is no model size limitation.*
- SSID can be sized to run on any machine. To date SSID has been successfully compiled and executed on 386 PC, Unix Workstation, as well as VAX and CRAY Mainframe computers.
- SSID has its own substructuring capability (currently allowing up to nine substructures.) Substructure models (physical, modal, Guyan–reduced) can be read into SSID separately and assembled within.
- SSID performs modal analysis and frequency response analysis for lightly damped structures.
- SSID is capable of estimating any mass and stiffness parameter which appears linearly in the equations of motion, including finite element and lumped parameters, linked finite element parameters, and submatrix scaling parameters. SSID also estimates system modal damping parameters including the off–diagonal elements of modal damping matrices.

Test Data

- SSID estimates model parameters based on any combination of eigenvalue and eigenvector (E/E) data, or any combination of FRF amplitude and phase data.
- E/E or FRF data can be combined from any number of test data files to create a data batch.
- There are no limitations on the amount of data which can be processed.

Parameter Estimation

- SSID offers two alternative Bayesian estimators, one for use when the number of data exceeds the number of parameters, and the other when the number of parameters exceeds the number of data. Both can be used in either case, efficiency and numerical stability being the determining factor.
- SSID processes data in either single batch or sequential batch estimation modes.
- SSID evaluates the statistical significance of all parameter estimates.

Although there are no theoretical limitations such as array size, practical limitations such as available memory and run time should not be overlooked.

- SSID provides a series of graphical outputs which summarize the estimation process.

A comprehensive description of SSID, including its mathematical basis, user instructions, and a more complete description of its capabilities and limitations are provided in References [5–1] through [5–3].

5.2 PDAC Modifications to SSID

There is a run option in SSID which allows the user to compute the eigenvalues, eigenvectors, and frequency response of the initial model without making an estimation run; no test data are required to exercise this option. This is the run option which was modified to incorporate PDAC. In simplest terms, PDAC adds the capability to compute interval response in conjunction with this response–only option.

Three types of interval response are computed by PDAC:

1. Response intervals of $\pm n\sigma$ based on linear covariance propagation,
2. Response possibility bounds based on $\pm n\sigma$ parameter intervals, and
3. Response distribution functions based on Monte Carlo simulation.

Linear covariance propagation is the easiest and most straight–forward of the three computations. It requires only the covariance matrix of modal parameters and the sensitivity of eigenvalues, eigenvectors and frequency response to those modal parameters. The derivatives of eigenvalues and eigenvectors to those modal parameters is particularly simple. Eigenvector derivatives do not require a modal summation in this case.

The Vertex Method for computing possibility bounds is the most complex portion of the code. It involves clustering to limit the parameter space, diagonalization of the modal parameter covariance matrix to preserve the correlation structure of the data, and detection and evaluation of included response maxima and minima within the rectangular hyperspace defined by parameter intervals. The evaluation of included maxima and minima is the critical part of this operation. Several user options are available, including (1) uniform grid search, (2) random search and (3) constrained optimization. These options are described in Section 4.2. Default options have been built into the code based on experience gained to date. These options may be overridden by the

user. Additional options allow the user to make trade–offs between accuracy and computation time. In this way, approximate results can be obtained at relatively little cost, while any desired level of accuracy may be attained with sufficient computational effort.

At the present time, there is no uncertainty database for damping, so the user must specify damping uncertainty in terms of a multiplicative uncertainty factor on the diagonal elements of the modal damping matrix. For example, a one–sigma uncertainty factor of 2.0 means that with the assumed lognormal damping distribution, the logarithmic mean plus one standard deviation will be twice the nominal damping value, and the logarithmic means minus one standard deviation will be one–half the nominal damping value. PDAC has been structured to accept a covariance matrix for all of the modal damping matrix elements, including off–diagonal as well as diagonal terms, so that at some future time when the data become available (and are considered to be important), this option may be activated.

6. DEMONSTRATION OF METHODOLOGY

This chapter discusses application of the methodology to practical problems. Applications to three real structures are presented, including comparisons with measured FRF data. The purpose of these comparisons is to show how test results compare with the intervals of predictive accuracy determined form actuarial data. The results, while encouraging, should be viewed cautiously because of the limited database and the limited number of applications which have so far been investigated.

Before presenting these applications, the issue of database sensitivity is considered. The question is, how sensitive are the computed uncertainty intervals to a particular database? Four different databases were presented in Chapter 2, three independent and one combined database. Rather than examine this question with respect to a particular structure belonging to one of the three independent databases, the 2–DOF spring–mass model is used as a neutral example.

6.1 Database Sensitivity

Table 2–7 compared the four databases in terms of the singular values and trace of their covariance matrices. The largest singular value is called the spectral radius, and the trace is equal to the sum of the singular values. As expected, the pretest models had the largest spectral radius (0.93), and the largest trace (1.547). The posttest models had the smallest trace (0.734), roughly half that of the pretest models. The traces of the research models and combined database fell between those of the pretest and posttest models, while the spectral radii of the LSS research models, the CSS posttest models and combined database were nearly the same, ranging from 0.57 to 0.60. In summary, the CSS pretest models exhibited the most uncertainty, the CSS posttest models the least uncertainty, with the other two somewhere in between.

Each of the four databases was used to evaluate the predictive accuracy of the 2–DOF model. The results are shown in Figures 6–1 through 6–4. Figure 6–3 corresponds to Figure 4–6 in that both reflect the CSS posttest database. The frequency range is extended to cover both modes, however. As expected, the uncertainty intervals computed with the CSS pretest model database are largest overall. Comparison of Figures 6–1 (LSS) and 6–3 (CSS posttest) reveals uncertainty intervals which are approximately the same, a

FUZZY BOUNDING ANALYSIS

FREQ-HZ	NOM DISPL/FORCE
7.00000E-02	3.95191E+00
7.20673E-02	4.20389E+00
7.41957E-02	4.50961E+00
7.63870E-02	4.88763E+00
7.86430E-02	5.36614E+00
8.09656E-02	5.99015E+00
8.33568E-02	6.83631E+00
8.58186E-02	8.04645E+00
8.83531E-02	9.91568E+00
9.09625E-02	1.31754E+01
9.36489E-02	2.02659E+01
9.64147E-02	4.69738E+01
9.92621E-02	9.03078E+01
1.02194E-01	2.35329E+01
1.05212E-01	1.29842E+01
1.08319E-01	8.76758E+00
1.11518E-01	6.50361E+00
1.14812E-01	5.09297E+00
1.18202E-01	4.13083E+00
1.21693E-01	3.43535E+00
1.25287E-01	2.90500E+00
1.28988E-01	2.49125E+00
1.32797E-01	2.15866E+00
1.36719E-01	1.88560E+00
1.40757E-01	1.65744E+00
1.44914E-01	1.46393E+00
1.49194E-01	1.29765E+00
1.53600E-01	1.15307E+00
1.58136E-01	1.02601E+00
1.62806E-01	9.13176E-01
1.67615E-01	8.11947E-01
1.72565E-01	7.20164E-01
1.77661E-01	6.35989E-01
1.82908E-01	5.57789E-01
1.88310E-01	4.84027E-01
1.93872E-01	4.13146E-01
1.99597E-01	3.43421E-01
2.05492E-01	2.72735E-01
2.11561E-01	1.98202E-01
2.17809E-01	1.15551E-01
2.24242E-01	2.36773E-02
2.30864E-01	1.19576E-01
2.37683E-01	3.21846E-01
2.44702E-01	7.20354E-01
2.51929E-01	2.06702E+00
2.59370E-01	6.26359E+00
2.67030E-01	1.68536E+00
2.74916E-01	1.03120E+00
2.83035E-01	7.66894E-01
2.91394E-01	6.19725E-01
3.00000E-01	5.23576E-01

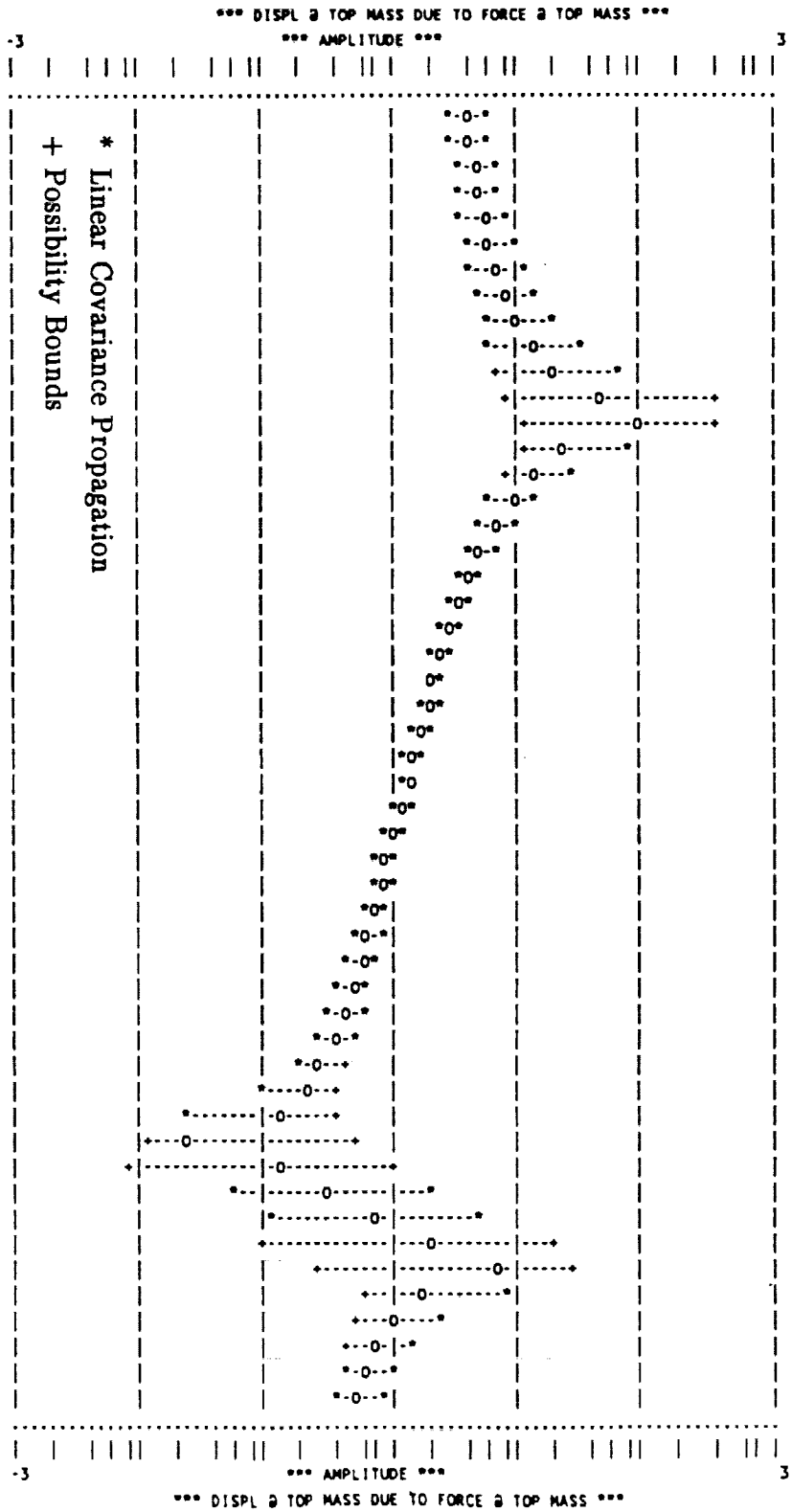

Figure 6–1a. One–Sigma Uncertainty Intervals on FRF Amplitude for 2–DOF Example, LSS Research Model Database.

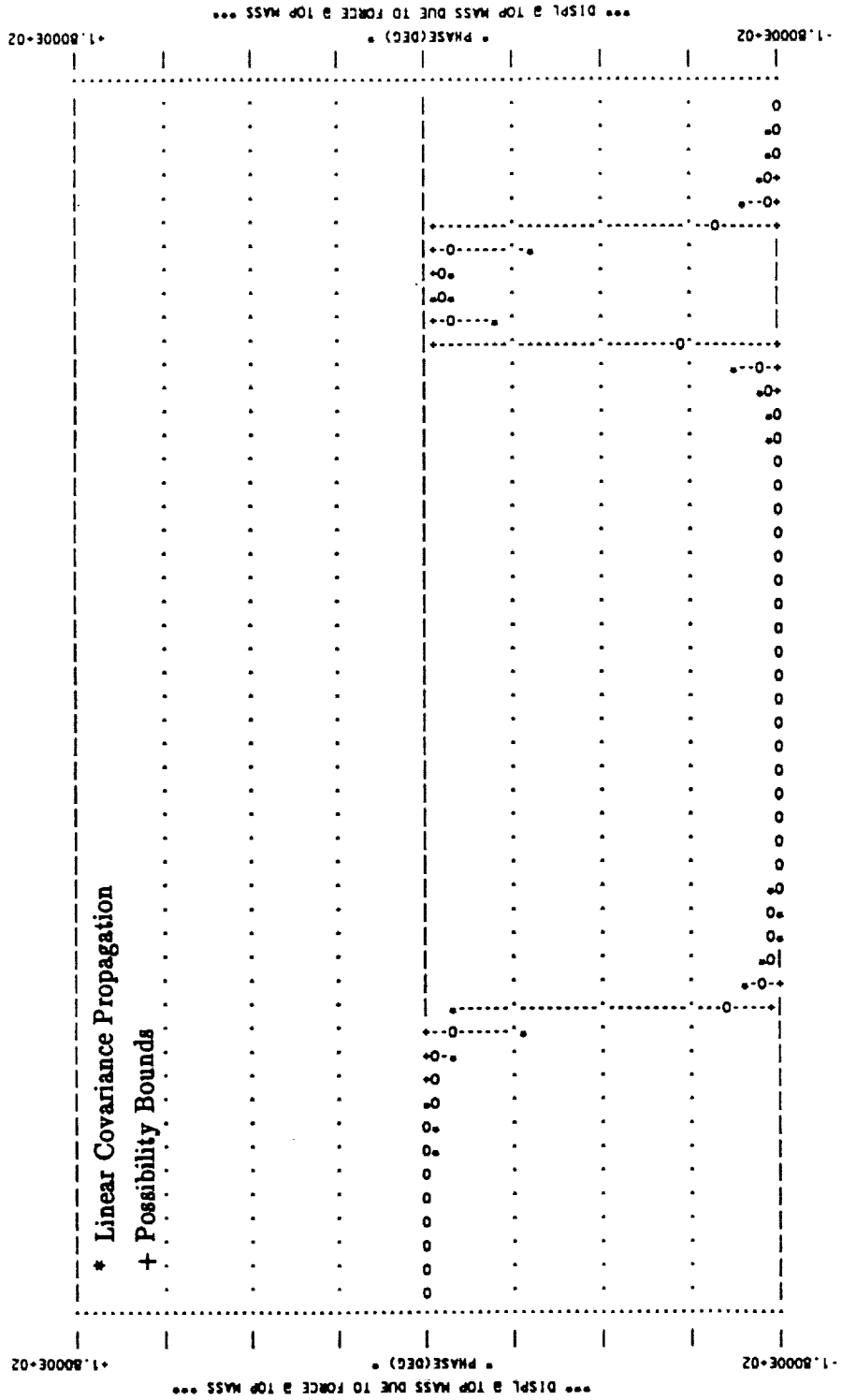

Figure 6–1b. One–Sigma Uncertainty Intervals on FRF Phase for 2–DOF Example, LSS Research Model Database.

FUZZY BOUNDING ANALYSIS

FREQ-HZ	NOM DISPL/FORCE
7.00000E-02	3.95191E+00
7.20673E-02	4.20389E+00
7.41957E-02	4.50961E+00
7.63870E-02	4.88763E+00
7.86430E-02	5.36614E+00
8.09656E-02	5.99015E+00
8.33568E-02	6.83631E+00
8.58186E-02	8.04645E+00
8.83531E-02	9.91568E+00
9.09625E-02	1.31754E+01
9.36489E-02	2.02659E+01
9.64147E-02	4.69738E+01
9.92621E-02	9.03078E+01
1.02194E-01	2.35329E+01
1.05212E-01	1.29842E+01
1.08319E-01	8.76758E+00
1.11518E-01	6.50361E+00
1.14812E-01	5.09297E+00
1.18202E-01	4.13083E+00
1.21693E-01	3.43335E+00
1.25287E-01	2.90500E+00
1.28988E-01	2.49125E+00
1.32797E-01	2.15866E+00
1.36719E-01	1.88560E+00
1.40757E-01	1.65744E+00
1.44914E-01	1.46393E+00
1.49194E-01	1.29765E+00
1.53600E-01	1.15307E+00
1.58136E-01	1.02601E+00
1.62806E-01	9.13176E-01
1.67615E-01	8.11947E-01
1.72565E-01	7.20164E-01
1.77661E-01	6.35989E-01
1.82908E-01	5.57789E-01
1.88310E-01	4.84027E-01
1.93872E-01	4.13146E-01
1.99597E-01	3.43421E-01
2.05492E-01	2.72735E-01
2.11561E-01	1.98202E-01
2.17809E-01	1.15551E-01
2.24242E-01	2.36773E-02
2.30864E-01	1.19576E-01
2.37683E-01	3.21846E-01
2.44702E-01	7.20354E-01
2.51929E-01	2.06702E+00
2.59370E-01	6.26359E+00
2.67030E-01	1.68536E+00
2.74916E-01	1.03120E+00
2.83035E-01	7.66894E-01
2.91394E-01	6.19725E-01
3.00000E-01	5.23576E-01

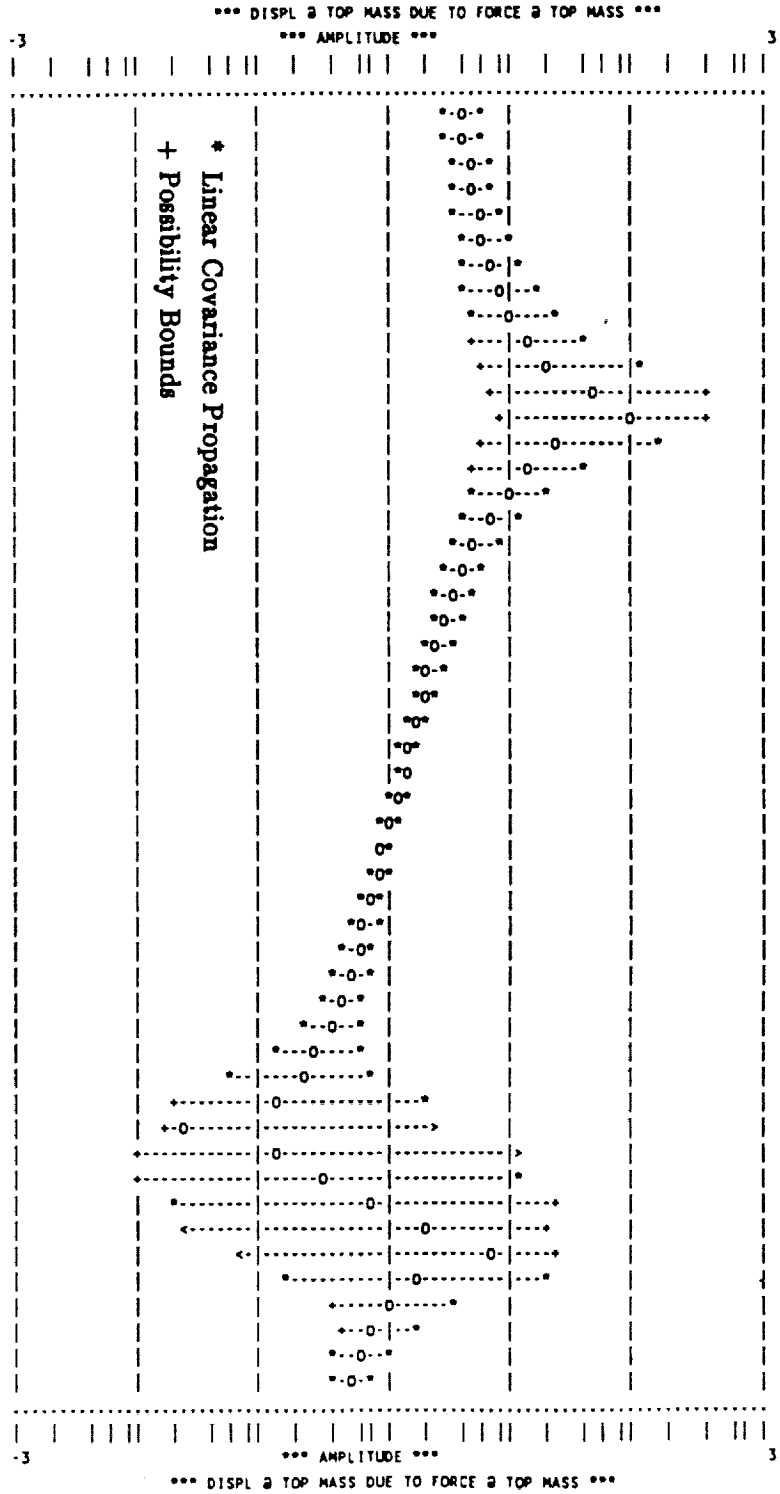

Figure 6–2a. One–Sigma Uncertainty Intervals on FRF Amplitude for 2–DOF Example, CSS Pretest Model Database.

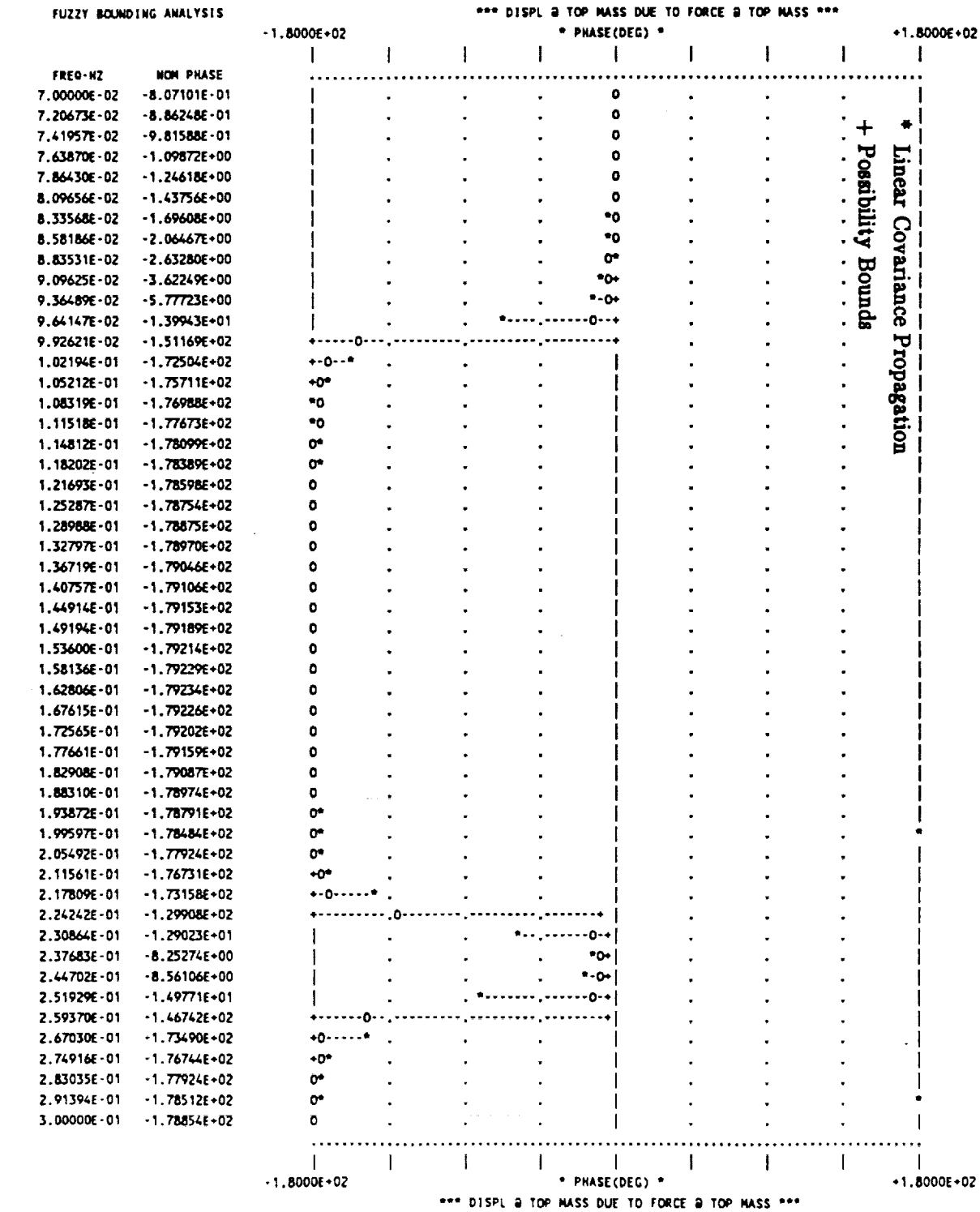

Figure 6–2b. One–Sigma Uncertainty Intervals on FRF Phase for 2–DOF Example, CSS Pretest Model Database.

FUZZY BOUNDING ANALYSIS

FREQ-HZ	NOM DISPL/FORCE
7.00000E-02	3.95191E+00
7.20673E-02	4.20389E+00
7.41957E-02	4.50961E+00
7.63870E-02	4.88763E+00
7.86430E-02	5.36614E+00
8.09656E-02	5.99015E+00
8.33568E-02	6.83631E+00
8.58186E-02	8.04645E+00
8.83531E-02	9.91568E+00
9.09625E-02	1.31754E+01
9.36489E-02	2.02659E+01
9.64147E-02	4.69738E+01
9.92621E-02	9.03078E+01
1.02194E-01	2.35329E+01
1.05212E-01	1.29842E+01
1.08319E-01	8.76758E+00
1.11518E-01	6.50361E+00
1.14812E-01	5.09297E+00
1.18202E-01	4.13083E+00
1.21693E-01	3.43335E+00
1.25287E-01	2.90500E+00
1.28988E-01	2.49125E+00
1.32797E-01	2.15866E+00
1.36719E-01	1.88560E+00
1.40757E-01	1.65744E+00
1.44914E-01	1.46393E+00
1.49194E-01	1.29765E+00
1.53600E-01	1.15307E+00
1.58136E-01	1.02601E+00
1.62806E-01	9.13176E-01
1.67615E-01	8.11947E-01
1.72565E-01	7.20164E-01
1.77661E-01	6.35989E-01
1.82908E-01	5.57789E-01
1.88310E-01	4.84027E-01
1.93872E-01	4.13146E-01
1.99597E-01	3.43421E-01
2.05492E-01	2.72735E-01
2.11561E-01	1.98202E-01
2.17809E-01	1.15551E-01
2.24242E-01	2.36773E-02
2.30864E-01	1.19576E-01
2.37683E-01	3.21846E-01
2.44702E-01	7.20354E-01
2.51929E-01	2.06702E+00
2.59370E-01	6.26359E+00
2.67030E-01	1.68536E+00
2.74916E-01	1.03120E+00
2.83035E-01	7.66894E-01
2.91394E-01	6.19725E-01
3.00000E-01	5.23576E-01

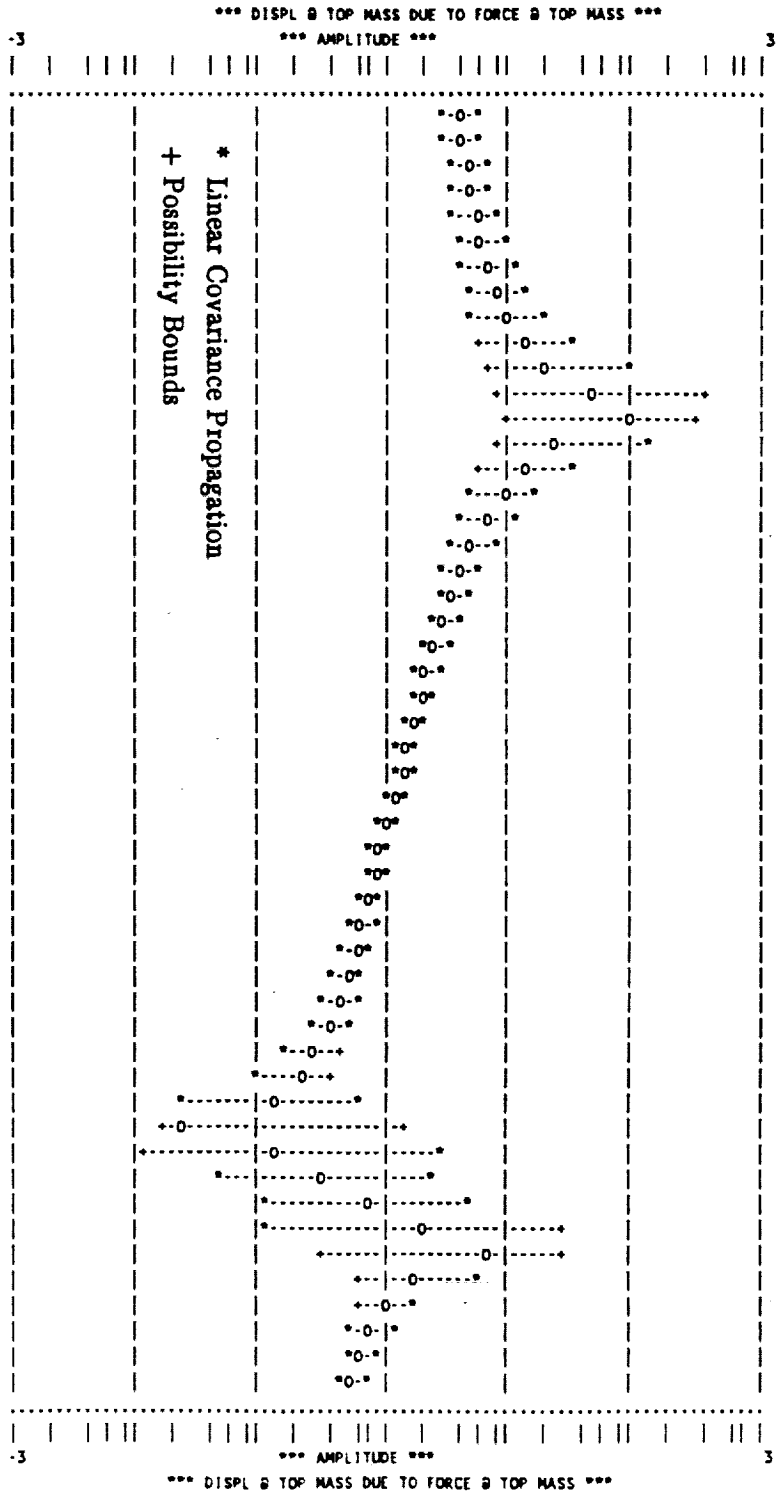

Figure 6–3a. One–Sigma Uncertainty Intervals on FRF Amplitude for 2–DOF Example, CSS Posttest Model Database.

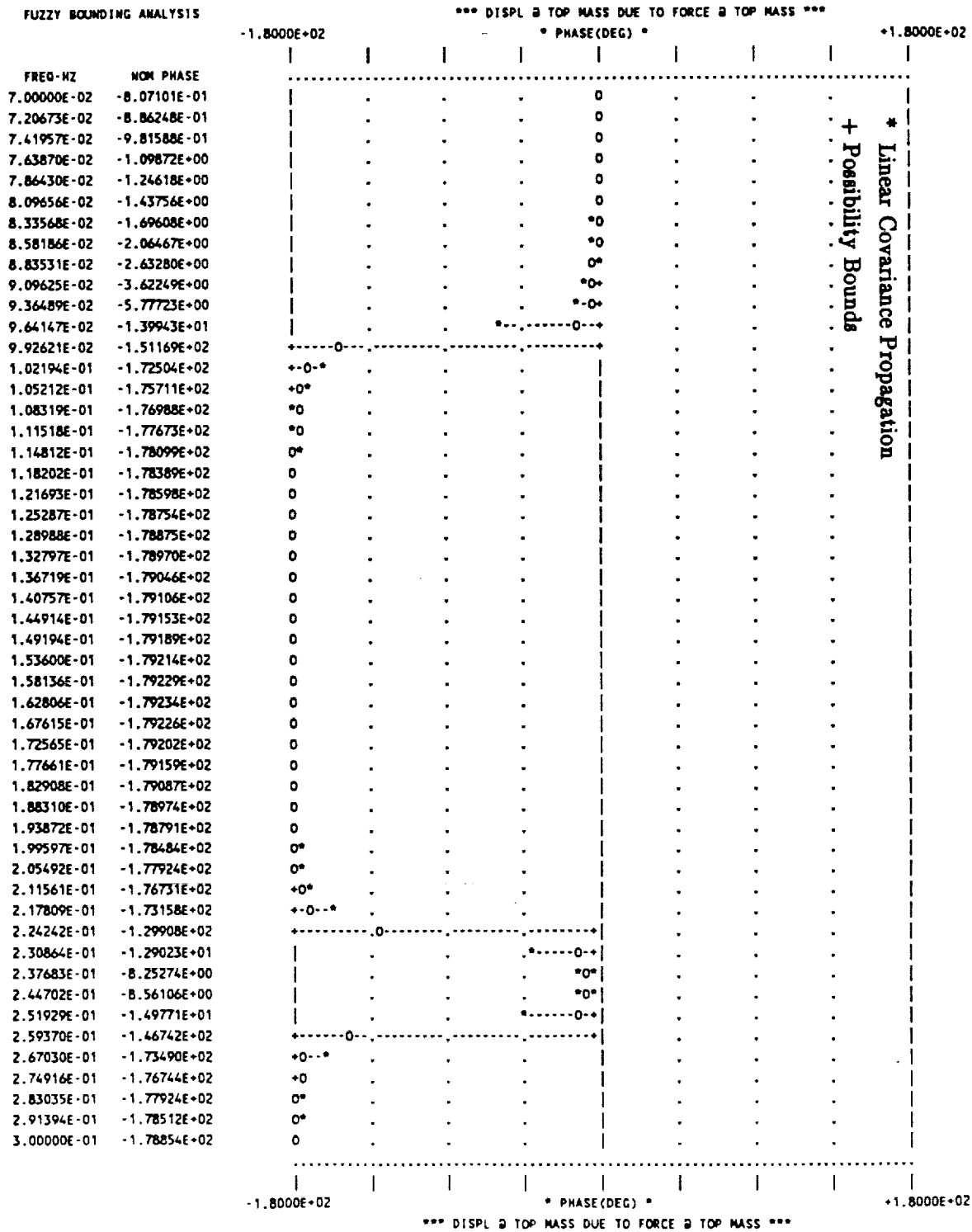

Figure 6–3b. One–Sigma Uncertainty Intervals on FRF Phase for 2–DOF Example, CSS Posttest Model Database.

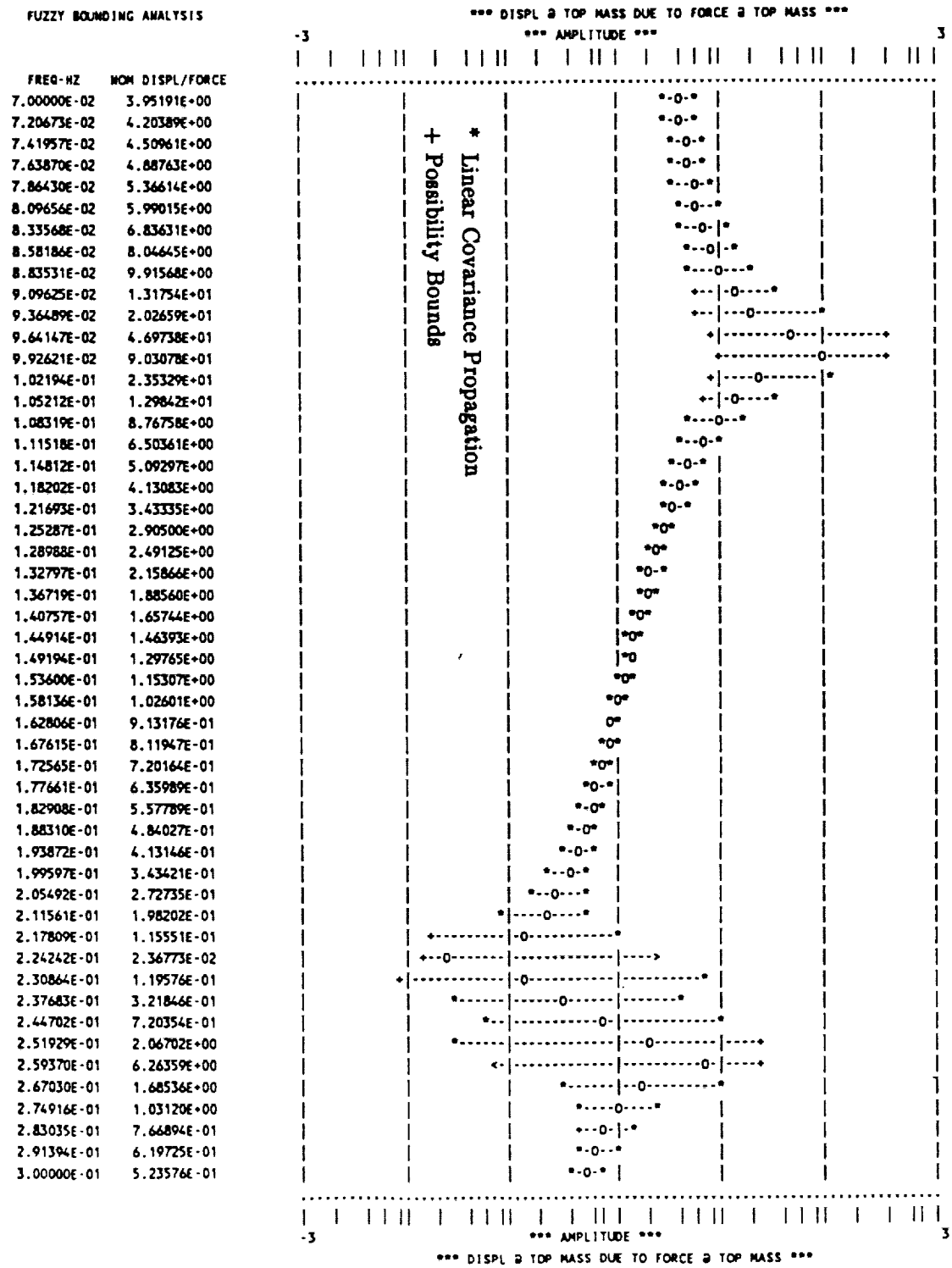

Figure 6–4a. One–Sigma Uncertainty Intervals on FRF Amplitude for 2–DOF Example, Combined Database.

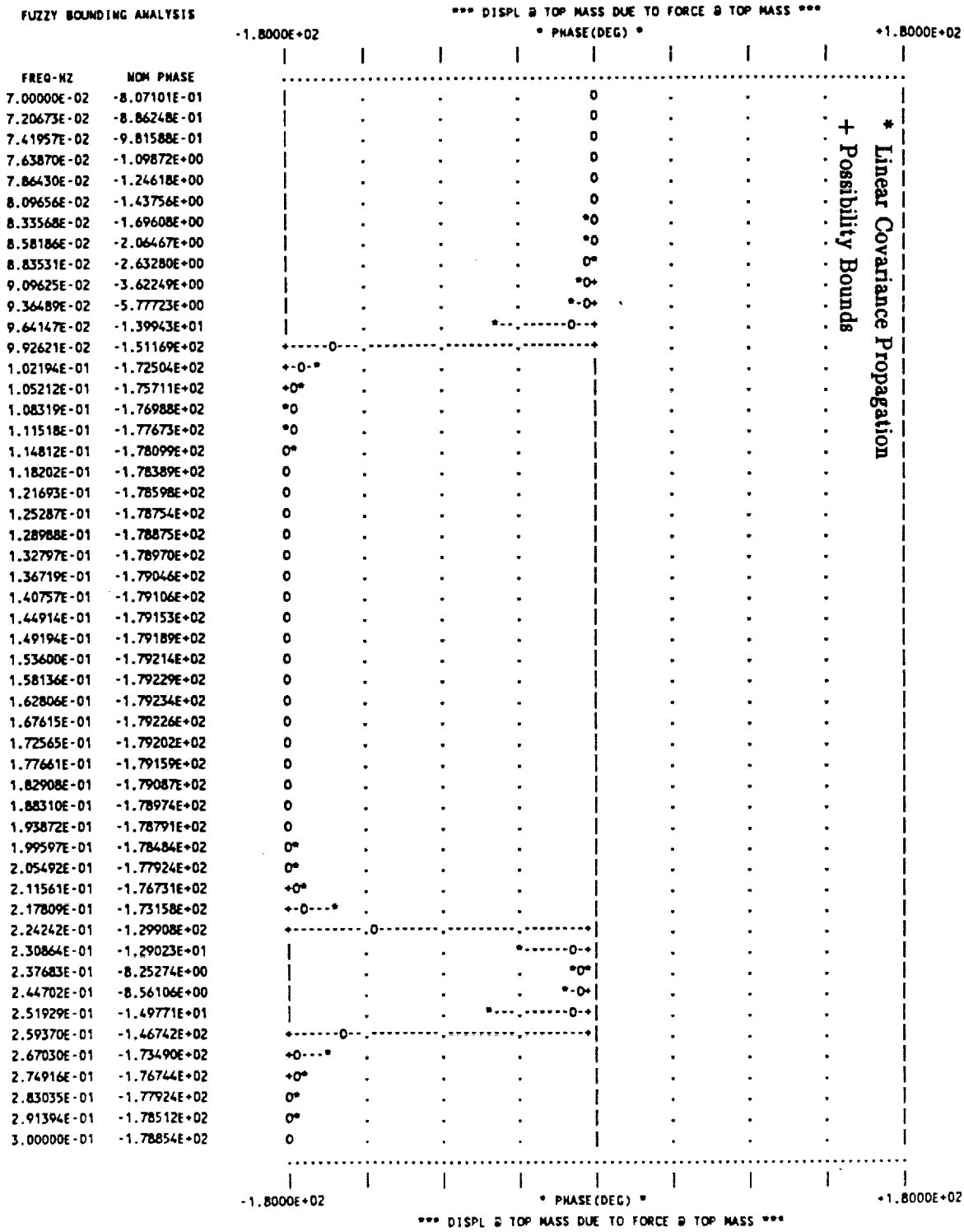

Figure 6–4b. One–Sigma Uncertainty Intervals on FRF Phase for 2–DOF Example, Combined Database.

little smaller for the LSS near the first mode and a little larger near the second mode. The combined database in Figure 6–4 appears to yield an average of the first three as it should. Between the first and second modes in the frequency range of approximately 0.1 to 0.2 Hz, there is very little difference among the four databases. The greatest difference is between the LSS and CSS pretest databases around 0.24 Hz, where the total uncertainty interval for the latter is three decades compared with only one and a half decades for the former, a difference of more than an order of magnitude. These results indicate that database differentiation can be important in some cases.

6.2 Mini–mast Structure

The LaRC Mini–mast structure introduced in Chapter 2 is the first structure selected to demonstrate the methodology. A finite element model for the structure was provided, along with measured FRF data [6–1]. Frequency response functions were computed using the LSS database.

Figure 6–5 shows the excitation and response locations for frequency response functions presented in [6–1]. Figures 6–6 through 6–8 show FRF amplitude and phase plots at Bays 6, 10 and 18 due to shaker input at Bay 9. These figures show both the test measurements (smooth lines) and analytical model predictions (lines with "+" symbols). Figures 6–9 through 6–11 show PDAC interval plots for the same FRF's. As in previously shown PDAC plots, the nominal response of the analytical model is denoted by "o" symbols. One sigma interval boundaries are denoted by " * " symbols when determined by linear covariance propagation, "+" symbols when determined by the fuzzy set approach (possibility bounds), and arrows when the interval exceeds two decades from the nominal in either direction.

FRF amplitude from test measurements are hand–plotted on the PDAC plots for direct comparison of predicted uncertainty intervals with test results. Where the test results exceed the $\pm\ 1\sigma$ intervals determined by covariance propagation (asterisks) the plotted intervals may be doubled (on the log scale) to determine $\pm\ 2\sigma$ uncertainty intervals. When an interval is delimited by plus signs, this cannot be done because the possibility bounds are not linear functions of parameter uncertainty. At these frequencies PDAC would have to be rerun to compute $\pm\ n\sigma$ intervals with $n > 1$, as illustrated in Figure 4–8.

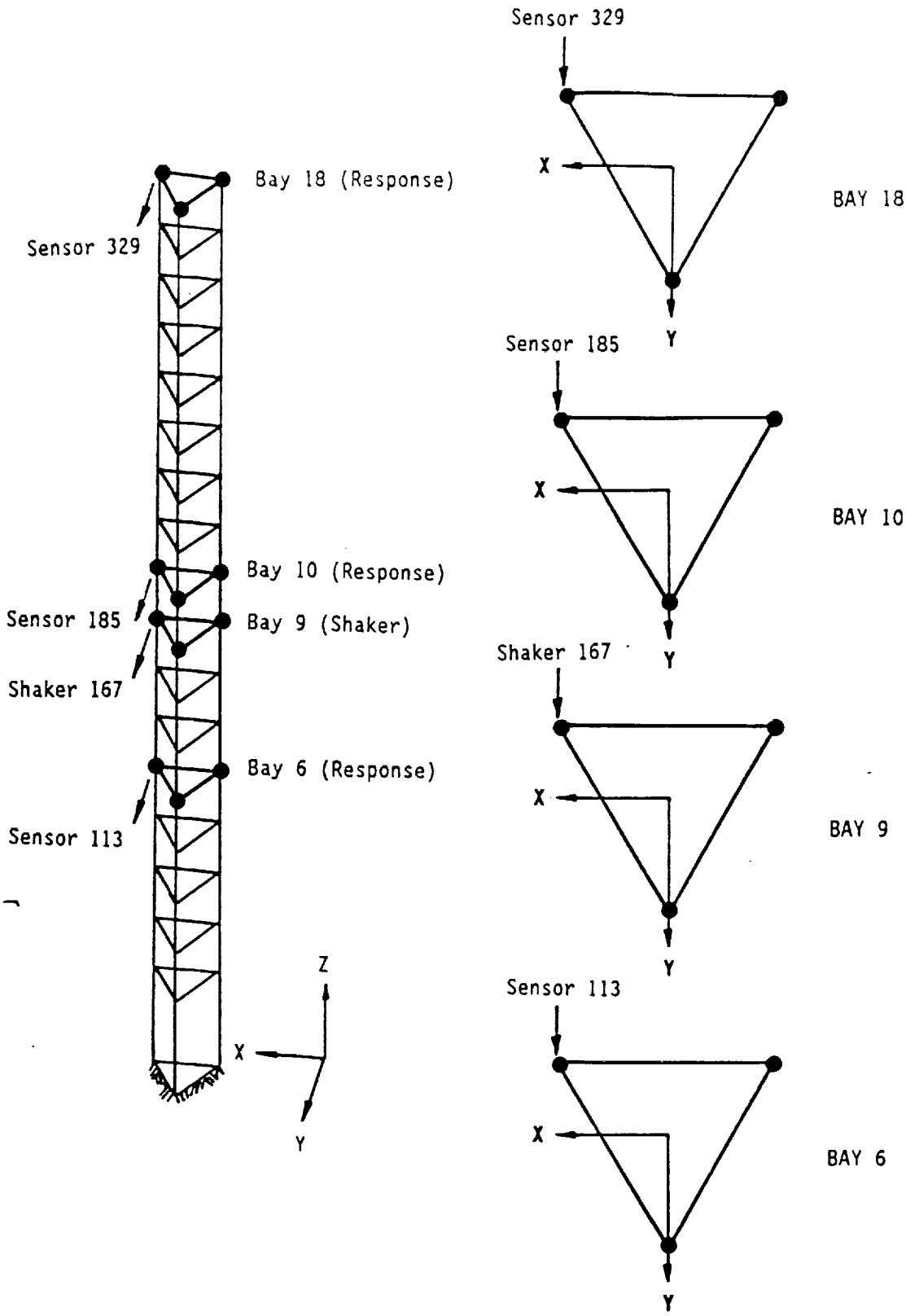

Figure 6–5. Excitation and Response Locations for the Mini–mast Structure.

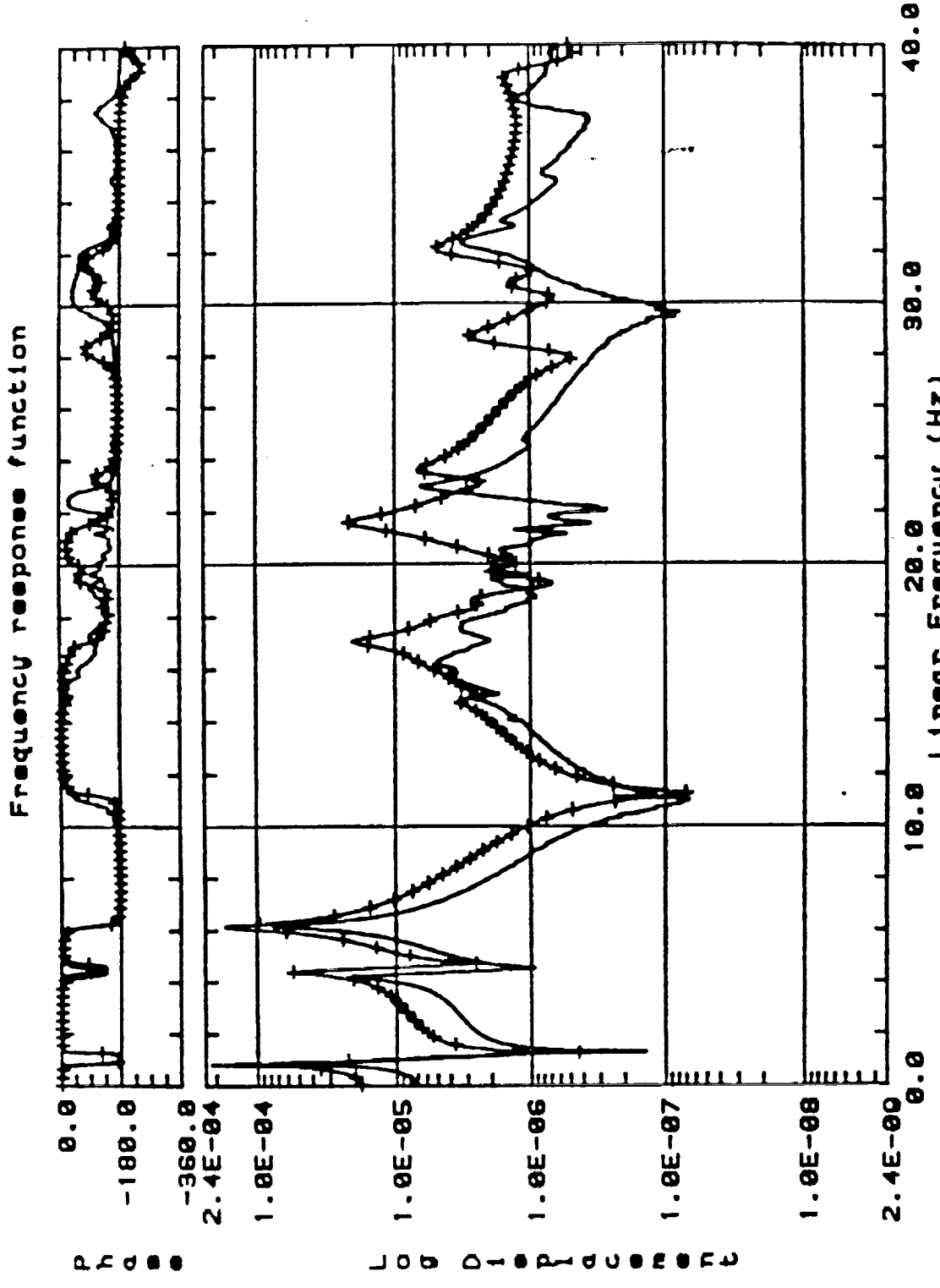

Figure 6–6. Displacement Frequency Response at Test Sensor 113 Due to Shaker 167 Input.

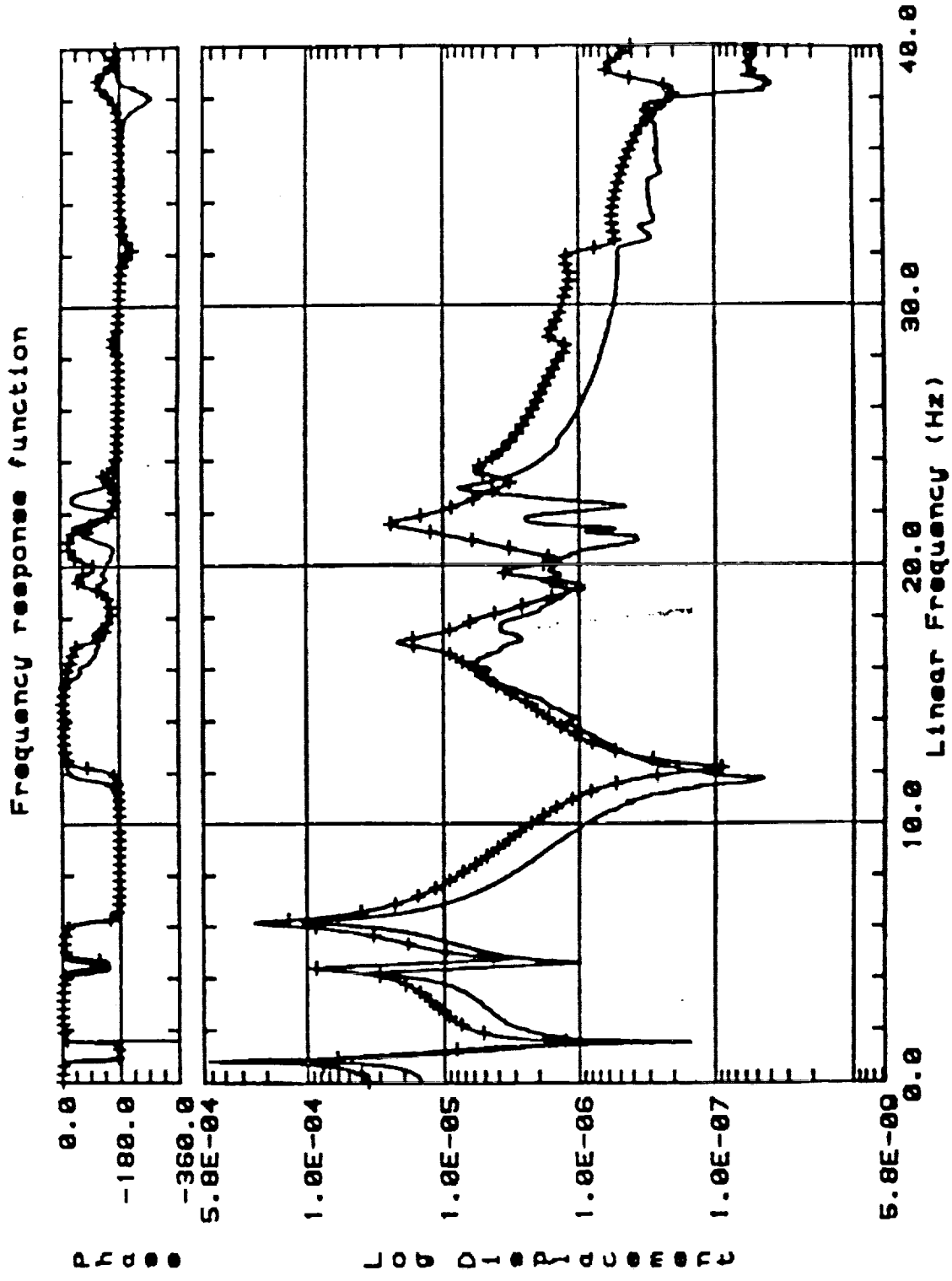

Figure 6–7. Displacement Frequency Response at Test Sensor 185 Due to Shaker 167 Input.

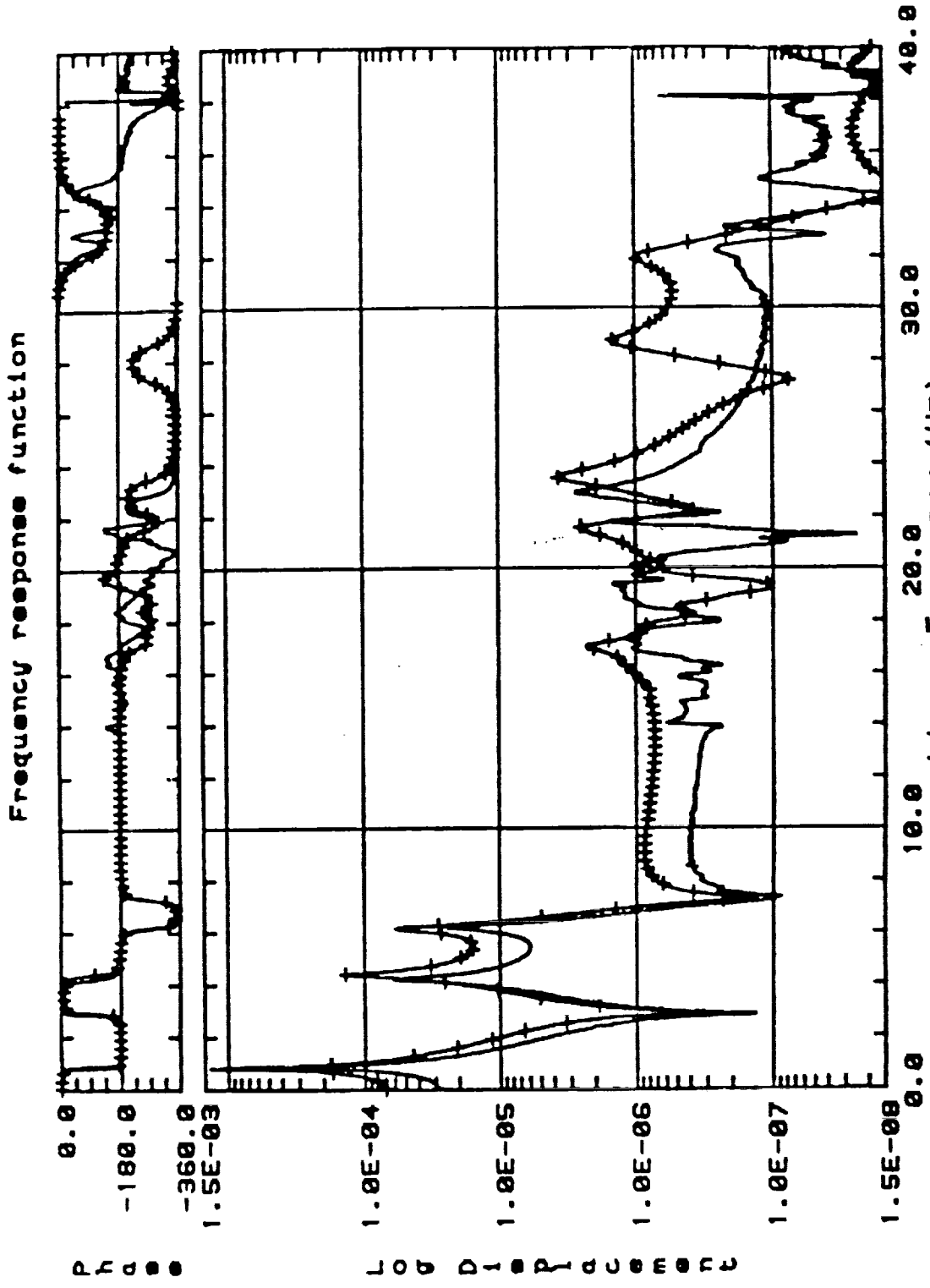

Figure 6–8. Displacement Frequency Response at Test Sensor 329 Due to Shaker 167 Input.

FUZZY BOUNDING ANALYSIS

FREQ-HZ	NOM DISPL/FORCE
5.00000E-01	2.12569E-05
5.30115E-01	2.24304E-05
5.62043E-01	2.39742E-05
5.95895E-01	2.60796E-05
6.31785E-01	2.90957E-05
6.69837E-01	3.37354E-05
7.10181E-01	4.17091E-05
7.52955E-01	5.83634E-05
7.98304E-01	1.11470E-04
8.46386E-01	2.07047E-04
8.97363E-01	5.84073E-05
9.51411E-01	2.82845E-05
1.00871E+00	1.64564E-05
1.06947E+00	1.02049E-05
1.13388E+00	6.35892E-06
1.20217E+00	3.76484E-06
1.27458E+00	1.90631E-06
1.35135E+00	5.48056E-07
1.43274E+00	6.64626E-07
1.51903E+00	1.51536E-06
1.61052E+00	2.23447E-06
1.70752E+00	2.84484E-06
1.81036E+00	3.37381E-06
1.91940E+00	3.84314E-06
2.03501E+00	4.27032E-06
2.15757E+00	4.67018E-06
2.28752E+00	5.05617E-06
2.42530E+00	5.44159E-06
2.57137E+00	5.84088E-06
2.72624E+00	6.27143E-06
2.89044E+00	6.75643E-06
3.06453E+00	7.33010E-06
3.24911E+00	8.04855E-06
3.44480E+00	9.01592E-06
3.65228E+00	1.04596E-05
3.87225E+00	1.30143E-05
4.10548E+00	1.94634E-05
4.35275E+00	5.47570E-05
4.61491E+00	6.46928E-06
4.89286E+00	2.87759E-06
5.18756E+00	6.94431E-06
5.50000E+00	1.14981E-05

Figure 6–9a. Predictive Accuracy of Mini–mast Model, FRF Amplitude at Sensor 113.

FUZZY BOUNDING ANALYSIS

FREQ-HZ	NOM PHASE
5.00000E-01	-1.61517E+00
5.30115E-01	-1.86762E+00
5.62043E-01	-2.19878E+00
5.95895E-01	-2.65095E+00
6.31785E-01	-3.30232E+00
6.69837E-01	-4.31419E+00
7.10181E-01	-6.07866E+00
7.52955E-01	-9.84611E+00
7.98304E-01	-2.25730E+01
8.46386E-01	-1.20619E+02
8.97363E-01	-1.62788E+02
9.51411E-01	-1.69476E+02
1.00871E+00	-1.71818E+02
1.06947E+00	-1.72716E+02
1.13388E+00	-1.72745E+02
1.20217E+00	-1.71765E+02
1.27458E+00	-1.68378E+02
1.35135E+00	-1.48438E+02
1.43274E+00	-1.96405E+01
1.51903E+00	-6.85137E+00
1.61052E+00	-3.89467E+00
1.70752E+00	-2.66148E+00
1.81036E+00	-2.02368E+00
1.91940E+00	-1.65891E+00
2.03501E+00	-1.44205E+00
2.15757E+00	-1.31560E+00
2.28752E+00	-1.25058E+00
2.42530E+00	-1.23212E+00
2.57137E+00	-1.25358E+00
2.72624E+00	-1.31440E+00
2.89044E+00	-1.42020E+00
3.06453E+00	-1.58539E+00
3.24911E+00	-1.84070E+00
3.44480E+00	-2.25375E+00
3.65228E+00	-2.99437E+00
3.87225E+00	-4.60499E+00
4.10548E+00	-9.85359E+00
4.35275E+00	-7.08914E+01
4.61491E+00	-1.44729E+02
4.89286E+00	-2.36546E+01
5.18756E+00	-7.09128E+00
5.50000E+00	-5.56173E+00

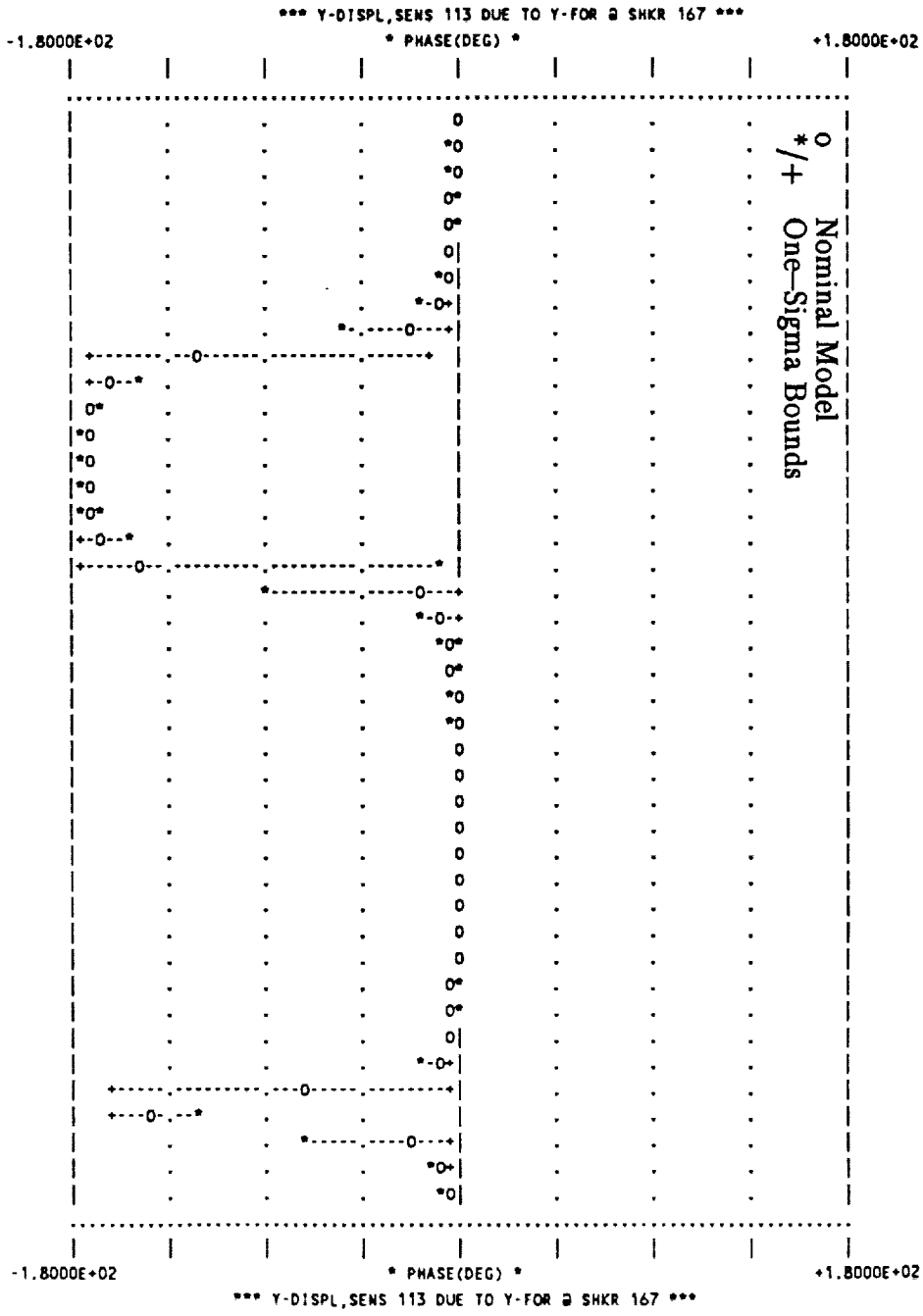

Figure 6–9b. Predictive Accuracy of Mini–mast Model, FRF Phase at Sensor 113.

FUZZY BOUNDING ANALYSIS

FREQ-HZ	NOM DISPL/FORCE
5.00000E-01	4.58191E-05
5.30115E-01	4.86246E-05
5.62043E-01	5.23166E-05
5.95895E-01	5.73532E-05
6.31785E-01	6.45713E-05
6.69837E-01	7.56790E-05
7.10181E-01	9.47776E-05
7.52955E-01	1.34695E-04
7.98304E-01	2.62179E-04
8.46386E-01	4.98326E-04
8.97363E-01	1.44785E-04
9.51411E-01	7.28272E-05
1.00871E+00	4.45616E-05
1.06947E+00	2.96277E-05
1.13388E+00	2.04476E-05
1.20217E+00	1.42615E-05
1.27458E+00	9.82720E-06
1.35135E+00	6.50380E-06
1.43274E+00	3.92772E-06
1.51903E+00	1.88209E-06
1.61052E+00	3.60102E-07
1.70752E+00	1.27224E-06
1.81036E+00	2.44946E-06
1.91940E+00	3.48370E-06
2.03501E+00	4.40487E-06
2.15757E+00	5.24367E-06
2.28752E+00	6.02766E-06
2.42530E+00	6.78287E-06
2.57137E+00	7.53604E-06
2.72624E+00	8.31767E-06
2.89044E+00	9.16665E-06
3.06453E+00	1.01386E-05
3.24911E+00	1.13232E-05
3.44480E+00	1.28855E-05
3.65228E+00	1.51847E-05
3.87225E+00	1.92244E-05
4.10548E+00	2.94171E-05
4.35275E+00	8.61649E-05
4.61491E+00	1.15292E-05
4.89286E+00	3.02208E-06
5.18756E+00	8.99192E-06
5.50000E+00	1.56709E-05

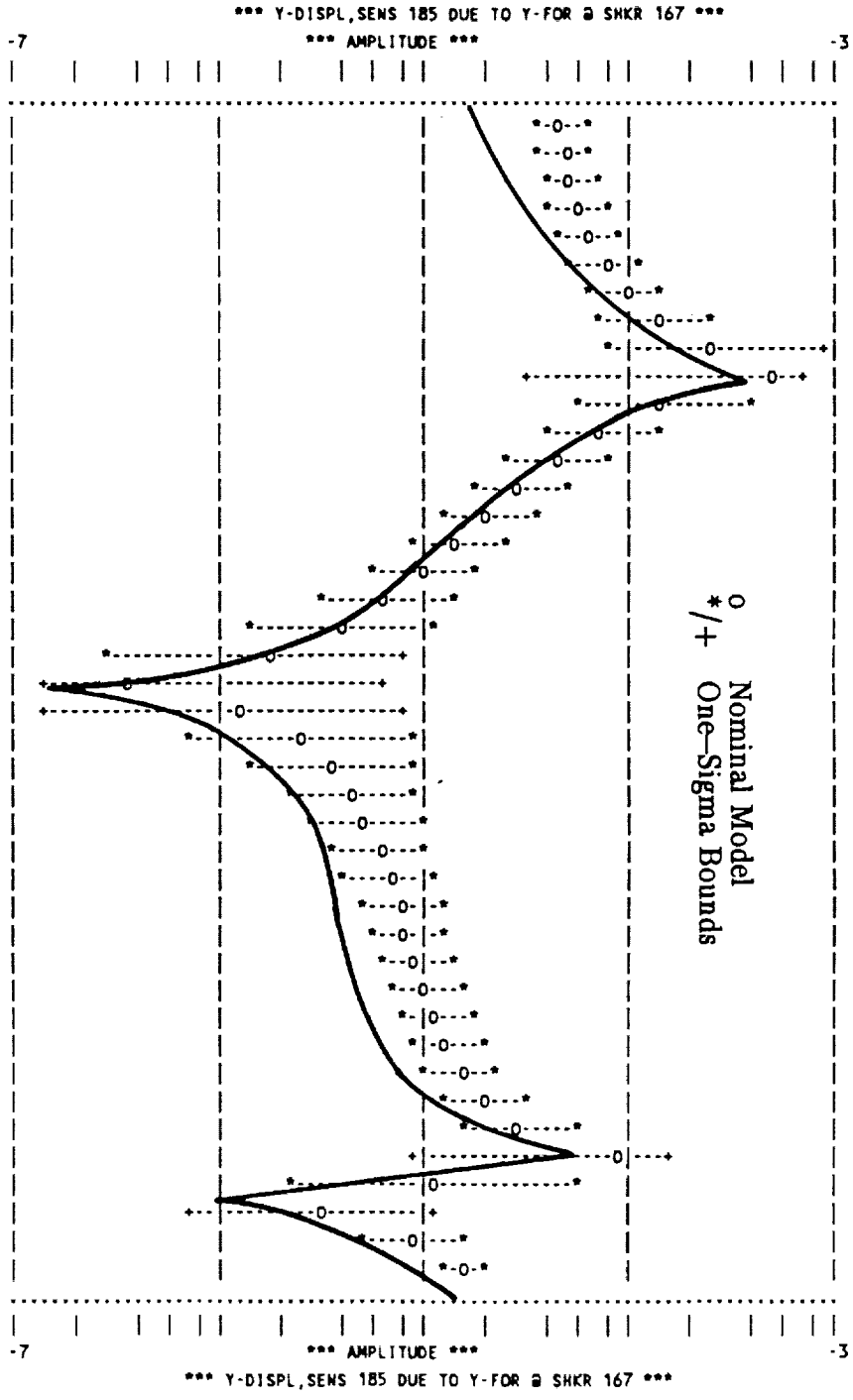

Figure 6–10a. Predictive Accuracy of Mini–mast Model, FRF Amplitude at Sensor 185.

C-3

FUZZY BOUNDING ANALYSIS

FREQ-HZ	NOM PHASE
5.00000E-01	-1.78114E+00
5.30115E-01	-2.04982E+00
5.62043E-01	-2.39977E+00
5.95895E-01	-2.87397E+00
6.31785E-01	-3.55146E+00
6.69837E-01	-4.59476E+00
7.10181E-01	-6.39768E+00
7.52955E-01	-1.02132E+01
7.98304E-01	-2.30035E+01
8.46386E-01	-1.21141E+02
8.97363E-01	-1.63402E+02
9.51411E-01	-1.70238E+02
1.00871E+00	-1.72800E+02
1.06947E+00	-1.74045E+02
1.13388E+00	-1.74677E+02
1.20217E+00	-1.74917E+02
1.27458E+00	-1.74806E+02
1.35135E+00	-1.74222E+02
1.43274E+00	-1.72683E+02
1.51903E+00	-1.67875E+02
1.61052E+00	-1.16368E+02
1.70752E+00	-1.23390E+01
1.81036E+00	-5.54393E+00
1.91940E+00	-3.50399E+00
2.03501E+00	-2.57844E+00
2.15757E+00	-2.08576E+00
2.28752E+00	-1.80821E+00
2.42530E+00	-1.65695E+00
2.57137E+00	-1.59146E+00
2.72624E+00	-1.59398E+00
2.89044E+00	-1.66095E+00
3.06453E+00	-1.80193E+00
3.24911E+00	-2.04574E+00
3.44480E+00	-2.46094E+00
3.65228E+00	-3.22277E+00
3.87225E+00	-4.88991E+00
4.10548E+00	-1.02835E+01
4.35275E+00	-7.18038E+01
4.61491E+00	-1.49360E+02
4.89286E+00	-3.59675E+01
5.18756E+00	-8.14916E+00
5.50000E+00	-5.91057E+00

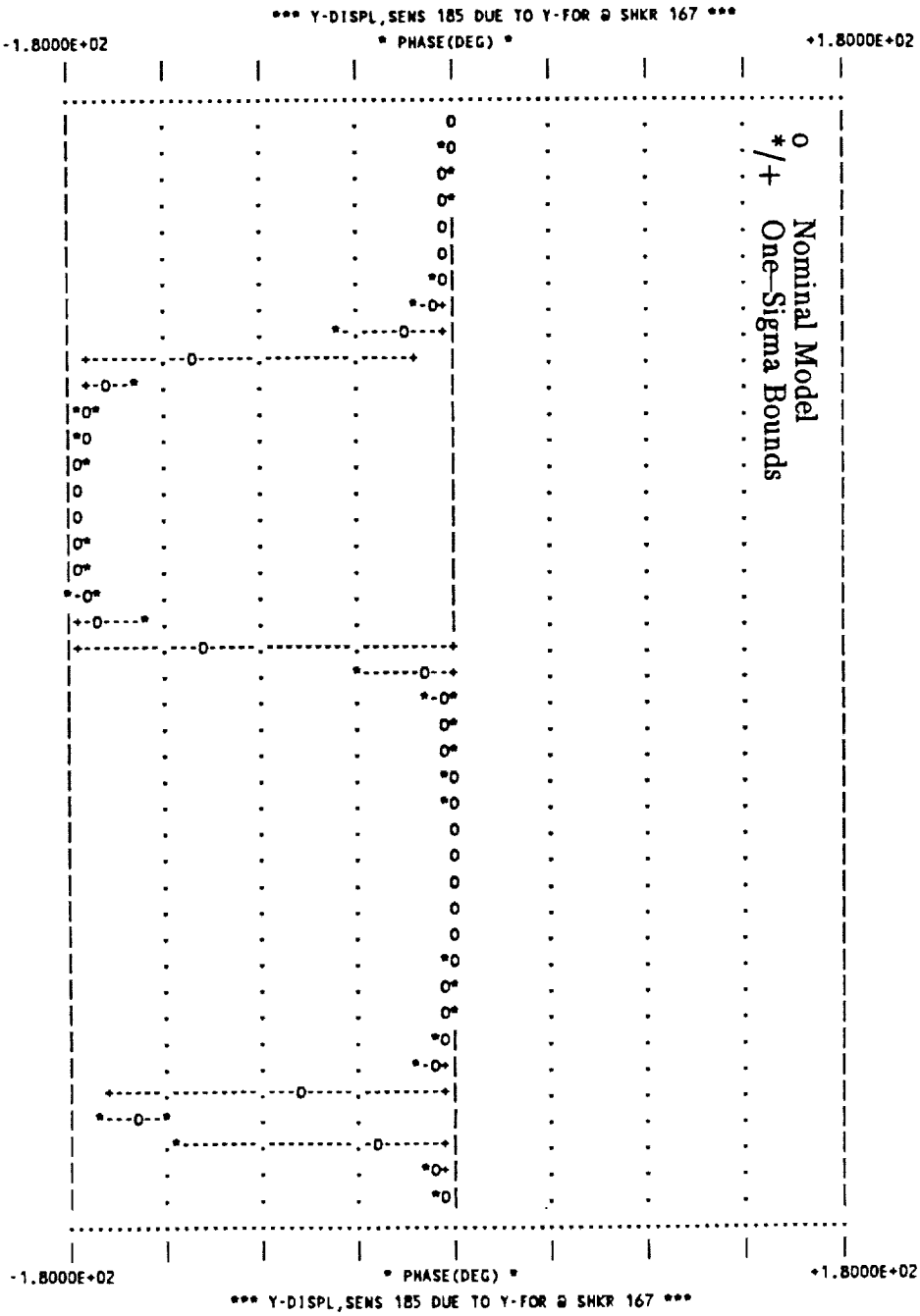

Figure 6–10b. Predictive Accuracy of Mini–mast Model, FRF Phase at Sensor 185.

FUZZY BOUNDING ANALYSIS

FREQ-HZ	NOM DISPL/FORCE
5.00000E-01	9.84553E-05
5.30115E-01	1.05531E-04
5.62043E-01	1.14846E-04
5.95895E-01	1.27558E-04
6.31785E-01	1.45785E-04
6.69837E-01	1.73847E-04
7.10181E-01	2.22127E-04
7.52955E-01	3.23121E-04
7.98304E-01	6.46325E-04
8.46386E-01	1.26798E-03
8.97363E-01	3.82641E-04
9.51411E-01	2.01383E-04
1.00871E+00	1.30149E-04
1.06947E+00	9.25307E-05
1.13388E+00	6.94336E-05
1.20217E+00	5.39000E-05
1.27458E+00	4.27976E-05
1.35135E+00	3.45097E-05
1.43274E+00	2.81173E-05
1.51903E+00	2.30592E-05
1.61052E+00	1.89730E-05
1.70752E+00	1.56133E-05
1.81036E+00	1.28077E-05
1.91940E+00	1.04306E-05
2.03501E+00	8.38749E-06
2.15757E+00	6.60434E-06
2.28752E+00	5.02099E-06
2.42530E+00	3.58576E-06
2.57137E+00	2.25202E-06
2.72624E+00	9.84183E-07
2.89044E+00	4.79837E-07
3.06453E+00	1.80551E-06
3.24911E+00	3.43173E-06
3.44480E+00	5.54456E-06
3.65228E+00	8.69428E-06
3.87225E+00	1.44768E-05
4.10548E+00	3.01398E-05
4.35275E+00	1.33930E-04
4.61491E+00	3.83080E-05
4.89286E+00	2.04522E-05
5.18756E+00	1.47868E-05
5.50000E+00	1.25986E-05

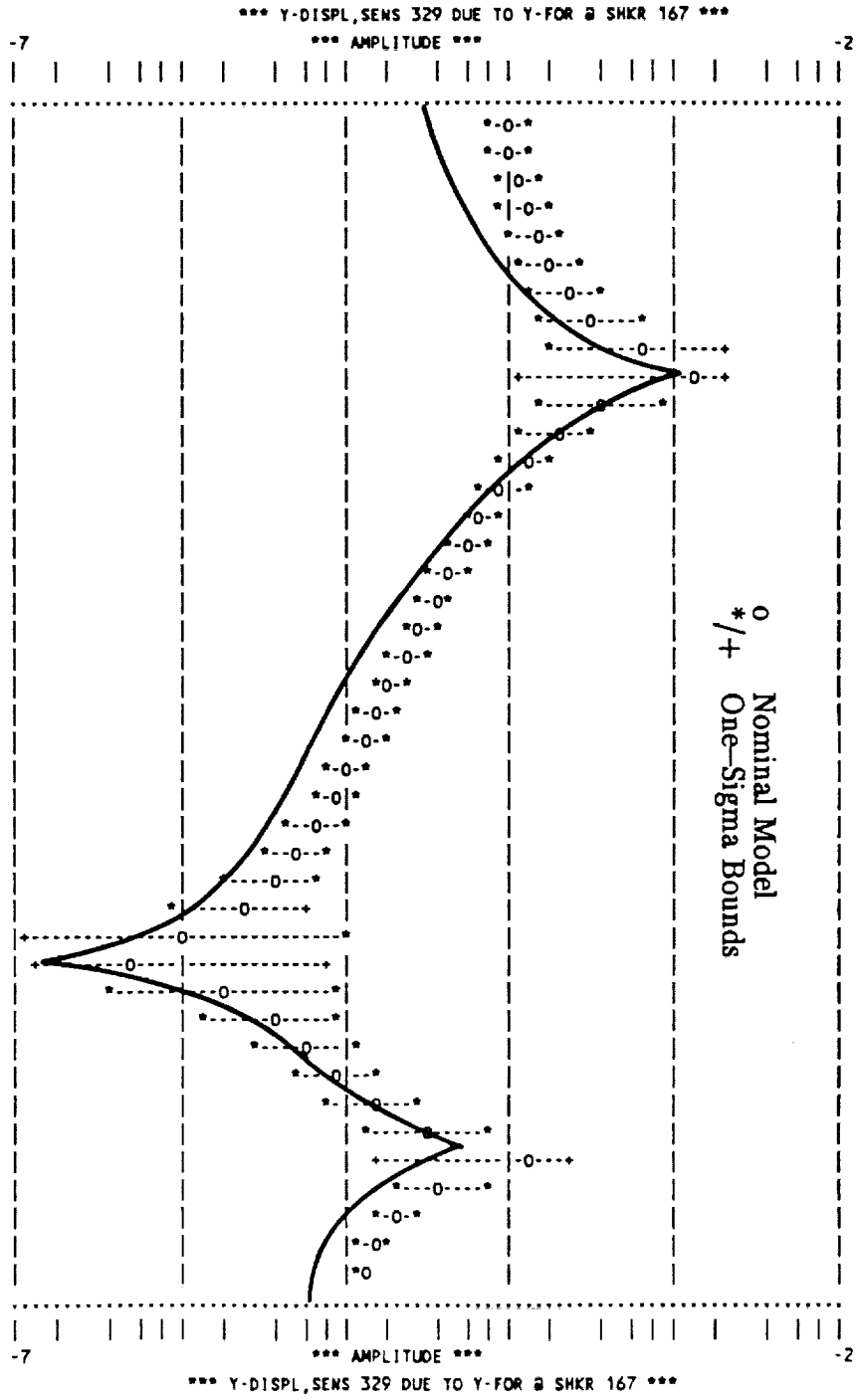

Figure 6–11a. Predictive Accuracy of Mini–mast Model, FRF Amplitude at Sensor 329.

FUZZY BOUNDING ANALYSIS

FREQ-HZ	NOM PHASE
5.00000E-01	-2.07589E+00
5.30115E-01	-2.36809E+00
5.62043E-01	-2.74431E+00
5.95895E-01	-3.24803E+00
6.31785E-01	-3.95895E+00
6.69837E-01	-5.04041E+00
7.10181E-01	-6.88736E+00
7.52955E-01	-1.07545E+01
7.98304E-01	-2.36076E+01
8.46386E-01	-1.21829E+02
8.97363E-01	-1.64164E+02
9.51411E-01	-1.71107E+02
1.00871E+00	-1.73806E+02
1.06947E+00	-1.75230E+02
1.13388E+00	-1.76106E+02
1.20217E+00	-1.76693E+02
1.27458E+00	-1.77108E+02
1.35135E+00	-1.77410E+02
1.43274E+00	-1.77633E+02
1.51903E+00	-1.77792E+02
1.61052E+00	-1.77899E+02
1.70752E+00	-1.77955E+02
1.81036E+00	-1.77957E+02
1.91940E+00	-1.77893E+02
2.03501E+00	-1.77739E+02
2.15757E+00	-1.77443E+02
2.28752E+00	-1.76896E+02
2.42530E+00	-1.75820E+02
2.57137E+00	-1.73287E+02
2.72624E+00	-1.63512E+02
2.89044E+00	-4.08807E+01
3.06453E+00	-1.20506E+01
3.24911E+00	-8.18448E+00
3.44480E+00	-7.22929E+00
3.65228E+00	-7.55726E+00
3.87225E+00	-9.38224E+00
4.10548E+00	-1.56372E+01
4.35275E+00	-7.95606E+01
4.61491E+00	-1.66595E+02
4.89286E+00	-1.74367E+02
5.18756E+00	-1.77186E+02
5.50000E+00	-1.79124E+02

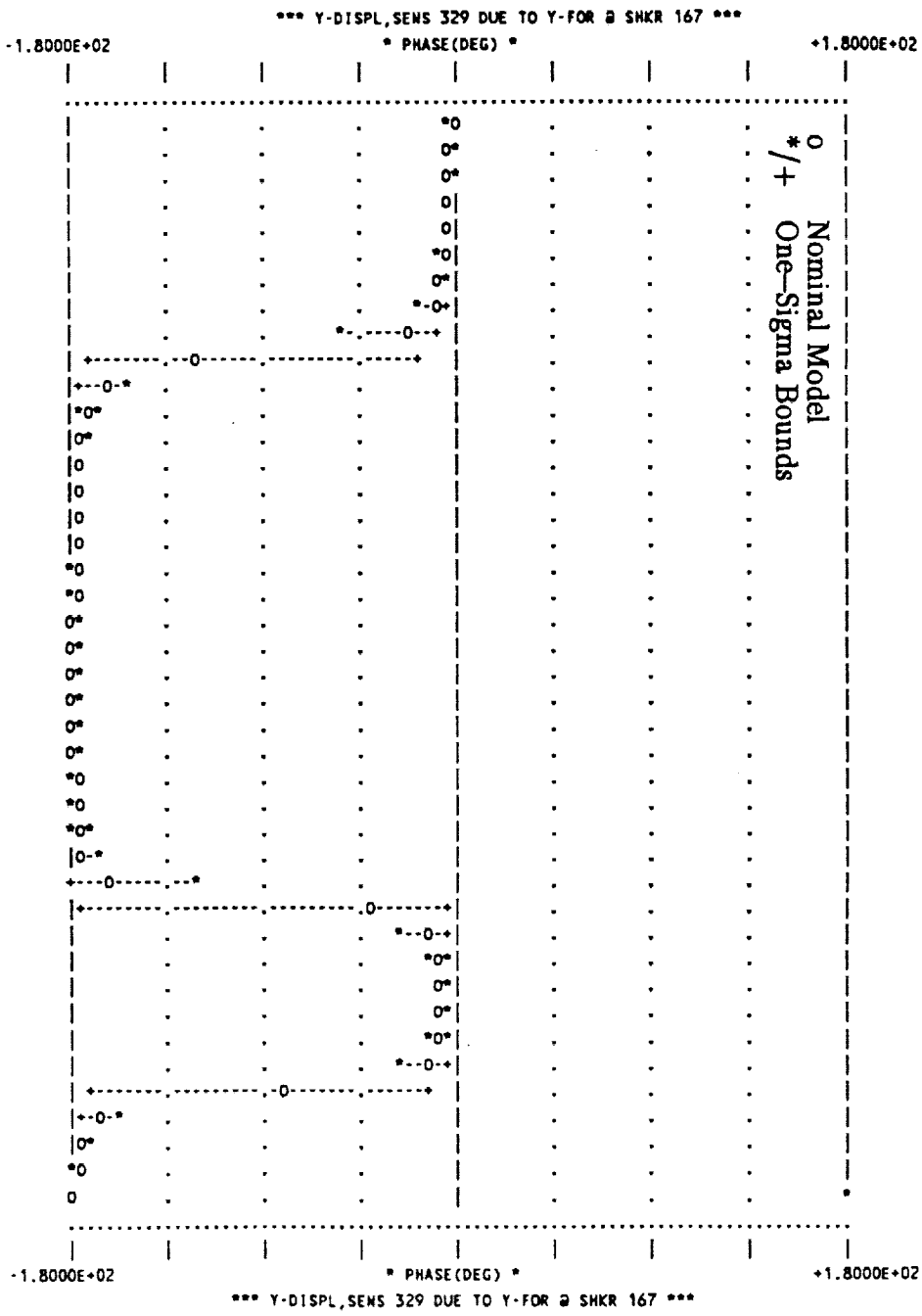

Figure 6–11b. Predictive Accuracy of Mini–mast Model, FRF Phase at Sensor 329.

Direct comparisons between PDAC response intervals and test data are not presented for FRF Phase. This is because the hard copy plots (e.g. Figures 6–6 through 6–8) available for comparison did not show sufficient detail; predicted and measured phase were too close to differentiate.

The Mini–mast demonstration case was selected to perform sensitivity analyses with respect to approximations employed by PDAC to limit run time. Sections 4.2.2.1 and 4.2.2.2 discussed modal parameter clustering and the diagonalization of the modal parameter covariance matrix. Clustering of the r–parameters is performed to reduce the size of the covariance matrix subjected to singular value decomposition (SVD) at each excitation frequency near a pole or zero. Figures 6–10, 6–12 and 6–13 illustrate the sensitivity of computed response intervals to the selected clustering thresholds. See Equations (4–47) through (4–49). The r–parameter thresholds are 5%, 2.5% and 10% at the poles, and 100%, 50% and 200% at the zeros in Figures 6–10, 6–12 and 6–13, respectively. These results show small but relatively insignificant differences, even at the highest threshold level.

All three of the above runs were executed with a 5% threshold on the s–parameters. See Equations (4–54), (4–48) and (4–49). The same problem (with 5% and 100% r–parameter thresholds at poles and zeros), was rerun at s–parameter thresholds of 10% and 15% to investigate the sensitivity of results to s–parameter truncation. These results are presented in Figures 6–14 and 6–15.

Again, the plots show small, insignificant differences. With the threshold at 5% a maximum of 21 s–parameters was required near the first zero (1.707 Hz); at 10% only 16 s–parameters; and at 15% only 12 s–parameters. At any given frequency, the elimination of each s–parameter reduces the computation time by half. The computation time with a 5% threshold was therefore $2^9 = 512$ times longer than the computation time at a threshold of 15%. Of course, these computations are not made at all frequencies. In this case the fuzzy set approach was applied at only those frequencies listed in Table 6–1. The number of s–parameters retained after truncation at each frequency for each threshold are shown for comparison.

FUZZY BOUNDING ANALYSIS

FREQ-HZ	NOM DISPL/FORCE
5.00000E-01	4.58191E-05
5.30115E-01	4.86246E-05
5.62043E-01	5.23166E-05
5.95895E-01	5.73532E-05
6.31785E-01	6.45713E-05
6.69837E-01	7.56790E-05
7.10181E-01	9.47776E-05
7.52955E-01	1.34695E-04
7.98304E-01	2.62179E-04
8.46386E-01	4.98326E-04
8.97363E-01	1.44785E-04
9.51411E-01	7.28272E-05
1.00871E+00	4.45616E-05
1.06947E+00	2.96277E-05
1.13388E+00	2.04476E-05
1.20217E+00	1.42615E-05
1.27458E+00	9.82720E-06
1.35135E+00	6.50380E-06
1.43274E+00	3.92772E-06
1.51903E+00	1.88209E-06
1.61052E+00	3.60102E-07
1.70752E+00	1.27224E-06
1.81036E+00	2.44946E-06
1.91940E+00	3.48370E-06
2.03501E+00	4.40487E-06
2.15757E+00	5.24367E-06
2.28752E+00	6.02766E-06
2.42530E+00	6.78287E-06
2.57137E+00	7.53604E-06
2.72624E+00	8.31767E-06
2.89044E+00	9.16665E-06
3.06453E+00	1.01386E-05
3.24911E+00	1.13232E-05
3.44480E+00	1.28855E-05
3.65228E+00	1.51847E-05
3.87225E+00	1.92244E-05
4.10548E+00	2.94171E-05
4.35275E+00	8.61649E-05
4.61491E+00	1.15292E-05
4.89286E+00	3.02208E-06
5.18756E+00	8.99192E-06
5.50000E+00	1.56709E-05

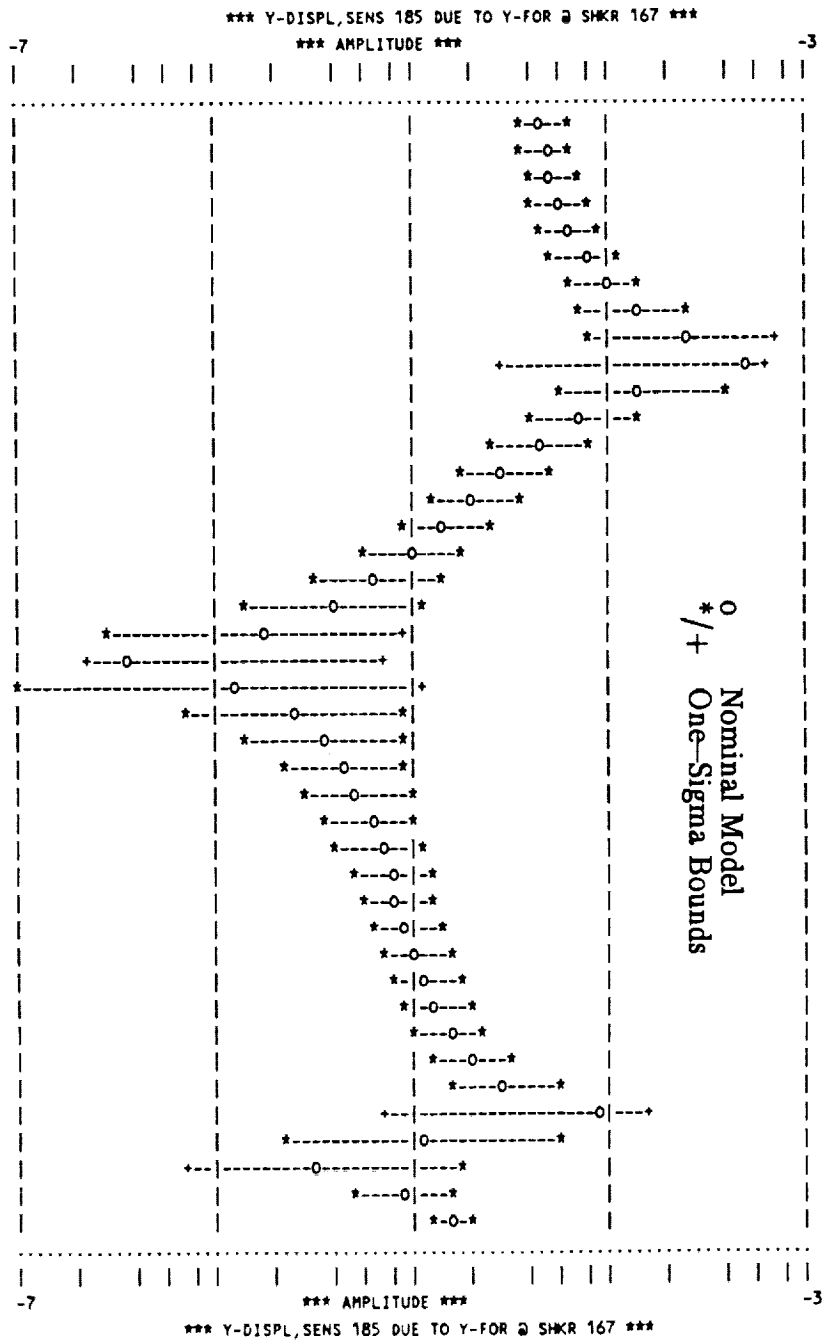

Figure 6–12a. Sensitivity of Interval Prediction on FRF Amplitude to r–parameter Truncation. Truncation Error Threshold is Half That of Figure 6–10.

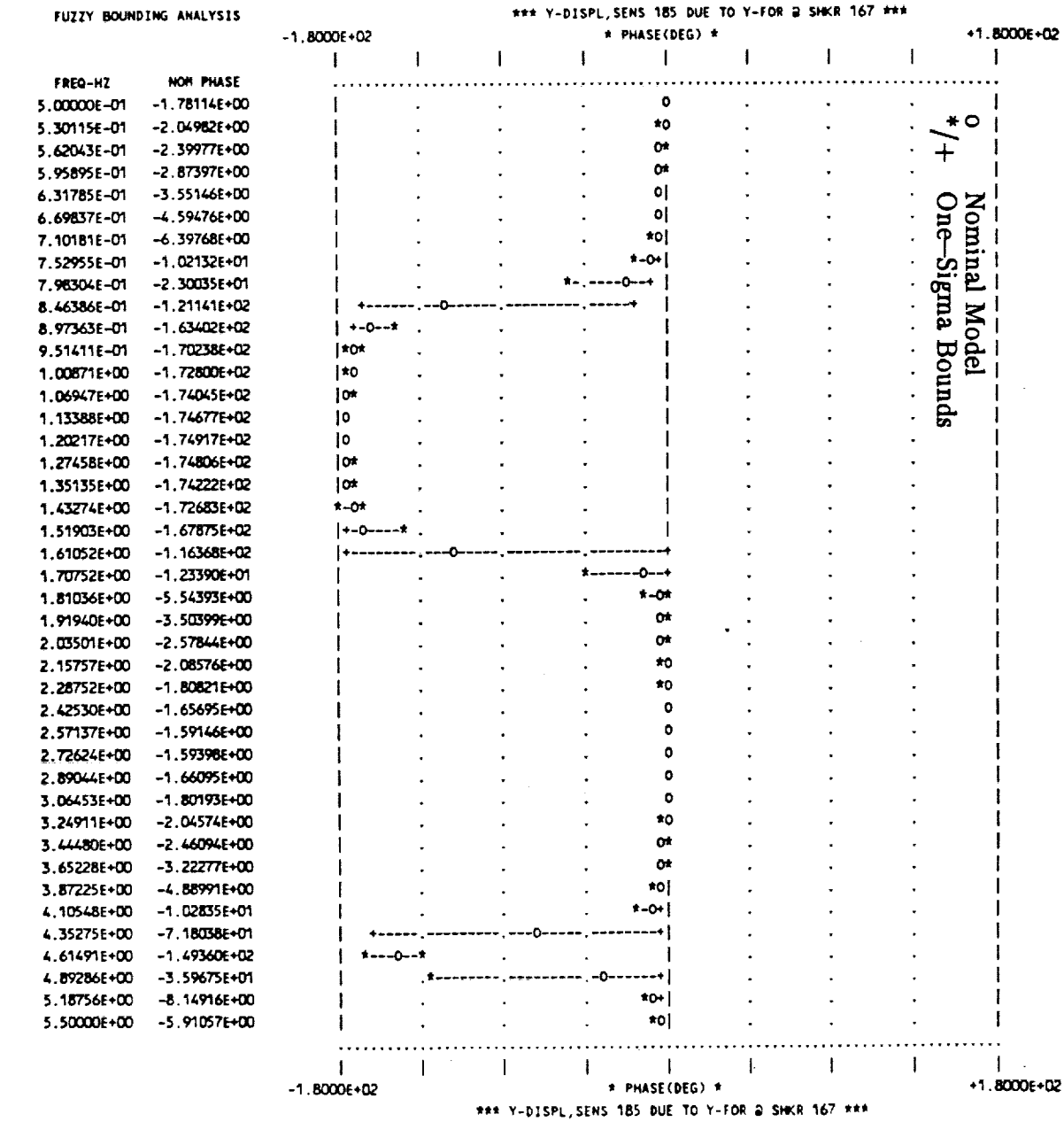

Figure 6–12b. Sensitivity of Interval Prediction on FRF Phase to r–parameter Truncation. Truncation Error Threshold is Half That of Figure 6–10.

FUZZY BOUNDING ANALYSIS

FREQ-HZ	NOM DISPL/FORCE
5.00000E-01	4.58191E-05
5.30115E-01	4.86246E-05
5.62043E-01	5.23166E-05
5.95895E-01	5.73532E-05
6.31785E-01	6.45713E-05
6.69837E-01	7.56790E-05
7.10181E-01	9.47776E-05
7.52955E-01	1.34695E-04
7.98304E-01	2.62179E-04
8.46386E-01	4.98326E-04
8.97363E-01	1.44785E-04
9.51411E-01	7.28272E-05
1.00871E+00	4.45616E-05
1.06947E+00	2.96277E-05
1.13388E+00	2.04476E-05
1.20217E+00	1.42615E-05
1.27458E+00	9.82720E-06
1.35135E+00	6.50380E-06
1.43274E+00	3.92772E-06
1.51903E+00	1.88209E-06
1.61052E+00	3.60102E-07
1.70752E+00	1.27224E-06
1.81036E+00	2.44946E-06
1.91940E+00	3.48370E-06
2.03501E+00	4.40487E-06
2.15757E+00	5.24367E-06
2.28752E+00	6.02766E-06
2.42530E+00	6.78287E-06
2.57137E+00	7.53604E-06
2.72624E+00	8.31767E-06
2.89044E+00	9.16665E-06
3.06453E+00	1.01386E-05
3.24911E+00	1.13232E-05
3.44480E+00	1.28855E-05
3.65228E+00	1.51847E-05
3.87225E+00	1.92244E-05
4.10548E+00	2.94171E-05
4.35275E+00	8.61649E-05
4.61491E+00	1.15292E-05
4.89286E+00	3.02208E-06
5.18756E+00	8.99192E-06
5.50000E+00	1.56709E-05

Figure 6–13a. Sensitivity of Interval Prediction on FRF Amplitude to r–parameter Truncation. Truncation Error Threshold is Twice That of Figure 6–10.

FUZZY BOUNDING ANALYSIS

FREQ-HZ	NOM PHASE
5.00000E-01	-1.78114E+00
5.30115E-01	-2.04982E+00
5.62043E-01	-2.39977E+00
5.95895E-01	-2.87397E+00
6.31785E-01	-3.55146E+00
6.69837E-01	-4.59476E+00
7.10181E-01	-6.39768E+00
7.52955E-01	-1.02132E+01
7.98304E-01	-2.30035E+01
8.46386E-01	-1.21141E+02
8.97363E-01	-1.63402E+02
9.51411E-01	-1.70238E+02
1.00871E+00	-1.72800E+02
1.06947E+00	-1.74045E+02
1.13388E+00	-1.74677E+02
1.20217E+00	-1.74917E+02
1.27458E+00	-1.74806E+02
1.35135E+00	-1.74222E+02
1.43274E+00	-1.72683E+02
1.51903E+00	-1.67875E+02
1.61052E+00	-1.16368E+02
1.70752E+00	-1.23390E+01
1.81036E+00	-5.54393E+00
1.91940E+00	-3.50399E+00
2.03501E+00	-2.57844E+00
2.15757E+00	-2.08576E+00
2.28752E+00	-1.80821E+00
2.42530E+00	-1.65695E+00
2.57137E+00	-1.59146E+00
2.72624E+00	-1.59398E+00
2.89044E+00	-1.66095E+00
3.06453E+00	-1.80193E+00
3.24911E+00	-2.04574E+00
3.44480E+00	-2.46094E+00
3.65228E+00	-3.22277E+00
3.87225E+00	-4.88991E+00
4.10548E+00	-1.02835E+01
4.35275E+00	-7.18038E+01
4.61491E+00	-1.49360E+02
4.89286E+00	-3.59675E+01
5.18756E+00	-8.14916E+00
5.50000E+00	-5.91057E+00

Figure 6—13b. Sensitivity of Interval Prediction on FRF Phase to r—parameter Truncation. Truncation Error Threshold is Twice That of Figure 6—10.

FUZZY BOUNDING ANALYSIS

FREQ-HZ	NOM DISPL/FORCE
5.00000E-01	4.58191E-05
5.30115E-01	4.86246E-05
5.62043E-01	5.23166E-05
5.95895E-01	5.73532E-05
6.31785E-01	6.45713E-05
6.69837E-01	7.56790E-05
7.10181E-01	9.47776E-05
7.52955E-01	1.34695E-04
7.98304E-01	2.62179E-04
8.46386E-01	4.98326E-04
8.97363E-01	1.44785E-04
9.51411E-01	7.28272E-05
1.00871E+00	4.45616E-05
1.06947E+00	2.96277E-05
1.13388E+00	2.04476E-05
1.20217E+00	1.42615E-05
1.27458E+00	9.82720E-06
1.35135E+00	6.50380E-06
1.43274E+00	3.92772E-06
1.51903E+00	1.88209E-06
1.61052E+00	3.60102E-07
1.70752E+00	1.27224E-06
1.81036E+00	2.44946E-06
1.91940E+00	3.48370E-06
2.03501E+00	4.40487E-06
2.15757E+00	5.24367E-06
2.28752E+00	6.02766E-06
2.42530E+00	6.78287E-06
2.57137E+00	7.53604E-06
2.72624E+00	8.31767E-06
2.89044E+00	9.16665E-06
3.06453E+00	1.01386E-05
3.24911E+00	1.13232E-05
3.44480E+00	1.28855E-05
3.65228E+00	1.51847E-05
3.87225E+00	1.92244E-05
4.10548E+00	2.94171E-05
4.35275E+00	8.61649E-05
4.61491E+00	1.15292E-05
4.89286E+00	3.02208E-06
5.18756E+00	8.99192E-06
5.50000E+00	1.56709E-05

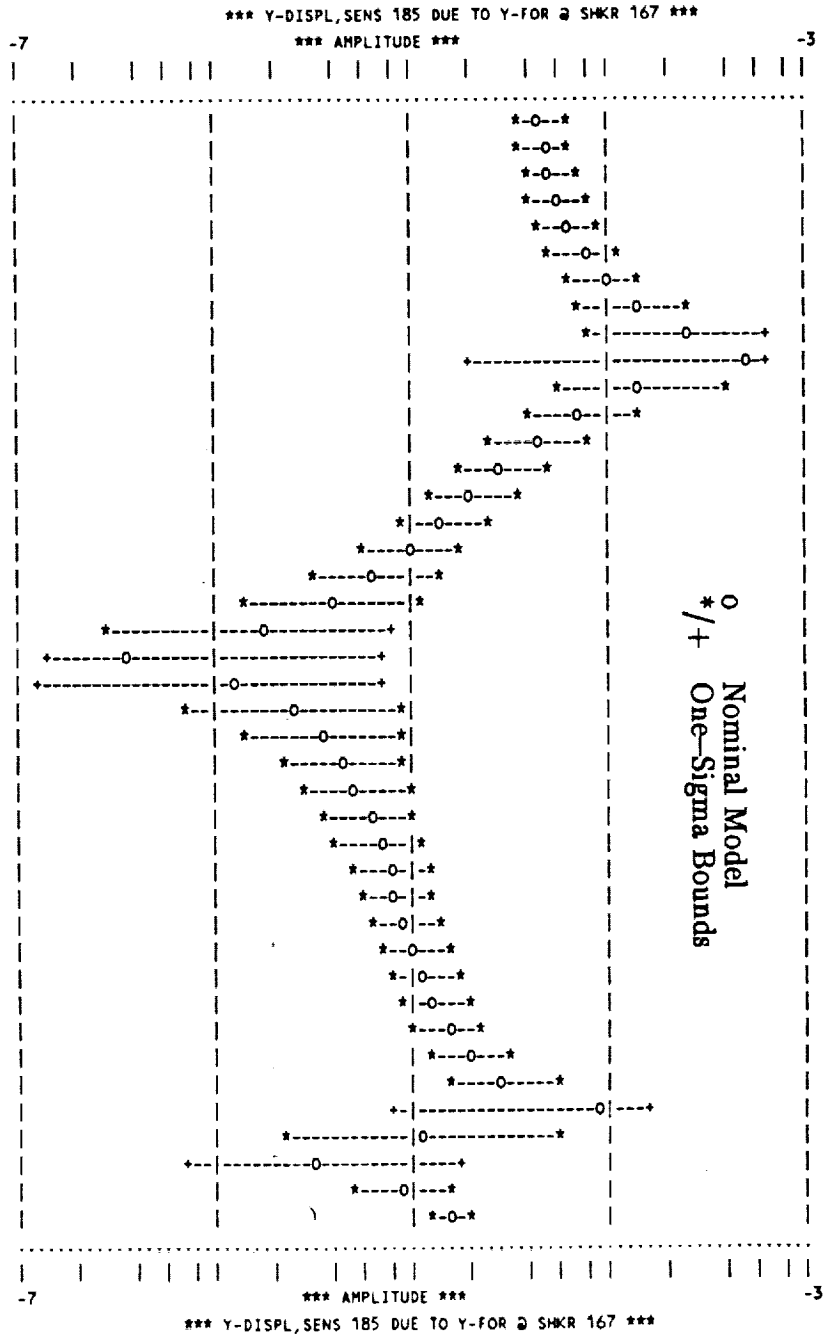

Figure 6-14a. Sensitivity of Interval Prediction on FRF Amplitude to s-parameter Truncation. Truncation Error Threshold is Twice That of Figure 6-10.

LE-9

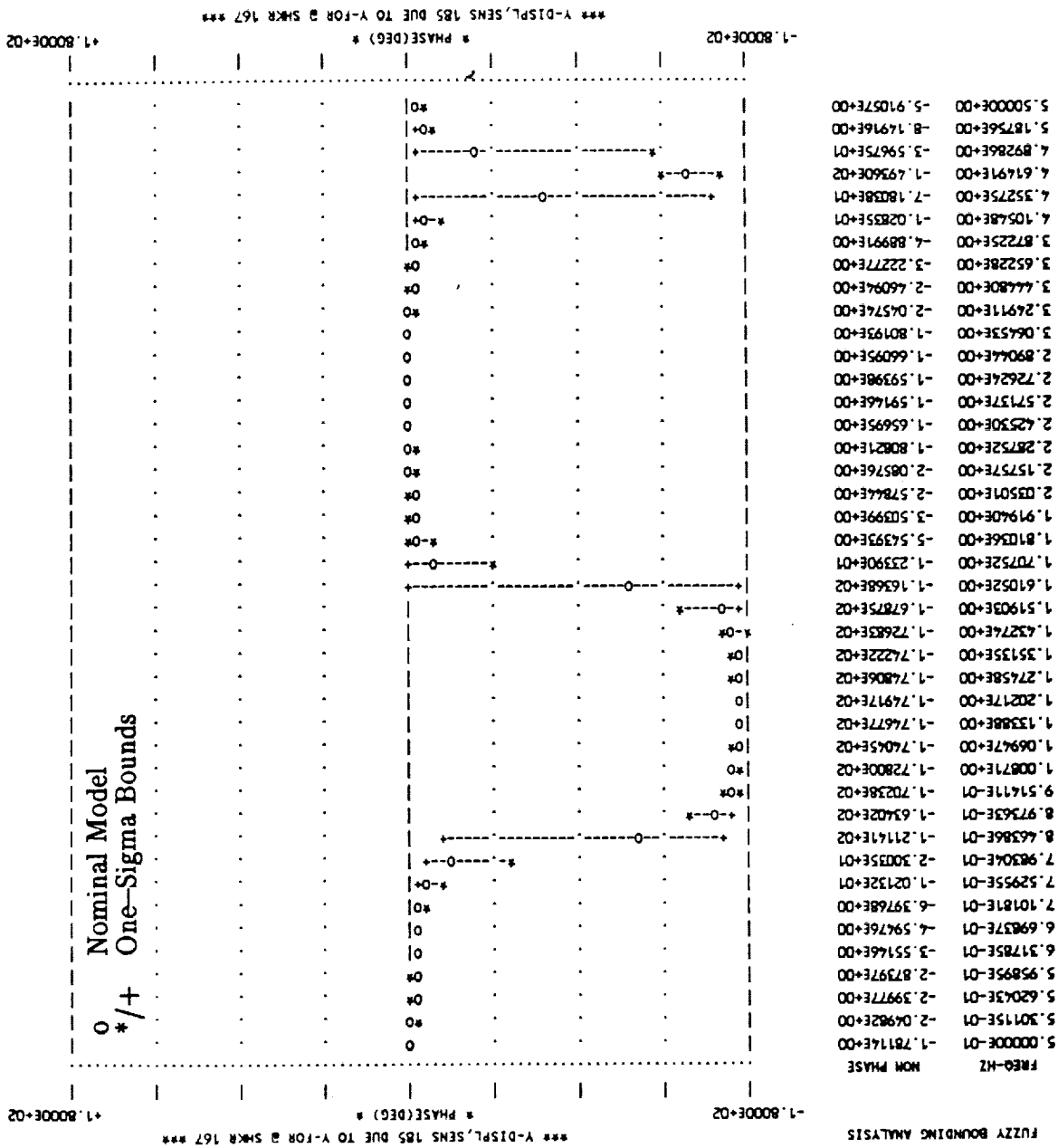

Figure 6–14b. Sensitivity of Interval Prediction on FRF Phase to s–parameter Truncation. Truncation Error Threshold is Twice That of Figure 6–10.

FUZZY BOUNDING ANALYSIS

FREQ-HZ	NOM DISPL/FORCE
5.00000E-01	4.58191E-05
5.30115E-01	4.86246E-05
5.62043E-01	5.23166E-05
5.95895E-01	5.73532E-05
6.31785E-01	6.45713E-05
6.69837E-01	7.56790E-05
7.10181E-01	9.47776E-05
7.52955E-01	1.34695E-04
7.98304E-01	2.62179E-04
8.46386E-01	4.98326E-04
8.97363E-01	1.44785E-04
9.51411E-01	7.28272E-05
1.00871E+00	4.45616E-05
1.06947E+00	2.96277E-05
1.13388E+00	2.04476E-05
1.20217E+00	1.42615E-05
1.27458E+00	9.82720E-06
1.35135E+00	6.50380E-06
1.43274E+00	3.92772E-06
1.51903E+00	1.88209E-06
1.61052E+00	3.60102E-07
1.70752E+00	1.27224E-06
1.81036E+00	2.44946E-06
1.91940E+00	3.48370E-06
2.03501E+00	4.40487E-06
2.15757E+00	5.24367E-06
2.28752E+00	6.02766E-06
2.42530E+00	6.78287E-06
2.57137E+00	7.53604E-06
2.72624E+00	8.31767E-06
2.89044E+00	9.16665E-06
3.06453E+00	1.01386E-05
3.24911E+00	1.13232E-05
3.44480E+00	1.28855E-05
3.65228E+00	1.51847E-05
3.87225E+00	1.92244E-05
4.10548E+00	2.94171E-05
4.35275E+00	8.61649E-05
4.61491E+00	1.15292E-05
4.89286E+00	3.02208E-06
5.18756E+00	8.99192E-06
5.50000E+00	1.56709E-05

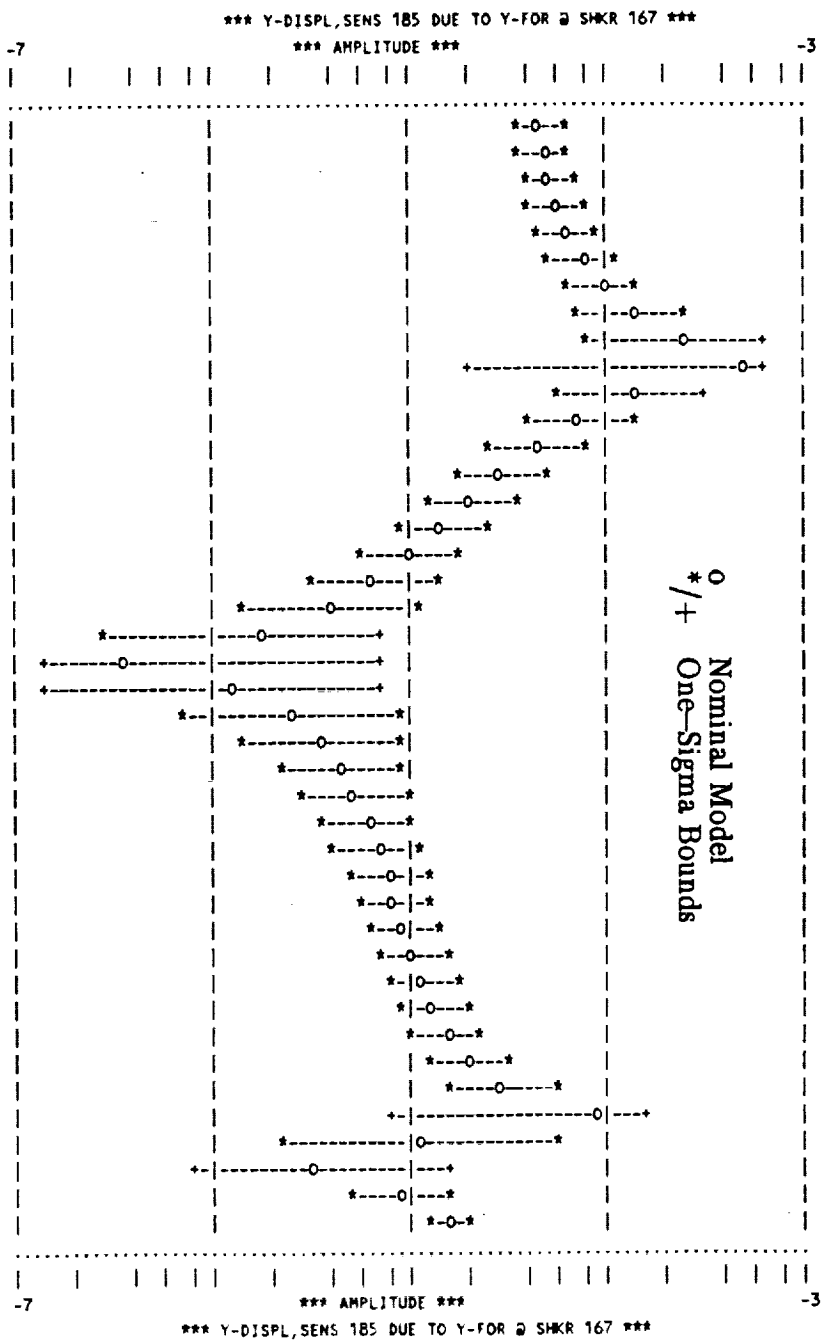

Figure 6—15a. Sensitivity of Interval Prediction on FRF Amplitude to s-parameter Truncation. Truncation Error Threshold is Three Times That of Figure 6—10.

FUZZY BOUNDING ANALYSIS

FREQ-HZ	NOM PHASE
5.00000E-01	-1.78114E+00
5.30115E-01	-2.04982E+00
5.62043E-01	-2.39977E+00
5.95895E-01	-2.87397E+00
6.31785E-01	-3.55146E+00
6.69837E-01	-4.59476E+00
7.10181E-01	-6.39768E+00
7.52955E-01	-1.02132E+01
7.98304E-01	-2.30035E+01
8.46386E-01	-1.21141E+02
8.97363E-01	-1.63402E+02
9.51411E-01	-1.70238E+02
1.00871E+00	-1.72800E+02
1.06947E+00	-1.74045E+02
1.13388E+00	-1.74677E+02
1.20217E+00	-1.74917E+02
1.27458E+00	-1.74806E+02
1.35135E+00	-1.74222E+02
1.43274E+00	-1.72683E+02
1.51903E+00	-1.67875E+02
1.61052E+00	-1.16368E+02
1.70752E+00	-1.23390E+01
1.81036E+00	-5.54393E+00
1.91940E+00	-3.50399E+00
2.03501E+00	-2.57844E+00
2.15757E+00	-2.08576E+00
2.28752E+00	-1.80821E+00
2.42530E+00	-1.65695E+00
2.57137E+00	-1.59146E+00
2.72624E+00	-1.59398E+00
2.89044E+00	-1.66095E+00
3.06453E+00	-1.80193E+00
3.24911E+00	-2.04574E+00
3.44480E+00	-2.46094E+00
3.65228E+00	-3.22277E+00
3.87225E+00	-4.88991E+00
4.10548E+00	-1.02835E+01
4.35275E+00	-7.18038E+01
4.61491E+00	-1.49360E+02
4.89286E+00	-3.59675E+01
5.18756E+00	-8.14916E+00
5.50000E+00	-5.91057E+00

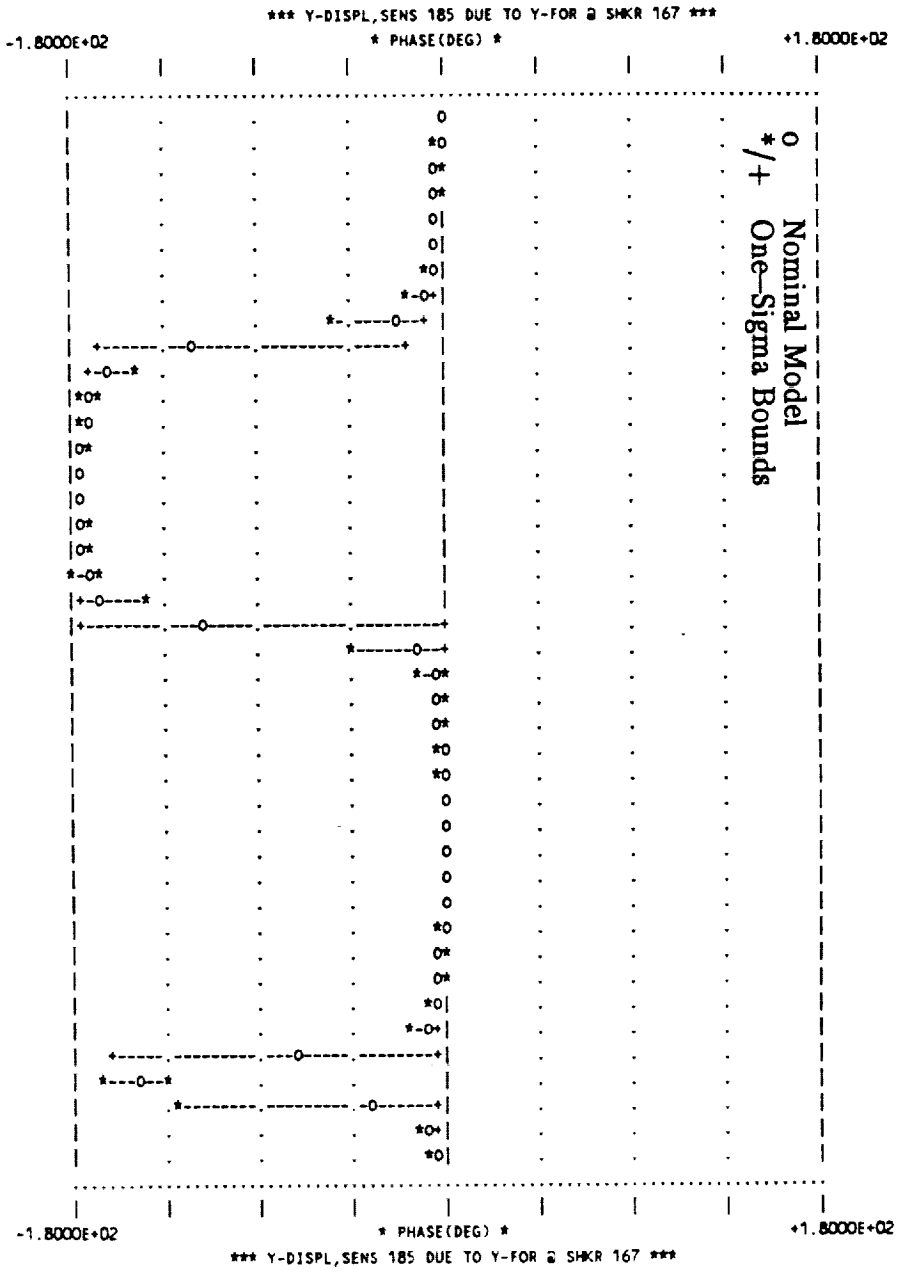

Figure 6–15b. Sensitivity of Interval Prediction on FRF Phase to s–parameter Truncation. Truncation Error Threshold is Three Times That of Figure 6–10.

Table 6–1. Number of S–Parameters Retained Above Error Threshold.

Frequency (Hz)	Error Threshold 5%	10%	15%
0.753	10	7	6
0.798	12	7	6
0.846	11	8	8
0.897	8	7	4
1.519	14*	10	9
1.611	15*	14*	11
1.707	21*	16*	12
4.105	11	8	7
4.353	10	9	7
4.615	16*	12	8
4.893	11	11	8
5.188	14*	11	7

*Note that in cases where more than 12 s–parameters were required to satisfy the given threshold, the number actually used was limited to 12 to conserve run time.

6.3 CSI Evolutionary Structure

The LaRC CSI Evolutionary Structure described in Reference [6–2] is the only one of the three structures selected to demonstrate the PDAC methodology which is not included in the present LSS database. However, it consists of truss beams and a rib antenna, as shown in Figure 6–16, which clearly qualify it as a member of the generic category of large space structures. The suspension system is not soft enough to approximate free–free modes, but this was not a requirement for the initial phase of testing. In fact, the structure has six suspension modes ranging from 0.147 Hz to 0.874 Hz. The first structural mode is 1.474 Hz. The first 43 modes of the structure and its suspension system are listed in Table 6–2.

Reference [6–2] presents preliminary analysis and test data for the CSI Evolutionary Structure, including analysis and test frequencies, analysis mode shapes and measured frequency response functions. Frequency response functions from an analytical model are also presented, however they do not seem to agree precisely with the analytical frequencies and mode shapes. Discussions with LaRC personnel confirm the possibility that in this preliminary report, the analytical models represented by the frequencies and mode shapes, and the FRF plots may be different, one of them representing a later version of the finite element model. This is of no consequence for purposes of the present demonstration, since the models appear to be reasonably close and interval prediction with either model should therefore suffice for comparison with the test data. The analytical model used herein is the one represented by the frequencies and numerical modal displacements contained in Tables 11 and 12 of [6–2].

A representative selection of four frequency response functions was made for interval prediction and comparison with FRF data. The four functions include Y–acceleration response at Coordinates 1, 3, 6 and 8 due to force input at Coordinate 1. See Figure 6–16. The nine modes indicated by asterisks in Table 6–2 were selected to represent the analytical model. These modes were chosen because of their contributions to response at the selected locations. Interval predictions for FRF amplitude and phase were computed over frequencies ranging from 1 to 6 Hz. As before, since FRF derivatives which involve a modal summation are used in these computations, the number of modes included in the model exceed the range of frequencies over which interval predictions are made.

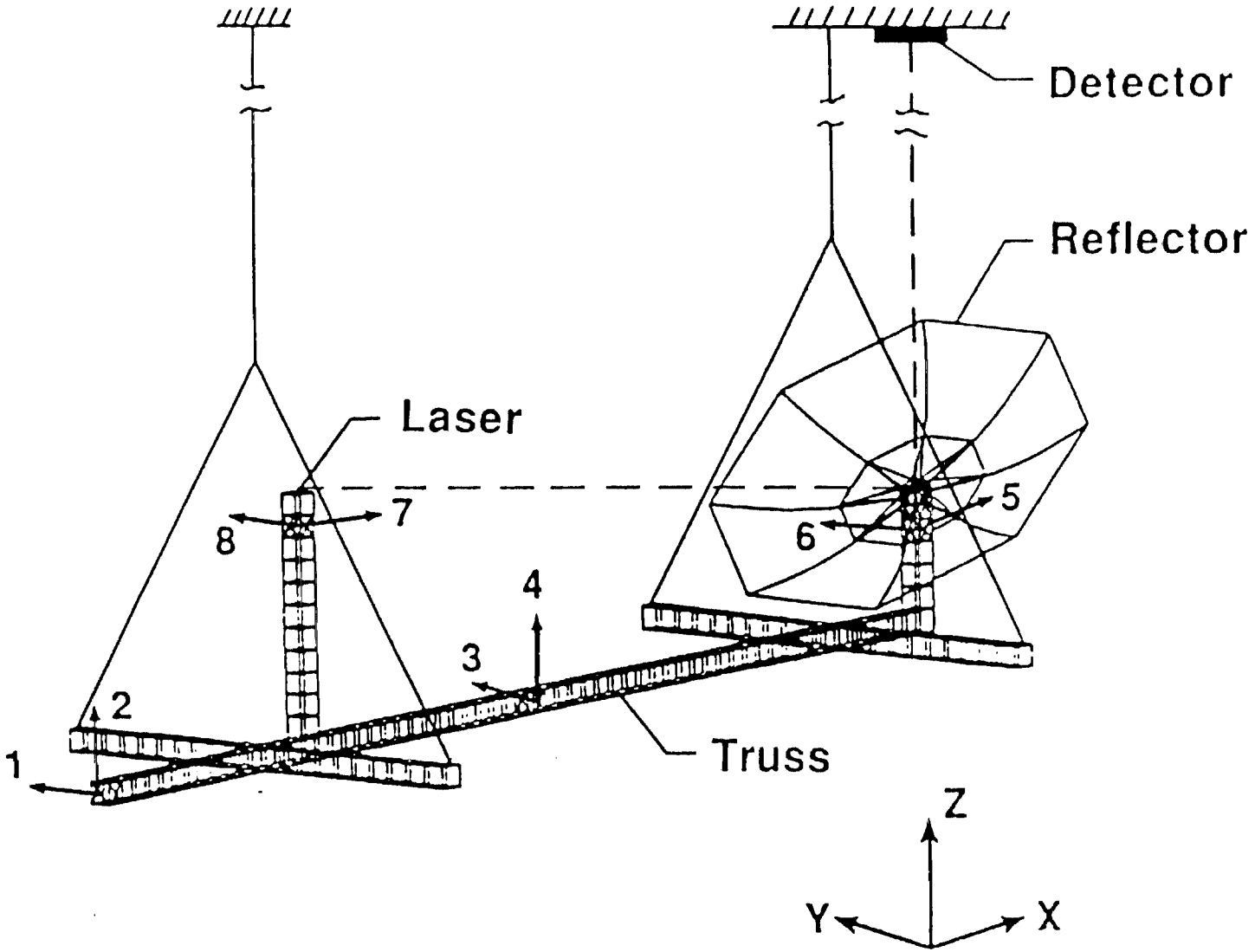

Figure 6–16. Schematic of CSI Evolutionary Structure Showing Collocated Thruster and Accelerometer Locations (Note: Diagonal Bracing in Bays not Shown).

Table 6-2. Modal Frequencies and Damping for CSI Evolutionary Structure

PDAC Mode	Mode No.	Test Frequency	Test Damping	Analysis Frequency	Analysis Damping	PDAC Mode Description
	1	0.145		0.147	5.7	
	2	0.149		0.149	7.5	
1	3*	0.148		0.155	7.5	Suspension
	4	0.718	1.5	0.730	0.7	
	5	0.740	1.2	0.748	0.7	
	6	0.900	0.6	0.874	0.2	
2	7*	1.500	0.4	1.474	0.2	1st Twist/1st Bending
	8	1.710	0.7	1.738	0.3	
3	9*	1.900	0.5	1.883	0.3	1st Bending/1st Twist
	10			2.301	0.1	
	11			2.535	0.1	
	12	2.570	2.1	2.839	0.1	
	13			3.419	0.1	
	14			3.486	0.1	
	15			3.587	0.1	
4	16*	4.040	0.4	4.015	0.1	2nd Bending
5	17*	4.300	0.9	4.032	0.1	2nd Bending
	18			4.206	0.1	
6	19			4.392	0.1	1st Vertical
	20			5.029	0.1	
	21			5.034	0.1	
7	22*	5.330	0.7	5.501	0.1	Refl Twist/Truss Bend
		5.920	1.1			
	23	6.140	0.3	6.180	0.1	
	24			6.231	0.1	
	25	6.650	0.3	6.471	0.1	
	26			6.670	0.1	
		6.790	0.2			
	27	7.240	0.6	7.372	0.1	
8	28*	8.260	0.3	8.293	0.1	3rd Bending
	29	9.110	0.2	8.409	0.1	
	30			8.456	0.1	
	31			8.824	0.1	
	32			8.926	0.1	
9	33*			8.966	0.1	Truss End LOC Bend
	34			9.235	0.1	
	35			9.527	0.1	
	36			9.901	0.1	
	37			12.486	0.1	
	38			13.615	0.1	
	39			14.315	0.1	
	40			14.718	0.1	
	41			15.886	0.1	
	42			16.853	0.1	
	43			16.993	0.1	

METHODS FOR EVALUATING THE PREDICTIVE ACCURACY OF STRUCTURAL DYNAMIC MODELS

PART 3

Figures 6–17 through 6–20 show measured FRF amplitude and phase plots at the four locations previously identified. The dashed lines represent an analytical model, but as discussed above, it is apparently different from the one used here.

Figures 6–21 through 6–24 show the analytical FRF amplitude and phase intervals computed by PDAC as well as the nominal response. Measured FRF amplitude from Figures 6–17 through 6–20 have been replotted in Figures 6–21 through 6–24 for purposes of direct comparison. These comparisons again show quite good agreement, with measured response falling within the $\pm$ 1σ intervals for the most part. The most obvious difference between predicted and measured response occurs near the frequency of 2.7 Hz where the test FRF's exhibit a mode not present in the analytical model. This mode shows up at Coordinates 3 and 6 and very weakly at Coordinate 1 (Figure 6–17). At Location 8 the amplitude is apparently too low to be accurately measured. The rest of the frequency range between 1 and 6 Hz appears to match the data reasonably well.

Phase was not plotted again because the resolution of the plots was inadequate. Nevertheless, there are some notable differences, for example at Coordinate 3 near 1.6 Hz where measured phase jumps from -180° to $+ 180^{\circ}$, while the predicted phase interval remains below 0°. This type of situation suggests the possibility that an analytical mode is missing. From approximately 2.0 to 2.7 Hz and from 2.9 to 4.0 Hz the measured phase is 180° while the predicted phase is -180°. In a sense, the two are equivalent because of the wrap–around feature of the plots. The omission of weakly participative analytical modes could conceivably cause this type of difference. On the other hand, the fact that measured FRF amplitude is small in this range lowers the accuracy of phase measurements.

Since analytical response computations, point predictions (nominal response) as well as interval predictions, both involve modal summations, a sensitivity study was made to investigate the effect of modal truncation on predicted response. Response at Coordinate 1 due to force at the same coordinate was selected for this purpose. Both FRF amplitude and phase response were computed over the frequency range of 1.0 to 2.5 Hz, including the first three modes, for solution based on 9, 7, 5 and 3 modes. The results are shown in Figures 6–25 through 6–28, respectively. These figures show that both the nominal and interval response predictions are nearly the same in all four cases, indicating low sensitivity to modal truncation.

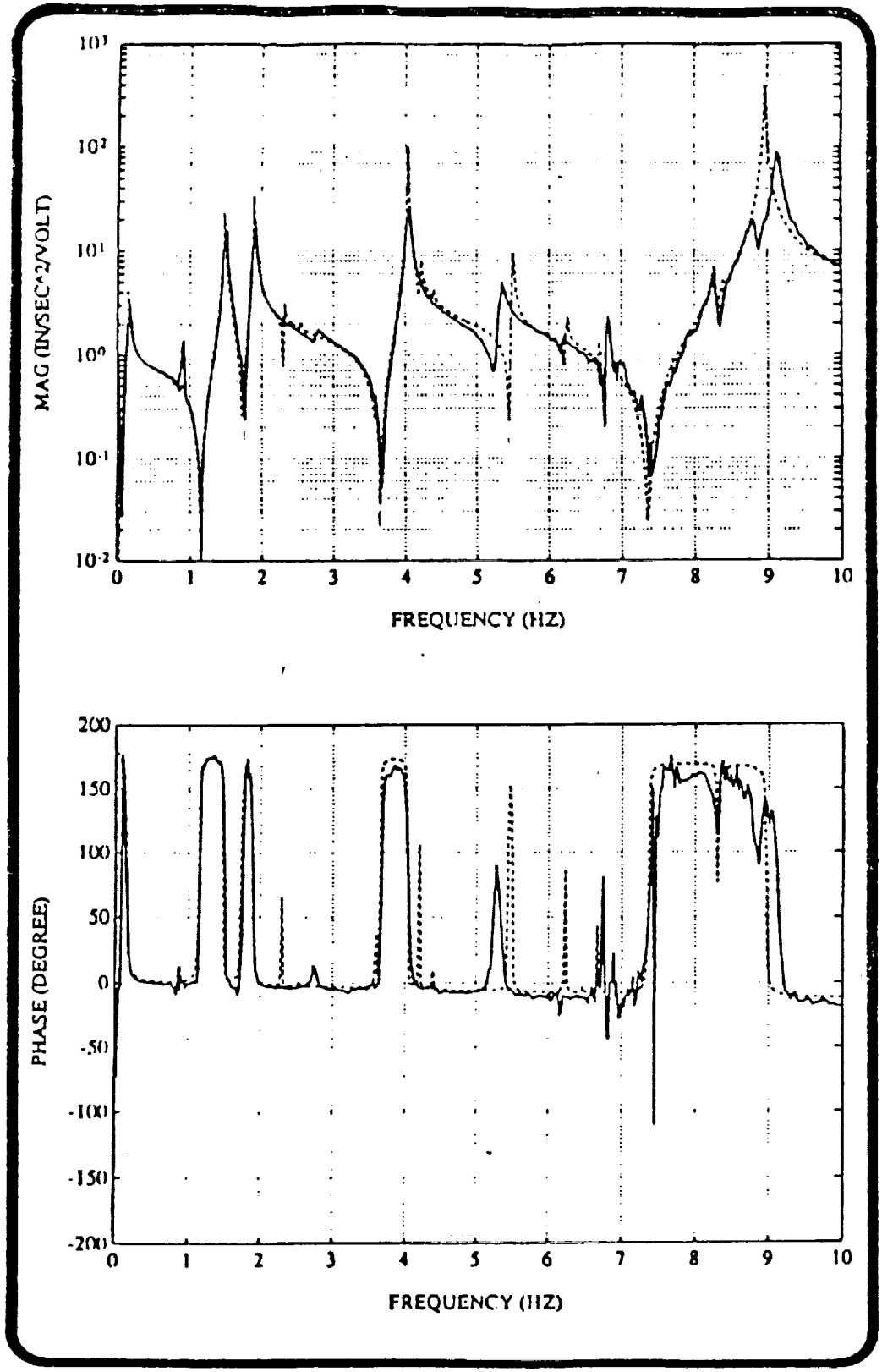

Figure 6–17. CSI FRF Comparison (Response at Thruster 1/Force at Thruster 1).

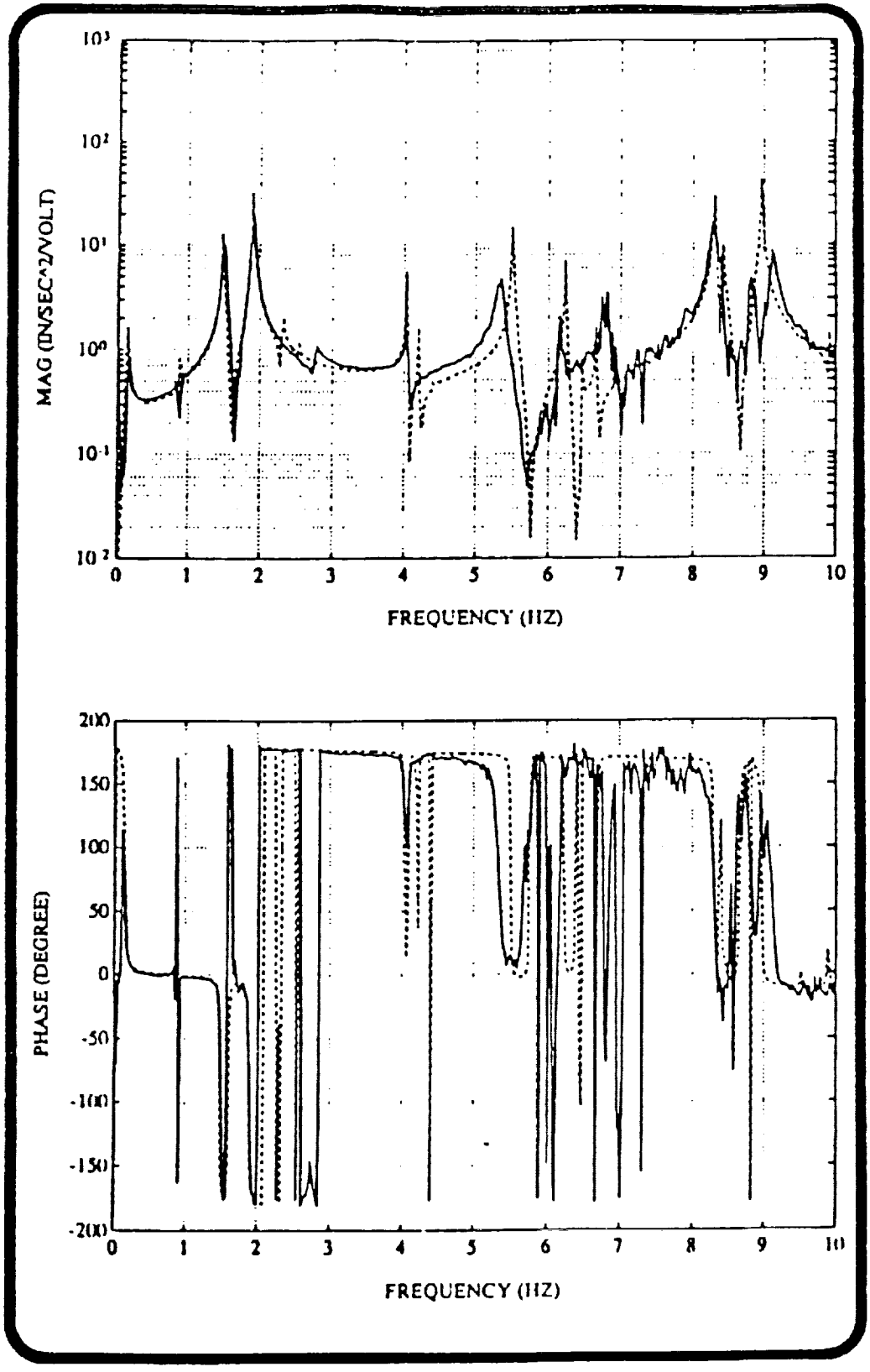

Figure 6–18. CSI FRF Comparison (Response at Thruster 3/Force at Thruster 1).

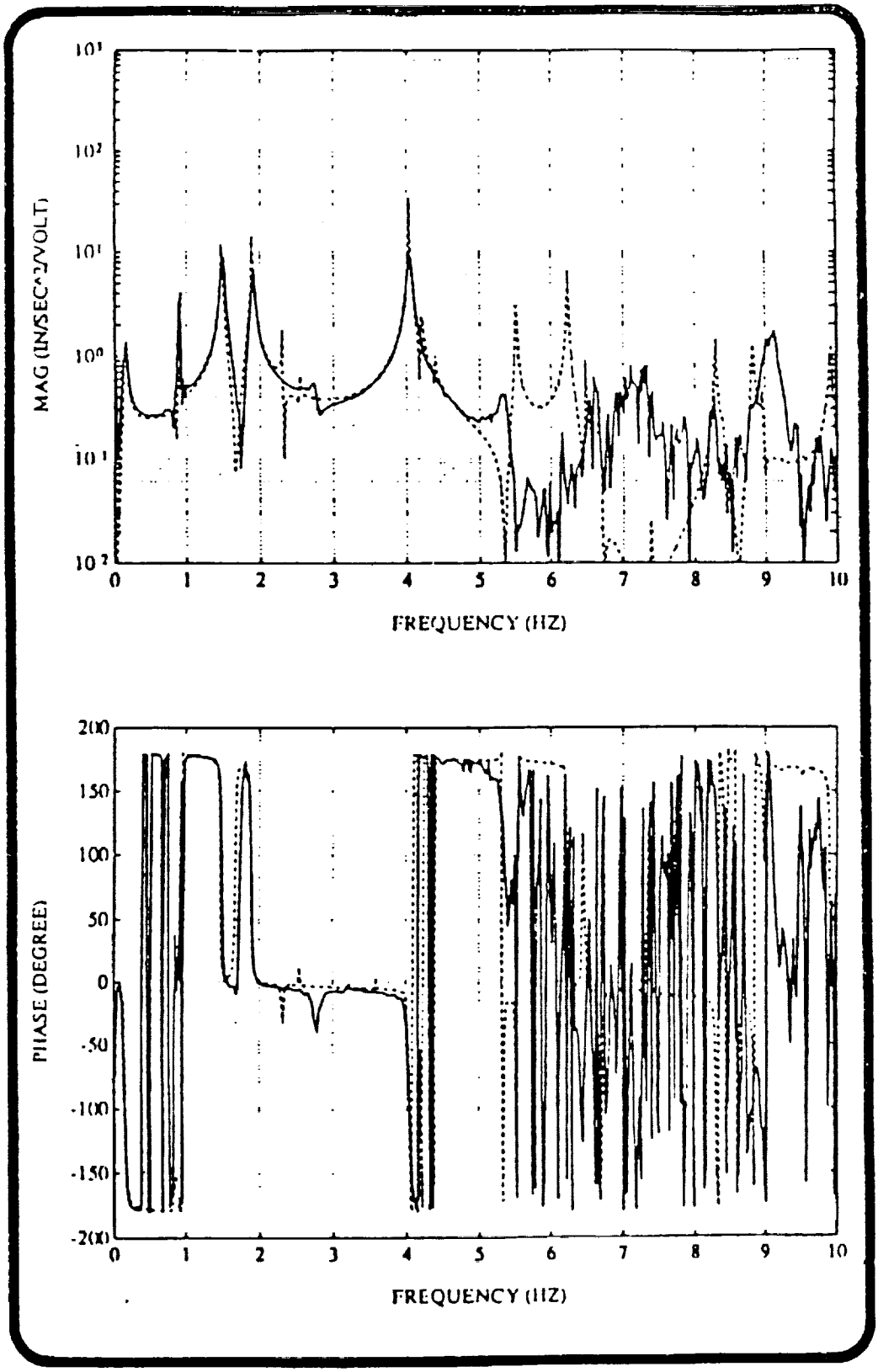

Figure 6–19. CSI FRF Comparison (Response at Thruster 6/Force at Thruster 1).

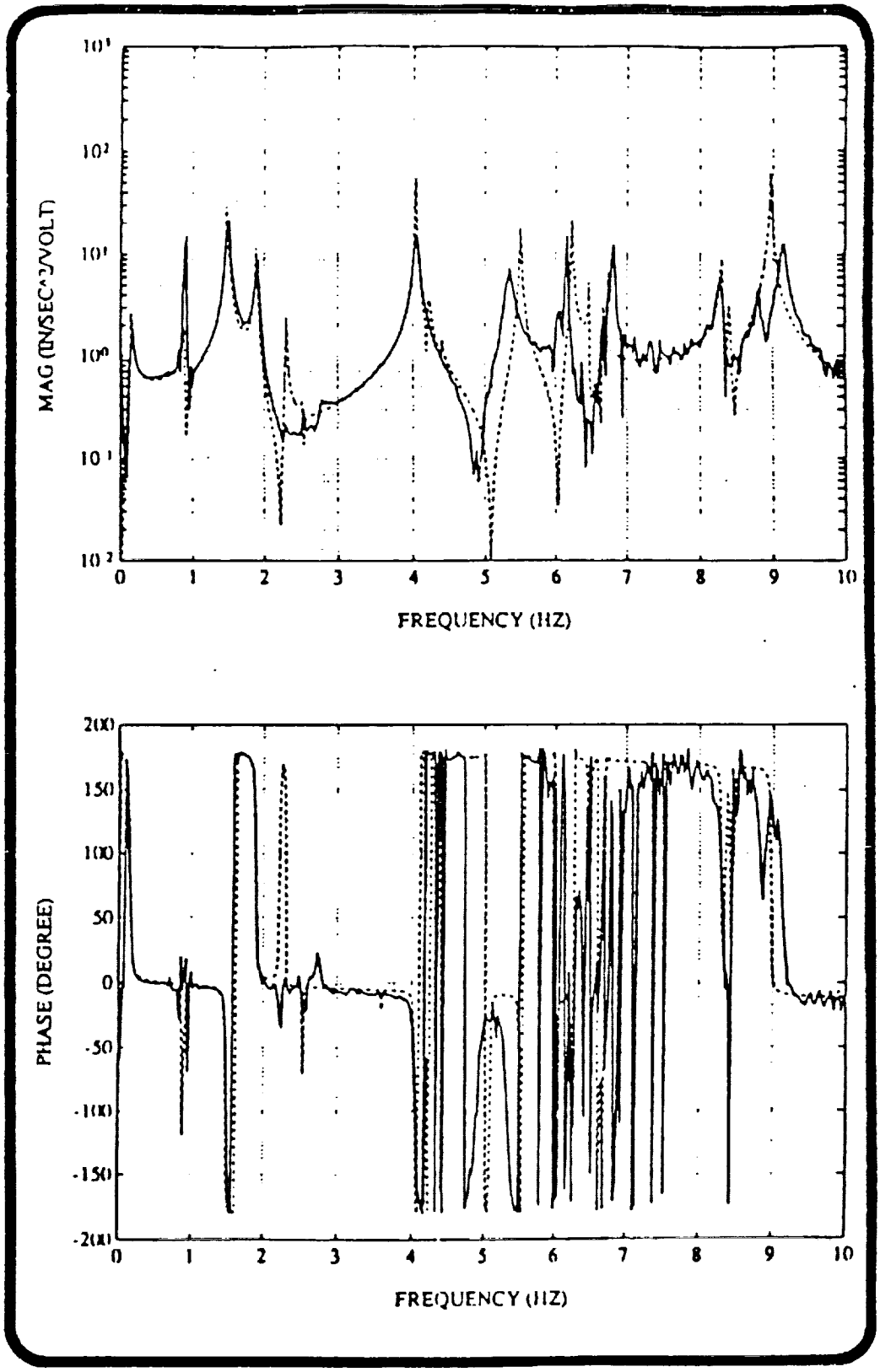

Figure 6–20. CSI FRF Comparison (Response at Thruster 8/Force at Thruster 1).

FUZZY BOUNDING ANALYSIS

FREQ-HZ	NOM ACCEL/FORCE
1.00000E+00	5.79282E-02
1.03649E+00	1.46373E-02
1.07430E+00	7.65442E-02
1.11350E+00	1.63857E-01
1.15412E+00	2.74495E-01
1.19623E+00	4.18945E-01
1.23988E+00	6.16554E-01
1.28511E+00	9.06308E-01
1.33200E+00	1.38094E+00
1.38060E+00	2.33258E+00
1.43097E+00	5.44740E+00
1.48318E+00	2.53237E+01
1.53729E+00	3.80099E+00
1.59338E+00	1.80768E+00
1.65151E+00	8.47754E-01
1.71177E+00	7.81357E-02
1.77422E+00	1.35597E+00
1.83896E+00	5.97190E+00
1.90605E+00	1.54749E+01
1.97559E+00	4.96097E+00
2.04767E+00	3.31814E+00
2.12238E+00	2.62525E+00
2.19982E+00	2.23037E+00
2.28008E+00	1.96767E+00
2.36327E+00	1.77484E+00
2.44949E+00	1.62282E+00
2.53886E+00	1.49586E+00
2.63149E+00	1.38432E+00
2.72750E+00	1.28158E+00
2.82701E+00	1.18246E+00
2.93016E+00	1.08222E+00
3.03706E+00	9.75754E-01
3.14787E+00	8.56505E-01
3.26272E+00	7.14786E-01
3.38176E+00	5.34158E-01
3.50514E+00	2.82587E-01
3.63303E+00	1.17017E-01
3.76558E+00	8.89674E-01
3.90297E+00	3.26468E+00
4.04537E+00	5.30700E+01
4.19296E+00	4.93861E+00
4.34594E+00	2.95164E+00
4.50450E+00	2.44315E+00
4.66885E+00	2.02107E+00
4.83919E+00	1.73722E+00
5.01575E+00	1.49402E+00
5.19875E+00	1.21241E+00
5.38843E+00	5.04928E-01
5.58503E+00	2.51848E+00
5.78880E+00	1.52266E+00
6.00000E+00	1.23639E+00

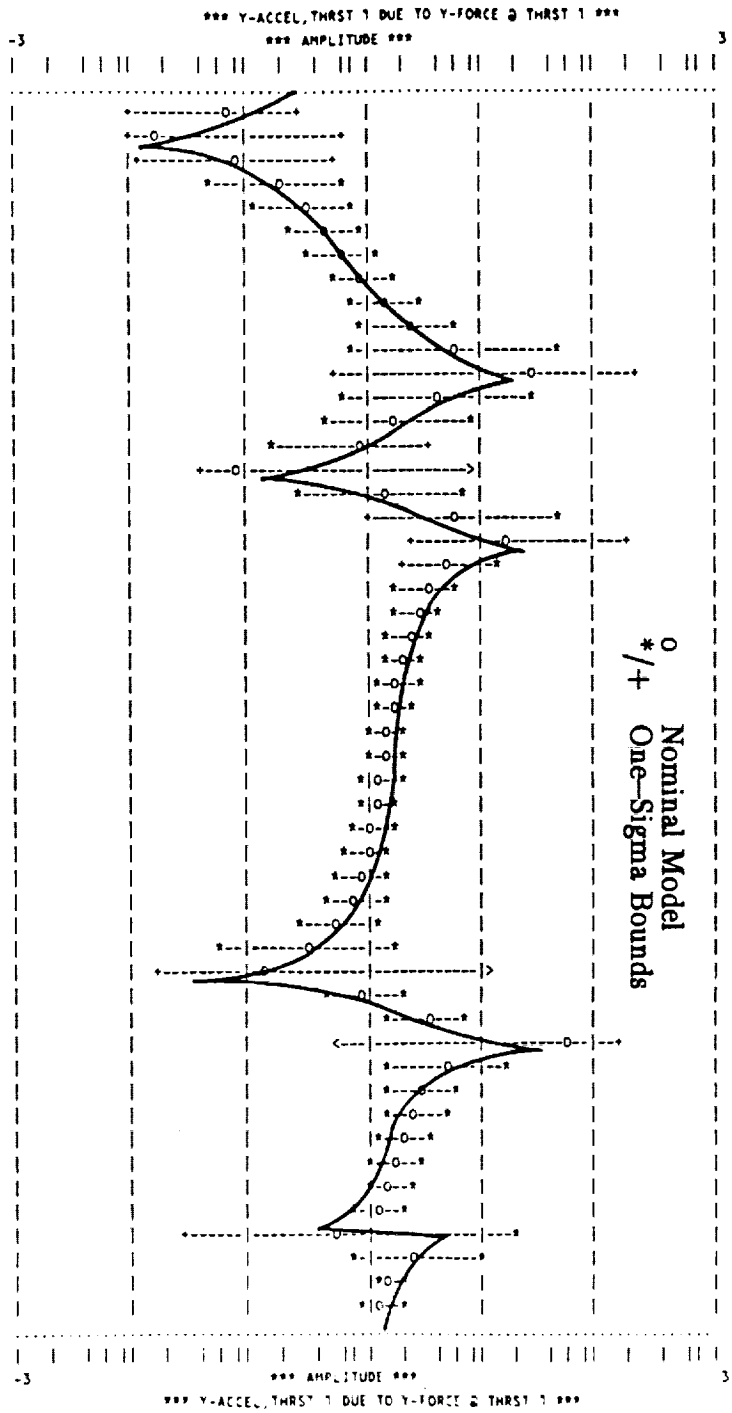

Figure 6–21a. Predictive Accuracy of CSI Evolutionary Structure Model.
FRF Amplitude, Coordinate 1 Acceleration/ Coordinate 1 Force.

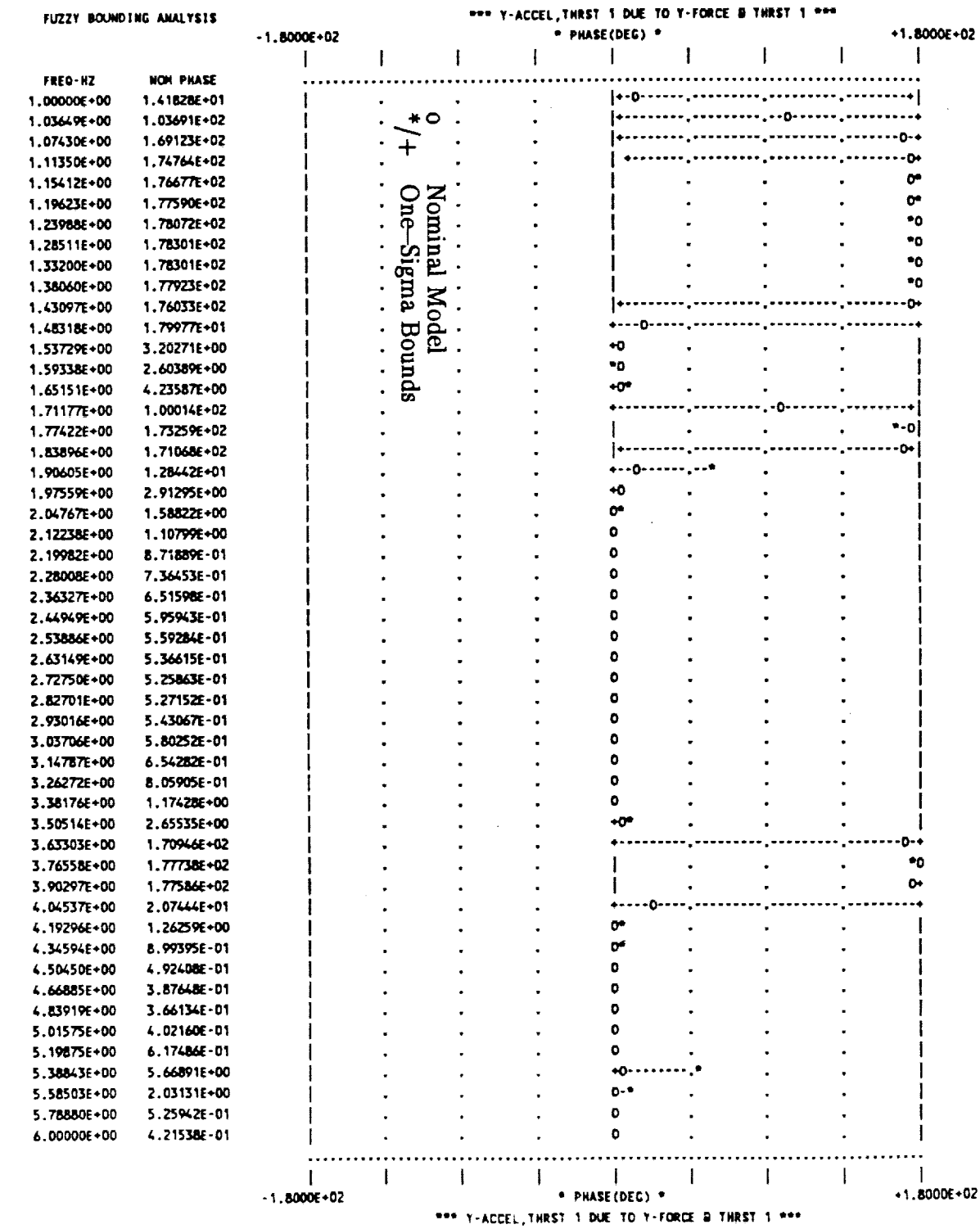

Figure 6–21b. Predictive Accuracy of CSI Evolutionary Structure Mode.
FRF Phase, Coordinate 1 Acceleration/ Coordinate 1 Force.

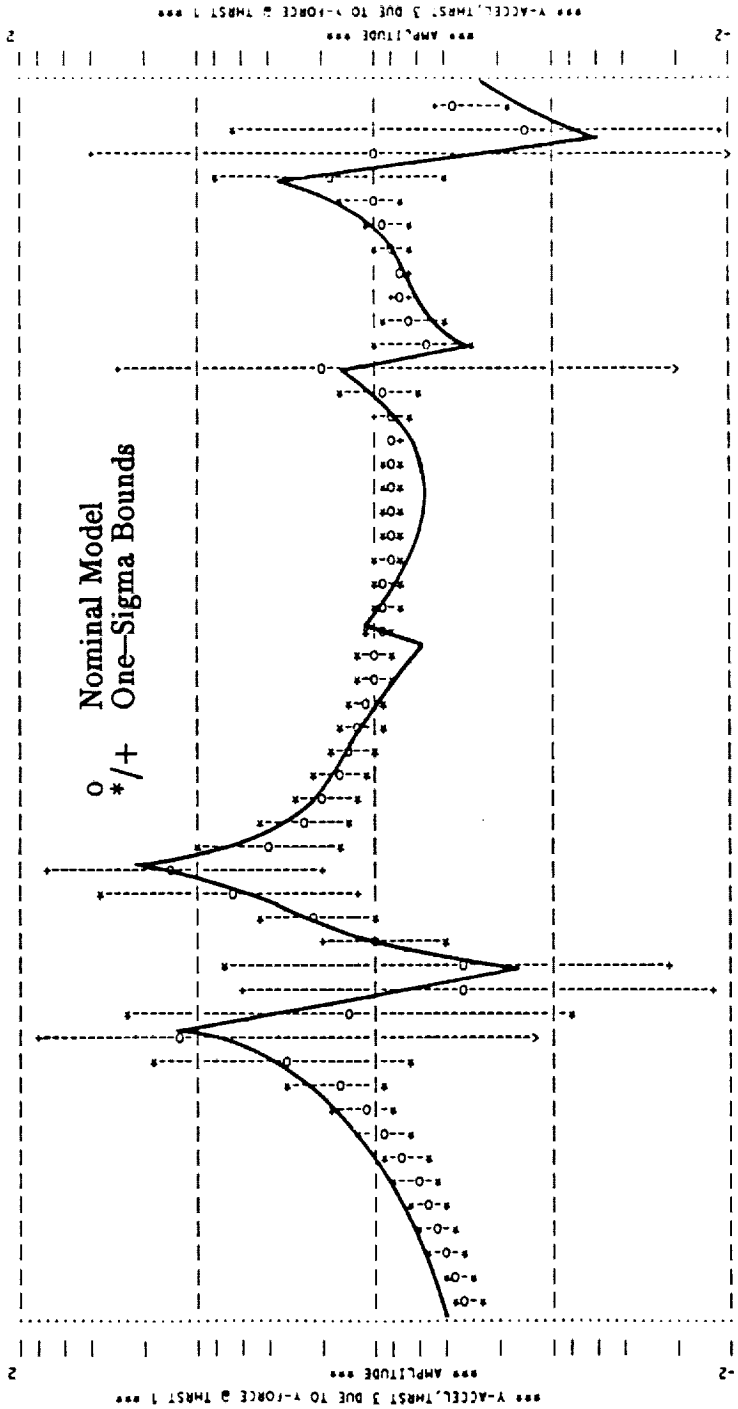

FUZZY BOUNDING ANALYSIS

FREQ-HZ	NOM ACCEL/FORCE
1.000000E+00	3.044876E-01
1.034696E+00	3.399796E-01
1.074308E+00	3.826236E-01
1.113506E+00	4.348066E-01
1.154126E+00	5.001946E-01
1.196236E+00	5.847726E-01
1.239888E+00	6.991206E-01
1.285116E+00	8.642456E-01
1.332006E+00	1.129536E+00
1.380606E+00	1.690886E+00
1.430976E+00	3.307036E+00
1.483186E+00	1.279006E+01
1.537296E+00	1.445796E+00
1.593388E+00	3.268406E-01
1.651516E+00	3.026706E-01
1.711776E+00	9.671106E-01
1.774226E+00	2.749236E+00
1.838966E+00	6.510796E+00
1.906056E+00	1.418636E+01
1.975596E+00	4.102706E+00
2.047676E+00	2.563226E+00
2.122386E+00	1.934436E+00
2.199826E+00	1.590506E+00
2.280086E+00	1.373126E+00
2.363276E+00	1.223446E+00
2.449496E+00	1.114496E+00
2.538866E+00	1.032116E+00
2.631496E+00	9.682066E-01
2.727506E+00	9.177776E-01
2.827016E+00	8.776276E-01
2.930166E+00	8.456486E-01
3.037066E+00	8.204636E-01
3.147876E+00	8.012336E-01
3.262726E+00	7.876106E-01
3.381766E+00	7.798236E-01
3.505146E+00	7.790796E-01
3.633036E+00	7.889056E-01
3.765586E+00	8.207806E-01
3.902976E+00	9.366156E-01
4.045376E+00	1.099536E+00
4.192966E+00	5.217556E-01
4.345946E+00	6.193036E-01
4.504506E+00	6.800066E-01
4.668856E+00	7.218476E-01
4.839196E+00	7.757496E-01
5.015756E+00	8.619476E-01
5.198756E+00	1.045496E+00
5.388436E+00	1.830916E+00
5.585036E+00	1.046346E+00
5.788806E+00	1.425526E-01
6.000006E+00	3.642236E-01

Figure 6–22a. Predictive Accuracy of CSI Evolutionary Structure Model, FRF Amplitude, Coordinate 3 Acceleration/Coordinate 1 Force.

FUZZY BOUNDING ANALYSIS

FREQ-HZ	NOM PHASE
1.00000E+00	-1.23763E-01
1.03649E+00	-1.66991E-01
1.07430E+00	-2.13477E-01
1.11350E+00	-2.65303E-01
1.15412E+00	-3.25728E-01
1.19623E+00	-4.00268E-01
1.23988E+00	-4.99226E-01
1.28511E+00	-6.44406E-01
1.33200E+00	-8.90894E-01
1.38060E+00	-1.42368E+00
1.43097E+00	-3.37652E+00
1.48318E+00	-1.61326E+02
1.53729E+00	-1.75587E+02
1.59338E+00	-1.71967E+02
1.65151E+00	-7.67390E+00
1.71177E+00	-3.52600E+00
1.77422E+00	-3.76843E+00
1.83896E+00	-7.78323E+00
1.90605E+00	-1.66547E+02
1.97559E+00	-1.76728E+02
2.04767E+00	-1.78196E+02
2.12238E+00	-1.78770E+02
2.19982E+00	-1.79074E+02
2.28008E+00	-1.79261E+02
2.36327E+00	-1.79388E+02
2.44949E+00	-1.79480E+02
2.53886E+00	-1.79550E+02
2.63149E+00	-1.79605E+02
2.72750E+00	-1.79651E+02
2.82701E+00	-1.79688E+02
2.93016E+00	-1.79721E+02
3.03706E+00	-1.79750E+02
3.14787E+00	-1.79776E+02
3.26272E+00	-1.79801E+02
3.38176E+00	-1.79826E+02
3.50514E+00	-1.79854E+02
3.63303E+00	-1.79894E+02
3.76558E+00	-1.79973E+02
3.90297E+00	1.79695E+02
4.04537E+00	2.85898E+01
4.19296E+00	1.79571E+02
4.34594E+00	-1.79969E+02
4.50450E+00	-1.79981E+02
4.66885E+00	-1.79999E+02
4.83919E+00	1.79962E+02
5.01575E+00	1.79874E+02
5.19875E+00	1.79631E+02
5.38843E+00	1.78211E+02
5.58503E+00	6.07690E+00
5.78880E+00	1.76058E+02
6.00000E+00	1.79480E+02

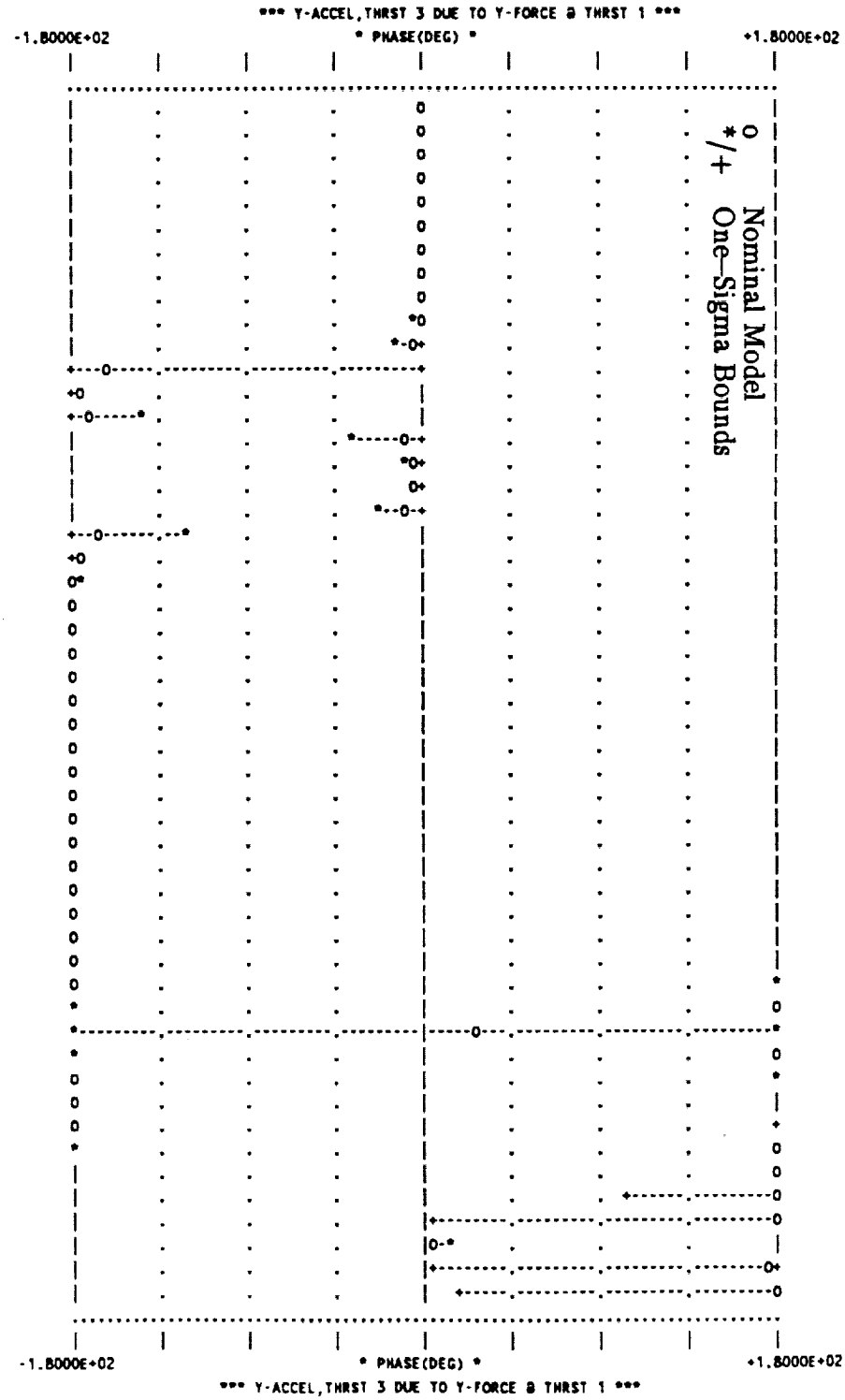

Figure 6–22b. Predictive Accuracy of CSI Evolutionary Structure Model, FRF Phase, Coordinate 3 Acceleration/Coordinate 1 Force.

FUZZY BOUNDING ANALYSIS

FREQ-HZ	NOM ACCEL/FORCE
1.00000E+00	5.89991E-01
1.03649E+00	6.14678E-01
1.07430E+00	6.44933E-01
1.11350E+00	6.82729E-01
1.15412E+00	7.31143E-01
1.19623E+00	7.95284E-01
1.23988E+00	8.84347E-01
1.28511E+00	1.01687E+00
1.33200E+00	1.23703E+00
1.38060E+00	1.68425E+00
1.43097E+00	3.16386E+00
1.48318E+00	1.15880E+01
1.53729E+00	1.28253E+00
1.59338E+00	3.46396E-01
1.65151E+00	9.16937E-02
1.71177E+00	4.62145E-01
1.77422E+00	1.02168E+00
1.83896E+00	2.92880E+00
1.90605E+00	5.94354E+00
1.97559E+00	1.58988E+00
2.04767E+00	9.15798E-01
2.12238E+00	6.36552E-01
2.19982E+00	4.82365E-01
2.28008E+00	3.84725E-01
2.36327E+00	3.18059E-01
2.44949E+00	2.70635E-01
2.53886E+00	2.36352E-01
2.63149E+00	2.11805E-01
2.72750E+00	1.95063E-01
2.82701E+00	1.85120E-01
2.93016E+00	1.81669E-01
3.03706E+00	1.85070E-01
3.14787E+00	1.96521E-01
3.26272E+00	2.18523E-01
3.38176E+00	2.56034E-01
3.50514E+00	3.19442E-01
3.63303E+00	4.33711E-01
3.76558E+00	6.76147E-01
3.90297E+00	1.46075E+00
4.04537E+00	1.76499E+01
4.19296E+00	1.34828E+00
4.34594E+00	6.85664E-01
4.50450E+00	5.47616E-01
4.66885E+00	4.21482E-01
4.83919E+00	3.45478E-01
5.01575E+00	2.85937E-01
5.19875E+00	2.18414E-01
5.38843E+00	3.16674E-02
5.58503E+00	6.41201E-01
5.78880E+00	3.73806E-01
6.00000E+00	3.19214E-01

Figure 6–23a. Predictive Accuracy of CSI Evolutionary Structure Model, FRF Amplitude, Coordinate 6 Acceleration/Coordinate 1 Force.

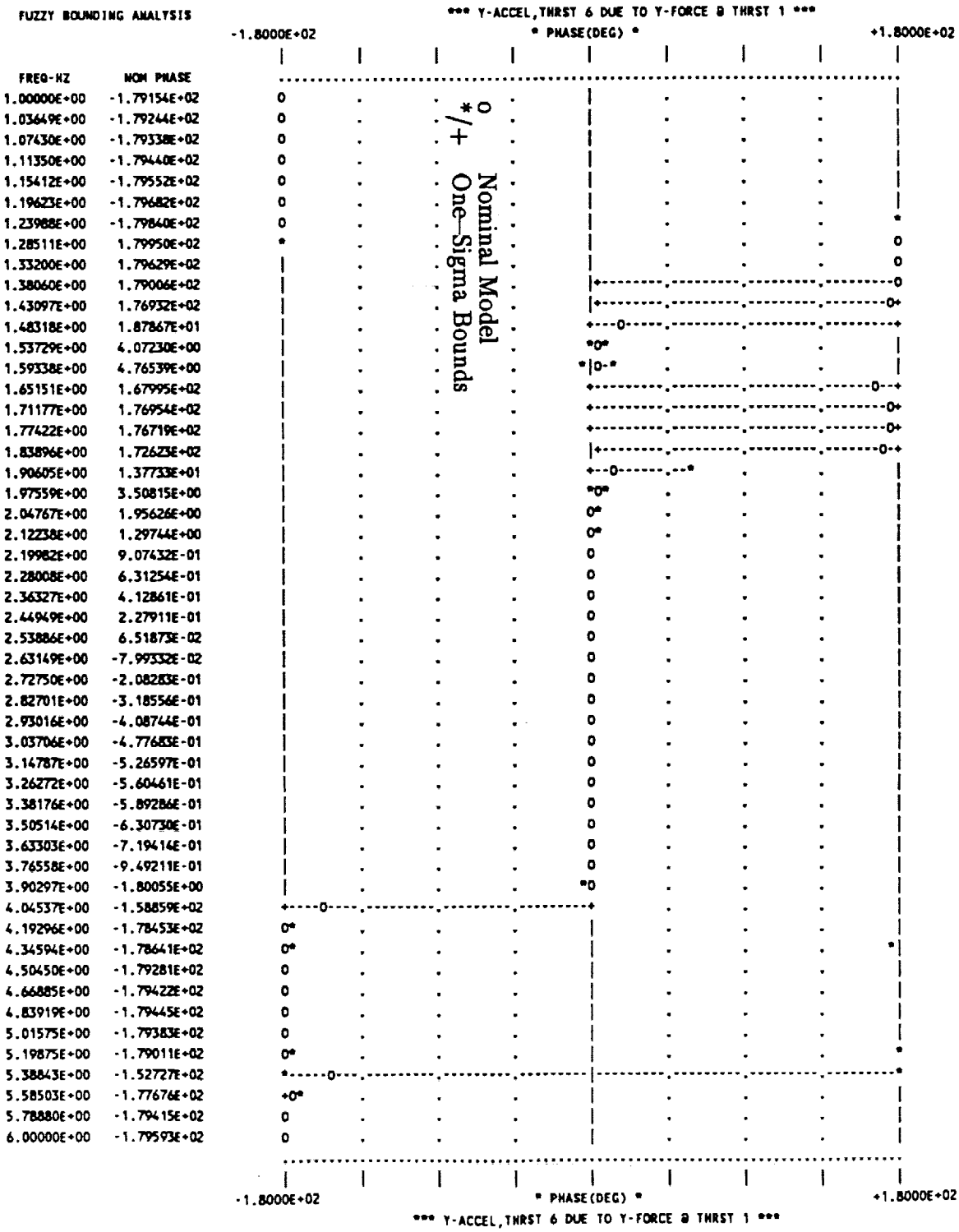

Figure 6–23b. Predictive Accuracy of CSI Evolutionary Structure Model, FRF Phase, Coordinate 6 Acceleration/Coordinate 1 Force.

FUZZY BOUNDING ANALYSIS

FREQ-HZ	NOM ACCEL/FORCE
1.00000E+00	5.80871E-01
1.03649E+00	6.27250E-01
1.07430E+00	6.85087E-01
1.11350E+00	7.58868E-01
1.15412E+00	8.55748E-01
1.19623E+00	9.87859E-01
1.23988E+00	1.17750E+00
1.28511E+00	1.47050E+00
1.33200E+00	1.97789E+00
1.38060E+00	3.05469E+00
1.43097E+00	6.76916E+00
1.48318E+00	3.12485E+01
1.53729E+00	4.97359E+00
1.59338E+00	2.81662E+00
1.65151E+00	2.09061E+00
1.71177E+00	1.83002E+00
1.77422E+00	1.93668E+00
1.83896E+00	3.23334E+00
1.90605E+00	4.08148E+00
1.97559E+00	6.86691E-01
2.04767E+00	2.42288E-01
2.12238E+00	9.69314E-02
2.19982E+00	3.85005E-02
2.28008E+00	1.54458E-02
2.36327E+00	9.37725E-03
2.44949E+00	1.25380E-02
2.53886E+00	2.21440E-02
2.63149E+00	3.66005E-02
2.72750E+00	5.53014E-02
2.82701E+00	7.84153E-02
2.93016E+00	1.06763E-01
3.03706E+00	1.41926E-01
3.14787E+00	1.86616E-01
3.26272E+00	2.45508E-01
3.38176E+00	3.27155E-01
3.50514E+00	4.48843E-01
3.63303E+00	6.51467E-01
3.76558E+00	1.06085E+00
3.90297E+00	2.34939E+00
4.04537E+00	2.86196E+01
4.19296E+00	2.18380E+00
4.34594E+00	1.10619E+00
4.50450E+00	8.30043E-01
4.66885E+00	6.04982E-01
4.83919E+00	4.45038E-01
5.01575E+00	2.83147E-01
5.19875E+00	2.59474E-02
5.38843E+00	9.64259E-01
5.58503E+00	2.58901E+00
5.78880E+00	1.13371E+00
6.00000E+00	8.78490E-01

Figure 6–24a. Predictive Accuracy of CSI Evolutionary Structure Model, FRF Amplitude, Coordinate 8 Acceleration/Coordinate 1 Force.

6-45

FUZZY BOUNDING ANALYSIS

FREQ-HZ	NOM PHASE
1.00000E+00	4.82450E-01
1.03649E+00	3.84681E-01
1.07430E+00	2.81679E-01
1.11350E+00	1.70642E-01
1.15412E+00	4.71936E-02
1.19623E+00	-9.59618E-02
1.23988E+00	-2.72023E-01
1.28511E+00	-5.07726E-01
1.33200E+00	-8.67055E-01
1.38060E+00	-1.55243E+00
1.43097E+00	-3.73611E+00
1.48318E+00	-1.62097E+02
1.53729E+00	-1.77331E+02
1.59338E+00	-1.78718E+02
1.65151E+00	-1.79387E+02
1.71177E+00	1.79992E+02
1.77422E+00	1.78928E+02
1.83896E+00	1.74742E+02
1.90605E+00	1.61346E+01
1.97559E+00	6.43676E+00
2.04767E+00	5.95753E+00
2.12238E+00	7.37600E+00
2.19982E+00	1.13555E+01
2.28008E+00	1.98763E+01
2.36327E+00	2.50147E+01
2.44949E+00	1.46674E+01
2.53886E+00	6.85306E+00
2.63149E+00	3.52546E+00
2.72750E+00	2.00509E+00
2.82701E+00	1.20861E+00
2.93016E+00	7.38563E-01
3.03706E+00	4.31714E-01
3.14787E+00	2.11972E-01
3.26272E+00	3.87462E-02
3.38176E+00	-1.14202E-01
3.50514E+00	-2.70668E-01
3.63303E+00	-4.66439E-01
3.76558E+00	-7.94591E-01
3.90297E+00	-1.73472E+00
4.04537E+00	-1.58877E+02
4.19296E+00	-1.78534E+02
4.34594E+00	-1.78899E+02
4.50450E+00	-1.79449E+02
4.66885E+00	-1.79587E+02
4.83919E+00	-1.79551E+02
5.01575E+00	-1.79125E+02
5.19875E+00	-1.57990E+02
5.38843E+00	-4.26137E+00
5.58503E+00	-1.76954E+02
5.78880E+00	-1.79376E+02
6.00000E+00	-1.79737E+02

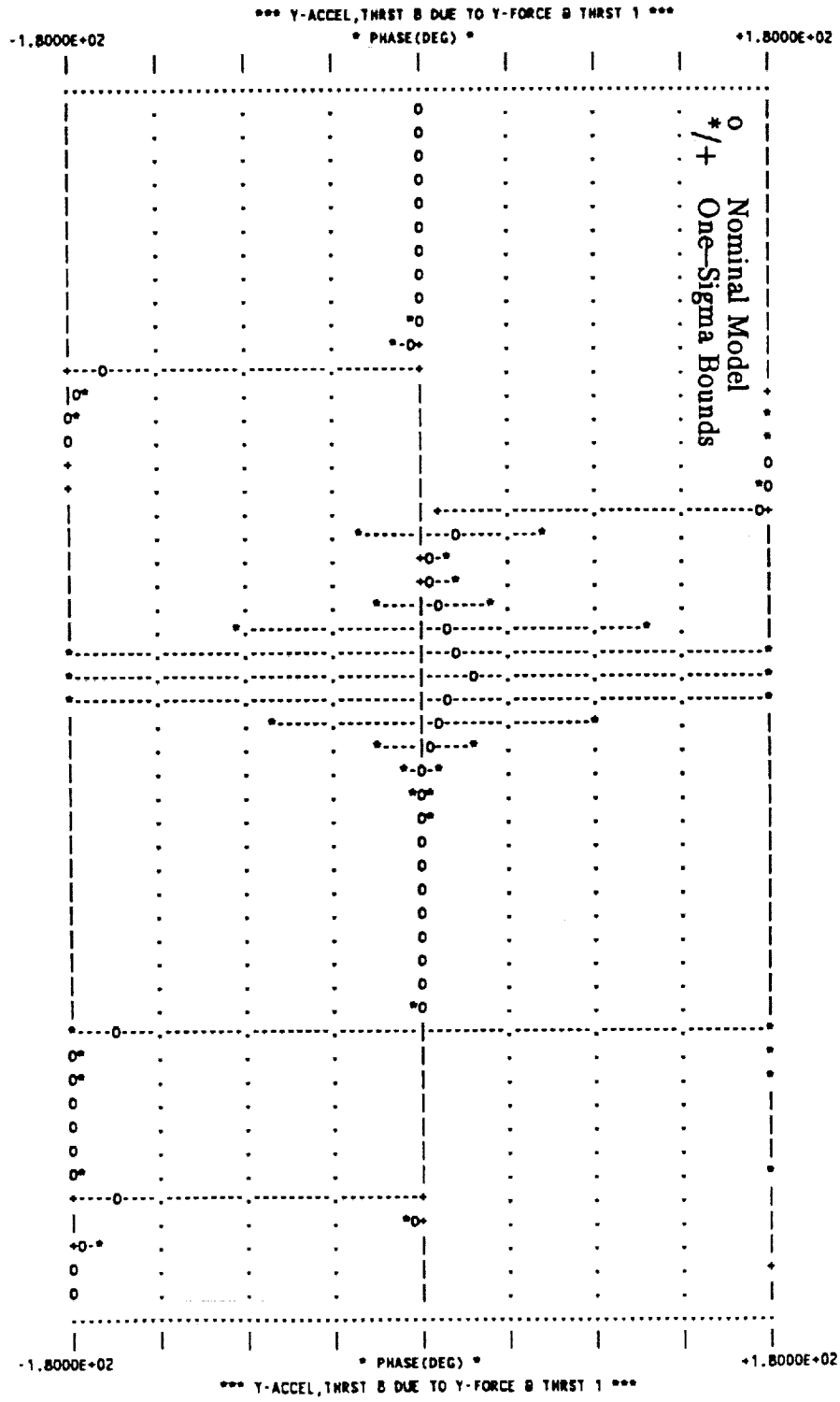

Figure 6–24b. Predictive Accuracy of CSI Evolutionary Structure Model, FRF Phase, Coordinate 8 Acceleration/Coordinate 1 Force.

Figure 6–25a. Sensitivity of Predictive Accuracy to Modal Truncation, CSI Evolutionary Structure, FRF Amplitude, 9–Mode Solution.

Figure 6–25b. Sensitivity of Predictive Accuracy to Modal Truncation, CSI Evolutionary Structure, FRF Phase, 9–Mode Solution.

Figure 6–26a. Sensitivity of Predictive Accuracy to Modal Truncation, CSI Evolutionary Structure, FRF Amplitude, 7–Mode Solution.

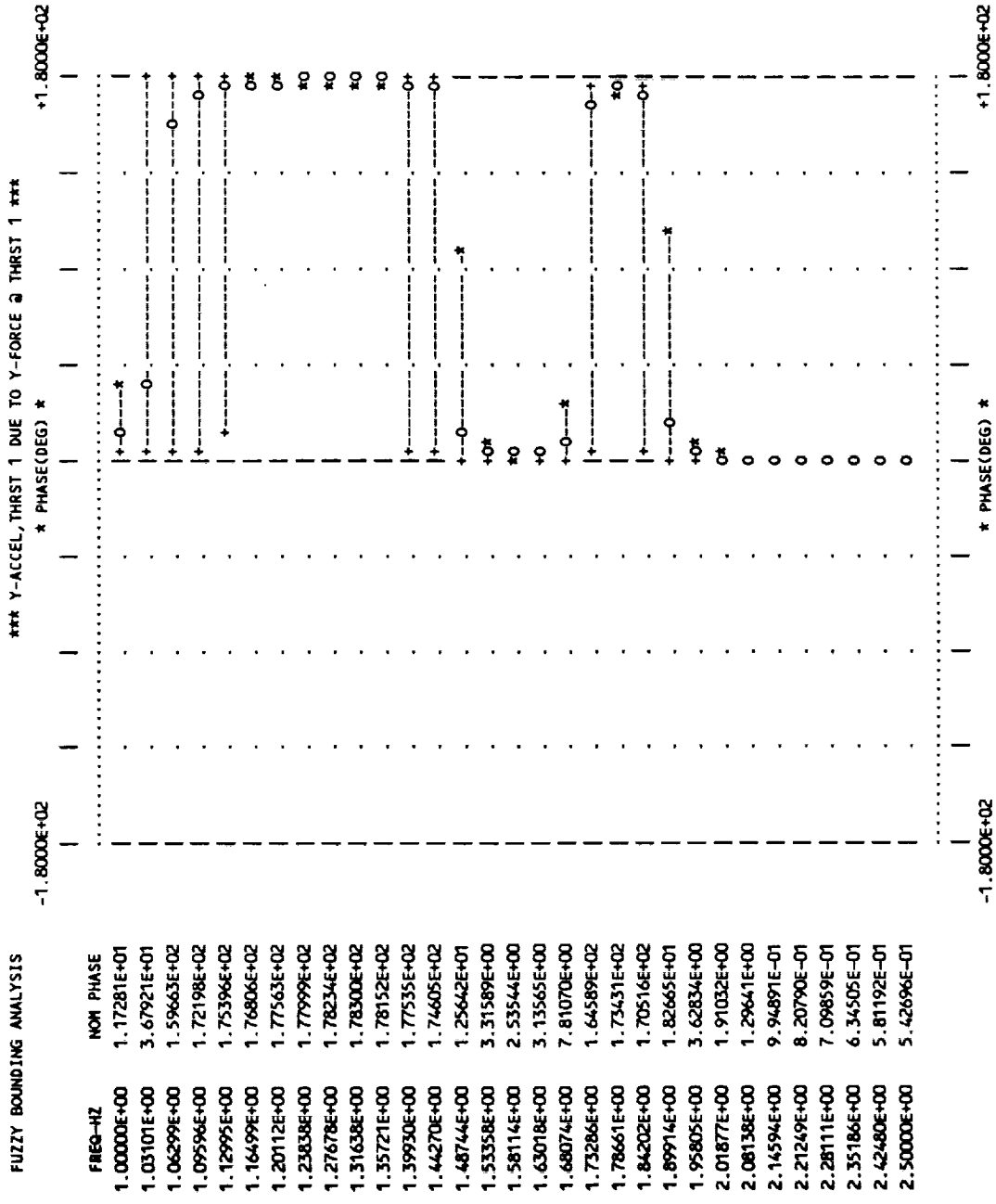

Figure 6–26b. Sensitivity of Predictive Accuracy to Modal Truncation, CSI Evolutionary Structure, FRF Phase, 7–Mode Solution.

Figure 6–27a. Sensitivity of Predictive Accuracy to Modal Truncation, CSI Evolutionary Structure, FRF Amplitude, 5–Mode Solution.

Figure 6–27b. Sensitivity of Predictive Accuracy to Modal Truncation, CSI Evolutionary Structure, FRF Phase, 5–Mode Solution.

Figure 6–28a. Sensitivity of Predictive Accuracy to Modal Truncation, CSI Evolutionary Structure, FRF Amplitude, 3–Mode Solution.

Figure 6–28b. Sensitivity of Predictive Accuracy to Modal Truncation, CSI Evolutionary Structure, FRF Phase, 3–Mode Solution.

6.4 Ten Bay Truss

Model verification has two goals: (1) to compare model predictions with appropriate test data and adjust the model so that it agrees with the data as closely as possible; and (2) to improve the predictive accuracy of the model so that it may be used with greater confidence in future applications. The words "appropriate" and "improve" are underscored to make the point that a model can be adjusted to match certain data without improving the model from the standpoint of its predictive accuracy. For example, the model might be tuned to match data in one range of frequencies and in the process become distorted so that it matches less well at other frequencies. Or it may be tuned to better match data at certain locations at the expense of matching less well at other locations. Or it may be tuned to match frequencies, only to find that it does not match mode shapes as well. A model should be verified for a specific use and its predictive accuracy quantified for that use.

When Bayesian parameter estimation is used in model verification, a covariance matrix of the parameter estimates is obtained. This covariance matrix provides a measure of confidence in the mean. It can be propagated forward to obtain uncertainty intervals on response, but these intervals reflect confidence in the estimated mean response; they do not reflect the degree of variation between the estimated mean response and the data, i.e. the sample covariance. The only way to obtain a sample covariance for a particular structure would be to have an ensemble of models to compare with test results (assuming the test results are repeatable). Since this is not possible, uncertainty intervals obtained from a generic database involving similar but different structures offers the best alternative.

In order to fully demonstrate Bayesian estimation with uncertainty intervals on both pretest and posttest response predictions, the following information is required:

1. A pretest analytical model of the structure;
2. Appropriate test data for that structure;
3. A pretest model uncertainty database; and
4. A posttest model uncertainty database.

The first three of these items were available for the LaRC Ten Bay Truss shown in Figure 2–2. The given analytical model is treated as a pretest model and the LSS research model uncertainty database is treated as a pretest model database for purposes of

demonstration. This treatment is consistent with the data since the analytical frequencies and mode shapes of this model were used in compiling the model uncertainty database. It is therefore appropriate to use the LSS uncertainty database to determine the predictive accuracy of the given model. This model can then be tuned to match available data and the nominal response of the tuned model compared with the original model and its predictive accuracy, as represented by uncertainty intervals on FRF amplitude and phase.

FRF data were not available to use in parameter estimation, so frequency and mode shape data were used instead. Nevertheless, FRF plots are obtained for both the original model and the refined model. The model refinement is reported in Reference [6–3], and included in Appendix B of this report. Figure 6–29 shows the nominal response of the original (given) model with uncertainty intervals based on the LSS database. The revised nominal response after tuning the model is shown by the dashed lines. Dashed lines are used instead of solid lines so that they will not be confused with actual test data which are plotted with solid lines in earlier plots.

Figure 6–30 shows the nominal response with uncertainty intervals in the out–of–plane direction. The nominal response is as one would expect, but the uncertainty intervals in the neighborhood of the primary bending modes are very large. In an attempt to avoid potential numerical problems with closely spaced modes, a minimum frequency separation of one half of one percent is arbitrarily enforced between close modes. To determine whether the closely spaced modes were causing the large uncertainty intervals, this frequency separator was increased to two percent. The results are shown in Figures 6–31 and 6–32 for both response directions.

This study shows that frequency separation does indeed have a major effect on out–of–plane response. Large uncertainty was expected near resonance, but not at frequencies well below resonance. A Monte Carlo run was therefore made to check the results obtained by linear covariance propagation. Distribution functions of FRF amplitude and phase were generated for frequencies of 10 Hz and 15 Hz. These distributions are presented in Figures 33 and 34 for the nominal case where frequency separation between modes was again set at a minimum of 0.5%.

The numerical simulation tends to confirm the results obtained by linear covariance propagation, in the sense that the intervals of uncertainty are indeed large. What is apparently happening here is that mass and stiffness uncertainties are causing

FUZZY BOUNDING ANALYSIS

FREQ-HZ	NOM DISPL/FORCE
1.00000E+01	3.86222E-03
1.05095E+01	4.04682E-03
1.10450E+01	4.27311E-03
1.16078E+01	4.55544E-03
1.21993E+01	4.91551E-03
1.28209E+01	5.38781E-03
1.34742E+01	6.03058E-03
1.41607E+01	6.95045E-03
1.48823E+01	8.36547E-03
1.56406E+01	1.07990E-02
1.64375E+01	1.58716E-02
1.72751E+01	3.12998E-02
1.81553E+01	5.25473E-02
1.90804E+01	1.77802E-02
2.00526E+01	9.75815E-03
2.10744E+01	6.44595E-03
2.21482E+01	4.65994E-03
2.32767E+01	3.54967E-03
2.44627E+01	2.79614E-03
2.57092E+01	2.25342E-03
2.70192E+01	1.84542E-03
2.83959E+01	1.52858E-03
2.98428E+01	1.27618E-03
3.13634E+01	1.07089E-03
3.29615E+01	9.00969E-04
3.46410E+01	7.58122E-04
3.64061E+01	6.36300E-04
3.82611E+01	5.30924E-04
4.02107E+01	4.38381E-04
4.22596E+01	3.55664E-04
4.44129E+01	2.80055E-04
4.66759E+01	2.08787E-04
4.90542E+01	1.38528E-04
5.15537E+01	6.47195E-05
5.41805E+01	3.36941E-05
5.69412E+01	1.65553E-04
5.98426E+01	4.91126E-04
6.28918E+01	3.16830E-03
6.60964E+01	5.93045E-04
6.94642E+01	2.78886E-04
7.30037E+01	1.43554E-04
7.67235E+01	4.73230E-05
8.06329E+01	5.64347E-05
8.47414E+01	2.01956E-04
8.90593E+01	5.82339E-04
9.35973E+01	4.18658E-03
9.83664E+01	6.93831E-04
1.03379E+02	3.79292E-04
1.08646E+02	2.61989E-04
1.14182E+02	1.97528E-04
1.20000E+02	1.55135E-04

Figure 6–29a. Predictive Accuracy of Ten Bay Truss Model, FRF Amplitude, Y–displacement at Node 2/Y–force at Node 2.

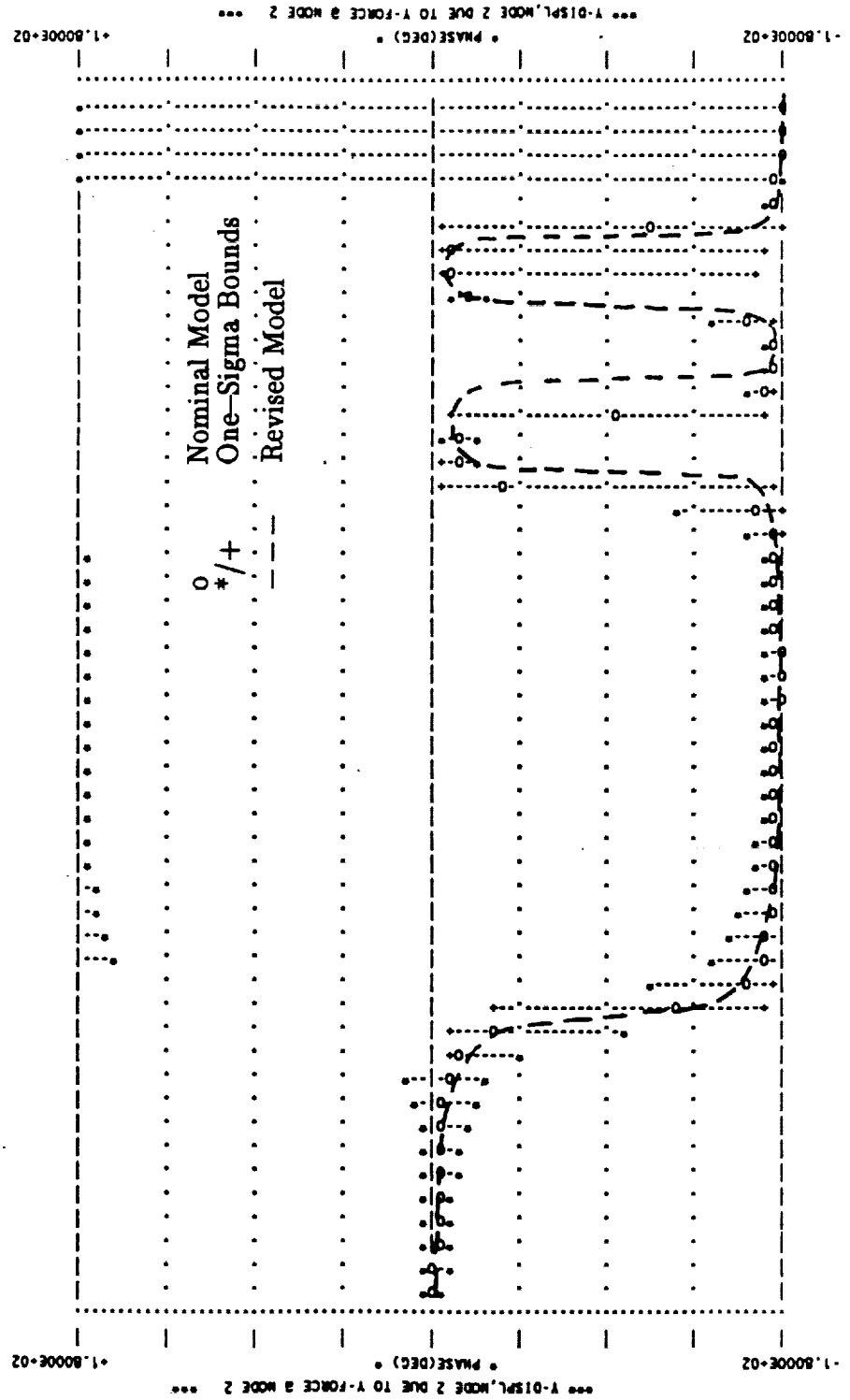

Figure 6–29b. Predictive Accuracy of Ten Bay Truss Model, FRF Phase, Y–displacement at Node 2/Y–force at Node 2.

FUZZY BOUNDING ANALYSIS

FREQ-HZ	NOM DISPL/FORCE
1.00000E+01	9.27748E-05
1.05095E+01	9.64361E-05
1.10450E+01	1.01318E-04
1.16078E+01	1.08041E-04
1.21993E+01	1.17669E-04
1.28209E+01	1.32137E-04
1.34742E+01	1.55223E-04
1.41607E+01	1.95051E-04
1.48823E+01	2.71582E-04
1.56406E+01	4.45080E-04
1.64375E+01	9.73548E-04
1.72751E+01	4.08351E-03
1.81553E+01	1.50188E-02
1.90804E+01	1.59715E-03
2.00526E+01	5.23405E-04
2.10744E+01	2.64029E-04
2.21482E+01	1.68585E-04
2.32767E+01	1.26191E-04
2.44627E+01	1.05581E-04
2.57092E+01	9.51822E-05
2.70192E+01	9.00152E-05
2.83959E+01	8.77574E-05
2.98428E+01	8.72768E-05
3.13634E+01	8.80154E-05
3.29615E+01	8.97127E-05
3.46410E+01	9.22803E-05
3.64061E+01	9.57478E-05
3.82611E+01	1.00248E-04
4.02107E+01	1.06029E-04
4.22596E+01	1.13506E-04
4.44129E+01	1.23352E-04
4.66759E+01	1.36714E-04
4.90542E+01	1.55667E-04
5.15537E+01	1.84371E-04
5.41805E+01	2.32525E-04
5.69412E+01	3.29103E-04
5.98426E+01	6.15777E-04
6.28918E+01	3.14123E-03
6.60964E+01	5.28320E-04
6.94642E+01	2.50707E-04
7.30037E+01	1.55415E-04
7.67235E+01	1.06910E-04
8.06329E+01	7.64286E-05
8.47414E+01	5.19782E-05
8.90593E+01	1.04497E-05
9.35973E+01	1.44897E-03
9.83664E+01	1.22781E-05
1.03379E+02	1.82974E-05
1.08646E+02	1.65325E-05
1.14182E+02	1.32490E-05
1.20000E+02	9.81051E-06

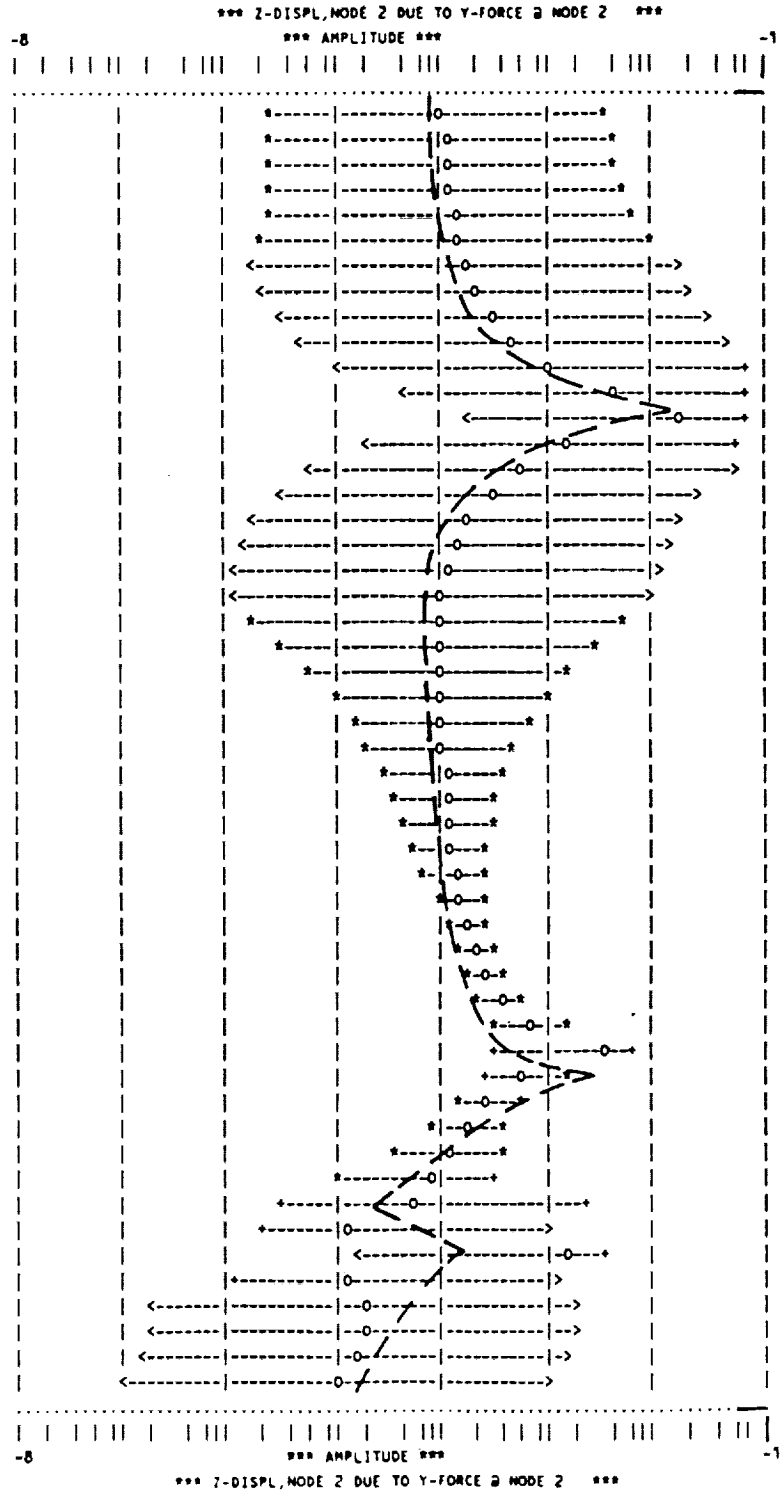

Figure 6–30a. Predictive Accuracy of Ten Bay Truss Model, FRF Amplitude, Z–displacement at Node 2/Y–force at Node 2.

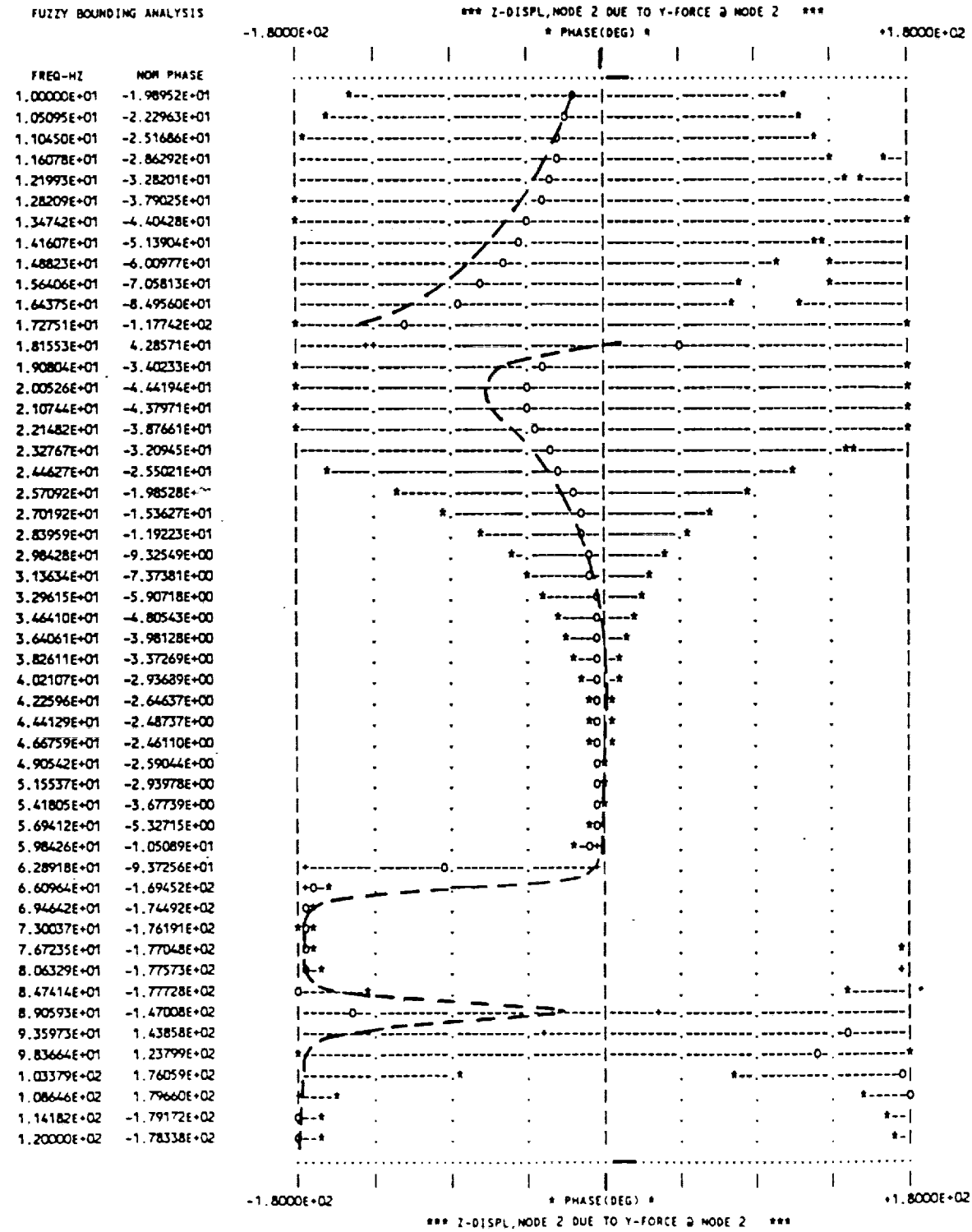

Figure 6–30b. Predictive Accuracy of Ten Bay Truss Model, FRF Phase, Z–displacement at Node 2/Y–force at Node 2.

FUZZY BOUNDING ANALYSIS

FREQ-HZ	NOM DISPL/FORCE
1.00000E+01	3.82286E-03
1.05095E+01	4.00371E-03
1.10450E+01	4.22520E-03
1.16078E+01	4.50118E-03
1.21993E+01	4.85262E-03
1.28209E+01	5.31267E-03
1.34742E+01	5.93713E-03
1.41607E+01	6.82760E-03
1.48823E+01	8.19024E-03
1.56406E+01	1.05143E-02
1.64375E+01	1.52843E-02
1.72751E+01	2.91375E-02
1.81553E+01	5.04492E-02
1.90804E+01	1.92155E-02
2.00526E+01	1.01140E-02
2.10744E+01	6.59286E-03
2.21482E+01	4.73585E-03
2.32767E+01	3.59423E-03
2.44627E+01	2.82459E-03
2.57092E+01	2.27272E-03
2.70192E+01	1.85915E-03
2.83959E+01	1.53876E-03
2.98428E+01	1.28400E-03
3.13634E+01	1.07710E-03
3.29615E+01	9.06057E-04
3.46410E+01	7.62418E-04
3.64061E+01	6.40034E-04
3.82611E+01	5.34261E-04
4.02107E+01	4.41443E-04
4.22596E+01	3.58546E-04
4.44129E+01	2.82832E-04
4.66759E+01	2.11521E-04
4.90542E+01	1.41273E-04
5.15537E+01	6.74749E-05
5.41805E+01	3.13303E-05
5.69412E+01	1.62429E-04
5.98426E+01	4.87713E-04
6.28918E+01	3.16859E-03
6.60964E+01	5.97545E-04
6.94642E+01	2.84399E-04
7.30037E+01	1.50593E-04
7.67235E+01	5.66747E-05
8.06329E+01	4.15093E-05
8.47414E+01	1.72180E-04
8.90593E+01	4.87819E-04
9.35973E+01	1.79309E-03
9.83664E+01	8.25642E-04
1.03379E+02	4.05605E-04
1.08646E+02	2.72356E-04
1.14182E+02	2.02924E-04
1.20000E+02	1.58449E-04

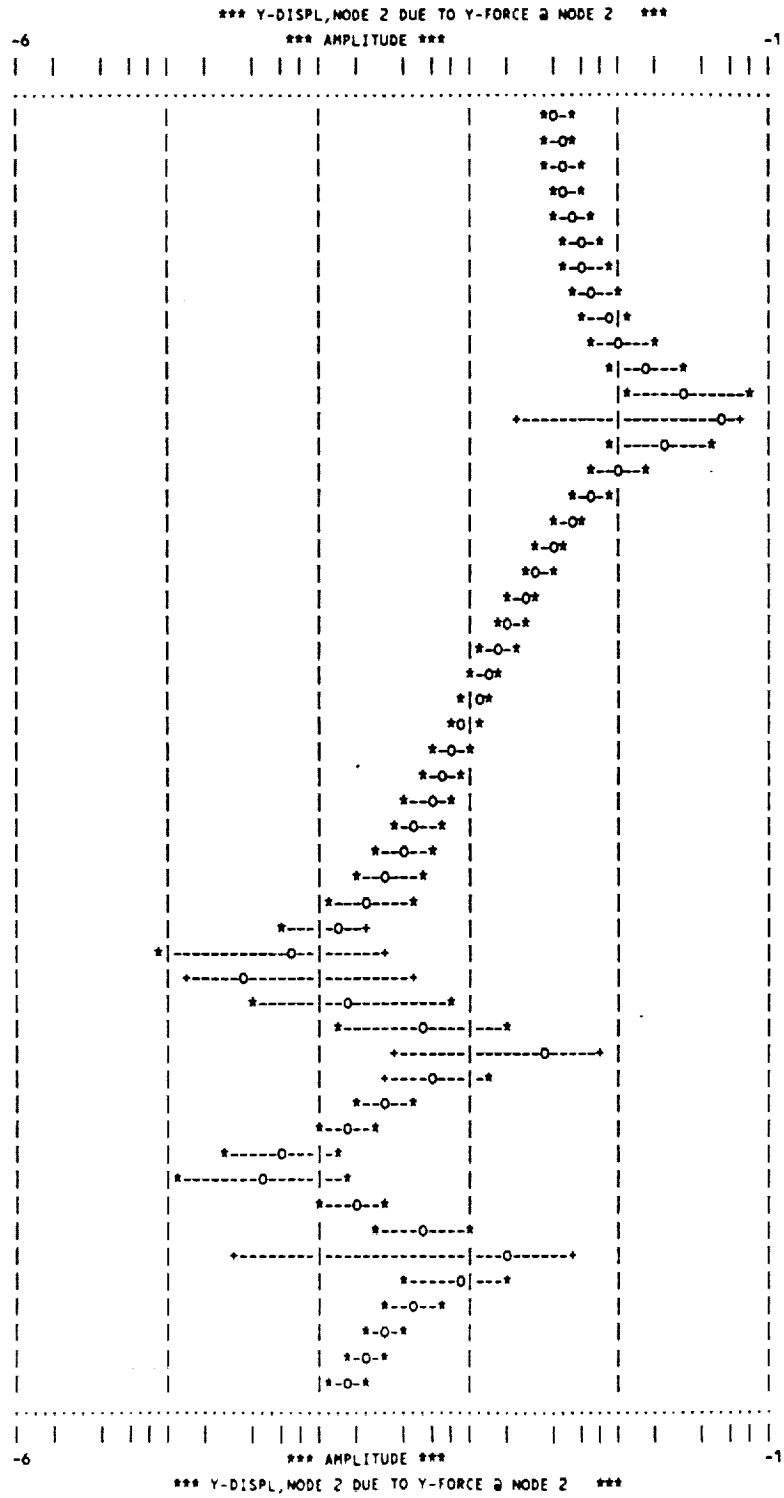

Figure 6–31a. Rerun of Figure 6–29a with 2% Minimum Frequency Separation Between Modes.

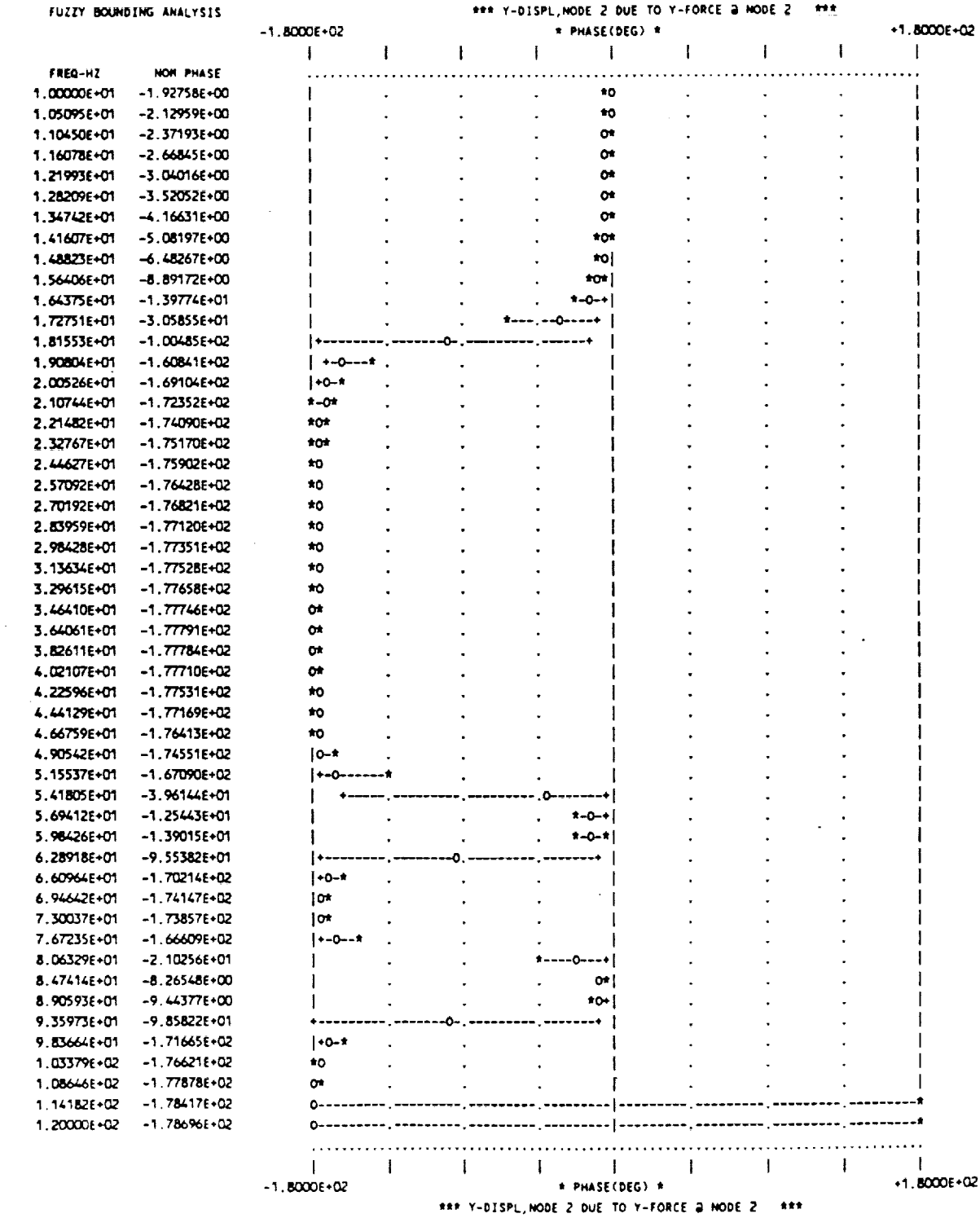

Figure 6–31b. Rerun of Figure 6–29b with 2% Minimum Frequency Separation Between Modes.

FUZZY BOUNDING ANALYSIS

FREQ-HZ	NOM DISPL/FORCE
1.00000E+01	1.58165E-04
1.05095E+01	1.67679E-04
1.10450E+01	1.79951E-04
1.16078E+01	1.96205E-04
1.21993E+01	2.18447E-04
1.28209E+01	2.50173E-04
1.34742E+01	2.97946E-04
1.41607E+01	3.75361E-04
1.48823E+01	5.14629E-04
1.56406E+01	8.08782E-04
1.64375E+01	1.62830E-03
1.72751E+01	5.66181E-03
1.81553E+01	3.18035E-02
1.90804E+01	3.56963E-03
2.00526E+01	9.95338E-04
2.10744E+01	4.62355E-04
2.21482E+01	2.75492E-04
2.32767E+01	1.91828E-04
2.44627E+01	1.48937E-04
2.57092E+01	1.25159E-04
2.70192E+01	1.11438E-04
2.83959E+01	1.03491E-04
2.98428E+01	9.91221E-05
3.13634E+01	9.71454E-05
3.29615E+01	9.69147E-05
3.46410E+01	9.80956E-05
3.64061E+01	1.00557E-04
3.82611E+01	1.04324E-04
4.02107E+01	1.09574E-04
4.22596E+01	1.16669E-04
4.44129E+01	1.26252E-04
4.66759E+01	1.39445E-04
4.90542E+01	1.58310E-04
5.15537E+01	1.86997E-04
5.41805E+01	2.35206E-04
5.69412E+01	3.31913E-04
5.98426E+01	6.18783E-04
6.28918E+01	3.14109E-03
6.60964E+01	5.24471E-04
6.94642E+01	2.45986E-04
7.30037E+01	1.49353E-04
7.67235E+01	9.85006E-05
8.06329E+01	6.32805E-05
8.47414E+01	2.68396E-05
8.90593E+01	7.57028E-05
9.35973E+01	2.47791E-03
9.83664E+01	1.14874E-04
1.03379E+02	6.47465E-06
1.08646E+02	7.82399E-06
1.14182E+02	8.81314E-06
1.20000E+02	7.20790E-06

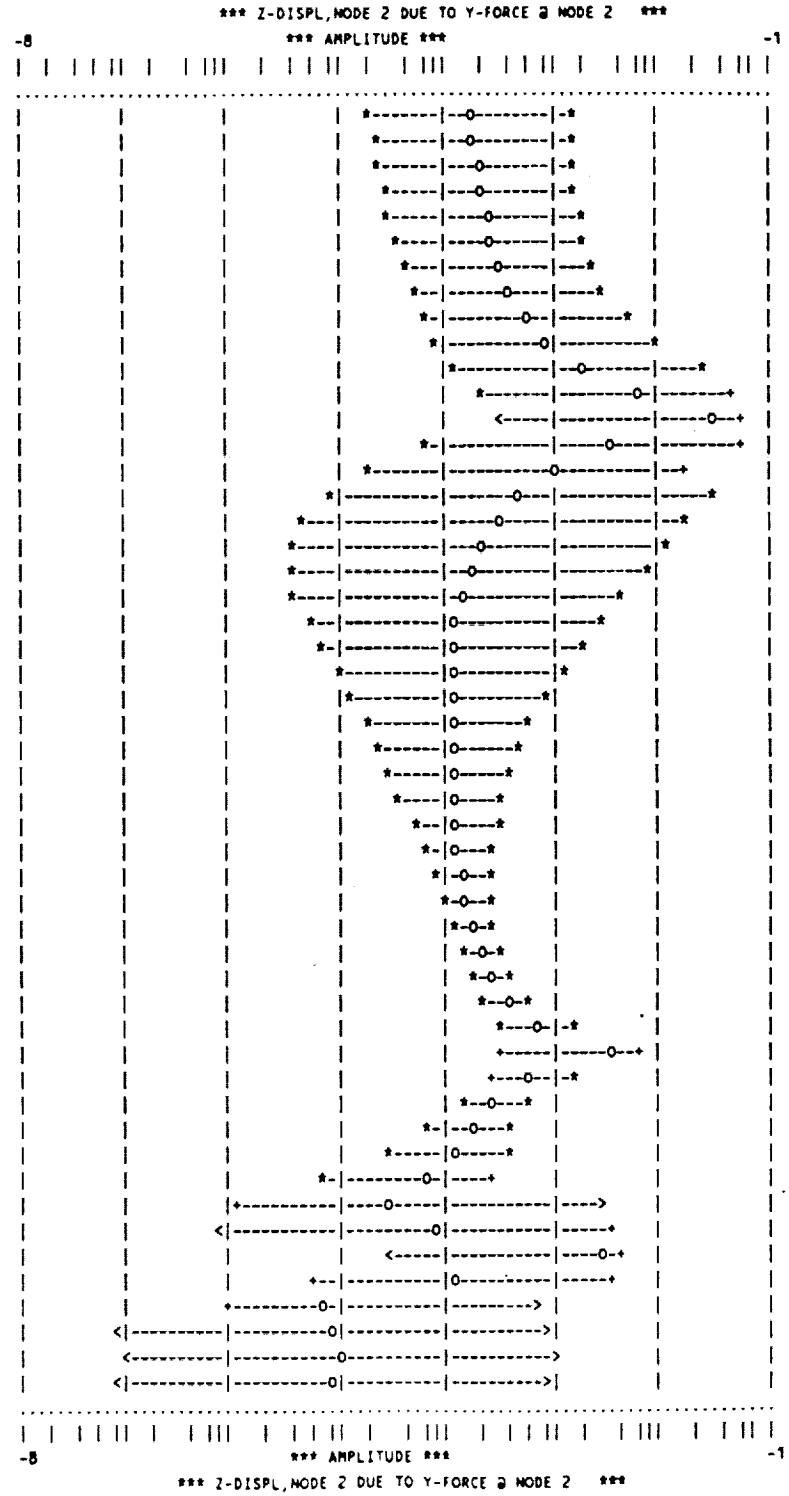

Figure 6–32a. Rerun of Figure 6–30a with 2% Minimum Frequency Separation Between Modes.

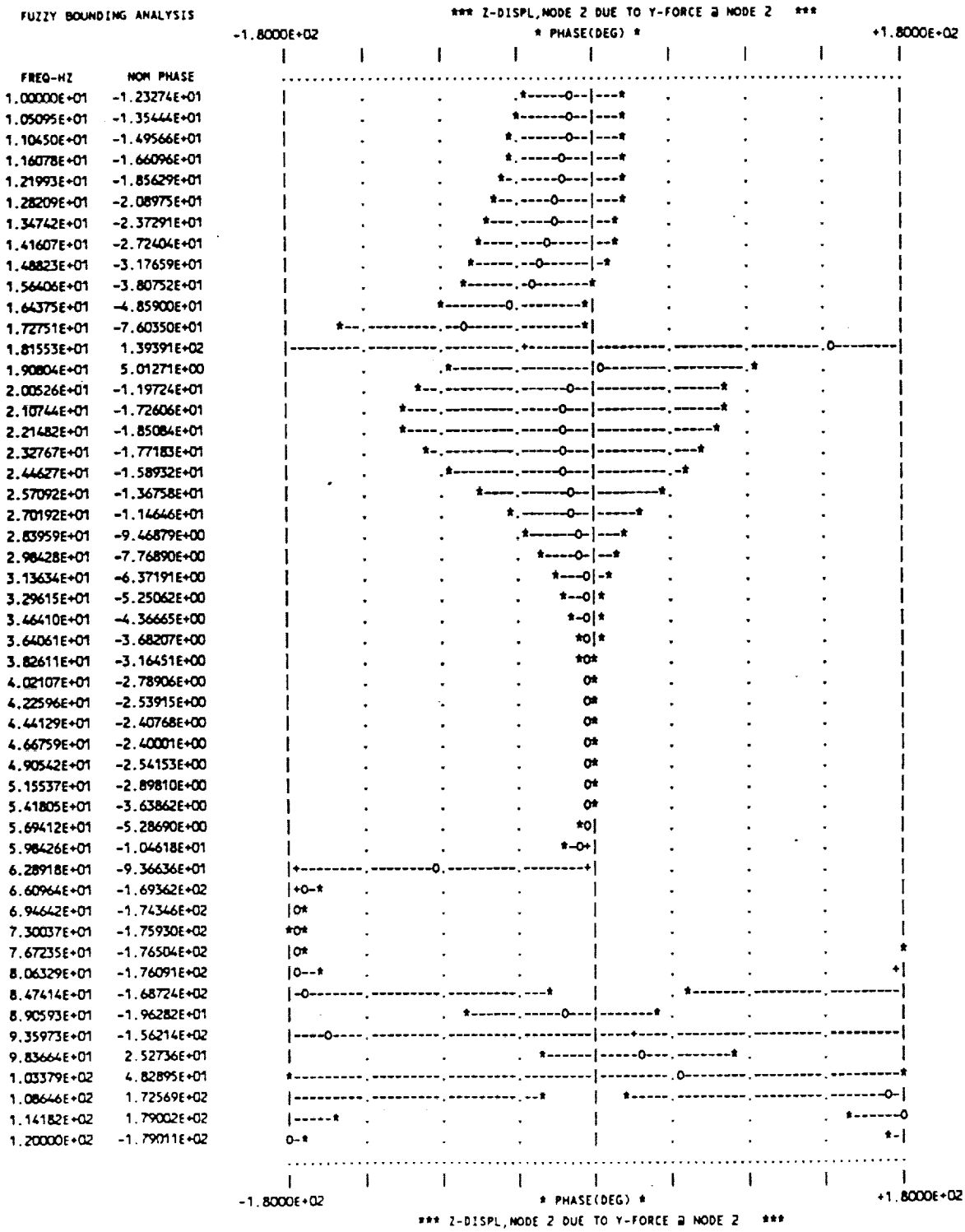

Figure 6–32b. Rerun of Figure 6–30b with 2% Minimum Frequency Separation Between Modes.

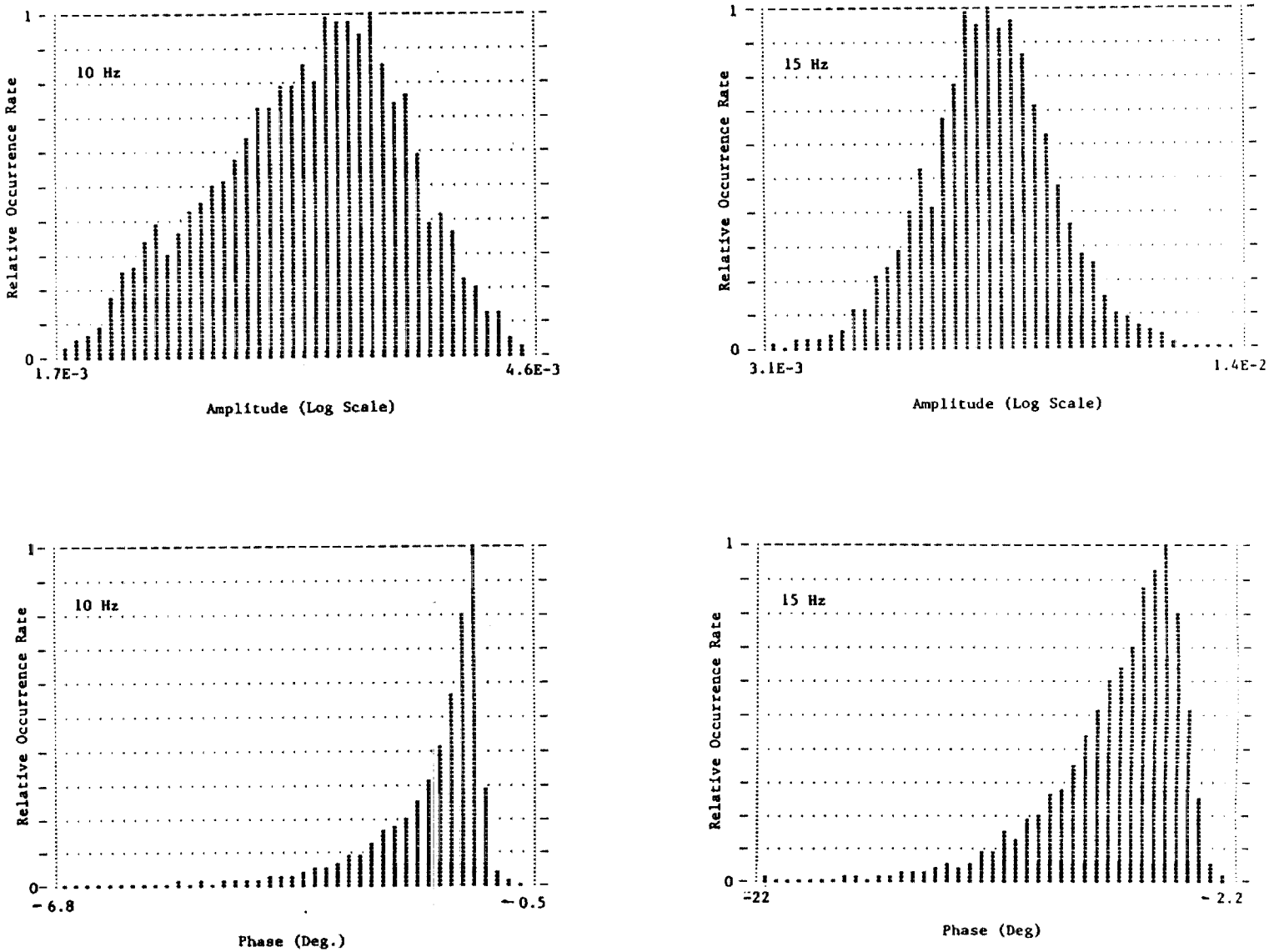

Figure 6–33. FRF Distribution for the Ten Bay Truss: Y–displacement at Node 2 due to Y–force at Node 2.

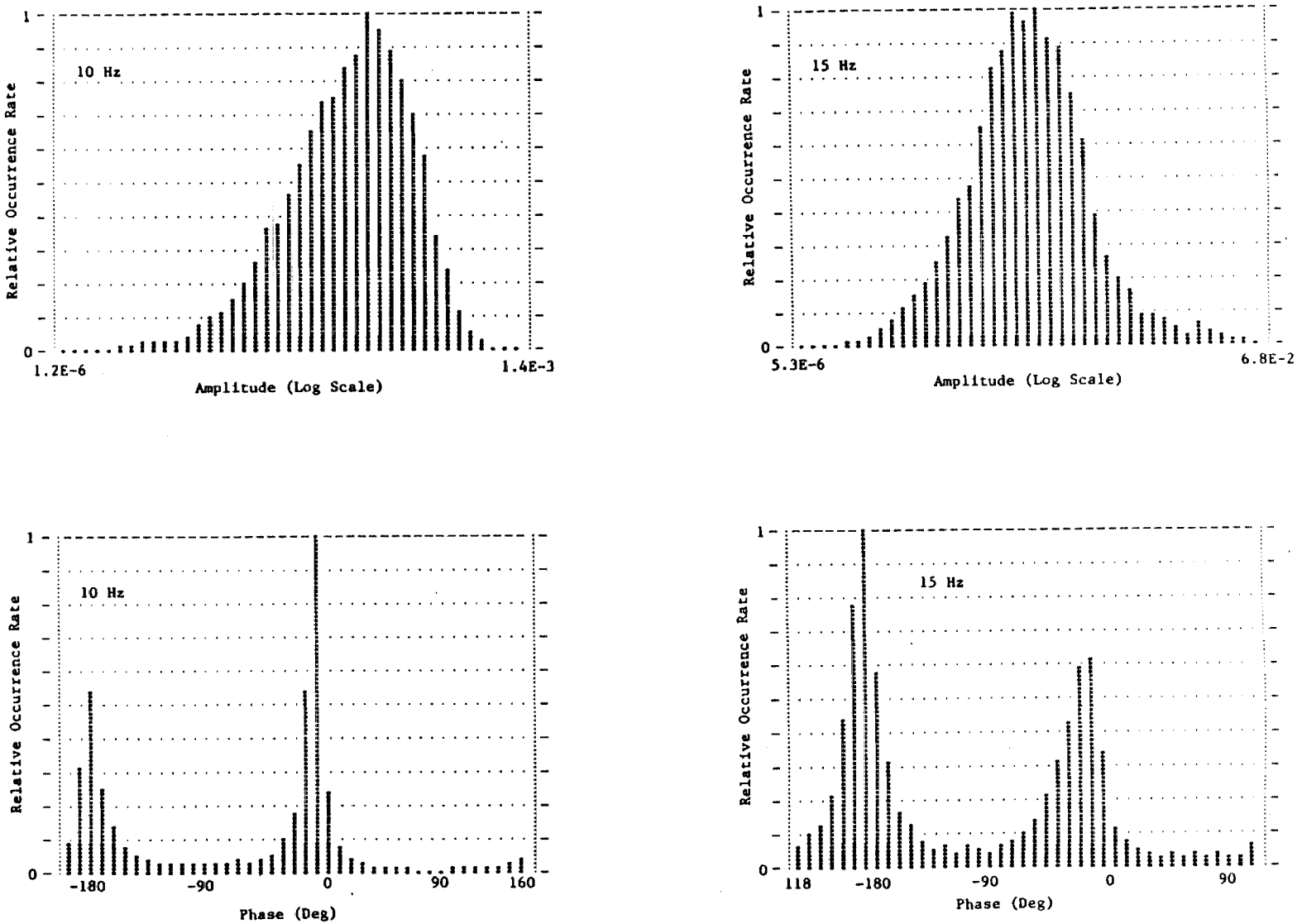

Figure 6–34. FRF Distributions for the Ten Bay Truss: Z–displacement at Node 2 due to Y–force at Node 2.

coupling between the first two bending modes because of the closely spaced frequencies. Whether or not this coupling is real or the result of inaccuracies in the uncertainty database is not known at this time. The numerical simulation appears to rule out the possibility of a numerical problem in the uncertainty propagation. It does not, however, rule out the possibility that small random variations in the database might cause this type of coupling when the frequencies of two modes are very close. One thing the study points out is that small asymmetries or eccentricities in the mass or stiffness properties of a structure with closely spaced modes may couple the modes in ways which are not expected. Further study of this phenomenon is warranted.

7. CONCLUSIONS AND RECOMMENDATIONS

The primary goal of this research has been to develop a practical tool for evaluating the predictive accuracy of structural dynamic models. The emphasis on practicality means that the tool must produce meaningful results, based on real data. It also implies that these data should be readily available and preferably incorporated as part of the tool. This goal has been accomplished. That is not to say that the tool is foolproof. While numerous sensitivity studies and varied practical applications have demonstrated the viability of the tool, much more remains to be done before a full appreciation of its capabilities and limitations can be realized. This appreciation will come only through use. As with any new tool, skillful application and refinement of the tool go hand in hand. Conversely, it is fair to say that if a tool is not used, it must relinquish its claim to practicality.

The following sections are intended to bring a sense of closure to the project and to establish a benchmark reference for future work, whether that work be in the nature of practical application or further research. To this end the next three sections are ordered according to the maturity of the technologies they address: Section 7.1 addresses the technology incorporated in the Predictive Accuracy code, PDAC. Section 7.2 addresses the estimation of a full modal damping matrix from measured complex modes. Section 7.3 addresses other research efforts which were eventually abandoned in favor of more fruitful endeavors. That is not to say that these efforts were not worthwhile, or that future efforts in pursuit of the same objectives would not be fruitful. Lessons were learned in the process which should benefit future research.

Finally, this chapter concludes with several recommendations. The recommendations extend the thinking of the project team beyond that which may be concluded from the work accomplished to date, and are offered as suggestions to those who may continue research in this area.

7.1 PDAC Methodology

Methods have been developed, implemented and demonstrated for evaluating the predictive accuracy of structural dynamic models. Primary implementation of the methods is embodied in the computer code, PDAC, an acronym for PreDictive ACcuracy.

Together, the methods comprise a methodology for "interval prediction", a capability which augments the "point prediction" of conventional structural dynamic analysis. The following subsections present the major conclusions drawn from each stage of this research effort.

7.1.1 Development

There are three major parts to the PDAC methodology: (1) the characterization of mass and stiffness uncertainty, (2) the characterization of damping uncertainty, and (3) the propagation of these uncertainties through the model to obtain response uncertainty in the form of response intervals.

Mass and stiffness uncertainty is cast in the form of a covariance matrix of modal mass and normalized modal stiffness matrix elements, derived from differences between predicted and measured eigenvalues and eigenvectors. The latter were expressed in terms of the modal cross–orthogonality matrix. This formulation has proven to be effective as a basis for computing frequency response intervals.

Whereas mass and stiffness uncertainty can be derived from prior analysis and test experience on generically similar structures, damping uncertainty must be treated differently because as yet there is no way to predict structural damping in general. Instead, damping must be determined experimentally, and damping uncertainty therefore must be expressed in terms of the variability among damping measurements or estimates. Although considerable effort was devoted to estimating a full modal damping matrix from experimentally derived complex modes, and this effort appears to have been successful, PDAC presently assumes that the modal damping matrix is diagonal. The use of a full modal damping matrix is beyond the current state–of–the–practice in structural dynamic analysis, and there were insufficient data available to construct a meaningful database.

Uncertainty propagation through a model proved to be the most difficult part of the methodology development. Phase I showed that linear covariance propagation could be used effectively away from poles and zeros, and that a fuzzy set approach involving the use of possibility intervals ought to provide meaningful results near poles and zeros. The practicality of the latter approach depends on whether frequency response near the poles and zeros can be approximated with only a few modal parameters. If so, the Vertex

Method provides an efficient means of bounding response in the vicinity of these frequencies. When the response surface includes maxima or minima internal to the rectangular hyperspace defined by the parameter intervals, special techniques must be used to evaluate the included maxima and minima. Random search and constrained optimization techniques were the most successful.

Use of the random search technique led to the use of numerical simulation as a means of estimating the distribution of response at a given frequency. This provided a third way of characterizing response uncertainty. At the outset it was thought that numerical simulation would be too costly because of the number of samples required to define a distribution for a multivariate system. This remains true in general. However, as an auxiliary method, numerical simulation can be quite valuable. It provides insight to the distribution of response that neither of the two interval methods offer. It too benefits from parameter truncation near the poles and zeros.

Perhaps the least obvious part of the methodology is the selection of parameter truncation thresholds. A clustering method is discussed in Section 4.2.2.1, and sensitivity analyses are presented in Section 6.2. Although this clustering method makes use of the derivatives, some of which become very large near the poles and zeros, it is the smaller (well–behaved) derivatives which control the clustering. The fact that some of the derivatives may be very large is of no consequence; they are simply used to identify the parameters which should be retained in the truncation.

7.1.2 Implementation

The foregoing methodology for FRF interval prediction is implemented in PDAC. One of the run options in an existing structural system identification code, SSID, was modified to incorporate PDAC. The combined code, SSID/PDAC, offers the capability to compute FRF amplitude and phase with uncertainty intervals on either pretest or posttest models. That is, predictive accuracy can be evaluated either before or after a model has been tuned to match experimental data.

SSID/PDAC is exceptionally easy to run in the PDAC mode. It requires no test data, and requires no modeling data other than modal frequencies and corresponding modal displacements at input/output locations. Mass and stiffness uncertainty databases

are stored internally and are selected by specifying the desired option. Current database options include:

- Large Space Structure (LSS) Research Models;
- Conventional Space Structures (CSS) Pretest Models;
- Conventional Space Structures (CSS) Posttest Models; and
- A Combined Database (including all of the first three).

At the present time, nine modes of data are available in each database, resulting in modal mass and normalized modal stiffness covariance matrices of dimension 90 x 90. In general, the dimension of this matrix will be $n^2 + n$, where n is the number of modes included. For a database including 30 modes, the covariance matrix would be of dimension 930 x 930.

The present databases are designed to be updated as more data become available. A summary of the currently available data is given in Tables 2–1 and 2–3 which list seven structures in the LSS database, and seven and eight structures, respectively in the CSS Pretest and Posttest databases. A continuing effort will be made to expand these databases during Phase III. Four additional structures have been identified for both the CSS Pretest and Posttest databases as of this writing.

7.1.3 Demonstration

PDAC has been demonstrated by application to three real structures for which both analysis and test data were available. In two of the three cases, the NASA Mini–mast and CSI Evolutionary Structures, measured FRF amplitude and phase data were available to compare with uncertainty intervals based on analytical frequencies and mode shapes, measured damping values, and the LSS database. The analyses span the first three modes of the Mini–mast Structure and the first seven modes of the CSI Evolutionary Structure, although in view of the modal sensitivity analysis performed on the latter, the analyses might have been extended to include five modes and nine modes, respectively. As it was, measured FRF amplitude and phase tended to fall within the ± one–sigma uncertainty intervals for the most part. One notable difference between the two cases is that the CSI Evolutionary Structure is not included in the LSS database, demonstrating that uncertainty data from generically similar structures can be used to effectively evaluate the predictive accuracy of other structures belonging to the same generic family.

A different capability was demonstrated with the Ten Bay Truss. In this case, FRF data were not available, but both analysis and test frequencies and mode shapes were available. The test frequencies and mode shapes were used to tune the original model using the parameter estimation capability of SSID. FRF plots were generated for both the original and revised models. Uncertainty intervals generated for the original model were shown to enclose the FRF amplitude and phase of the revised model.

Numerous sensitivity studies were conducted to test the validity of PDAC interval predictions. Different databases were run with the same model to examine the sensitivity of interval predictions to different databases. This study showed that while different databases can produce significantly different results at certain frequencies, the model itself tends to dominate the envelope of uncertainty as a function of frequency. One of the questions often raised about the validity of the method is whether the results are meaningful, considering the fact that different kinds of modes with inherently different characteristics tend to be averaged together in the statistical processing of the data. This question might be explored, for example, by creating a special database of structures within a very narrow generic classification (such as cantilevered truss beams) where the modes tend to have similar characteristics (e.g. a pair of bending modes followed by a twist mode followed by another pair of bending modes, etc.). Then interval prediction using this database could be compared with those using less homogeneous databases such as the ones developed here. Unfortunately, the present database does not support such a study because it does not contain a sufficient number of structures of any one type. However, the feeling is that because of all of the averaging (i.e. summing) taking place in the analysis, differences tend to be smoothed over so that the end results are indeed meaningful. It is worth noting the various summing operations which occur.

1. For any given structure, summing occurs when computing the cross–orthogonality coefficients, i.e. mode shape differences are integrated over the structure.

2. Opposing off–diagonal terms in the cross–orthogonality matrix are summed to obtain the differences in modal mass and stiffness.

3. Modal mass and stiffness differences are summed over a number of structures when computing the modal mass and stiffness covariance matrices.

4. Modal contributions to response uncertainty are summed when transforming response from modal coordinates to physical coordinates.

In short, the summations occur over the spatial geometry of each structure in the database for each structural mode, over the ensemble of structures in the database, and over a range of frequencies for the particular structure being analyzed.

Other sensitivity analyses examined the sensitivity of computed response intervals to parameter truncation and modal truncation, and found the sensitivity to be small in the limited number of cases studied.

7.2 Estimation of a Full Modal Damping Matrix

Research conducted nearly twenty years ago produced a method for estimating a full modal damping matrix from experimentally derived complex modes. Practical application of the method was of limited success because of difficulties inherent in the use of analog data acquisition and processing techniques. Yet, the full modal damping matrix is known to be useful in the synthesis of structural damping from substructure tests, and could be useful in identifying the source of damping by location and damping mechanism. This could open the door to pretest damping prediction, finding application in the prediction of on–orbit damping.

The earlier research was extended under this project to make use of available digital data acquisition and processing technology. Refinements to the earlier technology include a method for removing bias–type errors from the digitally processed complex modes, methods for orthogonalizing the complex modes, and a method for updating the mass matrix used in the computation of a full modal damping matrix.

The refined methodology was applied to two real structures for which experimentally derived digitally processed complex modes were available: the NASA Mini–mast Structure and Ten Bay Truss. Estimates of the modal damping matrix in each case based on multiple realizations of the complex modes by the ERA method showed good repeatability provided that consistent mode sets were used, i.e. where all modes were derived from the same realization. Mode sets constructed from different realizations produced much poorer results in terms of repeatability, i.e. uncertainties in the estimates were greater by an order of magnitude.

Another interesting observation was that the consistent mode sets in the case of the Mini–mast Structure yielded a much lower estimate of damping in the first mode, i.e. 0.59% compared with 1.94% derived from the constructed mode sets.. Frequency response plots appear to confirm the lower estimate, although the resolution is not good enough to be certain.

While the results of this effort are clearly encouraging, it would be premature to draw any strong conclusions on the basis of the limited data processed so far. Nevertheless, the positive results which have been achieved provide sound justification for testing the methodology in future applications.

7.3 Other Research Efforts

Several avenues of research were pursued which did not prove to be as fruitful. Even so, lessons were learned which are worth reporting. This section is included to report those findings.

An attempt was made to construct a simple knowledge based system (KBS) to facilitate model verification planning and execution. Several attempts were made to generate a rule base to operate on a given set of factual information so as to produce meaningful, nontrivial results. This effort was abandoned when it was realized how much effort would be required to produce a meaningful KBS, even for purposes of illustration. It was furthermore concluded that the knowledge available to build into such a KBS is presently inadequate. More practical experience with currently available model verification software like SSID is required before an adequate knowledge base can be formulated.

Another attempt was made to generate a KBS for purposes of pretest damping prediction. The first step was to try to estimate the distribution of damping in a structure by type of damping. Damping proportional to localized mass and stiffness submatrices was the assumed model. Attempts to estimate the distribution of damping in the Ten Bay Truss based on a 5 x 5 modal damping matrix were unsuccessful because of an inadequate database. Although only 10 parameters (5 mass proportionality constants and 5 stiffness proportionality constants) were being estimated from 15 modal damping matrix elements, only five independent estimates of the 5 x 5 modal damping matrix were available. This resulted in the 15 x 15 covariance matrix of modal damping matrix elements having a rank

of only 5. In essence, 10 parameters were being estimated from 5 pieces of information. The individual estimates were therefore meaningless. Failure to successfully complete this first step meant that the task could be pursued no further. Additional data were not available to compute additional modal damping matrices so the effort was abandoned.

Fuzzy clustering was one of the methods investigated for truncating parameters. While the method showed initial promise, it proved to be too difficult to use. The clustering depended on too many variables, including the number and type of features defined for each parameter, the number of clusters into which the parameters would be grouped, and the membership level which ultimately determines the truncation threshold. In retrospect, this was probably not an application well suited to fuzzy clustering. The simpler method described in Section 4.2.2.1 is more understandable and the threshold relates directly to truncation error.

7.4 Recommendations

As stated in the opening paragraph of the Chapter, the utility of the predictive accuracy tool developed under this project will not be realized until it is used. The first recommendation therefore is to install and use the SSID/PDAC code. Although the documentation is imposing, simple demonstration problems are provided to guide the prospective user so that he or she can be making successful runs within a few hours once the code is installed.

As the code receives broader usage, it is likely that needs will arise for capabilities which the present version of the code does not offer. Some possibilities which come to mind include interval prediction for eigenvectors, and interval prediction for the location of poles and zeros in the complex plane. A second recommendation therefore, is to identify alternative formats for evaluating and presenting the predictive accuracy of structural dynamic models to satisfy particular needs. The basic information and methodological framework are available to do so.

The third and final recommendation is to attempt further application of the method for estimating a full modal damping matrix. Damping synthesis based on substructure testing, and on–orbit damping prediction are two of the possible benefits to be derived. Additional benefits may accrue to the interpretation of the complex eigenvalues and eigenvectors derived by the ERA method and perhaps other methods as well.

REFERENCES

1–1 Pannossian, Hagop V., "Optimal Stochastic Modeling and Control of Flexible Structures," Report No. AFWAL–TR–88–3066, prepared for the Air Force Flight Dynamics Laboratory, Wright Aeronautical Laboratories by HR Textron, September, 1988.

1–2 Hasselman, T.K. and Hart, G.C., "Modal Analysis of Large Random Structures," ASCE Journal Engineering Mechanics Division, June, 1972.

2–1 Pappa, R., et. al., "Mini–Mast CSI Testbed User's Guide," NASA Langley Research Center, March, 1989.

2–2 Pappa, R. and Elliott, K., Transmittal of Analysis and Test Data for the NASA LaRC Ten Bay Truss and Mini–Mast Structure, NASA Langley Research Center, February 9, 1990.

2–3 Kissil, A., and Fanson, J.L., Transmittal of Analysis and Test Data for the JPL Precision Truss, Jet Propulsion Laboratory, April 26, 1990.

2–4 Kuo, C.P., Chen, G.–S, and Wada, B.K., "On–orbit System Identification Using Active Members," Paper No. AIAA–90–1129, Proceedings of the AIAA/ASME/ ASCE/AHS/ASC 31st SDM Conference, CP902, April 2–4, 1990.

2–5 Gehling, R.N., "Passive and Active Control of Space Structures, Volume 2, Dynamic Test Article Modal Survey: Test and Analysis Results," Report No. WRDC–TR–90–3044 Volume 2, Prepared for Wright Research and Development Center, by Martin Marietta Astronautics Group, September, 1990.

2–6 Klema, Virginia C. and Laub, Alan J., "The Singular Value Decomposition: its Computation and Some Applications," IEEE Transactions on Automatic Control, Vol AC–25, No. 2, April, 1980.

3–1 Hasselman, T.K., "Modal Coupling in Lightly Damped Structures," AIAA Journal, Vol. 14, No. 11, November, 1976.

3–2 Hasselman, T.K., "Damping Synthesis from Substructure Tests," AIAA Journal, Vol. 14, No. 10, Nov. 1976.

3–3 Hasselman, T.K., "Method for Constructing a Full Modal Damping Matrix from Experimental Measurements," AIAA Journal, Vol. 10, pp. 526–527, No. 4, April, 1972.

3–4 Smith, K., "Modal Testing Methodology at JPL," Report No. JPL D–4810, Jet Propulsion Laboratory, Pasadena, California, October, 1987.

3–5 Targoff, W.P., "Orthogonality Check and Correction of Measured Modes," AIAA Journal, Vol. 14, No. 2, February, 1976.

4–1 Hasselman, T.K., "Structural Uncertainty in Dynamic Analysis," Technical Paper No. 811049, SAE Transactions, 1981.

4–2 Hasselman, T.K. and Chrostowski, J.D., "Methods for Evaluating the Predictive Accuracy of Structural Dynamic Models," Technical Report No. 88–1146–1, Prepared by Engineering Mechanics Associates for the National Aeronautics and Space Administration, August, 1988.

4–3 Klir, G. and Folger T., "Fuzzy Sets, Uncertainty and Information," Prentice Hall, Englewood Cliffs, NJ, 1988.

4–4 Ross, T.J., and Hasselman, T.K., "Assessing Damping Uncertainty in Space Structures with Fuzzy Sets," Shock and Vibration Technology Review, Vol. 1, No. 10, Shock and Vibration Information Analysis Center, October, 1991.

4–5 Dong, W., and Shah, H., "Vertex Method for Computing Functions of Fuzzy Variables", Journal of Fuzzy Sets and Systems," Vol. 24, pp. 65–78, 1987.

4–6 Vanderplaats, G., Numerical Optimization Techniques for Engineering Design: With Applications, McGraw Hill, 1984.

5–1 "SSID/PDAC Theoretical Manual (Version 1.0)", Report No. TR–91–1152–1, prepared by Engineering Mechanics Associates for the National Aeronautics and Space Administration, December, 1991.

5–2 "SSID/PDAC User's Manual (Version 1.0)", Report No. TR–91–1152–2, prepared by Engineering Mechanics Associates for the National Aeronautics and Space Administration, December, 1991.

5–3 "SSID/PDAC Demonstration Manual (Version 1.0)", Volumes I and II, Report No. TR–91–1152–3, prepared by Engineering Mechanics Associates for the National Aeronautics and Space Administration, December, 1991.

6–1 Noll, C., Pappa, R. and Perez, S., "Comparisons of Mini–Mast Experimental and NASTRAN–Predicted Frequency Response Functions (CSI Configuration), Revised NASTRAN Model with Plate Dynamics," NASA Langley Research Center, September 12, 1989.

6–2 Hasselman, T.K. and Chrostowski, J.D., "A Recent Case Study in System Identification," Paper No. AIAA–91–1190, Proceedings of the 32nd SDM Conference, CP–911, April 8–10, 1991.

6–3 Belvin, W.K., et. al., "Langley's CSI Evolutionary Model: Phase 0," Preliminary Report, NASA Langley Research Center, August 12, 1991.

APPENDIX A

Mass and Stiffness Uncertainty Database

The mass and stiffness uncertainty database compiled under this project is contained in Tables A–1 through A–22. The data are grouped into three generic categories as follows:

Tables A–1 through A–7:	Research Models of Large Space Structures (LSS)
Tables A–8 through A–14:	Pretest Models of Conventional Space Structures (CSS)
Tables A–15 through A–22:	Posttest Models of Conventional Space Structures (CSS)

The tables are presented in two parts. Part (a) lists the paired modes, showing both analysis and test frequencies, the cross–orthogonality between analysis and test modes, and a general description of the modes. The mode description in the LSS portion of the database can be interpreted with reference to the information presented in Section 2. Since the identity of Conventional Space Structures is not disclosed in this report, the mode descriptions serve only to identify the general character of the modes as given by the contributing organizations. To some extent, local appendage modes can be distinguished from primary structural modes based on these descriptions. However, it is not possible to do so in all cases. Some of the abbreviations cannot be understood without identifying the structure, and the degree of coupling between appendage motion and motion of the primary structure is such that a clear distinction cannot always be made. Nevertheless, the mode descriptions are included for the useful information they do provide.

Two general criteria were used in selecting the modes to include in this database.

1. The analysis modes should (in some sense) be a complete representation of the mass and stiffness characteristics of the structure within the frequency range spanned by the modes.

2. The test modes should (in some sense) be completely represented by the analysis modes.

The sense in which each of these criteria are satisfied is discussed below.

Complete representation of the mass and stiffness characteristics of the structure within the frequency range spanned by the modes implies that no analysis modes are skipped within that frequency range. For the most part, analysis and test modes tend to correlate well at low frequencies, and poorly at higher frequencies. There is often a clear transition between the two regimes so that the modes can be truncated at a frequency below which every analysis mode correlates with one of the test modes. This was true for all of the structures in the LSS database. Within the frequency ranges spanned by the included modes, no analysis modes were skipped. Of the 61 modes included in the database, 77% had cross–orthogonalities of at least 0.90, and only 5% had cross–orthogonalities less than 0.70, the smallest being 0.64.

The CSS database is not as clear cut. Analysis modes are occasionally skipped and some of the cross–orthogonalities are lower, especially for the pretest models. Skipped modes and cross–orthogonalities less than 0.50 are noted in the tables. The intent is still to truncate the analysis modes when correlation with the test modes becomes poor. However, in a few cases no test mode could be found to correlate with an analysis mode, in which case the analysis mode was omitted. In one case (Table A–11) fourteen analysis modes are skipped between the 4th and 5th mode listed. However, all of these are identified as local appendage modes which do not contribute significantly to the effective mass of the structure at the spacecraft/launch vehicle interface. In fact, while the two skipped modes between the 2nd and 3rd listed modes could not be definitely identified as local appendage modes, they nevertheless do not contribute significantly to the effective mass and therefore are not important for calculating spacecraft/launch vehicle interface loads.

A general assumption has been made in the interpretation of these data. It is assumed that all of the important modes of the structure were recorded during testing, i.e. that the primary objective of the modal survey was accomplished. Completeness of the mass and stiffness representation of the structure is therefore guaranteed provided that the

second criterion is satisfied, i.e. that the test modes are "completely" represented by a linear combination of the corresponding analysis modes. Completeness in this case refers to the definition given in Equation (2–36) which is

$$\text{Percent completeness} = 100\% \sqrt{\psi_j^T \psi_j}$$

where ψ_j is the jth column of the cross–orthogonality matrix.

It may be noted that each column of the cross–orthogonality matrices presented in Part (b) of Tables A–1 through A–22 is followed by a number (close to unity) which is the sum of the squares ("SUM SQ") of the numbers in that column, i.e.

$$\text{SUM SQ} = \psi_j^T \psi_j$$

Thus, even when the cross–orthogonality between a particular analysis mode and test mode is not close to unity, as long as all of the significant modes are included in the test mode set, ϕ, and $\psi_j^T \psi_j$ is close to unity, the essential mass and stiffness characteristics of the model will be represented.

Table A-1. Analysis and Test Data for LSS 1, LaRC Mini-Mast Structure.

(a) Modal Frequencies

Mode No.	Analysis Freq. (Hz)	Test Freq. (Hz)	Cross Ortho	Mode Description
1.	0.801	0.854	0.78	1st bending, X and Y
2.	0.812	0.862	0.86	1st bending, X and Y
3.	4.410	4.100	0.98	1st twist
4.	6.189	6.054	0.95	2nd bending, X and Y
5.	6.232	6.109	0.96	2nd bending, X and Y

(b) Cross-orthogonality Matrix

Freq	0.85	0.86	4.10	6.05	6.11
0.80	0.78	-.49	0.12	0.00	-.02
0.81	0.61	0.86	0.08	-.03	0.00
4.41	0.09	-.05	0.98	0.00	-.04
6.19	-.02	0.03	-.02	0.95	-.25
6.23	-.07	0.00	-.04	0.28	0.96
SUM SQ	0.99	0.98	0.98	0.98	0.99

Table A-2. Analysis and Test Data for LSS 2, LaRC Ten Bay Truss.

(a) Modal Frequencies

Mode No.	Analysis Freq. (Hz)	Test Freq. (Hz)	Cross Ortho	Mode Description
1.	17.889	18.048	1.00	1st bending, Y and Z
2.	17.892	18.040	0.94	1st bending, Y and Z
3.	63.047	68.043	0.99	1st twist
4.	93.569	92.610	0.83	2nd bending, Y and Z
5.	94.011	91.634	0.96	2nd bending, Y and Z
6.	170.688	160.764	0.99	1st axial
7.	192.093	200.153	0.90	2nd twist
8.	219.786	200.195	0.89	3rd bending, Y and Z
9.	225.218	192.538	0.68	3rd bending, Y and Z

(b) Cross-orthogonality Matrix

Freq	18.05	18.04	68.04	92.61	91.63	160.76	200.15	200.20	192.54
17.89	1.00	-.35	0.06	0.04	0.06	0.03	-.09	-.07	0.07
17.89	0.02	0.94	0.00	-.02	-.06	0.01	-.05	-.10	0.20
63.05	0.00	0.03	0.99	-.02	0.00	0.02	-.10	-.04	-.12
93.57	0.01	0.00	-.03	0.83	-.19	0.02	0.10	0.21	-.03
94.01	-.02	0.02	-.02	0.53	0.96	0.02	-.07	-.16	0.24
170.69	0.00	0.00	-.01	0.04	0.02	0.99	0.20	0.04	0.06
192.09	-.01	0.01	0.04	-.04	-.07	-.06	0.90	0.04	0.28
219.79	0.00	0.00	-.01	-.07	-.06	-.02	0.17	0.89	0.48
225.22	-.01	0.03	0.03	0.02	-.03	0.00	-.25	-.30	0.68
SUM SQ	1.00	1.01	0.99	0.98	0.97	0.99	0.98	0.97	0.89

Table A-3. Analysis and Test Data for LSS 3, JPL Precision Truss Structure.

(a) Modal Frequencies

Mode No.	Analysis Freq. (Hz)	Test Freq. (Hz)	Cross Ortho	Mode Description
1.	8.21	8.31	0.90	1st bending, Z
2.	10.72	10.79	0.98	1st bending, Y
3.	11.31	11.51	0.98	1st twist
4.	34.99	35.52	0.97	2nd bending, Z

(b) Cross-orthogonality Matrix

Freq	8.31	10.79	11.51	35.53
8.21	0.90	-.07	0.04	0.00
10.72	0.05	0.98	0.17	-.01
11.32	-.04	-.05	0.98	0.03
34.99	0.00	0.02	-.01	0.97
SUM SQ	0.81	0.97	0.99	0.94

Table A-4. Analysis and Test Data for LSS 4, JPL Tetrahedral Bay Cantilevered Truss Beam.

(a) Modal Frequencies

Mode No.	Analysis Freq. (Hz)	Test Freq. (Hz)	Cross Ortho	Mode Description
1.	10.73	10.61	0.99	1st bending, vertical
2.	19.90	17.51	0.97	1st bending, horizontal
3.	37.87	37.99	0.99	1st twist
4.	54.27	55.02	0.99	2nd bending, vertical
5.	78.15	71.83	0.88	2nd bending, horizontal

(b) Cross-orthogonality Matrix

Freq	10.61	17.51	37.99	55.02	71.83
10.73	0.99	0.00	-.07	0.12	0.01
19.90	-.04	0.97	0.07	0.02	0.05
37.87	-.02	0.06	0.99	-.06	0.12
54.27	0.01	0.04	-.03	0.99	0.10
78.15	0.00	-.19	0.11	-.03	0.88
SUM SQ	0.98	0.98	1.00	1.00	0.80

Table A-5. Analysis and Test Data for LSS 5, JPL Tetrahedral Bay Free-Free Truss Beam.

(a) Modal Frequencies

Mode No.	Analysis Freq. (Hz)	Test Freq. (Hz)	Cross Ortho	Mode Description
1.	16.28	17.94	0.97	1st bending, vertical
2.	27.76	29.87	0.99	1st bending, horizontal
3.	33.31	34.13	0.99	1st twist
4.	42.04	45.66	0.96	2nd bending, vertical
5.	65.79	66.71	0.92	2nd bending, horizontal
6.	67.13	69.17	0.97	2nd twist

(b) Cross-orthogonality Matrix

Freq	17.94	29.87	34.13	45.66	66.71	69.17
16.28	0.97	0.00	0.05	-.12	0.03	0.04
27.76	0.02	0.99	-.05	0.00	0.11	-.16
33.31	0.00	-.04	0.99	0.05	0.01	-.01
42.04	0.02	-.02	0.01	0.96	0.00	0.01
65.79	0.01	0.02	-.02	-.02	0.92	0.02
67.13	0.00	0.03	0.00	0.00	0.01	0.97
SUM SQ	0.94	0.98	0.99	0.94	0.86	0.97

Table A-6. Analysis and Test Data for LSS 6, PACOSS Dynamic Test Article.

(a) Modal Frequencies

Mode No.	Analysis Freq. (Hz)	Test Freq. (Hz)	Cross Ortho	Mode Description
1.	1.00	1.03	0.96	1st blanket bending, solar array 1
2.	1.03	1.10	0.99	1st blanket bending, solar array 2
3.	2.61	2.61	0.97	1st symetric ring truss bending
4.	3.01	2.81	0.64	Symmetric horizontal solar array mast bending
5.	3.08	2.89	0.68	Anti-symmetric horizontal solar array mast bending
6.	3.29	3.25	0.93	Anti-symmetric solar array vertical bending w/box truss rocking
7.	3.50	3.53	0.88	Anti-symmetric solar array vertical bending w/tripod
8.	3.70	3.72	0.97	Equip platform vertical bending w/ tripod & solar array symmetric bending
9.	3.81	4.13	0.99	Equip platform horizontal bending
10.	4.14	4.15	0.91	1st blanket torsion, solar array 1
11.	4.15	4.24	0.93	1st blanket torsion, solar array 2
12.	4.60	4.83	0.88	Symmetric antenna bending w/tripod bending
13.	4.81	5.04	0.94	Symmetric antenna dish, equipment platform, tripod
14.	4.86	4.96	0.97	Tripod torsion
15.	5.32	5.42	0.98	2nd blanket bending, solar array 2
16.	5.32	5.43	0.95	2nd blanket bending, solar array 1
17.	6.12	6.48	0.91	Anti-symmetric tripod bending w/box rocking & solar array vertical bending
18.	7.52	9.40	0.76	Symmetric antenna dish bending
19.	8.94	8.89	0.96	2nd blanket torsion, solar array 1
20.	8.95	9.32	0.99	2nd blanket torsion, solar array 2
21.	9.04	8.92	0.97	Anti-symmetric tripod bending
22.	9.28	9.26	0.88	Symmetric tripod bending w/antenna and ring bending

Table A-6. Analysis and Test Data for LSS 6, PACOSS Dynamic Test Article (Cont'd).

(b) Cross-orthogonality Matrix

Freq	1.03	1.10	2.61	2.81	2.89	3.25	3.53	3.72	4.13
1.00	0.96	0.00	-.14	0.46	-.23	-.11	0.00	-.10	0.00
1.03	0.21	0.99	0.00	0.55	-.63	0.00	0.00	0.00	0.00
2.61	0.00	0.00	0.97	-.14	0.00	0.00	0.00	0.00	0.00
3.01	0.00	0.00	0.00	0.64	0.13	0.00	0.00	0.00	0.00
3.08	0.00	0.00	0.00	-.11	0.68	0.00	0.00	0.00	0.00
3.29	0.00	0.00	0.00	0.00	0.00	0.93	-.35	0.00	0.00
3.50	0.00	0.00	0.00	0.00	0.00	0.30	0.88	0.00	0.00
3.70	0.00	0.00	0.00	0.00	0.00	0.00	0.00	0.97	0.00
3.81	0.00	0.00	0.00	0.00	0.00	0.00	0.00	0.00	0.99
SUM SQ	0.97	0.98	0.96	0.96	0.93	0.97	0.90	0.95	0.98

Table A-7. Analysis and Test Data for LSS 7, PACOSS Solar Array.

(a) Modal Frequencies

Mode No.	Analysis Freq. (Hz)	Test Freq. (Hz)	Cross Ortho	Mode Description
1.	0.89	0.93	0.99	1st blanket/TMD (blanket and TMDs in phase)
2.	2.90	2.8	0.93	Blanket/mast horizontal bending
3.	3.75	3.7	0.82	1st mast/blanket torsion mode
4.	4.07	4.0	0.97	Vertical mast bending
5.	5.36	5.3	0.99	2nd horizontal blanket bending mode (TMD second mode coupled)
6.	8.84	9.0	0.99	2nd blanket/mast torsion
7.	10.51	9.8	0.95	3rd blanket horizontal bending
8.	12.43	12.8	0.93	3rd blanket torsion
9.	15.95	16.6	1.00	4th blanket torsion

(b) Cross-orthogonality Matrix

Freq	0.93	2.80	3.70	4.00	5.30	9.00	9.80	12.80	16.60
0.89	0.99	-.18	0.40	0.18	0.00	0.00	0.00	0.00	0.00
2.90	0.00	0.93	0.00	0.00	0.00	0.00	0.00	0.00	0.00
3.75	0.14	0.29	0.82	-.14	0.00	0.00	0.00	0.00	0.00
4.07	0.00	0.16	-.29	0.97	0.00	0.00	0.00	0.00	0.00
5.36	0.00	0.00	0.00	0.00	0.99	-.12	0.00	0.00	0.00
8.84	0.00	0.00	0.00	0.00	0.00	0.99	0.18	0.00	0.00
10.51	0.00	0.00	0.00	0.00	0.00	0.10	0.95	-.30	0.00
12.43	0.00	0.00	0.00	0.00	0.00	0.00	0.25	0.93	0.00
15.95	0.00	0.00	0.00	0.00	0.00	0.00	0.00	0.15	1.00
SUM SQ	1.00	1.01	0.92	0.99	0.98	1.00	1.00	0.98	1.00

Table A-8. Analysis and Test Data for for CSS 1, Pretest Model.

(a) Modal Frequencies

Mode No.	Analysis Freq. (Hz)	Test Freq. (Hz)	Cross Ortho	Mode Description
1.	13.49	13.71	0.97	HGA bending X
2.	13.74	13.69	0.96	HGA bending Y
3.	16.44	18.59	0.96	Science boom X
4.	18.15	17.95	0.86	Core bending +Y, -X
5.	18.83	17.66	0.71	Core bending +X, -Y
6.	20.42	23.08	0.53	RTG Z; probe Y; science boom Z
7.	20.52	21.60	0.78	RTG Z; RPM bus X
8.	21.27	24.85	0.94	Torsion
9.	22.97	23.58	0.57	RTG Z; probe Y; science boom Z

(b) Cross-orthogonality Matrix

Freq	13.71	13.69	18.59	17.95	17.66	23.08	21.60	24.85	23.58
13.49	0.97	0.06	0.13	0.15	0.49	0.01	-.04	0.03	-.01
13.74	-.05	0.96	0.02	-.29	-.07	0.03	0.02	0.02	-.01
16.44	0.07	-.02	0.96	-.19	-.33	0.04	-.11	-.08	-.02
18.15	0.00	0.20	-.01	0.86	0.21	-.20	-.03	-.03	0.08
18.83	-.15	-.05	0.39	0.22	0.71	0.04	-.02	0.02	-.03
20.42	-.04	0.02	0.03	0.08	0.07	0.53	0.58	0.09	-.35
20.52	0.01	-.09	0.07	0.02	0.09	-.52	0.78	-.02	0.28
21.27	0.02	0.00	-.04	0.03	0.00	-.03	-.02	0.94	-.07
22.97	0.02	-.07	0.02	0.00	0.00	-.36	0.08	0.13	0.57
SUM SQ	0.97	0.98	1.10	0.94	0.92	0.73	0.97	0.92	0.54

Table A-9. Analysis and Test Data for CSS 2, Pretest Model.

(a) Modal Frequencies

Mode No.	Analysis Freq. (Hz)	Test Freq. (Hz)	Cross Ortho	Mode Description
1.	14.51	16.27	1.00	First Y bending
2.	15.20	17.08	1.00	First X bending
3.	39.14	52.70	0.97	Probe fixture Y
4.	41.11 (1)	44.96	1.00	Bounce
5.	44.18	49.92	0.99	Torsion

Note:
(1) Analysis mode at 39.37 Hz. was skipped. Maximum cross-orthogonality of this mode with respect to test modes listed above is 0.14.

(b) Cross-orthogonality Matrix

Freq	16.27	17.08	52.70	44.96	49.92
14.51	1.00	0.01	-.17	-.01	-.01
15.20	-.01	1.00	-.05	0.00	0.00
39.14	-.12	0.02	0.97	0.04	0.12
41.11	0.02	0.00	-.02	1.00	-.02
44.18	0.01	0.00	-.11	0.01	0.99
SUM SQ	1.01	1.00	0.98	1.00	1.00

Table A-10. Analysis and Test Data for CSS 3, Pretest Model.

(a) Modal Frequencies

Mode No.	Analysis Freq. (Hz)	Test Freq. (Hz)	Cross Ortho	Mode Description
1.	13.54	14.49	0.97	First Y bending
2.	14.17	15.41	0.97	First X bending
3.	18.83	18.28	0.94	Second Y bending
4.	19.58	19.63	0.96	Second X bending
5.	40.62 (1)	44.49	1.00	Bounce
6.	44.16	49.97	0.99	Torsion

Note:
(1) Analysis modes skipped at 39.01 and 39.24 Hz. Maximum cross-orthogonality of these modes with respect to test modes listed above is 0.12.

(b) Cross-orthogonality Matrix

Freq	14.49	15.41	18.28	19.63	44.49	49.97
13.54	0.97	-.07	-.29	-.02	0.01	-.01
14.17	0.04	0.97	-.01	-.20	0.00	0.00
18.83	0.29	-.02	0.94	-.11	0.00	0.00
19.58	0.05	0.25	0.08	0.96	0.00	0.00
40.62	-.01	0.00	0.01	-.01	1.00	0.02
44.16	0.01	0.00	-.01	0.00	-.02	0.99
SUM SQ	1.03	1.01	0.97	0.97	1.00	0.98

Table A-11. Analysis and Test Mode Frequencies for CSS 4, Pretest Model.

(a) Modal Frequencies

Mode No.	Analysis Freq. (Hz)	Test Freq. (Hz)	Cross Ortho	Mode Description
1.	13.42	14.45	0.94	First Y bending
2.	14.05	15.42	0.90	First X bending
3.	18.85 (1)	18.31	0.63	Second Y bending
4.	19.55	19.59	0.95	Second X bending
5.	40.60 (2)	44.77	0.97	Bounce
6.	45.02	50.29	0.95	Torsion

Notes:

(1) Analysis modes skipped at 18.65 and 18.74 Hz. Maximum cross-orthogonality of these modes with respect to test modes listed above is 0.31.

(2) Fourteen analysis modes skipped in frequency range of 20.26 - 39.65 Hz. Maximum cross-orthogonality with respect to test modes listed above is 0.29.

(b) Cross-orthogonality Matrix

Freq	14.45	15.42	18.31	19.59	44.77	50.29
13.42	0.94	-.04	-.25	0.01	-.04	0.00
14.05	0.05	0.90	-.02	0.17	0.02	-.02
18.85	0.23	-.02	0.63	0.05	0.00	0.00
19.55	-.05	-.22	-.08	0.95	0.00	0.01
40.60	0.00	0.02	-.01	-.02	0.97	-.02
45.02	0.01	0.00	0.00	0.00	0.03	0.95
SUM SQ	0.94	0.86	0.47	0.93	0.94	0.90

Table A-12. Analysis and Test Data for CSS 5, Pretest Model.

(a) Modal Frequencies

Mode No.	Analysis Freq. (Hz)	Test Freq. (Hz)	Cross Ortho	Mode Description
1.	29.81	29.38	0.90	Primary reflector rocking about X axis
2.	34.92	29.88	0.91	X translation
3.	41.21	40.13	0.83	Primary reflector in-plane translation
4.	42.11	35.55	0.49 (1)	Radiometer +X, reflector -X
5.	46.19	41.66	0.97	Radiometer torsion about Y axis
6.	55.20	46.34	0.76	Secondary reflector X
7.	59.99	59.54	0.68	Secondary reflector Z
8.	66.83	68.60	0.64	Secondary reflector torsion
9.	106.35 (2)	95.99	0.91	Radiometer Y

Notes:

(1) Although the cross-orthogonality of this mode pair is less than 0.50, the test mode is 94% represented by a linear combination of the analysis modes listed above.

(2) Four local analysis modes skipped in frequency range of 77.76 - 104.57 Hz. Maximum cross-orthogonality of these modes with respect to test modes listed above is 0.20.

Table A-12. Analysis and Test Data for CSS 5, Pretest Model (Cont'd).

(b) Cross-orthogonality Matrix

Freq	29.38	29.88	40.13	35.55	41.66	46.34	59.54	68.60	95.99
29.81	0.90	-.10	0.07	-.16	-.02	0.15	0.26	-.28	0.00
34.92	0.29	0.91	-.17	0.46	0.12	0.33	-.17	0.00	0.03
41.21	-.02	-.17	0.83	0.41	-.14	0.37	0.32	0.23	0.02
42.11	0.00	-.18	-.55	0.49	-.20	0.38	-.39	-.13	-.04
46.19	-.07	-.02	-.13	0.02	0.97	0.17	-.08	0.05	-.13
55.20	-.09	-.18	0.10	-.49	0.01	0.76	-.03	-.18	0.11
59.99	0.21	-.01	0.03	0.02	0.00	-.06	0.68	-.67	-.07
66.83	-.06	-.06	0.17	-.03	-.04	0.12	0.67	0.64	-.01
106.35	0.01	0.14	0.09	-.01	-.01	-.03	-.05	0.00	0.91
SUM SQ	0.96	0.96	1.09	0.89	1.02	1.04	1.27	1.04	0.87

Table A-13. Analysis and Test Data for CSS 6, Pretest Model.

(a) Modal Frequencies

Mode No.	Analysis Freq. (Hz)	Test Freq. (Hz)	Cross Ortho	Mode Description
1.	16.13	15.11	0.97	S/C X translation
2.	20.80	23.56	0.95	S/C Y translation
3.	23.73	27.08	0.72	S/C symmetric bending about Y axis
4.	24.99	25.70	0.69	EGRET/BATSE Y bending
5.	27.35	28.40	0.82	S/C torsion about Z axis

(b) Cross-orthogonality Matrix

Freq	15.11	23.56	27.08	25.70	28.40
16.13	0.97	-.01	-.06	0.23	-.03
20.80	0.01	0.95	0.00	0.09	0.15
23.73	0.13	0.03	0.72	-.58	-.02
24.99	-.11	-.04	0.57	0.69	-.11
27.35	0.00	-.18	0.10	0.09	0.82
SUM SQ	0.97	0.94	0.86	0.88	0.71

Table A-14. Analysis and Test Data for CSS 11, Pretest Model.

(a) Modal Frequencies

Mode No.	Analysis Freq. (Hz)	Test Freq. (Hz)	Cross Ortho	Mode Description
1.	15.00	16.15	0.99	Y bending fundamental
2.	16.03	18.24	0.97	X bending fundamental
3.	22.32	28.52	0.92	Thruster X
4.	23.03	24.15	0.95	Thruster Y
5.	26.03	26.58	0.87	Subnadir
6.	26.76	25.71	0.98	OX tank 2 torsion
7.	31.18 (1)	31.59	0.94	OX1 OX2 lateral
8.	32.18	31.36	0.76	Subnadir
9.	34.01	35.50	0.72	OX 2 tank lateral
10.	34.34	36.12	0.97	OX1 OX2 X

Note:
(1) Analysis mode skipped at 27.24 Hz. Maximum cross-orthogonality of this mode with respect to test modes listed above is 0.30.

Table A-14. Analysis and Test Data for CSS 11, Pretest Model (Cont'd).

(b) Cross-orthogonality Matrix

Freq	16.15	18.24	28.52	24.15	26.58	25.71	31.59	31.36	35.50
15.00	0.99	0.11	0.00	0.00	0.00	0.00	0.00	0.00	0.00
16.03	0.00	0.97	0.00	0.00	0.00	0.00	0.00	0.00	0.00
22.32	0.00	0.00	0.92	-.29	0.00	0.00	0.00	0.00	0.00
23.03	0.00	0.00	0.28	0.95	0.00	0.00	0.00	0.00	0.00
26.03	0.00	0.00	0.00	0.00	0.87	0.00	0.00	0.16	0.00
26.76	0.00	0.00	0.00	0.00	0.00	0.98	0.00	0.00	0.00
31.18	0.00	0.00	0.14	0.00	0.00	0.00	0.94	-.19	0.00
32.18	0.00	0.00	0.00	0.00	-.14	0.00	0.18	0.76	-.46
34.01	0.00	0.00	0.00	0.00	-.11	0.00	0.00	0.40	0.72
SUM SQ	0.98	0.95	0.94	0.99	0.79	0.96	0.92	0.80	0.73

Table A-15. Analysis and Test Data for CSS 2, Posttest Model.

(a) Modal Frequencies

Mode No.	Analysis Freq. (Hz)	Test Freq. (Hz)	Cross Ortho	Mode Description
1.	16.27	16.27	0.98	First Y bending
2.	17.18	17.08	0.98	First X bending
3.	45.21	44.96	0.97	Bounce
4.	50.76	49.92	0.95	Torsion
5.	58.09	52.70	0.98	Probe fixture Y

(b) Cross-orthogonality Matrix

Freq	16.27	17.08	44.96	49.92	52.70
16.27	0.98	0.05	0.05	-.01	-.03
17.18	0.01	0.98	0.00	-.02	0.00
45.21	-.01	0.00	0.97	0.02	0.08
50.76	0.00	0.00	-.02	0.95	0.04
58.09	0.06	0.00	-.04	-.12	0.98
SUM SQ	0.96	0.96	0.95	0.92	0.97

Table A-16. Analysis and Test Data for CSS 3, Posttest Model.

(a) Modal Frequencies

Mode No.	Analysis Freq. (Hz)	Test Freq. (Hz)	Cross Ortho	Mode Description
1.	14.75	14.49	0.99	First Y bending
2.	15.51	15.41	0.99	First X bending
3.	18.64	18.28	0.98	Second Y bending
4.	19.40	19.63	0.98	Second X bending
5.	44.67	44.49	0.97	Bounce
6.	46.80	49.97	0.94	Torsion

(b) Cross-orthogonality Matrix

Freq	14.49	15.41	18.28	19.63	44.49	49.97
14.75	0.99	0.04	-.08	-.06	0.03	-.01
15.51	-.06	0.99	-.01	-.04	0.00	-.01
18.64	0.06	0.03	0.98	-.09	-.02	0.01
19.40	0.03	-.01	0.09	0.98	0.00	-.01
44.67	-.01	0.00	0.01	0.00	0.97	-.02
46.80	0.00	0.01	0.00	0.01	0.02	0.94
SUM SQ	0.99	0.98	0.98	0.97	0.94	0.88

Table A-17. Analysis and Test Data for CSS 5, Posttest Model.

(a) Modal Frequencies

Mode No.	Analysis Freq. (Hz)	Test Freq. (Hz)	Cross Ortho	Mode Description
1.	29.35	29.39	0.97	Primary reflector rocking about X axis
2.	29.94	29.88	0.92	X translation
3.	35.79	35.55	0.89	Radiometer +X, reflector -X
4.	39.64	40.13	0.93	Primary reflector in-plane translation
5.	41.40	41.66	0.92	Radiometer torsion about Y axis
6.	46.13	46.34	0.95	Secondary reflector X
7.	60.53	59.54	0.64	Secondary reflector Z
8.	67.05	68.60	0.63	Secondary reflector torsion
9.	94.20 (1)	95.99	0.97	Radiometer Y

Note:
(1) Three analysis modes skipped in frequency range of 77.08 - 86.86 Hz. Maximum cross-orthogonality of these modes with respect to test modes listed above is 0.15.

Table A-17. Analysis and Test Data for CSS 5, Posttest Model (Cont'd).

(b) Cross-orthogonality Matrix

Freq	29.39	29.88	35.55	40.13	41.66	46.34	59.54	68.60	95.99
29.35	0.97	0.25	-.09	-.04	0.01	-.01	-.12	-.10	0.01
29.94	0.12	0.92	-.30	0.03	0.02	0.16	-.09	0.06	0.06
35.79	-.01	0.21	0.89	-.08	0.05	-.14	0.11	-.05	0.10
39.64	0.03	0.01	0.09	0.93	0.37	0.10	0.22	-.08	-.01
41.40	-.05	-.06	-.03	-.21	0.92	-.05	-.13	0.05	0.01
46.13	-.07	-.15	0.24	-.08	-.07	0.95	-.43	0.06	0.00
60.53	0.09	0.02	-.06	-.06	0.01	0.05	0.64	0.68	-.01
67.05	-.04	-.03	0.12	0.20	-.04	-.07	-.48	0.63	-.02
94.20	-.01	-.03	-.02	0.00	-.08	0.02	-.03	0.01	0.97
SUM SQ	0.97	0.98	0.98	0.97	1.00	0.97	0.93	0.89	0.96

Table A-18. Analysis and Test Data for CSS 7, Posttest Model.

(a) Modal Frequencies

Mode No.	Analysis Freq. (Hz)	Test Freq. (Hz)	Cross Ortho	Mode Description
1.	6.97	7.04	0.84	Primary bending Y
2.	7.06	7.16	0.86	Primary bending Z
3.	14.12	14.30	0.85	Solid rocket motor Y
4.	14.59	14.69	0.74	Solid rocket motor Z, Y
5.	14.61	14.56	0.69	Solid rocket motor Z, Y
6.	15.25	15.46	0.98	Appendage Z
7.	16.74	16.51	0.98	Appendage Z
8.	17.44	17.26	0.95	Appendage Y
9.	19.08	19.97	0.95	Appendage Z, Y
10.	20.44	20.21	0.85	Appendage Y
11.	20.67	20.65	0.92	Tank Z
12.	21.40	21.47	0.94	Primary axial
13.	23.21	23.65	0.94	Secondary bending X, Y
14.	24.56	24.23	0.95	Secondary bending, X, Y, Z
15.	25.17	24.86	0.94	Tanks X, Y
16.	26.03	25.79	0.83	Tank Y
17.	26.69	27.06	0.72	Solid rocket motor X
18.	26.99	27.53	0.88	Tanks Y, Z
19.	27.38	27.77	0.88	Tank Z
20.	27.69	28.11	0.84	Tank Z

Table A-18. Analysis and Test Data for CSS 7, Posttest Model.

(a) Modal Frequencies (Cont'd)

Mode No.	Analysis Freq. (Hz)	Test Freq. (Hz)	Cross Ortho	Mode Description
21.	29.99 (1)	29.83	0.74	Tanks X, Y
22.	30.13	29.99	0.54	Tank X
23.	31.23	30.49	0.81	Tanks X, Y
24.	31.99	31.44	0.86	Tanks X, Y
25.	32.52	32.66	0.82	Tank Z
26.	37.37	36.04	0.78	Tank X, Z
27.	37.66	35.67	0.88	Tanks X, Y, Z
28.	37.86	35.49	0.71	Tanks X, Y, Z
29.	40.49	40.36	0.90	Appendage X
30.	43.05	38.38	0.91	Tanks X, Y, RX, RY
31.	43.79	42.23	0.92	Tanks X, RX, RY
32.	47.43	45.29	0.69	N/A
33.	49.46 (2)	44.36	0.90	N/A
34.	50.52	46.50	0.92	N/A

Note:

(1) Analysis mode skipped at 29.24 Hz. Maximum cross orthogonality of this mode with respect to test modes listed above is 0.23.

(2) Analysis mode skipped at 48.09 Hz. Maximum cross orthogonality of this mode with respect to test modes listed above is 0.28.

Table A-18. Analysis and Test Data for CSS 7, Posttest Model (Cont'd).

(b) Cross-orthogonality Matrix

Freq	7.04	7.16	14.30	14.69	14.56	15.48	16.51	17.26	19.97
6.97	0.84	0.49	-.02	-.02	0.02	-.02	0.00	-.02	0.00
7.06	-.50	0.86	0.00	-.02	0.01	0.00	0.00	0.02	-.01
14.12	0.03	0.00	0.85	-.30	0.37	-.02	-.01	0.04	0.04
14.59	-.02	0.01	0.45	0.74	-.42	0.00	0.02	-.02	-.06
14.61	0.06	0.02	-.11	0.58	0.69	-.08	-.03	0.04	-.03
15.25	0.02	0.00	-.01	0.06	0.08	0.98	0.00	0.11	-.03
16.74	0.00	0.00	-.02	0.01	0.07	0.02	0.98	-.15	0.04
17.44	0.00	-.01	-.02	0.00	0.00	-.12	0.15	0.95	-.14
19.08	0.00	0.01	-.02	0.09	-.03	0.00	-.01	0.18	0.95
SUM SQ	0.96	0.98	0.94	0.99	0.80	0.98	0.98	0.97	0.93

Table A-19. Analysis and Test Data for CSS 8, Posttest Model.

(a) Modal Frequencies

Mode No.	Analysis Freq. (Hz)	Test Freq. (Hz)	Cross Ortho	Mode Description
1.	37.13	41.64	0.98	X axis translation
2.	41.52	44.91	0.96	Z axis translation
3.	64.55	75.18	0.95	Y axis rotation
4.	80.57	93.77	0.83	Local radiator bending

(b) Cross-orthogonality Matrix

Freq	41.64	44.91	75.18	93.77
37.13	0.98	-.18	-.01	-.01
41.52	0.14	0.97	0.01	0.06
64.55	-.06	0.02	0.95	-.30
80.57	0.03	0.01	-.03	0.83
SUM SQ	0.98	0.97	0.90	0.78

Table A-20. Analysis and Test Data for CSS 9, Posttest Model.

(a) Modal Frequencies

Mode No.	Analysis Freq. (Hz)	Test Freq. (Hz)	Cross Ortho	Mode Description
1.	6.13	5.84	0.98	Fundamental Z
2.	7.36	7.31	0.94	Fundamental X
3.	9.98	10.86	0.98	MMS-Y; CLAES-Y
4.	10.59	10.36	0.73	IM-Z; MMS-Z; SSPP-Z
5.	12.71	12.80	0.84	Fundamental Y
6.	16.33	16.87	0.79	SSPP-X,Y; MMS-Y; IM-Y
7.	18.09	17.32	0.85	CLAES-Z; MMS-Z; SA-Z
8.	18.59	18.23	0.64	SSPP-Z,X; SA-Z
9.	19.00	20.41	0.66	Outrigger mode
10.	20.42	19.60	0.42 (1)	SSPP-Z; IM/X; CLAES-Z
11.	20.95	21.41	0.93	Keel mode
12.	22.05	23.48	0.71	HALOE-X; SSPP-Z; SA-Y,Z
13.	22.43	20.97	0.79	Outrigger mode
14.	24.79	24.51	0.57	SSPP-X,Z; CLASE-Y

Note:
(1) Although the cross orthogonality of this mode pair is less than 0.50, the test mode is 85% represented by a linear combination of the analysis modes listed above.

Table A-20. Analysis and Test Data for CSS 9, Posttest Model (Cont'd)

(b) Cross-orthogonality Matrix

Freq	5.84	7.31	10.86	10.36	12.80	16.87	17.32	18.23	20.41
6.13	0.99	-.13	0.01	-.05	0.06	0.03	0.03	-.04	0.01
7.36	0.12	0.94	0.07	-.16	-.17	0.08	-.01	-.05	0.02
9.98	-.01	-.07	0.98	-.01	0.04	0.01	0.01	0.05	-.02
10.59	-.04	0.07	-.03	0.73	0.45	0.30	0.14	0.07	-.01
12.71	0.02	0.11	0.02	-.39	0.84	-.14	-.15	-.09	-.04
16.33	-.02	-.08	-.02	-.22	-.04	0.79	-.28	-.14	-.02
18.09	-.07	0.03	-.04	-.11	0.06	0.24	0.85	-.17	0.07
18.59	0.01	0.02	0.01	0.06	0.00	0.11	0.05	0.64	0.30
19.00	-.02	-.02	0.01	0.00	0.00	-.05	-.02	-.13	0.66
SUM SQ	1.00	0.93	0.97	0.78	0.95	0.81	0.85	0.49	0.53

Table A-21. Analysis and Test Data for CSS 10, Posttest Model.

(a) Modal Frequencies

Mode No.	Analysis Freq. (Hz)	Test Freq. (Hz)	Cross Ortho	Mode Description
1.	11.21	12.50	1.00	Fundamental Y-bending
2.	12.04	13.46	0.99	Fundamental X-bending
3.	18.43	21.47	0.97	Fundamental longitudinal Z
4.	20.61	22.91	0.78	Tank rotations
5.	22.59	23.45	0.85	Tank rotations
6.	23.77	25.57	0.87	Tank rotations
7.	23.90	30.59	0.89	Local S/A (+Y) flat panel mode
8.	25.22	27.56	0.91	Torsional mode
9.	27.13	33.82	0.88	Local S/A (-Y) flat panel mode
10.	29.09	29.89	0.88	S/A(+Y) flat panels + tanks
11.	30.18	31.55	0.89	S/A(+Y), tanks, cyl
12.	33.21	35.67	0.85	S/A($\pm$Y) panels (out of phase)

Table A-21. Analysis and Test Data for CSS 10, Posttest Model (Cont'd).

(b) Cross-orthogonality Matrix

Freq	12.50	13.46	21.47	22.91	23.45	25.57	30.59	27.56	33.82
11.21	1.00	-.08	0.00	0.02	-.02	-.03	0.01	0.01	0.00
12.04	0.04	0.99	0.00	-.03	0.00	0.04	0.01	-.01	-.02
18.43	-.02	0.02	0.97	0.11	-.07	-.06	-.02	-.12	-.03
20.61	0.03	0.02	-.15	0.78	-.46	-.26	-.03	0.01	0.01
22.59	0.00	0.00	0.01	0.52	0.85	0.00	0.13	-.03	0.07
23.77	-.01	-.01	0.05	0.26	-.11	0.87	-.13	0.19	0.02
23.90	-.01	0.00	-.01	-.01	-.14	0.22	0.89	-.26	-.04
25.22	0.02	0.00	0.12	-.09	-.04	-.05	0.24	0.91	-.08
27.13	0.00	0.00	0.01	-.02	-.03	0.01	0.05	0.10	0.88
SUM SQ	1.00	0.99	0.98	0.97	0.97	0.88	0.89	0.96	0.79

Table A-22. Analysis and Test Data for CSS 11, Posttest Model.

(a) Modal Frequencies

Mode No.	Analysis Freq. (Hz)	Test Freq. (Hz)	Cross Ortho	Mode Description
1.	16.60	16.15	0.99	Y-bending fundamental
2.	17.70	18.24	0.98	X-bending fundamental
3.	24.82	24.15	0.94	Thruster Y
4.	25.70	25.71	0.98	OX tank 2 torsion
5.	26.12 (1)	26.58	0.95	Subnadir
6.	28.71	28.52	0.92	Thruster X
7.	29.65	29.63	0.90	Cruciform
8.	30.20	29.76	0.91	Subnadir; Cruciform
9.	31.47	31.36	0.95	Subnadir
10.	31.66	31.59	0.98	OX1 OX2 lateral
11.	33.66	33.30	0.91	Subnadir; OX2 tank
12.	35.12	34.56	0.90	North panel
13.	35.38	35.50	0.94	OX2 tank lateral
14.	36.09	36.47	0.89	South panel
15.	37.58	36.12	0.95	OX1 OX2 X
16.	38.21	38.03	0.93	South panel
17.	38.77	37.87	0.94	North panel
18.	39.23	39.24	0.91	OX1 OX2 lateral
19.	41.76	40.43	0.91	Fuel 2 torsion
20.	42.42	42.46	0.88	Fuel 2 Y

Note:
(1) Analysis mode skipped at 26.04 Hz. Maximum cross orthogonality of this mode with respect to test modes listed above is 0.26.

Table A-22. Analysis and Test Data for CSS 11, Posttest Model.

(a) Modal Frequencies (Cont'd)

Mode No.	Analysis Freq. (Hz)	Test Freq. (Hz)	Cross Ortho	Mode Description
21.	42.67	43.43	0.73	Fuel 1 torsion; Fuel 1, 2 lateral
22.	42.88	42.91	0.93	Fuel 1 torsion
23.	44.50	46.60	0.89	Bus Z
24.	47.70	46.89	0.86	Fuel 1 X Fuel 2 Y
25.	47.98	47.30	0.86	Fuel 2 X Fuel 1 Y
26.	49.37	49.92	0.96	North, south panel
27.	50.15	50.76	0.91	North, south bus and battery Z

(b) Cross-orthogonality Matrix

Freq	16.15	18.24	24.15	25.71	26.58	28.52	29.63	29.76	31.36
16.60	0.99	0.00	0.00	0.00	0.00	0.00	0.00	0.00	0.00
17.70	0.00	0.98	0.00	0.00	0.00	0.00	0.00	0.00	0.00
24.82	0.00	0.00	0.94	0.00	0.00	0.31	0.00	0.00	0.00
25.70	0.00	0.00	0.00	0.98	0.00	0.00	0.00	0.00	0.00
26.12	0.00	0.00	0.00	0.00	0.95	0.00	0.00	0.00	0.00
28.71	0.00	0.00	-.33	0.00	0.00	0.92	0.00	0.00	0.00
29.65	0.00	0.00	0.00	0.00	0.00	0.00	0.90	0.00	0.00
30.20	0.00	0.00	0.00	0.00	0.00	0.00	0.00	0.91	-.13
31.47	0.00	0.00	0.00	0.00	0.00	0.00	0.00	0.10	0.95
SUM SQ	0.98	0.96	0.99	0.96	0.90	0.94	0.81	0.84	0.92

APPENDIX B

AIAA PAPER NO. AIAA–91–1190:
"A Recent Case Study in System Identification"

AIAA-91-1190

A Recent Case Study in System Identification

T.K. Hasselman and J.D. Chrostowski
Engineering Mechanics Associates

AIAA 32nd Structures, Structural Dynamics, and Materials Conference
April 8 - 10, 1991 / Baltimore, MD

A RECENT CASE STUDY IN SYSTEM IDENTIFICATION

T.K. Hasselman* and J.D. Chrostowski
Engineering Mechanics Associates

Abstract

A recent survey on system identification for large space structures [1] disclosed that the great majority of papers in the published literature present methods demonstrated with simulated data (i.e. "data" generated by perturbing an analytical model) or present the results of particular case studies in which selected parameters of a particular model were identified using a particular method with selected data. Few publications have addressed the practical problem of verifying a model of a real structure using real test data where the correctness of the model, correctness of the data, selection of parameters, and selection of data are critical issues.

One of the major drawbacks is the flexibility of available system identification software. This limitation has been partially alleviated by the development of a code called SSID (for Structural System Identification). This code interfaces with standard finite element modeling codes such as NASTRAN and offers numerous options for modeling, parameterization and data selection.

This paper presents a recent case study of a ten bay truss structure modeled and tested at the NASA Langley Research Center. Of particular interest are comparisons of results obtained by using different types of vibration test data including both eigenvalues and eigenvectors.

Introduction

System identification is the process of using the observed input to a system and its observed response (or output) to derive an analytical model. System identification applied to structural systems appeared in the technical literature during the 1960's and became a popular research topic during the 1970's. Hundreds of papers, numerous survey articles and several textbooks have since been written on the subject. One report [1] recently prepared by an ASCE committee of eight members including representatives from the Government, universities and private industry contains 207 references and a bibliography of over 500 publications. The great majority of these articles are essentially theoretical, some with numerical demonstrations. Relatively few address practical applications.

The development of system identification for structural dynamic applications may be grouped into three distinct areas, including identification of:

1. Input–output relationships,
2. Modal characteristics, and
3. Model parameters.

The first is well developed, particularly along the lines of frequency–domain spectral analysis. The second is still evolving but has seen extensive practical application during the past decade. The third area is just beginning to receive attention for practical application. One of the difficulties is that to be of practical use, model parameter identification must be linked to currently used modeling codes. This requirement has resulted in severe limitations, including cost, time and flexibility.

All methods for model parameter identification require the computation of parameter sensitivity to either modal characteristics or structural response. Some general modeling codes such as NASTRAN have a capability for design sensitivity analysis and compute these derivatives. NASTRAN, for example, computes derivatives of eigenvalues and eigenvectors with respect to model parameters. Several efforts have recently been reported where parameter estimation algorithms have been linked to NASTRAN. Some use only the eigenvalue sensitivities computed in NASTRAN [2] while others have attempted to use both eigenvalue and eigenvector sensitivities [3, 4, 5]. Limited studies have shown that parameter estimation based only on eigenvalue data can improve the eigenvalues while allowing the eigenvectors to deteriorate [6].

On the other hand, it is computationally expensive to compute eigenvector derivatives in NASTRAN. NASTRAN uses Nelson's method [7] for computing eigenvector derivatives which requires that the complete stiffness matrix be used in solving a full set of linear algebraic equations for every eigenvector derivative; i.e. the sensitivity of each eigenvector to every estimated parameter in every iterative cycle of the estimation must be evaluated. Bronowicki [5] has found a way to use intermediate NASTRAN output to implement Fox's method [8] of modal summation, thereby significantly reducing the computational effort. NASTRAN must still be called in each cycle of the iterative parameter estimation, however.

Another issue of practical concern is the selection of an estimation algorithm. Hasselman and Chrostowski, Ojalvo and Fries, among others, have used least square and Bayesian–type estimators [9, 3, 10], Martinez and Simonian have used Kalman filtering [11, 12, 13], while Bronowicki, Flanagan and Allen have used optimization algorithms [5, 2, 4]. Kalman filter algorithms have been used only with frequency response data, whereas optimization algorithms have so far been used only with eigenvalue and eigenvector data. Bayesian estimation algorithms have been used with all three. There is no reason, however, why any of the three algorithms could not be used with all three types of data. In fact, it is desirable to have the option of selecting the estimation algorithm as well as the type of data for any given application.

These are some of the issues which have motivated development of the code SSID (an acronym for Structural System Identification). SSID is a model verification code designed to improve existing analytical models, e.g. NASTRAN models, using vibration test data. SSID updates the original estimates of selected model parameters based on selected test data. The sections which follow highlight the features of SSID, and present some results of its application to a practical problem.

*President, Engineering Mechanics Associates
Member AIAA

SSID Code

SSID was developed for Sandia National Laboratories to be used as a research and production tool. As a research tool it was designed to be flexible, modular and expandable. As a production tool it was designed to be efficient and machine independent. It utilizes dynamic memory management and skyline matrix storage and has been run on machines ranging from a PC to a CRAY.

An important feature of SSID is its ability to interface with standard finite element codes. This, requires that an interface code be written to extract the necessary data files form the finite element code and translate them into SSID format. Such an interface code has been written by Sandia for NASTRAN, although some additional effort is presently required to generate the mass and stiffness sensitivity matrices which are not yet available from NASTRAN.

Other system identification codes have been written which interface with NASTRAN, e.g. [5, 6, 7]. These codes require looping back through NASTRAN in each cycle of the iterative parameter estimation. An iterative solution is required because the estimation problem is inherently nonlinear; eigenvalues, eigenvectors and frequency response are all nonlinear functions of the parameters being estimated. SSID, on the other hand, is designed to operate in a stand–alone mode once the basic modeling data are read in. The advantage of this feature is a large gain in efficiency making it possible to execute small to medium sized problems on a PC or a workstation. For example, 15 parameters of a 240 degree–of–freedom structure were updated after five estimation cycles using 33 eigenvalue and eigenvector data elements in approximately three minutes on an IBM PC–386/16 MHZ machine running under DOS and a 640K RAM ceiling The same problem on a Unix–based Silicon Graphics Personal Iris workstation ran ten times faster. The disadvantage is that while typical finite element codes compute mass and stiffness sensitivity matrices for purposes of design optimization and/or eigenvalue and eigenvector derivatives, they are treated as intermediate results and are not yet directly accessible. This situation is likely to change, however, as a need is established.

A top level flow diagram illustrating the operations performed in the finite element code (NASTRAN in this case) and SSID is shown in Figure 1. Three return loops are shown for updating the model after an iteration has been completed. The solid line represents the option implemented in the initial version of SSID. This loop enables SSID to execute in a stand–alone mode after receiving modeling data from NASTRAN. The inner loop will allow the updated model to be rerun in a reduced set of modal coordinates. This speeds up execution for large models. The outer loop will facilitate direct updating of the finite element model (in this case the NASTRAN bulk data deck). This will allow the estimation of parameters which appear nonlinearly in the mass or stiffness matrices, such as the thickness of a plate or the depth of a beam. When the mass or stiffness matrix are nonlinear in an estimation parameter, derivatives of the matrix must (in general) be reevaluated after each iteration. This necessitates looping back through the FEM code which is time consuming. When the mass and stiffness matrices are linear functions of the parameters, their derivatives are constant and need only be evaluated once. The FEM code does not need to be recalled until the final parameter estimates are ready to be run.

Finite Element Model of the NASA LaRC Ten Bay Truss

Figure 2 shows the nodal geometry of the NASA Langley Research Center (LaRC) Ten Bay Truss. A NASTRAN model was furnished by NASA. It consists of bar elements having six degrees of freedom per node. With 40 free nodes (the base being fixed) the model has 240 DOF. Mass was lumped at the nodes as point masses, which as it turns out, introduced a slight modeling error. The mass was distributed too far from the centerline of the truss. This resulted in the mass moment of inertia about the x–axis being too large, which caused the frequency of the first twisting mode to be too low by about 7%.

Vibration Test Data

Vibration testing was conducted on the Ten Bay Truss with its base fixed to ground. Multiple shakers were located at mid–span and the free end. Triaxial accelerometers were located at diagonally opposed corners at every other bay as shown in Figure 2. Multiple uncorrelated random inputs were applied by the shakers. Test modes computed by the ERA method produced complex modes. These modes were furnished by NASA. They were normalized to obtain a least squares fit on the phase angles in the complex plane, and a largest eigenvector element magnitude of 100. The procedure used by NASA and others for converting these complex modes to real modes is to compute the magnitude of each complex element and give it the sign of the dominant (real or imaginary) part of the eigenvector. The dominant part of the complex vector is that vector whose Euclidean norm is the greatest. The frequencies and self–orthogonality of these test modes is shown in Table 1. The test frequencies are obtained from the imaginary part of the complex eigenvector, $\lambda = \sigma + i\omega$, as

$$f_j = \omega_j/2\pi \tag{1}$$

the self–orthogonality matrix is

$$^{o}m = \phi_R^T \, {}^{o}M \phi_R \tag{2}$$

where ^{o}M is the original analytical mass matrix for the Test Analysis Model or TAM, reduced from the finite element model to the set of measurement coordinates, and ϕ_R is a matrix of the real test modes. Perfect self–orthogonality would result in $^{o}m = I$ where the test modes, ϕ_R, have been normalized to unit modal mass.

As can be seen in Table 1, orthogonality between the three sets of bending modes (Modes 1 and 2, 4 and 5, 8 and 9) and between the second twist mode (Mode 7) and the third set of bending modes is not particularly good due to the closeness in frequency between the modes and the consequent difficulty of obtaining "pure" experimental modes.

An attempt was made to condition these modes based on the orthogonalization method presented in Reference [14]. This method does two things in sequence: First, it renormalizes the phase angles of the complex modes such that the cross–orthogonality between the real and imaginary parts of the complex eigenvector is zero.

If the original jth complex mode is denoted by

$$\hat{\phi}_j = \hat{\phi}_{R_j} + i\,\hat{\phi}_{I_j} \tag{3}$$

this condition requires that the cross–orthogonality product with respect to the analytical mass matrix is zero.

$$\hat{\phi}_{R_j}^T \circ M \, \hat{\phi}_{I_j} = 0 \tag{4}$$

In this case, $\hat{\hat{\phi}}_{R_j}$ and $\hat{\hat{\phi}}_{I_j}$ are expressed as functions of the normalizing phase angles θ_{o_j}, by the following:

$$\hat{\hat{\phi}}_{R_{kj}} = A_{kj} \cos(\hat{\theta}_{kj} - \theta_{o_j}) \tag{5a}$$

$$\hat{\hat{\phi}}_{I_{kj}} = A_{kj} \sin(\hat{\theta}_{kj} - \theta_{o_j}) \tag{5b}$$

where

$$A_{kj} = (\hat{\hat{\phi}}^2_{R_{kj}} + \hat{\hat{\phi}}^2_{I_{kj}})^{1/2} \tag{6a}$$

$$\hat{\theta}_{kj} = \tan^{-1}(\hat{\hat{\phi}}_{I_{kj}} / \hat{\hat{\phi}}_{R_{kj}}) \tag{6b}$$

This renormalization typically results in phase correction angles on the order of 10° or less. The renormalization process produces a revised set of complex modes denoted by

$$\hat{\phi}_j = \hat{\phi}_{R_j} + i \, \hat{\phi}_{I_j} \tag{7}$$

The second step involves orthogonalization of the real parts of the modes by Targoff's procedure [15] to produce an orthogonal set of real modes, ϕ_{R_j}, which are linear combinations of the modes $\hat{\phi}_{R_j}$.

The effect of this conditioning on the test modes is shown in Table 2 which compares three self–orthogonality matrices:

1. Based on the real parts, $\hat{\phi}_R$, of the original test eigenvectors,
2. Based on the conventional procedure for using the magnitudes of eigenvector elements with the sign of the dominant (real or imaginary) part of the complex vector, and
3. Based on the conditioning procedure described above.

The rotation angles produced by Equation (4) and reflected in the conditioned eigenvectors used in Table 2(c) are shown in Table 3.

System Identification Using SSID

The results of three system identification runs are presented. The first run uses both eigenvalue and eigenvector data to estimate 14 parameters. The 14 parameters include two stiffness parameters for each of 5 two–bay sections. One of the two parameters is a scaling coefficient on the longerons and battens of the two–bay section. The other is a scaling parameter on the diagonals. A mass parameter is also included for each of the top four two–bay sections*. It is the mass moment of inertia about the x–axis at each node. Since the original model had no mass moments of inertia, this parameter was initially zero. The stiffness scaling parameters were initially set to unity. Eigenvalue and eigenvector data from the first five modes were used to estimate these parameters. Eigenvector data included the y and z modal displacements at Nodes 2, 8 22 and 32 (see Figure 2).

SSID uses a Bayesian Estimator [1, 16, 17] which requires uncertainties to be defined for the initial parameter estimates and the data. Uncertainties on the parameter estimates were specified as coefficients of variation (C.O.V.) of 20%. Uncertainties on the test frequencies were specified as C.O.V. of 2% while uncertainties on the test eigenvectors were specified as C.O.V. of 20%. The results of this run are summarized in Tables 4(a, b, c) where part (a) compares the original and revised frequencies, (b) compares the original and revised eigenvectors and (c) compares the original and revised parameter estimates. It is of interest to note that for the most part, the stiffness estimates changed by less than 20% except for stiffness parameters near the base where the largest change was 80%. This represented a change of four standard deviations relative to the initial parameter uncertainty. This change was considered too large to accept. It is also interesting to note that estimates of the mass parameters ranged from –0.0068 to –0.0198. The calculated correction factor based on the actual mass distribution was –0.0140.

Interpretation of these results led to the conclusion that a different set of parameters should be estimated, a set that allowed for some asymmetry in the stiffness properties near the base of the structure. This conclusion was partially influenced by feedback from engineers at LaRC who commented that a loose strut in the lower bay had been discovered after the test.

The alternate set of parameters included the same 12 mass and stiffness parameters for the first 8 bays (counted from the top), but replaced the two symmetric stiffness parameters which had been defined for the last two bays by the following ten parameters:

Bay 9 & 10 longerons, +y, +z, corner
Bay 9 & 10 longerons, –y, +z, corner
Bay 9 & 10 longerons, –y, –z, corner
Bay 9 & 10 longerons, +y, –z, corner
Bay 9 battens and in–plane diagonal
Bay 10 battens and in–plane diagonal
Bay 9 & 10 diagonals, –y face
Bay 9 & 10 diagonals, +y face
Bay 9 & 10 diagonals, +z face
Bay 9 & 10 diagonals, –z face

The same data used in the previous run were used to estimate these parameters, which were also assigned coefficients of variation of 20%. The results of this estimation run are summarized in Tables 5(a, b, c) which compare original and revised frequencies, eigenvectors and parameter estimates, respectively. Frequency errors in this case were reduced from a maximum of 7.63% to 2.19% compared with a reduction to 4.79% in the previous case. Eigenvector errors were roughly the same in both cases, the maximum error being about 36%.

*It was omitted from the fifth section to achieve parity with a subsequent run.

The most striking difference was between the parameter estimates in the two cases. Whereas in the 14 parameter case one parameter was changed by 80%, the maximum change in the 22 parameter case was in the stiffness of the say 9 & 10 diagonals on the –y face which decreased by only 38%.

A third run was made where the 22 parameters from the second run were estimated using only the frequencies of the first five modes. This run resulted in a somewhat greater reduction of the frequency errors but the eigenvectors deteriorated significantly from the original eigenvectors. The maximum error in this case increased from approximately 36% to 60%. The results of this run are summarized in Tables 6(a, b, c).

SSID Graphics

One of the most difficult aspects of system identification is the interpretation of results. Without exception, the behavior of a parameter estimation run must be scrutinized to ascertain its validity. The following questions typically arise:

- Have the eigenvalues converged, and if so how smoothly?
- Have the eigenvectors converged and have they improved on the average? Have they improved in terms of the maximum error of any single element relative some norm of the vector?
- How have the parameter estimates converged? Have they converged? Has convergence been monotonic or oscillatory? Have there been any large jumps in the estimates?
- What is the statistical significance of the estimates?
- How has the estimator converged relative to minimizing the overall objective function?

Answers to these questions are facilitated by the graphical output of SSID. This graphics capability is illustrated in Figures 4 through 8. Each figure presents two examples. Part (a) shows the graphical output from a successful run, while part (b) shows the same output for an unsuccessful run.

Figures 4, 5, 6 and 8 are fairly self explanatory. Figure 7 requires some explanation. Figure 7 shows how the estimated value of each parameter has changed as the result of Bayesian estimation, relative to its initial estimate. The horizontal axis of the figure is labeled in values ranging from –4 to +4. These numbers represent the number of standard deviations from the mean or initial value of the estimate. For example, if the original estimate of a parameter is 10, and its uncertainty is specified as a C.O.V. of 20%, then zero on the ordinate of the graph implies a value of 10, –4 implies a value of 2, and +4 implies a value of 18.

Corresponding to each of the estimated parameters an interval is depicted. The interval is symmetric about the center symbolized by a zero. A shift of this zero to the right or left corresponds to the change in the estimated parameter value. For example, if the zero shifts to a value of +2, it means that the value of the parameter has increased by two standard deviations. In the case of a parameter with an initial value of 10, and a C.O.V. of 20%, such a shift would indicate a 40% increase in the parameter value to 14.

The width of the interval signifies the degree to which the uncertainty of the parameter has been reduced. If the uncertainty has not been reduced at all, the width of the interval will be ± 2 or a total of 4, indicating approximately the ± 95% confidence bounds in the estimate. If the width of the interval shrinks to 2, it means that the revised standard deviation, and the ±95% confidence interval on the estimate is half as large as it was to begin with. An interpretation of these results has been presented in earlier papers [1, 16].

Conclusions

This paper presents the results of a recent case study in system identification. The case involves a real structure modeled and tested at the NASA Langley Research Center.

The first part of the paper discusses the conditioning of complex eigenvectors derived by the ERA method. The conditioning involves a phase angle rotation to remove bias errors from the small imaginary part of the eigenvector, and a Targoff orthogonalization to improve the orthogonality of the eigenvectors, particularly for closely spaced modes. Off–diagonal terms of the orthogonality matrix were reduced by an order of magnitude in the worst case, e.g. from 32% to 2%.

The second part of the paper presents results of parameter estimation using the SSID code. Results for three cases are presented. The first two cases use both eigenvalue (frequency) and eigenvector data from the first five modes. The conditioned eigenvectors were used in both cases. One run estimated 14 symmetric parameters. The second run estimated 12 of the original 14 parameters plus an additional 10 asymmetric parameters replacing two of the symmetric parameters in the lower two bays. In the first case, some of the parameter estimates exceeded reasonable bounds (considered to be two to three standard deviations from the initial estimate). In the second case, all of the estimates were considered reasonable. In addition, the frequency errors were reduced to approximately half of those obtained in the first case.

A third run was made to investigate the importance of eigenvector data in the estimation. A run similar to the second run was made, but with frequency data only. The residual frequency errors were somewhat smaller in this case than in the case where eigenvectors were used, but the eigenvectors of the revised model deteriorated significantly.

On the basis of this experience, as well as other experience not reported here, it is concluded that (1) parameter estimation based on modal data should include eigenvectors as well as eigenvalues, (2) the eigenvectors should be orthogonalized when the orthogonality is poor due to closely spaced modes (provided that one has confidence in the analytical mass matrix), and (3) the parameters used in the estimation should enable the model to match the data.

Finally, the paper presents examples of the graphical output provided by SSID. These graphics have proven to be a valuable tool in the practical application of system identification and model verification.

Acknowledgements

The results presented in this paper are based on research supported in part by NASA under contract NAS7–1064. The authors are grateful for the support provided by John Garba, Technical Monitor at the Jet Propulsion Laboratory. The authors also wish to thank Richard Pappa and Ken Elliott of the Langley Research Center for providing the analytical and test data used in this study. Mr. Elliott was responsible for the testing, whle Mr. Pappa performed the data reduction. Mr. Pappa was extremely cooperative in providing the data requested. Finally, the authors wish to acknowledge the support provided by Sandia Laboratories in the development of SSID. Dr. David Martinez was the Technical Monitor on this effort.

References

1. Denman, et. al., "Identification of Large Space Structures on Orbit," Report No. AFRPL TR–86–054, Air Force Rocket Propulsion Laboratory, September, 1986.

2. Flanagan, C.C., "Test/Analysis Correlation Using Design Sensitivity and Optimization," SAE Technical Paper 871743, October, 1987.

3. Ojalvo, I., Ting, T., Pilon, D., "PAREDYM – a Parameter Refinement Computer Code for Structural Dynamic Models," Proceedings of the 10th IMAC, Orlando, FL, 1988.

4. Allen, J.A., and Martinez, D.R., "Techniques for Implementing Structural Model Identification Using Test Data," SAND–1885, June, 1990.

5. Bronowicki, A.J., Lukich, M.S. and Kuritz, S.P., "Application of Physical Parameter Identification to Finite Element Models," First NASA/DOD CSI Technology Conference, Norfolk, VA, November, 1986.

6. Martinez, D.R., and Redhorse, J., AIAA/ASME/ASCE/AHS/ASC 32nd Structures, Structural Dynamics, and Materials Conference, Baltimore, MD, April, 8–10, 1991.

7. Nelson, R.B., "Simplified Calculation of Eigenvector Derivatives," AIAA Journal, Vol. 14, No. 9, pp. 1201–1205, September, 1976.

8. Fox, R.L., and Kapoor, M.P., "Rates of Change of Eigenvalues and Eigenvectors," AIAA Journal, Vol. 6, pp. 2426–2429, December, 1968.

9. Hasselman, T.K. and Chrostowski, J.D., "Dynamic Model Verification of a Multi–Component System," Paper No. 841585, SAE Aerospace Congress & Exposition, Long Beach, CA, October, 1984.

10. Fries, R.H. and N.K. Cooperrider, "Bayesian Estimation of Transit Rail Vehicle Parameters," ASME Journal of Dynamic System, Measurements, and Control, June, 1985, Vol. 107, pp. 151–158.

11. Martinez, D.R., "Estimation Theory Applied to Improving Dynamic Structural Models," Sandia Report No. SAND82–0572, Sandia National Laboratories, Albuquerque, NM, November, 1984.

12. Simonian, Stepan, S., "Inverse Problems in Structural Dynamics–1. Theory," International Journal for Numerical Methods in Engineering, Vol. 17, pp. 357–365, 1981.

13. Simonian, Stepan, S., "Inverse Problems in Structural Dynamics–II. Applications," International Journal for Numerical Methods in Engineering, Vol. 17, pp. 367–386, 1981.

14. Hasselman, T.K. and Chrostowski, J.D., "Estimation of Nonproportional Damping from Experimental Data," to be presented at the Damping '91 Conference, San Diego, CA, February 13–15, 1991.

15. Targoff, W.P., "Orthogonality Check and Correction of Measured Modes," AIAA Journal, Vol. 14, No. 2, February, 1976, pp. 164–167.

16. Hasselman, T.K., "A Perspective on Dynamic Model Verification," Modal Testing and Model Refinement – AMD Vol. 59, November, 1983.

17. Isenberg, Jerold, "Progressing from Least Squares to Bayesian Estimation," Paper No. 79–Wa/DSC–16 ASME Winter Annual Meeting, New York, NY, December 2–7, 1979.

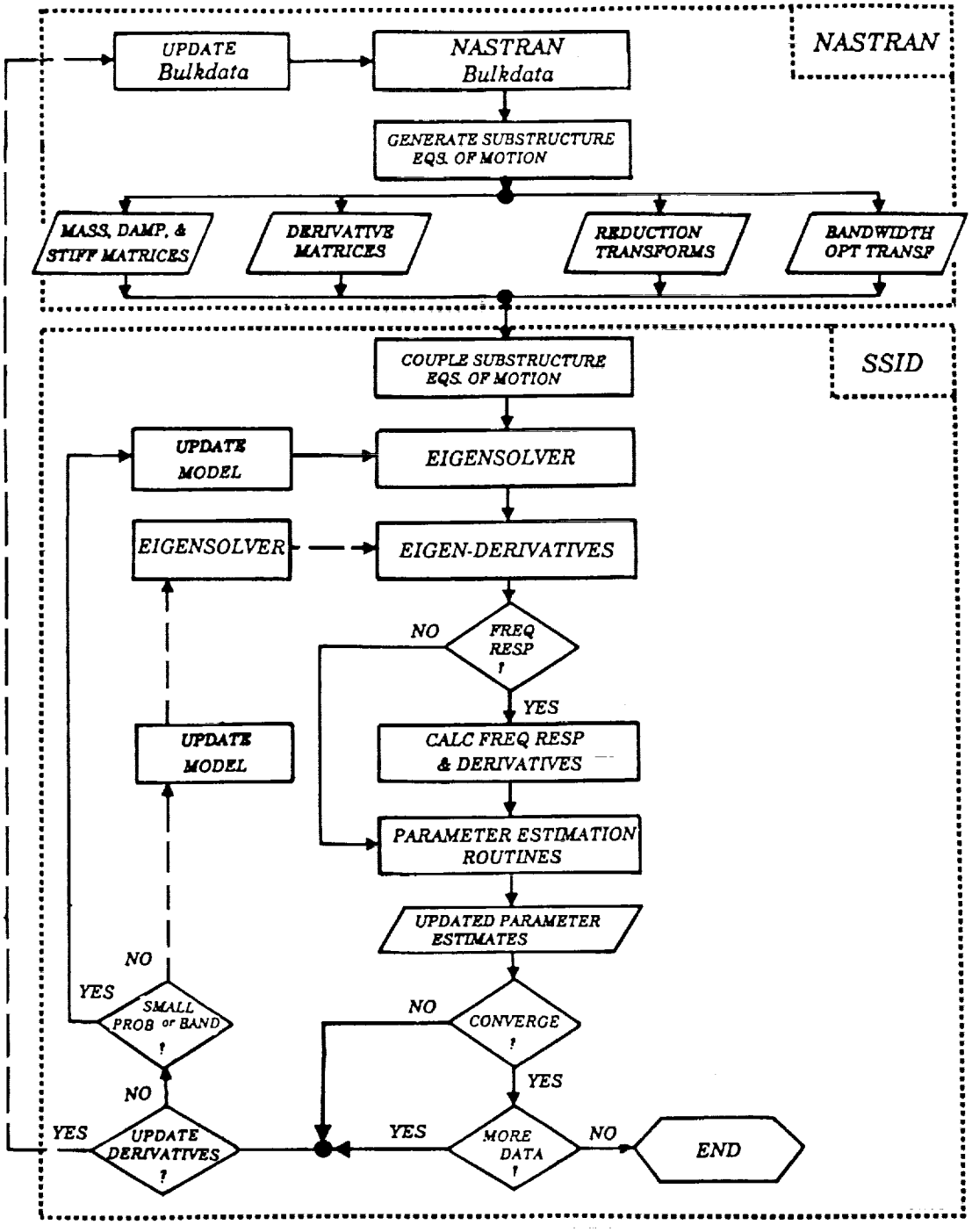

Figure 1. Flow Diagram Illustrating Operations Performed within NASTRAN and SSID

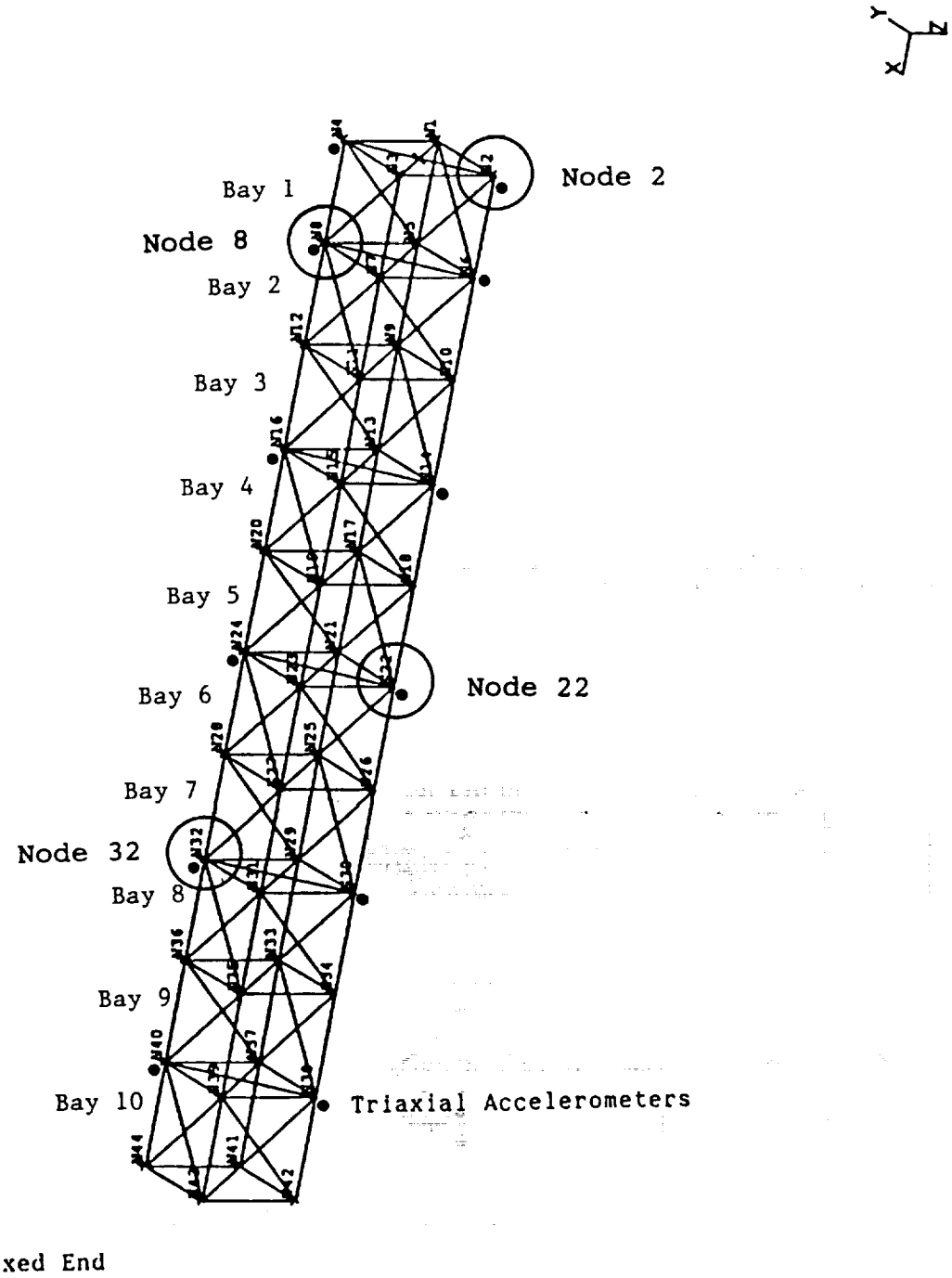

Figure 2. Nodal Geometry of LaRC Ten Bay Truss Structure

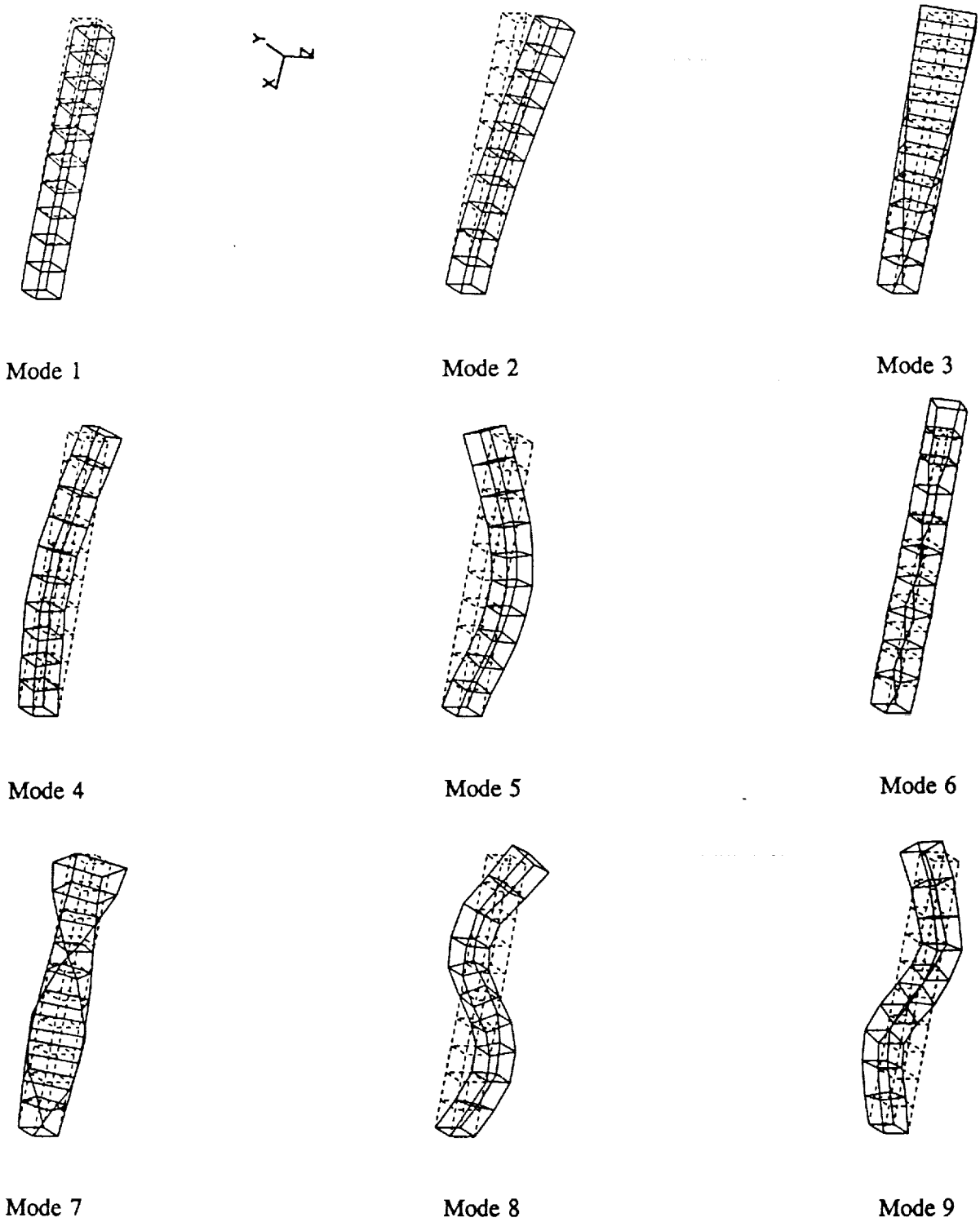

Figure 3. Analytical modes of the NASA LaRC Ten Bay Truss.

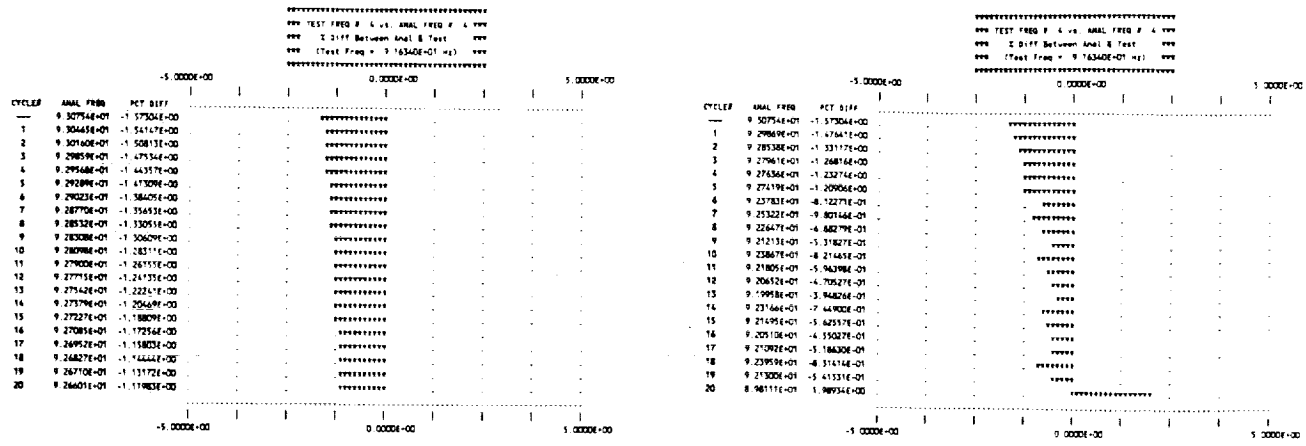

(a) Successful Run

(b) Unsucessful Run

Figure 4. Iterative Convergence of a Modal Frequency During a SSID Run

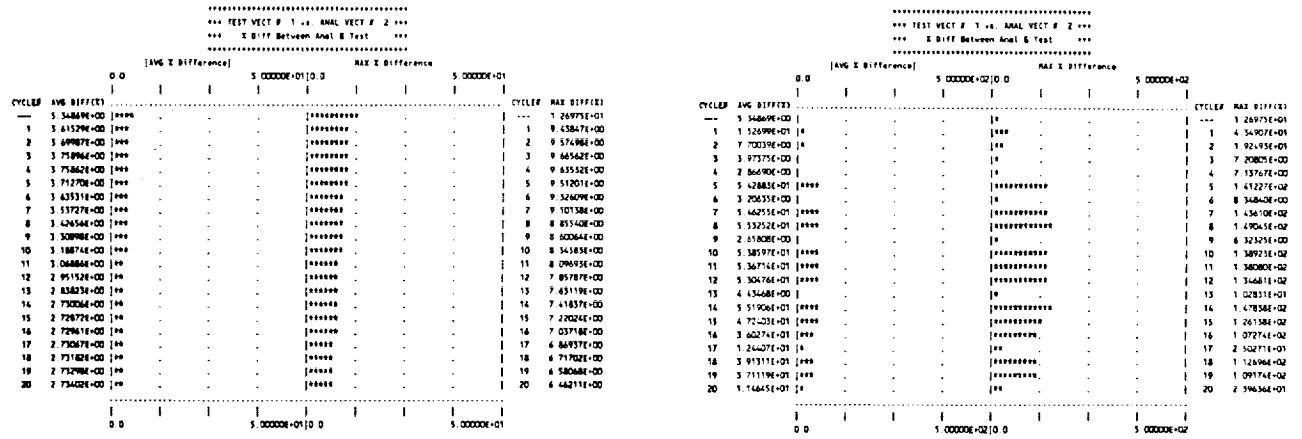

(a) Successful Run

(b) Unsuccessful Run

Figure 5. Iterative Convergence of an Eigenvector During a SSID Run

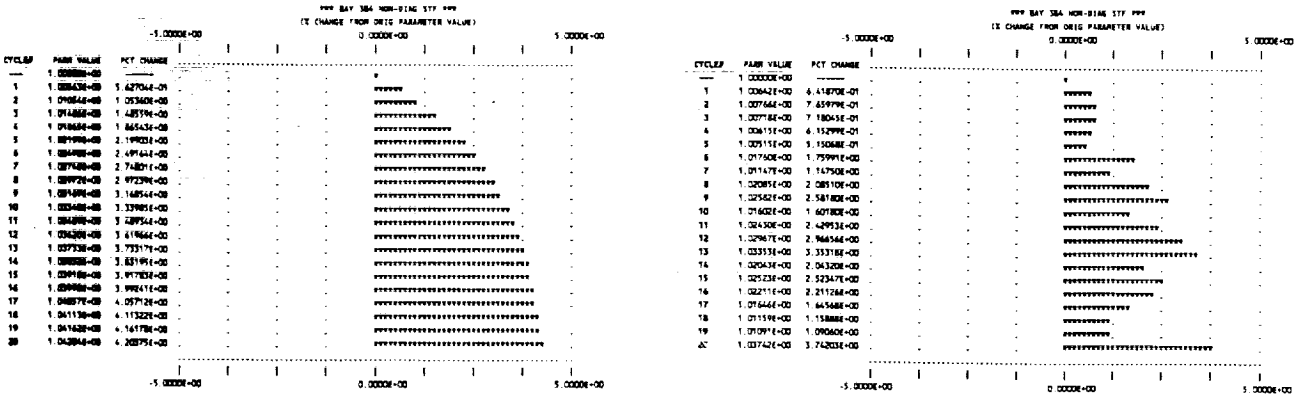

(a) Successful Run

(b) Unsuccessful Run

Figure 6. Iterative Convergence of a Parameter Estimate During a SSID Run

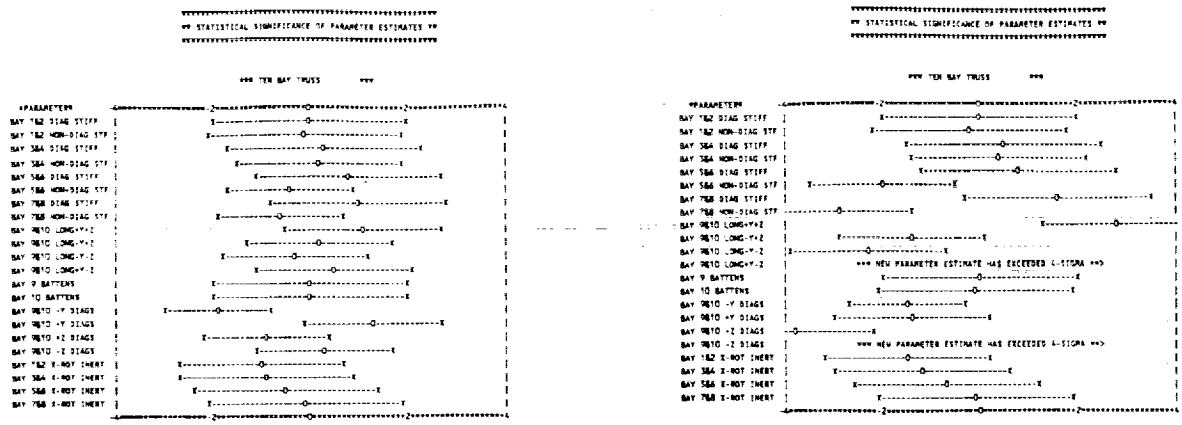

(a) Successful Run (b) Unsuccessful Run

Figure 7. Statistical Significance of Parameter Estimates from SSID Run

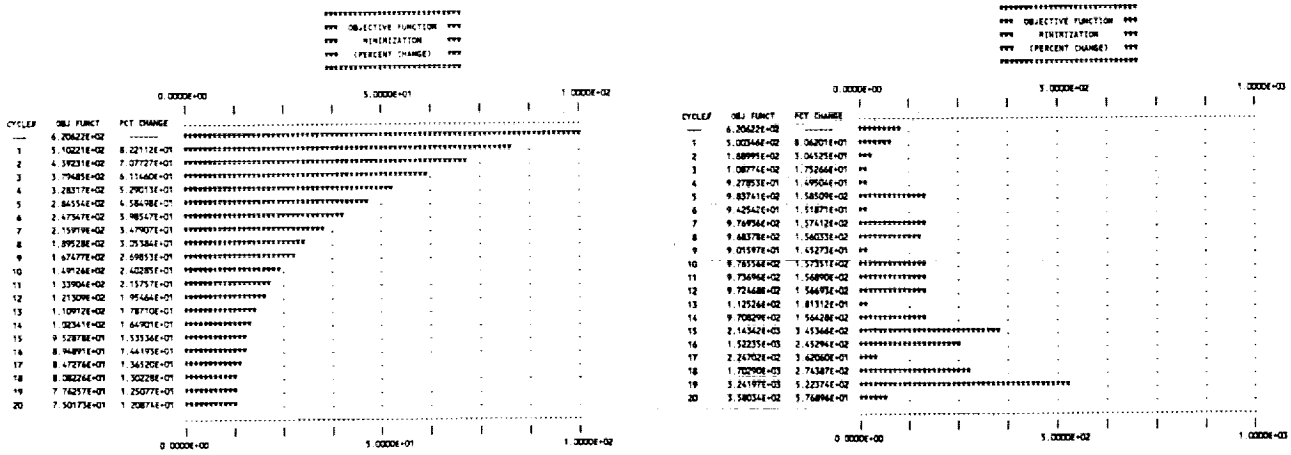

(a) Successful Run (b) Unsuccessful Run

Figure 8. Iterative Minimization of the Objective Function During a SSID Run

Table 1. Frequencies and Orthogonality of Original Test Modes

		** [Phi-real(orig)]-t[M(orig)][Phi-real(orig)] **								
Mode	Freq(Hz)									
1	18.040	1.0000	-.3250	.0073	.0592	-.0130	-.0067	.0757	.0105	.0803
2	18.048	-.3250	1.0000	.0584	-.0521	.0289	-.0248	.0557	.0609	.0737
3	68.043	.0073	.0584	1.0000	.0148	-.0483	-.0011	-.0209	.0403	.0644
4	91.634	.0592	-.0521	.0148	1.0000	-.3350	.0461	-.0623	-.1081	-.2457
5	92.609	-.0130	.0289	-.0483	-.3350	1.0000	-.0624	.0371	.0172	-.0194
6	160.765	-.0067	-.0248	-.0011	.0461	-.0624	1.0000	-.0778	.1660	.0228
7	192.537	.0757	.0557	-.0209	-.0623	.0371	-.0778	1.0000	-.2827	-.2255
8	200.154	.0105	.0609	.0403	-.1081	.0172	.1660	-.2827	1.0000	.1614
9	200.195	.0803	.0737	.0644	-.2457	-.0194	.0228	-.2255	.1614	1.0000

Table 2. Comparison of Orthogonality Matrices

(a) Based on Real Parts of Original Complex Eigenvectors

```
        ** [Phi-real(orig)]-t[M(orig)][Phi-real(orig)] **

1.0000  -.3250   .0073   .0592  -.0130  -.0067   .0757   .0105   .0803
-.3250  1.0000   .0584  -.0521   .0289  -.0248   .0557   .0609   .0737
 .0073   .0584  1.0000   .0148  -.0483  -.0011  -.0209   .0403   .0644
 .0592  -.0521   .0148  1.0000  -.3350   .0461  -.0623  -.1081  -.2457
-.0130   .0289  -.0483  -.3350  1.0000  -.0624   .0371   .0172  -.0194
-.0067  -.0248  -.0011   .0461  -.0624  1.0000  -.0778   .1660   .0228
 .0757   .0557  -.0209  -.0623   .0371  -.0778  1.0000  -.2827  -.2255
 .0105   .0609   .0403  -.1081   .0172   .1660  -.2827  1.0000   .1614
 .0803   .0737   .0644  -.2457  -.0194   .0228  -.2255   .1614  1.0000
```

(b) Based on Conventional Procedure for Converting Complex Eigenvectors to Real Eigenvectors

```
 *** [Phi-raw(mag)]-t[Mass-Orig][Phi-raw(mag)] ***

1.0000  -.2075   .0085   .0626  -.0143  -.0018   .0881   .0193   .0597
-.2075  1.0000   .0570  -.0475   .0334  -.0231   .0649   .0475   .0970
 .0085   .0570  1.0000   .0143  -.0532   .0036  -.0313   .1139   .0480
 .0626  -.0475   .0143  1.0000  -.1941   .0184  -.0409  -.0805  -.2894
-.0143   .0334  -.0532  -.1941  1.0000  -.0589   .0457   .0283  -.0187
-.0018  -.0231   .0036   .0184  -.0589  1.0000  -.0901   .1614   .0235
 .0881   .0649  -.0313  -.0409   .0457  -.0901  1.0000  -.3326  -.1764
 .0193   .0475   .1139  -.0805   .0283   .1614  -.3326  1.0000   .1559
 .0597   .0970   .0480  -.2894  -.0187   .0235  -.1764   .1559  1.0000
```

(c) Based on Real Parts of Conditioned Eigenvectors

```
        ** [Phi-real(new)]-t[M(orig)][Phi-real(new)] **
1.0000  -.0387   .1346   .0062   .0400   .1433   .1093   .0888  -.0006
-.0387  1.0000  -.0691   .0139  -.0061  -.1098   .0485  -.0092  -.0019
 .1346  -.0691  1.0000  -.0346   .0108  -.0198  -.0171  -.0272   .0615
 .0062   .0139  -.0346  1.0000  -.0334   .0249  -.0811  -.0007  -.0430
 .0400  -.0061   .0108  -.0334  1.0000   .0064  -.0256   .0055   .0067
 .1433  -.1098  -.0198   .0249   .0064  1.0000  -.0097   .0223  -.0161
 .1093   .0485  -.0171  -.0811  -.0256  -.0097  1.0000   .0834  -.0353
 .0888  -.0092  -.0272  -.0007   .0055   .0223   .0834  1.0000  -.1697
-.0006  -.0019   .0615  -.0430   .0067  -.0161  -.0353  -.1697  1.0000
```

Table 3. Rotation Angles Computed in the Renormalization of Complex Test Modes

```
MODE # 1 ROTATION ANGLE = -8.9180E-02 DEG
MODE # 2 ROTATION ANGLE =  8.2883E-02 DEG
MODE # 3 ROTATION ANGLE =  2.5080E-01 DEG
MODE # 4 ROTATION ANGLE =  2.3497E+00 DEG
MODE # 5 ROTATION ANGLE = -1.7157E+00 DEG
MODE # 6 ROTATION ANGLE =  3.3203E-01 DEG
MODE # 7 ROTATION ANGLE =  9.0292E+00 DEG
MODE # 8 ROTATION ANGLE = -3.2233E+00 DEG
MODE # 9 ROTATION ANGLE = -4.6475E-02 DEG
```

Table 4. Summary of SSID Results for Case 1.

(a) Comparison of Original and Revised Frequencies (below)
(c) Comparison of Original and Revised Parameter Estimates (right)

MODE NO.	ORIG MODEL FREQ (Hz)	REVISED MODEL FREQ (Hz)	TEST FREQ (Hz)	ORIG DIFF(%)	PREV CYC DIFF(%)	CURR CYC DIFF(%)
1	1.78857D+01	1.76384D+01	1.80480D+01	0.90	2.29	2.27
2	1.78868D+01	1.76474D+01	1.80400D+01	0.85	2.19	2.18
3	6.28527D+01	6.47857D+01	6.80430D+01	7.63	4.86	4.79
4	9.30754D+01	9.36383D+01	9.16340D+01	-1.57	-2.10	-2.19
5	9.31229D+01	9.37216D+01	9.26090D+01	-0.55	-1.12	-1.20
6	1.68636D+02	1.66739D+02	*Not Used*	------	------	------
7	1.87045D+02	2.00493D+02	*Not Used*	------	------	------
8	2.13381D+02	2.04978D+02	*Not Used*	------	------	------
9	2.13732D+02	2.05352D+02	*Not Used*	------	------	------

PARAMETER NAME	ORIG EST	PREV CYCLE EST	CURR CYCLE EST
BAY 1&2 DIAG STIFF	1.00000000D+00	9.47731730-01	9.39939980-01
BAY 1&2 NON-DIAG STF	1.00000000+00	8.59185200-01	8.64001290-01
BAY 3&4 DIAG STIFF	1.00000000+00	1.35651620+00	1.35602650+00
BAY 3&4 NON-DIAG STF	1.00000000+00	1.22817200+00	1.21681020+00
BAY 5&6 DIAG STIFF	1.00000000+00	9.68293420-01	9.76078800-01
BAY 5&6 NON-DIAG STF	1.00000000+00	1.12269580+00	1.13206830+00
BAY 7&8 DIAG STIFF	1.00000000+00	1.17531700+00	1.16450160+00
BAY 7&8 NON-DIAG STF	1.00000000+00	2.03334710-01	1.90342410-01
BAY 9&10 DIAG STIFF	1.00000000+00	6.20867060-01	6.24683900-01
BAY 9&10 NON-DIAG SF	1.00000000+00	1.48623650+00	1.49749280+00
BAY 1&2 X-ROT INERT	0.00000000+00	-1.95807170-02	-1.98371020-02
BAY 3&4 X-ROT INERT	0.00000000+00	-1.68974020-02	-1.71004510-02
BAY 5&6 X-ROT INERT	0.00000000+00	-1.24332530-02	-1.26148990-02
BAY 7&8 X-ROT INERT	0.00000000+00	-6.76497010-03	-6.85167320-03

Table 5. Summary of SSID Results for Case 2.

(a) Comparison of Original and Revised Frequencies (below)
(c) Comparison of Original and Revised Parameter Estimates (right)

MODE NO.	ORIG MODEL FREQ (Hz)	REVISED MODEL FREQ (Hz)	TEST FREQ (Hz)	ORIG DIFF(%)	PREV CYC DIFF(%)	CURR CYC DIFF(%)
1	1.78857D+01	1.79177D+01	1.80480D+01	0.90	0.73	0.72
2	1.78868D+01	1.79188D+01	1.80400D+01	0.85	0.67	0.67
3	6.28527D+01	6.65513D+01	6.80430D+01	7.63	2.29	2.19
4	9.30754D+01	9.26601D+01	9.16340D+01	-1.57	-1.13	-1.12
5	9.31229D+01	9.27998D+01	9.26090D+01	-0.55	-0.22	-0.21
6	1.68636D+02	1.67196D+02	*Not Used*	------	------	------
7	1.87045D+02	1.92705D+02	*Not Used*	------	------	------
8	2.13381D+02	2.14701D+02	*Not Used*	------	------	------
9	2.13732D+02	2.15450D+02	*Not Used*	------	------	------

PARAMETER NAME	ORIG EST	PREV CYCLE EST	CURR CYCLE EST
BAY 1&2 DIAG STIFF	1.00000000D+00	9.97471990-01	9.97298720-01
BAY 1&2 NON-DIAG STF	1.00000000+00	9.78302100-01	9.78541450-01
BAY 3&4 DIAG STIFF	1.00000000+00	1.05967980+00	1.05925620+00
BAY 3&4 NON-DIAG STF	1.00000000+00	1.04161770+00	1.04203750+00
BAY 5&6 DIAG STIFF	1.00000000+00	1.16796680+00	1.16999350+00
BAY 5&6 NON-DIAG STF	1.00000000+00	9.14215790-01	9.13032030-01
BAY 7&8 DIAG STIFF	1.00000000+00	1.19757020+00	1.20147010+00
BAY 7&8 NON-DIAG STF	1.00000000+00	8.81381840-01	8.81319370-01
BAY 9&10 LONG+Y+Z	1.00000000+00	1.21422080+00	1.21685980+00
BAY 9&10 LONG-Y+Z	1.00000000+00	1.04621710+00	1.04705880+00
BAY 9&10 LONG-Y-Z	1.00000000+00	9.47006170-01	9.45312800-01
BAY 9&10 LONG+Y-Z	1.00000000+00	1.10505870+00	1.10472760+00
BAY 9 BATTENS	1.00000000+00	9.98077690-01	9.97993200-01
BAY 10 BATTENS	1.00000000+00	9.98518570-01	9.98435680-01
BAY 9&10 -Y DIAGS	1.00000000+00	6.23516120-01	6.16737180-01
BAY 9&10 +Y DIAGS	1.00000000+00	1.25461710+00	1.25737320+00
BAY 9&10 +Z DIAGS	1.00000000+00	8.24802610-01	8.23644980-01
BAY 9&10 -Z DIAGS	1.00000000+00	1.07183180+00	1.06932590+00
BAY 1&2 X-ROT INERT	0.00000000+00	-1.37178590-02	-1.40443020-02
BAY 3&4 X-ROT INERT	0.00000000+00	-1.16435040-02	-1.19361570-02
BAY 5&6 X-ROT INERT	0.00000000+00	-7.24457060-03	-7.43723270-03
BAY 7&8 X-ROT INERT	0.00000000+00	-1.93813600-03	-1.98641210-03

Table 6. Summary of SSID Results for Case 3.

(a) Comparison of Original and Revised Frequencies (below)
(c) Comparison of Original and Revised Parameter Estimates (right)

MODE NO.	ORIG MODEL FREQ (Hz)	REVISED MODEL FREQ (Hz)	TEST FREQ (Hz)	ORIG DIFF(%)	PREV CYC DIFF(%)	CURR CYC DIFF(%)
1	1.78857D+01	1.80017D+01	1.80480D+01	0.90	0.27	0.26
2	1.78868D+01	1.80163D+01	1.80400D+01	0.85	0.14	0.13
3	6.28527D+01	6.64307D+01	6.80430D+01	7.63	2.45	2.37
4	9.30754D+01	9.25313D+01	9.16340D+01	-1.57	-0.99	-0.98
5	9.31229D+01	9.27109D+01	9.26090D+01	-0.55	-0.12	-0.11
6	1.68636D+02	1.68853D+02	*Not Used*	------	------	------
7	1.87045D+02	1.92799D+02	*Not Used*	------	------	------
8	2.13381D+02	2.13898D+02	*Not Used*	------	------	------
9	2.13732D+02	2.14736D+02	*Not Used*	------	------	------

PARAMETER NAME	ORIG EST	PREV CYCLE EST	CURR CYCLE EST
BAY 1&2 DIAG STIFF	1.00000000D+00	9.99432340-01	9.99409510-01
BAY 1&2 NON-DIAG STF	1.00000000+00	9.93529440-01	9.93421920-01
BAY 3&4 DIAG STIFF	1.00000000+00	1.03594090+00	1.03648780+00
BAY 3&4 NON-DIAG STF	1.00000000+00	9.42514220-01	9.41602210-01
BAY 5&6 DIAG STIFF	1.00000000+00	1.09250020+00	1.09373400+00
BAY 5&6 NON-DIAG STF	1.00000000+00	9.29951080-01	9.28944620-01
BAY 7&8 DIAG STIFF	1.00000000+00	1.11404190+00	1.11549350+00
BAY 7&8 NON-DIAG STF	1.00000000+00	1.04202250+00	1.04265410+00
BAY 9&10 LONG+Y+Z	1.00000000+00	1.01106310+00	1.01129680+00
BAY 9&10 LONG-Y+Z	1.00000000+00	1.01363660+00	1.01384800+00
BAY 9&10 LONG-Y-Z	1.00000000+00	1.01106470+00	1.01129850+00
BAY 9&10 LONG+Y-Z	1.00000000+00	1.01405240+00	1.01427290+00
BAY 9 BATTENS	1.00000000+00	1.00045400+00	1.00046120+00
BAY 10 BATTENS	1.00000000+00	1.00047760+00	1.00048710+00
BAY 9&10 -Y DIAGS	1.00000000+00	1.02057030+00	1.02078960+00
BAY 9&10 +Y DIAGS	1.00000000+00	1.02057020+00	1.02078940+00
BAY 9&10 +Z DIAGS	1.00000000+00	1.04303640+00	1.04384600+00
BAY 9&10 -Z DIAGS	1.00000000+00	1.04314680+00	1.04395800+00
BAY 1&2 X-ROT INERT	0.00000000+00	-9.98493140-03	-1.01544100-02
BAY 3&4 X-ROT INERT	0.00000000+00	-8.42712260-03	-8.56981080-03
BAY 5&6 X-ROT INERT	0.00000000+00	-5.62077650-03	-5.71496550-03
BAY 7&8 X-ROT INERT	0.00000000+00	-2.69351970-03	-2.73957420-03

Table 4(b). Comparison of Original and Revised Eigenvectors

*** TEST MODE NO. 1 vs ANALYSIS MODE NO. 2 for TEST SETUP NO. 1 ***

COMP NO.	NODE NO.	DOF	ORIG MODEL VECTOR	REVISED MODEL VECTOR	TEST VECTOR	ORIG DIFF(%)	PREV DIFF(%)	CURR DIFF(%)	COORDINATE DESCRIPTION
1	2	Y	2.8328D+00	2.5949D+00	2.3348D+00	-21.33	-11.19	-11.14	Y-MOTION @ NODE 2
1	2	Z	-4.9399D+00	-5.2217D+00	-5.6584D+00	12.70	7.78	7.72	Z-MOTION @ NODE 2
1	8	Y	2.4599D+00	2.2426D+00	1.9095D+00	-28.83	-17.51	-17.45	Y-MOTION @ NODE 8
1	8	Z	-4.2793D+00	-4.4707D+00	-4.3206D+00	0.96	-3.43	-3.47	Z-MOTION @ NODE 8
1	22	Y	1.0295D+00	8.6664D-01	7.1352D-01	-44.29	-21.70	-21.46	Y-MOTION @ NODE 22
1	22	Z	-1.7198D+00	-1.6330D+00	-1.7511D+00	1.79	6.63	6.74	Z-MOTION @ NODE 22
1	32	Y	4.6924D-01	3.5289D-01	5.2674D-01	10.92	32.73	33.01	Y-MOTION @ NODE 32
1	32	Z	-7.0236D-01	-5.0554D-01	-4.9413D-01	-42.14	-3.05	-2.31	Z-MOTION @ NODE 32

*** TEST MODE NO. 2 vs ANALYSIS MODE NO. 1 for TEST SETUP NO. 1 ***

COMP NO.	NODE NO.	DOF	ORIG MODEL VECTOR	REVISED MODEL VECTOR	TEST VECTOR	ORIG DIFF(%)	PREV DIFF(%)	CURR DIFF(%)	COORDINATE DESCRIPTION
1	2	Y	4.9406D+00	5.2250D+00	5.1027D+00	3.18	-2.33	-2.40	Y-MOTION @ NODE 2
1	2	Z	2.8320D+00	2.5940D+00	1.4127D+00	-100.47	-83.70	-83.62	Z-MOTION @ NODE 2
1	8	Y	4.2781D+00	4.4718D+00	4.6797D+00	8.58	4.48	4.44	Y-MOTION @ NODE 8
1	8	Z	2.4603D+00	2.2437D+00	1.8668D+00	-31.80	-20.25	-20.19	Z-MOTION @ NODE 8
1	22	Y	1.7193D+00	1.6318D+00	1.8399D+00	6.55	11.20	11.31	Y-MOTION @ NODE 22
1	22	Z	1.0293D+00	8.6585D-01	8.9305D-01	-15.26	2.86	3.05	Z-MOTION @ NODE 22
1	32	Y	7.0202D-01	5.1095D-01	6.7476D-01	-4.04	23.75	24.28	Y-MOTION @ NODE 32
1	32	Z	4.6883D-01	3.5181D-01	2.9290D-01	-60.06	-20.61	-20.11	Z-MOTION @ NODE 32

*** TEST MODE NO. 3 vs ANALYSIS MODE NO. 3 for TEST SETUP NO. 1 ***

COMP NO.	NODE NO.	DOF	ORIG MODEL VECTOR	REVISED MODEL VECTOR	TEST VECTOR	ORIG DIFF(%)	PREV DIFF(%)	CURR DIFF(%)	COORDINATE DESCRIPTION
1	2	Y	3.0090D+00	3.0815D+00	3.0478D+00	1.27	-0.94	-1.11	Y-MOTION @ NODE 2
1	2	Z	2.9947D+00	3.0704D+00	2.5395D+00	-17.93	-20.73	-20.91	Z-MOTION @ NODE 2
1	8	Y	-2.9510D+00	-3.0320D+00	-3.0019D+00	1.70	-0.89	-1.00	Y-MOTION @ NODE 8
1	8	Z	-2.9513D+00	-3.0313D+00	-2.7146D+00	-8.72	-11.54	-11.66	Z-MOTION @ NODE 8
1	22	Y	2.0850D+00	2.3391D+00	2.3913D+00	12.81	2.38	2.18	Y-MOTION @ NODE 22
1	22	Z	2.0851D+00	2.3375D+00	1.9628D+00	-6.23	-18.86	-19.09	Z-MOTION @ NODE 22
1	32	Y	-1.3338D+00	-1.5505D+00	-1.6426D+00	18.80	5.57	5.60	Y-MOTION @ NODE 32
1	32	Z	-1.3338D+00	-1.5526D+00	-1.2674D+00	-5.24	-22.54	-22.50	Z-MOTION @ NODE 32

*** TEST MODE NO. 4 vs ANALYSIS MODE NO. 4 for TEST SETUP NO. 1 ***

COMP NO.	NODE NO.	DOF	ORIG MODEL VECTOR	REVISED MODEL VECTOR	TEST VECTOR	ORIG DIFF(%)	PREV DIFF(%)	CURR DIFF(%)	COORDINATE DESCRIPTION
1	2	Y	3.1266D+00	1.5633D+00	2.4579D+00	-27.21	35.41	36.40	Y-MOTION @ NODE 2
1	2	Z	3.5464D+00	3.9405D+00	3.2864D+00	-7.91	-19.54	-19.90	Z-MOTION @ NODE 2
1	8	Y	1.5494D+00	7.2454D-01	2.8151D-01	-450.40	-162.52	-157.38	Y-MOTION @ NODE 8
1	8	Z	1.8239D+00	1.9462D+00	2.3174D+00	21.29	16.08	16.02	Z-MOTION @ NODE 8
1	22	Y	-2.7924D+00	-1.5408D+00	-2.0835D+00	-34.02	24.86	26.05	Y-MOTION @ NODE 22
1	22	Z	-3.0536D+00	-3.7913D+00	-3.4366D+00	11.14	-9.96	-10.32	Z-MOTION @ NODE 22
1	32	Y	-2.1951D+00	-1.4119D+00	-1.7867D+00	-22.86	19.61	20.98	Y-MOTION @ NODE 32
1	32	Z	-2.5201D+00	-3.5065D+00	-3.5649D+00	29.31	1.81	1.64	Z-MOTION @ NODE 32

*** TEST MODE NO. 5 vs ANALYSIS MODE NO. 5 for TEST SETUP NO. 1 ***

COMP NO.	NODE NO.	DOF	ORIG MODEL VECTOR	REVISED MODEL VECTOR	TEST VECTOR	ORIG DIFF(%)	PREV DIFF(%)	CURR DIFF(%)	COORDINATE DESCRIPTION
1	2	Y	3.5677D+00	3.9688D+00	3.2863D+00	-8.56	-20.39	-20.77	Y-MOTION @ NODE 2
1	2	Z	-3.1116D+00	-1.5524D+00	-2.3022D+00	-35.16	31.51	32.57	Z-MOTION @ NODE 2
1	8	Y	1.8141D+00	1.9384D+00	2.7155D+00	33.20	28.68	28.62	Y-MOTION @ NODE 8
1	8	Z	-1.5627D+00	-7.3023D-01	-1.0050D+00	-55.48	25.89	27.34	Z-MOTION @ NODE 8
1	22	Y	-3.0328D+00	-3.7743D+00	-3.3549D+00	9.60	-12.13	-12.50	Y-MOTION @ NODE 22
1	22	Z	2.8109D+00	1.5452D+00	1.5358D+00	-83.03	-2.24	-0.61	Z-MOTION @ NODE 22
1	32	Y	-2.5040D+00	-3.4660D+00	-3.6064D+00	30.57	4.06	3.89	Y-MOTION @ NODE 32
1	32	Z	2.2106D+00	1.4318D+00	1.8305D+00	-20.76	20.44	21.78	Z-MOTION @ NODE 32

Table 5(b). Comparison of Original and Revised Eigenvectors

*** TEST MODE NO. 1 vs ANALYSIS MODE NO. 2 for TEST SETUP NO. 1 ***

COMP NO.	NODE NO.	DOF	ORIG MODEL VECTOR	REVISED MODEL VECTOR	TEST VECTOR	ORIG DIFF(%)	PREV DIFF(%)	CURR DIFF(%)	COORDINATE DESCRIPTION
1	2	Y	2.8328D+00	2.2188D+00	2.3348D+00	-21.33	4.33	4.97	Y-MOTION @ NODE 2
1	2	Z	-4.9399D+00	-5.2927D+00	-5.6584D+00	12.70	6.58	6.46	Z-MOTION @ NODE 2
1	8	Y	2.4599D+00	1.9412D+00	1.9095D+00	-28.83	-2.32	-1.66	Y-MOTION @ NODE 8
1	8	Z	-4.2793D+00	-4.5557D+00	-4.3206D+00	0.96	-5.32	-5.44	Z-MOTION @ NODE 8
1	22	Y	1.0295D+00	7.9080D-01	7.1352D-01	-44.29	-11.58	-10.83	Y-MOTION @ NODE 22
1	22	Z	-1.7198D+00	-1.8005D+00	-1.7511D+00	1.79	-2.70	-2.82	Z-MOTION @ NODE 22
1	32	Y	4.6924D-01	3.7787D-01	5.2674D-01	10.92	27.92	28.26	Y-MOTION @ NODE 32
1	32	Z	-7.0236D-01	-7.0771D-01	-4.9413D-01	-42.14	-43.07	-43.22	Z-MOTION @ NODE 32

*** TEST MODE NO. 2 vs ANALYSIS MODE NO. 1 for TEST SETUP NO. 1 ***

COMP NO.	NODE NO.	DOF	ORIG MODEL VECTOR	REVISED MODEL VECTOR	TEST VECTOR	ORIG DIFF(%)	PREV DIFF(%)	CURR DIFF(%)	COORDINATE DESCRIPTION
1	2	Y	4.9406D+00	5.2933D+00	5.1027D+00	3.18	-3.61	-3.74	Y-MOTION @ NODE 2
1	2	Z	2.8320D+00	2.2338D+00	1.4127D+00	-100.47	-59.17	-58.12	Z-MOTION @ NODE 2
1	8	Y	4.2781D+00	4.5550D+00	4.6797D+00	8.58	2.78	2.67	Y-MOTION @ NODE 8
1	8	Z	2.4603D+00	1.9217D+00	1.8668D+00	-31.80	-3.63	-2.94	Z-MOTION @ NODE 8
1	22	Y	1.7193D+00	1.7994D+00	1.8399D+00	6.55	2.31	2.20	Y-MOTION @ NODE 22
1	22	Z	1.0293D+00	8.0920D-01	8.9305D-01	-15.26	8.82	9.39	Z-MOTION @ NODE 22
1	32	Y	7.0202D-01	7.0477D-01	6.7476D-01	-4.04	-4.32	-4.45	Y-MOTION @ NODE 32
1	32	Z	4.6883D-01	3.5874D-01	2.9290D-01	-60.06	-23.19	-22.48	Z-MOTION @ NODE 32

*** TEST MODE NO. 3 vs ANALYSIS MODE NO. 3 for TEST SETUP NO. 1 ***

COMP NO.	NODE NO.	DOF	ORIG MODEL VECTOR	REVISED MODEL VECTOR	TEST VECTOR	ORIG DIFF(%)	PREV DIFF(%)	CURR DIFF(%)	COORDINATE DESCRIPTION
1	2	Y	3.0090D+00	2.9351D+00	3.0478D+00	1.27	3.74	3.70	Y-MOTION @ NODE 2
1	2	Z	2.9947D+00	2.7052D+00	2.5395D+00	-17.93	-6.77	-6.52	Z-MOTION @ NODE 2
1	8	Y	-2.9510D+00	-3.1129D+00	-3.0019D+00	1.70	-3.63	-3.70	Y-MOTION @ NODE 8
1	8	Z	-2.9513D+00	-3.2372D+00	-2.7146D+00	-8.72	-19.01	-19.25	Z-MOTION @ NODE 8
1	22	Y	2.0850D+00	2.3014D+00	2.3913D+00	12.81	3.86	3.76	Y-MOTION @ NODE 22
1	22	Z	2.0851D+00	2.4790D+00	1.9628D+00	-6.23	-25.86	-26.30	Z-MOTION @ NODE 22
1	32	Y	-1.3338D+00	-1.3097D+00	-1.6426D+00	18.80	20.44	20.27	Y-MOTION @ NODE 32
1	32	Z	-1.3338D+00	-1.0812D+00	-1.2674D+00	-5.24	14.29	14.69	Z-MOTION @ NODE 32

*** TEST MODE NO. 4 vs ANALYSIS MODE NO. 4 for TEST SETUP NO. 1 ***

COMP NO.	NODE NO.	DOF	ORIG MODEL VECTOR	REVISED MODEL VECTOR	TEST VECTOR	ORIG DIFF(%)	PREV DIFF(%)	CURR DIFF(%)	COORDINATE DESCRIPTION
1	2	Y	3.1266D+00	2.2320D+00	2.4579D+00	-27.21	8.60	9.19	Y-MOTION @ NODE 2
1	2	Z	3.5464D+00	4.5812D+00	3.2864D+00	-7.91	-38.96	-39.40	Z-MOTION @ NODE 2
1	8	Y	1.5494D+00	5.5312D-01	2.8151D-01	-450.40	-102.69	-96.49	Y-MOTION @ NODE 8
1	8	Z	1.8239D+00	1.7311D+00	2.3174D+00	21.29	22.58	22.71	Z-MOTION @ NODE 8
1	22	Y	-2.7924D+00	-1.5684D+00	-2.0835D+00	-34.02	23.64	24.72	Y-MOTION @ NODE 22
1	22	Z	-3.0536D+00	-3.5688D+00	-3.4366D+00	11.14	-3.74	-3.85	Z-MOTION @ NODE 22
1	32	Y	-2.1951D+00	-1.3692D+00	-1.7867D+00	-22.86	22.60	23.36	Y-MOTION @ NODE 32
1	32	Z	-2.5201D+00	-3.1195D+00	-3.5649D+00	29.31	12.73	12.49	Z-MOTION @ NODE 32

*** TEST MODE NO. 5 vs ANALYSIS MODE NO. 5 for TEST SETUP NO. 1 ***

COMP NO.	NODE NO.	DOF	ORIG MODEL VECTOR	REVISED MODEL VECTOR	TEST VECTOR	ORIG DIFF(%)	PREV DIFF(%)	CURR DIFF(%)	COORDINATE DESCRIPTION
1	2	Y	3.5677D+00	4.2555D+00	3.2863D+00	-8.56	-29.27	-29.49	Y-MOTION @ NODE 2
1	2	Z	-3.1116D+00	-1.8649D+00	-2.3022D+00	-35.16	18.11	19.00	Z-MOTION @ NODE 2
1	8	Y	1.8141D+00	2.1519D+00	2.7155D+00	33.20	20.94	20.76	Y-MOTION @ NODE 8
1	8	Z	-1.5627D+00	-9.1425D-01	-1.0050D+00	-55.48	7.90	9.03	Z-MOTION @ NODE 8
1	22	Y	-3.0328D+00	-3.7446D+00	-3.3549D+00	9.60	-11.35	-11.62	Y-MOTION @ NODE 22
1	22	Z	2.8109D+00	1.7608D+00	1.5358D+00	-83.03	-15.89	-14.65	Z-MOTION @ NODE 22
1	32	Y	-2.5040D+00	-3.0873D+00	-3.6064D+00	30.57	14.60	14.40	Y-MOTION @ NODE 32
1	32	Z	2.2106D+00	1.3770D+00	1.8305D+00	-20.76	23.96	24.78	Z-MOTION @ NODE 32

Table 6(b). Comparison of Original and Revised Eigenvectors

*** TEST MODE NO. 1 vs ANALYSIS MODE NO. 2 for TEST SETUP NO. 1 ***

COMP NO.	NODE NO.	DOF	ORIG MODEL VECTOR	REVISED MODEL VECTOR	TEST VECTOR	ORIG DIFF(%)	PREV DIFF(%)	CURR DIFF(%)	COORDINATE DESCRIPTION
1	2	Y	2.8328D+00	4.4988D+00	2.3348D+00	-21.33	-------	-92.68	Y-MOTION @ NODE 2
1	2	Z	-4.9399D+00	-3.5263D+00	-5.6584D+00	12.70	-------	37.68	Z-MOTION @ NODE 2
1	8	Y	2.4599D+00	3.8958D+00	1.9095D+00	-28.83	-------	-104.02	Y-MOTION @ NODE 8
1	8	Z	-4.2793D+00	-3.0477D+00	-4.3206D+00	0.96	-------	29.46	Z-MOTION @ NODE 8
1	22	Y	1.0295D+00	1.5869D+00	7.1352D-01	-44.29	-------	-122.40	Y-MOTION @ NODE 22
1	22	Z	-1.7198D+00	-1.1938D+00	-1.7511D+00	1.79	-------	31.82	Z-MOTION @ NODE 22
1	32	Y	4.6924D-01	6.9232D-01	5.2674D-01	10.92	-------	-31.43	Y-MOTION @ NODE 32
1	32	Z	-7.0236D-01	-4.7111D-01	-4.9413D-01	-42.14	-------	4.66	Z-MOTION @ NODE 32

*** TEST MODE NO. 2 vs ANALYSIS MODE NO. 1 for TEST SETUP NO. 1 ***

COMP NO.	NODE NO.	DOF	ORIG MODEL VECTOR	REVISED MODEL VECTOR	TEST VECTOR	ORIG DIFF(%)	PREV DIFF(%)	CURR DIFF(%)	COORDINATE DESCRIPTION
1	2	Y	4.9406D+00	3.5267D+00	5.1027D+00	3.18	-------	30.89	Y-MOTION @ NODE 2
1	2	Z	2.8320D+00	4.4967D+00	1.4127D+00	-100.47	-------	-218.31	Z-MOTION @ NODE 2
1	8	Y	4.2781D+00	3.0466D+00	4.6797D+00	8.58	-------	34.90	Y-MOTION @ NODE 8
1	8	Z	2.4603D+00	3.8960D+00	1.8668D+00	-31.80	-------	-108.71	Z-MOTION @ NODE 8
1	22	Y	1.7193D+00	1.1936D+00	1.8399D+00	6.55	-------	35.13	Y-MOTION @ NODE 22
1	22	Z	1.0293D+00	1.5876D+00	8.9305D-01	-15.26	-------	-77.78	Z-MOTION @ NODE 22
1	32	Y	7.0202D-01	4.7003D-01	6.7476D-01	-4.04	-------	30.34	Y-MOTION @ NODE 32
1	32	Z	4.6883D-01	6.9357D-01	2.9290D-01	-60.06	-------	-136.79	Z-MOTION @ NODE 32

*** TEST MODE NO. 3 vs ANALYSIS MODE NO. 3 for TEST SETUP NO. 1 ***

COMP NO.	NODE NO.	DOF	ORIG MODEL VECTOR	REVISED MODEL VECTOR	TEST VECTOR	ORIG DIFF(%)	PREV DIFF(%)	CURR DIFF(%)	COORDINATE DESCRIPTION
1	2	Y	3.0090D+00	3.1057D+00	3.0478D+00	1.27	-------	-1.90	Y-MOTION @ NODE 2
1	2	Z	2.9947D+00	3.0915D+00	2.5395D+00	-17.93	-------	-21.74	Z-MOTION @ NODE 2
1	8	Y	-2.9510D+00	-3.0472D+00	-3.0019D+00	1.70	-------	-1.51	Y-MOTION @ NODE 8
1	8	Z	-2.9513D+00	-3.0472D+00	-2.7146D+00	-8.72	-------	-12.25	Z-MOTION @ NODE 8
1	22	Y	2.0850D+00	2.1396D+00	2.3913D+00	12.81	-------	10.52	Y-MOTION @ NODE 22
1	22	Z	2.0851D+00	2.1395D+00	1.9628D+00	-6.23	-------	-9.01	Z-MOTION @ NODE 22
1	32	Y	-1.3338D+00	-1.3888D+00	-1.6426D+00	18.80	-------	15.45	Y-MOTION @ NODE 32
1	32	Z	-1.3338D+00	-1.3891D+00	-1.2674D+00	-5.24	-------	-9.60	Z-MOTION @ NODE 32

*** TEST MODE NO. 4 vs ANALYSIS MODE NO. 4 for TEST SETUP NO. 1 ***

COMP NO.	NODE NO.	DOF	ORIG MODEL VECTOR	REVISED MODEL VECTOR	TEST VECTOR	ORIG DIFF(%)	PREV DIFF(%)	CURR DIFF(%)	COORDINATE DESCRIPTION
1	2	Y	3.1266D+00	9.9924D-01	2.4579D+00	-27.21	-------	59.35	Y-MOTION @ NODE 2
1	2	Z	3.5464D+00	4.6355D+00	3.2864D+00	-7.91	-------	-41.05	Z-MOTION @ NODE 2
1	8	Y	1.5494D+00	4.6995D-01	2.8151D-01	-450.40	-------	-66.94	Y-MOTION @ NODE 8
1	8	Z	1.8239D+00	2.3477D+00	2.3174D+00	21.29	-------	-1.31	Z-MOTION @ NODE 8
1	22	Y	-2.7924D+00	-9.6659D-01	-2.0835D+00	-34.02	-------	53.61	Y-MOTION @ NODE 22
1	22	Z	-3.0536D+00	-4.0431D+00	-3.4366D+00	11.14	-------	-17.65	Z-MOTION @ NODE 22
1	32	Y	-2.1951D+00	-6.7514D-01	-1.7867D+00	-22.86	-------	62.21	Y-MOTION @ NODE 32
1	32	Z	-2.5201D+00	-3.2272D+00	-3.5649D+00	29.31	-------	9.47	Z-MOTION @ NODE 32

*** TEST MODE NO. 5 vs ANALYSIS MODE NO. 5 for TEST SETUP NO. 1 ***

COMP NO.	NODE NO.	DOF	ORIG MODEL VECTOR	REVISED MODEL VECTOR	TEST VECTOR	ORIG DIFF(%)	PREV DIFF(%)	CURR DIFF(%)	COORDINATE DESCRIPTION
1	2	Y	3.5677D+00	4.6674D+00	3.2863D+00	-8.56	-------	-42.02	Y-MOTION @ NODE 2
1	2	Z	-3.1116D+00	-9.9532D-01	-2.3022D+00	-35.16	-------	56.77	Z-MOTION @ NODE 2
1	8	Y	1.8141D+00	2.3313D+00	2.7155D+00	33.20	-------	14.15	Y-MOTION @ NODE 8
1	8	Z	-1.5627D+00	-4.7692D-01	-1.0050D+00	-55.48	-------	52.55	Z-MOTION @ NODE 8
1	22	Y	-3.0328D+00	-4.0203D+00	-3.3549D+00	9.60	-------	-19.83	Y-MOTION @ NODE 22
1	22	Z	2.8109D+00	9.7366D-01	1.5358D+00	-83.03	-------	36.60	Z-MOTION @ NODE 22
1	32	Y	-2.5040D+00	-3.1987D+00	-3.6064D+00	30.57	-------	11.30	Y-MOTION @ NODE 32
1	32	Z	2.2106D+00	6.8062D-01	1.8305D+00	-20.76	-------	62.82	Z-MOTION @ NODE 32